MICRO AND NANO–MANUFACTURING PROCESS CHAINS: MATURITY ASSESSMENT AND BULK METALLIC GLASS ENABLED MANUFACTURING ROUTES

by PIERRE VELLA

A thesis submitted to
The University of Birmingham
for the degree of
DOCTOR OF PHILOSOPHY

School of Mechanical Engineering
University of Birmingham
April 2015

UNIVERSITY OF
BIRMINGHAM

University of Birmingham Research Archive

e-theses repository

ABSTRACT

The integration of complementary technologies in process chains is widely considered as a way forward to achieve cost effective and high throughput production of miniaturised devices. At the same time it is recognised that there are no methodologies to analyse and evaluate systematically process chains and thus to inform their further development and design new ones for micro fabrication. In this context, this research first proposes a methodology for assessing the maturity of micro and nano- manufacturing (MNM) technologies and their interfaces in process chains. The applicability and benefits of using the methodology as a tool for assessing the maturity levels of individual processes and their pairs or chains is demonstrated on existing proven and emerging MNM platforms. In addition, the methodology was also used to identify process pairs that are potentially suitable for integration in process chains.

Then, process pairs were identified to address the growing requirements for function and length scale integration (FLSI) in devices. In particular, two novel master-making process chains were designed and validated for serial replication of polymer components with sub-micron and micro size functional features. Through the use of a Zr-based Bulk Metallic Glass (BMG) these two process chains integrate the capabilities of complementary technologies, Picosecond (PS) Laser ablation with Focussed Ion Beam (FIB) Milling; and Miro-Mechanical Milling (μMilling) with Hot embossing (HE) and FIB Milling respectively. The empirical research showed that the use of BMG workpieces with their intrinsic atomic level homogeneity enables the integration of MNM technologies to achieve FLSI in replication inserts, especially incorporating both micro and nano-scale functional features. Furthermore,

the capabilities of such inserts were validated by employing them as replication masters for serial production of polymer based FLSI devices using injection moulding.

The advantages that partially crystalline BMG workpieces can offer in terms of enhanced wear and fatigue properties were investigated for master-making, especially in implementing the μMilling + HE + FIB Milling process chain. It was experimentally demonstrated that it is possible to produce partially crystalline BMG inserts incorporating micro and nano-scale features with the required resolution and surface integrity that can be applied for injection moulding of thermoplastic FLSI devices. The effects of the Zr-BMG's partial crystallisation on the insert's wear and fatigue life was studied and it was demonstrated, that: (i) the wear resistance of the insert was improved by introducing crystalline nano phases in the monolithic-amorphous Zr-based BMG and (ii) the fatigue performance of the insert can be affected significantly by the preceding stages in the process chain.

Finally, key component technologies in both master-making process chains were investigated to develop further their capabilities. The investigations revealed that the nanosecond laser machining regime is also a very promising method for cost-effective micro-structuring of the Zr-based BMGs and can therefore replace PS laser in the PS Laser + FIB process chain for more cost effective master-making. For the μMilling + HE + FIB Milling process chain, it was shown that the FIB milling response of both the fully amorphous and partially crystalline workpieces is similar. Furthermore, the overall performance of this master manufacturing route can be substantially improved by optimising both material(s) microstructure and processing parameters and set-ups.

ACKNOWLEDGEMENTS

TABLE OF CONTENTS

LIST OF FIGURES

LIST OF TABLES

NOTATION

μEDM   Micro electrical discharge machining

μIM   Micro-injection moulding

μm   Micrometre

μMilling   Micro milling

1D   One dimensional

2D   Two dimensional

3C   Capability, compatibility and complementarity

3D   Three dimensional

AFM   Atomic force microscope

AR   Aspect ratio

BD   Blu-ray disc

BMG   Bulk metallic glass

C_b Compatibility score

C_{cw} Normalised combined complementarity and compatibility weighted score

CD   Compact disc

CMM   Capability maturity model

CMMI   Capability maturity model integration

COC	Cyclic olefin copolymer
C_r	Complementarity score
CVD	Chemical vapour deposition
DOE	Design of experiments
DRIE	Deep reactive ion etching
DVD	Digital video disc
E	Elastic modulus
EB	Electron beam
ECMM	Electrochemical micro machining
EDM	Electrical discharge machining
EDS	Energy dispersive spectroscopy
EUV	Extreme ultraviolet
FIB	Focused ion beam
FLSI	Function and length scale integration
F_p	Applied force
Gpa	Giga pascals
H	Hardness
HAZ	Heat-affected zone
HE	Hot embossing
Hv	Vickers hardness

IB	Ion beam
IC	Integrated circuit
IM	Injection moulding
IPL	Ion projection lithography
k	Coverage factor
KPCA	Key process capability area
KPCP	Key process capability parameter
LIGA	Lithography, electroplating and moulding
l_m	Feature dimension of the master
l_{mr}	Feature dimension of the replicated part
MEMS	Micro-electromechanical systems
MET	Micro engineering technologies
ML	Maturity level
MNM	Micro and nano manufacturing
MNT	Micro and nano technologies
MOEMS	Micro-opto-electromechanical systems
MST	Micro systems technologies
NEMS	Nano-electromechanical systems
nm	Nanometre
NS	Nanosecond

PA+20%GF   Polyamide filled with 20% glass fibre

PC   Polycarbonate

P_h Holding pressure

PMI   Process maturity indicator

PML   Process maturity level

PMLIBP   Projection mask-less ion beam patterning

PMMA   Polymethyl methacrylate

PP   Polypropylene

PP_ML   Process pair maturity level

PPMM   Process pair maturity matrix

PS   Picosecond

PVD   Physical vapour deposition

PVD   Physical vapour deposition

QR   Quick response

R2R   Roll-to-roll

Ra   Arithmetic mean roughness

RIE   Reactive ion etching

S Shrinkage/expansion

SCL   Supercooled liquid

SCLR   Supercooled liquid region

SEI	Software engineering institute
SEM	Scanning electron microscope
SPF	Superplastic forming
T_b	Melt temperature
T_g	Glass transition temperature
t_h	Holding pressure duration
T_m	Mould temperature
T_p	Processing temperature
t_p	Overall process time
TPF	Thermoplastic forming
TRL	Technology readiness level
T_x	Crystallisation temperature
U	Expanded uncertainty
$u(art)$	Uncertainty of the calibration of the reference artefact
$u(cal)$	Uncertainty of the calibration of the measuring equipment
$u(hardness)$	Uncertainty due to variations in the hardness of the sample
$u(noise)$	Uncertainty due to background noise of the instrument
$u(P)$	SEM measurement uncertainty
$u(proc)$	Uncertainty due to the repeatability of the manufacturing process
$u(rep)$	Uncertainty due to the repeatability of the measurement process

u(res)	Uncertainty due to the measuring equipment resolution
u(step)	Uncertainty due to the confocal microscope scan step height
u(temp)	Uncertainty due to temperature variations
u_c	Combined standard uncertainty
UFG	Ultra fine grained
UV	Ultraviolet
V_i	Injection speed
XRD	X-ray diffraction
v_{eff}	Effective degrees of freedom

CHAPTER 1
INTRODUCTION

1.1 Background and Motivation

The global market for miniaturised products has been increasing continuously in the last decade ((HLG), 2011; Koc and Ozel, 2011). This trend is a direct consequence of the growing needs and demands across a range of industry sectors (e.g. biotechnology, energy, medical, optoelectronics, micro-optics, printed electronics and ultraprecision engineering) to integrate multiple functionality in the smallest possible enclosures/packages by combining the latest advances in functional materials and high throughput micro- and nano-manufacturing (MNM) technologies. Thus, it is not surprising that this trend for function integration in current and new emerging products has motivated researchers to look for new ways to 'harness' the latest advances in functional materials and MNM technologies to create manufacturing capabilities for function and length scale integration (FLSI) at part and product levels (Bigot et al., 2011). These capabilities underpin the development of new miniaturised devices that depend on the manufacture of components incorporating functional features covering the whole range of sizes from few 100 μm to sub-100 nm. In addition, to achieve FLSI in a single part, it is very important to explore the opportunities that new specially developed materials can offer and thus to benefit from their 'optimised' properties for micro- and nano-scale processing (Dimov et al., 2012).

Micro- and nano-manufacturing technologies that underpin the development of multifunctional miniaturised products are limited in their capabilities for producing structures with different length scale features cost-effectively, from a few millimetres down to nanometres, in different materials (Dimov et al., 2012). Therefore, the capabilities of

complementary and at the same time compatible manufacturing technologies are usually combined in process chains to produce miniaturised devices incorporating different length scale features. Such process chains can provide the necessary manufacturing solutions for achieving both high throughput and cost-effective production of micro- and nano-structured parts and devices. However, as will be disclosed in more detail in chapter 2, the manufacture of micro-products using such process chains is still in its infancy, and thus further research is required to characterize process chains, and also to develop new ones for the fabrication of novel miniaturised multi-material products (Dimov et al., 2012).

1.2   Research Hypothesis and Objectives

The abovementioned two underlying requirements prompted the two main hypotheses followed in this research.

The first hypothesis is that a methodology for assessing the maturity of micro and nano-manufacturing technologies and their interfaces in process chains will enable the systematic analysis and evaluation of such manufacturing routes; and thus provide an objective means to inform about the further development of existing process chains and to design new ones for the fabrication of novel miniaturized products (Dimov et al., 2012).

As stated earlier, further research is required to develop new process chains for the fabrication of novel multifunctional miniaturized products. In particular there is a need to develop cost-effective processing capabilities for mass producing components and devices incorporating micro and nano-scale features (Dimov et al., 2012). The gateway to develop manufacturing capabilities for mass producing FLSI products and components is to combine multiscale master making technologies with high throughput replication capability. However, it is really a challenging task to design and implement successfully such process chains aiming at FLSI

in innovative miniaturised products. Especially, it is necessary to address various specific technology integration issues (Bigot et al., 2011) in developing process chains   for producing replication masters incorporating multi-length scale features. The utilisation of materials that are compatible with all or the majority of manufacturing processes integrated in such process chains is one of important consideration in their development. Thus, when designing a process chain and selecting an appropriate material to address the requirements of the replication master, the processing constraints of its component micro and nano manufacturing technologies should be considered. This means that the selected material should have a microstructure with a favourable response to processing both at meso/macro and micro/nano scales. To satisfy this requirement, the material should have specific characteristics, such as being homogeneous and inclusion free at the considered processing scales and thus to minimise uncertainties in micro and nano manufacturing. Bulk metallic glasses (BMGs) are intrinsically homogeneous down to nanoscale and at the same time possess unique mechanical and thermal properties which can fulfil the functional and technical requirements of master-making materials**.** Thus BMGs are a very good candidate material for fabricating micro and nano structured replication masters (Kumar et al., 2009a; Kawasegi et al., 2006; Li et al., 2007b; Loffler et al., 2007; Quintana et al., 2009; Browne et al., 2012; Schroers and Paton, 2006).

Within this perspective, the second hypothesis is that taking into account bulk metallic glasses' atomic level homogeneity, these materials can undergo multi-scale patterning successfully and therefore can be used to design and implement FLSI enabling master-making process chains. At the same time, due to the functional and technical requirements of such masters, two important characteristics of BMGs are their wear and fatigue properties; however as will be disclosed in more detail in chapters 2 & 5, the literature review revealed some contradictory views concerning the effects of introducing some nano crystallisation on

their properties (Greer et al., 2002; Pan et al., 2010; Suryanarayana and Inoue, 2011). In particular, based on these findings, it can be assumed that morphological changes could be controlled to achieve a better wear resistance and fatigue properties whilst simultaneously retaining a satisfactory machining response at the submicron and nano scales.

In this context, the overall aims of this research were to develop a systematic approach for assessing the maturity of MNM technologies and to investigate cost-effective implementations of BMG enabled master-making process chains for serial replication of thermoplastic polymer based FLSI devices. To achieve the overall aims of the research, the following objectives were set:

- **Objective 1 :** To develop and validate a systematic approach for assessing the maturity of manufacturing technologies in the micro and nano manufacturing (MNM) domain at both the technological and platform levels. **(Chapter 3)**

- **Objective 2:** To design and experimentally investigate new master making process chains enabled by the use of bulk metallic glasses (BMGs) as a means to combine the capabilities of complementary technologies for producing micro and nano scale structures. **(Chapters 4 & 5 & 6)**

- **Objective 3:** To validate experimentally BMG replication masters for serial production of polymer based FLSI devices and at the same time to investigate systematically the factors affecting their performance. **(Chapters 4 & 5 & 6)**

- **Objective 4:** To investigate the effects of partially crystalline BMG workpieces both on micro and nano structuring technologies integrated in master making process chains and the robustness of such BMG masters when utilized for serial replication of polymer based FLSI devices. **(Chapters 5 & 6)**

- **Objective 5:** To study systematically the capabilities of key component technologies in BMG-enabled master making process chains and then to optimise and/or potentially develop them further to meet specific application requirements. **(Chapters 4 & 6)**

These objectives were set in order to address the open research issues identified in the literature review chapter.

1.3   Thesis Organisation

The remainder of this thesis consists of seven chapters. The main investigations of the research are presented in Chapters 3 to 6, whilst chapters 2 and 7 provide the literature review and a summary of the contributions to knowledge respectively. Following the main chapters are the Appendices, References and List of Publications section respectively. The latter section provides a list of publications based on some of the work described in the thesis.

Chapter 2 provides the background for the research carried out in this thesis. It first sets out to discuss the various integration issues encountered when combining and integrating micro- and nano-fabrication technologies into process chains. Then, the chapter proceeds to discuss the development of process chains for the fabrication of devices/ components incorporating micro and nano- length scale features. In particular, it discusses the concepts of (i) a systematic approach to assess process chains and (ii) material-enabled process chain development. In addition, an overview of the available MNM technologies which can be integrated into process chains is carried out together with an analysis of their capabilities and limitations. Subsequently, the chapter continues with a review and discussion on the use of bulk metallic glasses for the design and implementation of master-making process chains as fabrication routes for serial production of polymer based devices incorporating micro and nanoscale features. Finally, the chapter provides a summary of the open research issues.

In **chapter 3** the objective of the research is to develop and validate a systematic approach for assessing the maturity of technologies in the micro and nano manufacturing domain. After reviewing a number of maturity assessment techniques, the chapter proposes a novel method for assessing the maturity levels of individual MNM processes and the combined maturity of pairs or chains of processes. Then, a pilot application of this methodology on a set of MNM processes is described to demonstrate its capabilities. Finally, the results from this pilot application are discussed and conclusions are made about the viability of the proposed methodology.

In **chapter 4,** a novel process chain for serial production of polymer-based devices incorporating both micro- and nanoscale features is proposed and implemented. The proposed manufacturing route consists of two pairs of processes, identified in Chapter 3 as suitable to be integrated into process chains. Furthermore, the process chain is enabled by the use of a Zr-based BMG to achieve the necessary level of compatibility and complementarity between its component technologies. In particular, it integrates two different technologies, namely pico-second (PS) laser ablation and focused ion beam (FIB) milling for micro-structuring and sub-micron patterning respectively, in order to fabricate BMG inserts incorporating different length scale functional features. An alternative laser source, namely nano-second (NS) is also considered as another potential candidate for the first step in this master-making process chain. The capabilities of the component technologies together with some issues associated with their integration are studied. Micro-injection moulding (µIM) trials are carried out to validate the replication performance of the produced Zr-based BMG master. Furthermore, an experimental study is also carried out to determine whether it would be possible by NS laser ablation to structure the Zr-based BMG workpieces with a high surface integrity whilst retaining the BMG's non-crystalline morphology. The chapter begins by discussing process and material-related issues that have to be considered in achieving length scale integration in

master making process chains. It also provides an overview of the component technologies investigated this research. Then, the experimental set-up employed to carry out the above mentioned investigations is described. Finally, the obtained results are presented and discussed, and conclusions are made.

In Chapter 5 another novel process chain for serial production of polymer-based devices incorporating both micro- and nanoscale features is proposed and implemented. In the previous chapter, the capabilities of PS laser machining as a micro-structuring technology were successfully combined with those of the FIB milling to fabricate BMG replication inserts incorporating multi-scale structures. At the same time, it should be noted that the optimisation of the laser processing parameters will not be enough to produce sufficiently smooth surfaces on the microscale features for direct follow up FIB sub-micron and nano structuring. Thus in this chapter an alternative novel BMG enabled master-making process chain is investigated in order to overcome this issue and also to develop cost effective manufacturing capabilities for achieving FLSI in products incorporating 3D features. In particular, in the proposed process chain, the PS Laser + FIB milling pair of processes is replaced by the Micro milling (μMilling) + Hot embossing (HE) and HE + FIB process pairs, which were also identified in Chapter 3 as being suitable to be integrated in process chains. Furthermore, as outlined in Chapter 2, partially crystalline BMGs with their enhanced wear and fatigue properties, can offer potential advantages when utilised to fabricate replication tooling. Thus this research also explores the concept that the morphology of the BMG workpiece could be controlled to achieve a better wear resistance and fatigue properties whilst simultaneously retaining a satisfactory machining response at the submicron and nano scales.

Within this context, the three complementary technologies, namely μMilling, HE, and FIB are integrated to produce a Zr-based BMG replication tool incorporating micro and nano scale functional features. The machining response of the partially crystalline Zr-based BMG

workpiece is also studied to investigate the robustness of the proposed process chain and its effects on the master's properties, especially when utilized for micro-injection moulding. Furthermore micro-injection moulding trials are carried out to validate the replication performance of the partially crystalline Zr-based BMG insert. The chapter starts by presenting the rationale behind the design of the proposed master-making process chain. The component technologies utilised to achieve FLSI in the fabricated BMG masters and replicated polymer parts are also described. Then, the experimental set-up for the implementation and validation of the process chain is presented. Finally, the results are discussed and conclusions are made about the capability of the proposed process chain route for achieving FLSI in products.

Chapter 6 reports follow-up research work to investigate further the component technologies of the FLSI enabling master-making process chain designed and validated in chapter 5. In particular, supplementary trials to investigate potential improvements to the surface integrity of the Al masters generated by the μMilling process are presented. Also, an experimental study of the thermoplastic forming (TPF) process is carried out to investigate its constraints in regards to the achievable replication quality. The FIB machining response of a fully amorphous Zr-based BMG insert is also systematically studied and subsequently compared with the previously reported results for partially crystalline Zr-based BMG inserts and thus to determine whether there are any differences in the achievable nanoscale feature resolution and surface integrity. Finally, μIM trials are carried out to understand the broader applicability of the proposed FLSI enabling master-making process chain. The effects of BMG partial crystallisation on the insert's wear and fatigue life response is also studied in the context of the proposed process chain. The chapter starts by describing the experimental set-up including the design of the test device and processing conditions for each technology, as well as measuring and inspection equipment and procedures utilised to carry out the above mentioned investigations. Then, the obtained results are discussed, and conclusions are made.

Finally, **chapter 7** summarises the main contributions to knowledge and conclusions of the thesis, and also proposes some possible directions for further research work.

CHAPTER 2
LITERATURE REVIEW

2.1   Chapter Overview

In this chapter, a review on micro and nano-manufacturing (MNM) process chains is presented. In this research, the definitions for micro- and nano-manufacturing are adopted from Madou (2002). Specifically, micro-manufacturing refers to the production of products or components where the dimensions of at least one feature are in the micrometre range. Similarly, nano-manufacturing refers to the fabrication of devices or components where some of the feature dimensions are in the nanometre range. In this research work, feature/ component dimensions in the range of 1µm to 500µm are considered to be in the micrometre range, whilst those between 1nm and 999nm are deemed to be in the nanometre range. The chapter covers the state-of-the-art of the main topics addressed by this research and also discusses the related open research issues. It first sets out to discuss the various factors and processing constraints encountered when combining and integrating micro- and nano-fabrication technologies into process chains. Then, the chapter proceeds to discuss the development of process chains for the fabrication of devices/ components incorporating micro and nano- length scale features. In particular, it discusses the need (i) for a systematic approach to assess process chains at the technology and platform levels and (ii) to utilise materials that are compatible with all or the majority of the component processes when designing and implementing micro and nano-manufacturing process chains. In addition, an overview of the available micro and nano-manufacturing technologies which can be integrated into process chains is carried out together with an analysis of their capabilities and limitations. Subsequently the chapter elaborates further on the concept of utilising suitable

workpiece materials to develop process chains. In particular, it discusses the advantages that bulk metallic glasses can offer with regards to their use in the design and implementation of FLSI enabling master-making process chains, and also as a candidate replication tool material for serial production of polymer based devices incorporating micro and nanoscale features. A brief overview of bulk metallic glasses (BMGs) and the technologies used for the fabrication of micro and nano-scale features on metallic glass based workpieces is also provided. Finally, a summary of the open research issues is presented.

2.2   Product Development Trends

The global market for miniaturised products has been increasing continuously in the last decade ((HLG), 2011). This demand for micro-products and components has risen rapidly across many industrial sectors, especially in the electronics, optics, medical, biotechnology, automotive, communication and avionic industries (Alting et al., 2003; DeVor and Ehmann, 2005) . Examples of specific applications/products are medical implants, micro-scale pumps, valves and mixing devices, micro-fluidic systems, micro-optics, micro-nozzles and micro-molds. This trend towards product miniaturization has brought with it a number of associated product development trends. In particular, designers aim and tend to develop new products that integrate a variety of functions, thus broadening the products' application areas whilst simultaneously significantly reducing cost, size, material usage and power consumption.To satisfy specific functional and technical requirements, single components in such devices often exploit the latest advances in functional materials and also by integrating different length scale functional features/structures from meso down to nano scales. This generic trend in miniaturising devices can be concisely defined as an integration of functional multi-scale structures or features into a single component or in short Function and Length Scale Integration (FLSI) (Dimov et al., 2012; Bigot et al., 2011). In literature, there are also specific

examples of product ideas and concepts based on FLSI, such as polymer based lab-on chip platform for protein detection (Nestler et al., 2010), fused silica lab-on-chip device incorporating the functionalities of a biological laboratory on a single substrate (Vazquez et al., 2009) and a biocompatible polymer based contact lens encapsulating micron-scale metal interconnects and including light-emitting diodes (Ho et al., 2008).

Incorporating various functions in a single component is a difficult task due to the necessity to manufacture different length scale features reliably and cost effectively from nanometre through micro to meso scales. Thus, this FLSI trend has to be underpinned by the development of innovative, reliable and cost effective manufacturing methods for mass producing components with multi-scale features in a variety of materials (e.g metals, polymers, composites and ceramics) (Koc and Ozel, 2011; Dimov et al., 2012; Brousseau et al., 2010) . The various issues associated with meeting this requirement are discussed in more detail in the following sections.

2.3   Function and Length Scale Integration Issues

The fabrication methods for achieving FLSI can be classified into three groups: assembly, single process structuring and multi-process fabrication of a single component. However, based on the evidence found in a survey performed on European research projects, the typical issues that arise when designing and manufacturing products incorporating functional features with different length scales can be classified in two main categories, namely, assembly and multi-scale machining related issues (Bigot et al., 2011) . Only the latter category is pertinent to this research, and consequently some of the various integration issues related to the multi-scale machining category will be presented here.

2.3.1 Multi-scale machining related issues

Assembly steps should ideally be avoided for a variety of economic and technical reasons. So, it is usually better to achieve the required functionality of components or devices by using the minimum number of parts, and consequently minimising or even eliminating the use of assembly operations in order to achieve FLSI in products. In order to eliminate such assembly operations, features with different length scales are integrated by fabricating them directly on a single component. Typically the preferred option to fabricate such multi-scale features is the implementation of a sequence of compatible and complementary processes (i.e. a process chain) working on a single component. A wide range of processes can be integrated into such process chains to manufacture these multi-scale features.

Nevertheless, there are a number of integration issues associated with this multi-length scale machining approach, which are related to the use of: (i) a single manufacturing process or (ii) a process chain to produce the functional features cost effectively (Bigot et al., 2011).

2.3.1.1 Single process multiple scales

In order to minimise the number of processes used in a process chain and consequently reduce the overall production time and cost, a single process can sometimes be applied to achieve the necessary FLSI on a single component. Nevertheless, this approach requires significant R&D efforts to implement in scale-up manufacture, as in the case of micro injection moulding, hot embossing or electroforming. In particular, it is necessary to apply ''design for manufacture'' approaches during product development stage in order to take into account the specific manufacturing constraints of the selected high throughput technologies. In addition there are also issues related to the optimisation of such technologies in order to meet the specific product requirements. For example, issues for injection moulding are related to the replication fidelity. In particular, due to the difference in length scales, various features might require

different levels of process control in order to achieve the correct replication output. Thus, optimising part design and process parameters becomes increasingly challenging.

Another issue is that, the machine setup has to allow for the accurate setting up of the working coordinate systems and tool handling in order to achieve the necessary repeatability in producing batches of parts.

Finally, there are also issues due to limitations of the manufacturing equipment/ technology being utilised. (Bigot et al., 2011) . For instance, regarding processes that depend on optics, such as lithography and laser ablation, the limitations imposed by diffraction or focusing limits have to be taken into consideration (Dobrev, 2006).

2.3.1.2 Multiple processes multiple scales

Often, devices having a complex geometry, which incorporate different scales' features, are difficult or impossible to produce in a given material by employing a single process. In such cases it is necessary to integrate several compatible and at the same time complementary manufacturing technologies into process chains to achieve the necessary FLSI. However when using such process chains, there are integration issues related to achieving the necessary dimensional accuracy of the various functional features produced using multiple machine setups; due to handling, alignment and referencing errors. The most common problem is related to alignment difficulties. Consequently, alignment marks have to be considered at the early stages of component design, whilst also requiring the use of accurate vision and measuring equipment to manufacture the micro- and nano- features on the single component. (Bigot et al., 2011) .

When process chains are employed, the objective is to use each technology integrated in them in its most cost-effective processing window. Thus, another type of integration issue that may

arise is associated with the compatibility of subsequent processes in a given chain. In particular, it mainly involves aspects related to the material properties and the resulting surface integrity after machining by employing different physical phenomena. (Bigot et al., 2011) . Thus utilisation of materials that are compatible with all or the majority of manufacturing processes integrated in such process chains is therefore an important consideration in their design and implementation.

It is also imperative, that a process chain for the manufacturing of multi-scale features should be carefully designed and optimised in order to take into account the constraints of each manufacturing technology and the influence that they can have on previously machined features or subsequent processes in a chain (Bigot et al., 2011) and thus to minimise its overall uncertainty.

As can be observed from the discussion above, there are many important factors and processing constraints that need to be considered when combining and integrating micro- and nano-fabrication technologies into process chains. Furthermore, the wide range of available micro and nano-manufacturing technologies also makes it difficult to select the most appropriate manufacturing route. Therefore, overall, it is really a challenging task to design and implement successfully process chains aiming at FLSI in innovative miniaturised products.

2.4   Process Chains in Micro- and Nano- Manufacturing

As stated earlier, the capabilities of complementary and at the same time compatible manufacturing technologies are usually combined in process chains to produce miniaturised devices incorporating different length scale features. Such process chains can provide the necessary manufacturing solutions for achieving both high throughput and cost-effective

production of micro- and nano-structured parts and devices. So, it is not surprising that the efforts of research groups are focused on designing, validating and implementing process chains that satisfy the specific functional and technical requirements of new emerging multifunctional miniaturised products and thus to create the necessary prerequisites for their scale-up manufacture. (Scholz et al., 2011; Tosello et al., 2008; Velkova et al., 2010; Calaon et al., 2011; Lalev et al., 2009; Velkova et al., 2011) . Nevertheless, despite all these successful implementations, the manufacture of micro products using such process chains is still in its infancy, and thus further research is required to characterize existing process chains, and also to develop new ones for the fabrication of miniaturized multi-material products (Dimov et al., 2012).

2.4.1 Systematic approaches to assess process chains

These underlying requirements prompt the need to look for systematic approaches to assess such process chains at the technology and platform levels. At the technology level, the interfaces between component manufacturing technologies in such process chains should be analyzed in order to assess both their individual and combined capabilities, and also their compatibility and complementarity. While at the platform level, it is important to develop a tool for evaluating the "maturity" of process chains as potential manufacturing platforms for producing miniaturized products. Both types of analysis will also lead to ideas for new process chains, and will represent an objective means for assessing the risks associated with the adoption and implementation of these technologies and the manufacturing platforms underpinned by them. (Brousseau et al., 2009; Dimov et al., 2012) . In addition, the ability to assess the "maturity" of the technologies in process chains will also provide a means for benchmarking them. Such benchmarking could be used for ranking purposes, and therefore could eventually be applied for process chain selection when there are alternative competing solutions for the fabrication of a given micro component.

2.4.2 Material enabled process chains for achieving FLSI

As stated earlier, further research is required to develop new process chains for the fabrication of novel miniaturized multi-material products. In particular there is a need to develop manufacturing routes for achieving high throughput and cost-effective production of micro- and nano-structured components and devices (Dimov et al., 2012). From a product development viewpoint, polymer devices and components are very attractive as they could be mass produced with multi-scale features cost effectively. In particular, thermoplastic polymers together with their respective composites are a very large class of materials with diverse physical and mechanical properties to suit a wide range of applications (Becker and Gärtner, 2008; Heckele and Schomburg, 2004; Mani et al., 2013; Yao, 2011) and also for achieving FLSI in single components. In addition, the cost of the raw materials in most cases is negligibly low while replication technologies, e.g. micro-injection moulding and hot-embossing, are readily available for mass production of polymer components (Becker and Gärtner, 2008; Heckele and Schomburg, 2004; Yao, 2011) . Thus, it is not surprising that the replication route is very attractive for serial manufacture of polymer-based FLSI components. However, the quality and performance of the produced micro-parts is highly dependent on the quality and performance of the respective replication masters (Uriarte et al., 2006) and also the employed replication process. Hence, it is necessary for the FLSI enabling process chains to combine the capabilities of high throughput replication technologies with those for master making. This is a very active research area and there are constant advances in enabling technologies and new ways for combining their capabilities in process chains are emerging. However, further research is necessary to address many challenges in achieving length-scale integration and 3D patterning simultaneously. Especially, it is necessary to address various specific technology integration issues in developing process chains for producing replication masters. As discussed earlier in section 2.3.1.2 , the utilisation of materials that are compatible

with all or the majority of manufacturing processes integrated in such process chains is one important consideration in their design and implementation. In particular, to develop master-making process chains, it is necessary to identify material–process combinations for achieving the targeted features' sizes and surface integrity, and then to combine them with other complementary and compatible processes (Dimov et al., 2012) . The processing constraints of its component micro and nano manufacturing technologies in conjunction with the selection of an appropriate material for the inserts should be considered when designing a process chain to address the requirements of the replication master. This means that the material chosen should have a microstructure with a favourable response to processing both at meso/macro and micro/nano scales. This material enabled concept to process chain development will be discussed in more detail in section 2.6. However, first the various micro and nano manufacturing technologies which can be utilised in FLSI enabling process chains will be discussed in the following section.

2.5   Micro and Nano Manufacturing Technologies

As stated earlier, process chains formed by merging multiscale master making technologies with high throughput replication capabilities are the gateway to the serial manufacture of polymer-based FLSI components. The extent of available micro and nano-manufacturing technologies makes it difficult to design the most appropriate manufacturing route. Therefore, in order to select the proper manufacturing processes and sequence them into reliable, cost effective and high throughput process chains, a thorough knowledge of the constituent processes' capabilities and limitations is necessary (Dimov et al., 2006) . Within this context, this section presents an overview of the main micro- and nano- manufacturing technologies, considered as viable for implementation in master-making manufacturing routes and serial replication of polymer components.

As stated above, a wide range of technologies exists for micro- and nano-manufacturing, and the physical principles implemented in them are also very diverse. Various classification schemes have been proposed to categorise these technologies (Masuzawa, 2000; Madou, 2002; Dimov et al., 2006; Brinksmeier et al., 2001) . The most well-known classification appears to be that proposed by Brinksmeier et al. (2001) which is shown in Fig. 2.1. The authors divided the micromanufacturing processes into two generic technology groups, namely: Micro System Technologies (MST) and Micro Engineering Technologies (MET). MST includes the processes for the manufacture of microelectromechanical systems (MEMS) and micro-opto-electromechanical systems (MOEMS) while MET encompasses the processes for the production of highly precise mechanical components, moulds and microstructured surfaces. The replication processes are assigned a class of their own. The authors also emphasise that there can also be an overlap between the categories. The following review of the various micro- and nano- manufacturing processes is based on this taxonomy.
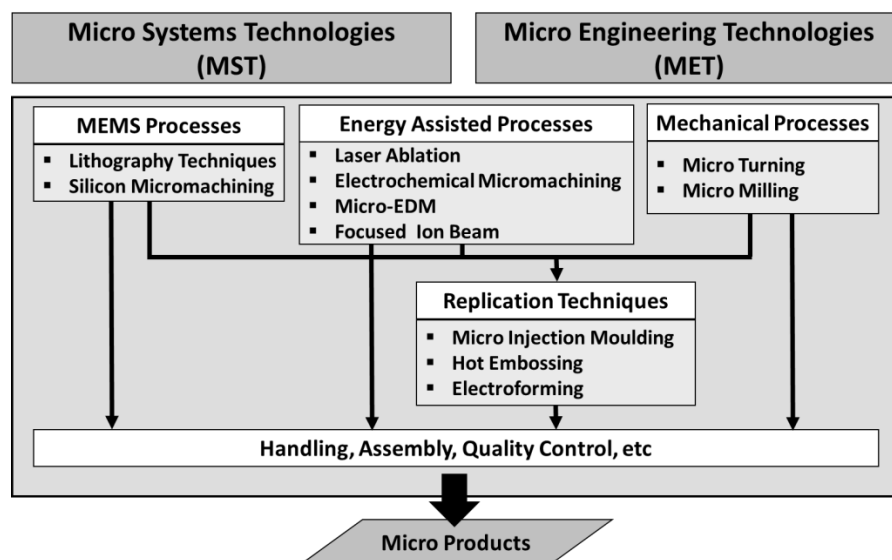
Figure 2.1 Process technologies for micro-manufacturing (adapted from (Brinksmeier et al., 2001)

2.5.1 Micro System Technologies

This review of the MST microfabrication technologies is organised into two sections: (1) silicon layering processes, and (2) the LIGA (German acronym for lithography, electroplating, and moulding) technique.

2.5.1.1 MEMS processes

2.5.1.1.1 Silicon Micromachining Processes

Since, silicon is widely used as the substrate material to produce MEMS, the basic processing technologies are those used to produce integrated circuits (ICs) (Groover, 2007). The manufacturing processes related to the MEMS/MOEMS and microelectronics fields are based on 2D or planar technologies. This implies that components or products are fabricated on or in initially flat wafers. The two general methods used to integrate multiple patterned materials together to fabricate a completed MEMS device, are surface micromachining and bulk micromachining (Jia and Madou, 2006b; Judy, 2001; Alting et al., 2003) . In particular, the surface micromachining technique produces MEMS by depositing, patterning and etching a sequence of thin films, typically 1–100 μm thick, on the silicon substrate. Whereas, in bulk micromachining, the single-crystal silicon substrate, is patterned and shaped to form important functional components of the device. By exploiting the predictable anisotropic etching characteristics of single-crystal silicon, various high-precision complex shapes, such as channels, V-grooves, pyramidal cavities, vias and nozzles, can be formed (Judy, 2001; Groover, 2007; Alting et al., 2003; Cui, 2005; Jia and Madou, 2006b) . The number of different fabrication processes and the derived process variants used in both methods is huge. Therefore the remainder of this section will provide an overview rather than discuss in detail all the specific processes. The sequence of technologies related to silicon machining starts from a prepared wafer. The silicon wafer is cleaned and oxidised and if necessary doped to obtain changed material characteristics. The MEMS devices and integrated circuits are then

formed by creating patterns in the various layers of the wafer. Pattern creation consists of the photographical transfer of the required pattern to a photosensitive film covering the wafer, followed by a chemical or physical process to etch or deposit material in order to produce the pattern. This cycle is then repeated until the desired component has been fabricated. (Alting et al., 2003; Franssila, 2004; Judy, 2001; Jia and Madou, 2006b) .

Ultraviolet (UV) photolithography is the principal process that enables ICs and MEMS to be produced reliably with microscopic dimensions and in high volumes. The technique is used to precisely define the shape of micro machined structures. The process begins by coating a silicon wafer with a UV sensitive polymer called a photoresist. There are two types of photoresist, termed positive and negative. Next, by projecting UV light through a mask, consisting of a transparent supporting medium with precisely patterned opaque regions, a highly detailed shadow is cast onto the photoresist. The regions exposed to the ultraviolet light are chemically altered. After exposure, the photoresist is immersed in a developer solution that removes either the exposed regions (positive process) or the unexposed regions (negative process) (Judy, 2001). Other lithography techniques such as extreme ultraviolet (EUV), electron beam (E-beam) lithography, X-ray lithography, and ion lithography can be used to produce a higher image resolution than conventional UV photolithography. For each technique, specific resist materials are required that react to the particular type of radiation being applied (Groover, 2007; Cui, 2005) .

After the developing process, the wafer is cleaned and dried, and the remaining photoresist can be used as a mask for a subsequent chemical or physical process to etch or deposit material in order to create the pattern. Finally, the photoresist is selectively removed, resulting in the micromachined substrate (Cui, 2005; Judy, 2001; Franssila, 2004; Groover, 2007). The various subsequent chemical or physical processes are shown in Fig 2.2. The specific

sequence of processes to fabricate the completed MEMs device is defined by the designer (Alting et al., 2003) .

Finally, apart from the production of ICs and MEMS devices, some of these well-developed processes have also been used for the fabrication of silicon based replication tools with micro and nano- scale features for thermo-mechanical forming of polymer devices (Henann et al., 2009; Barbero et al., 2007; Giboz et al., 2007; Guo, 2007).

Thin Film Deposition Processes	Etching Processes
Chemical Vapour Deposition	**Wet Etching**
▪ *Low Pressure*	▪ *Anisotropic Wet Etching*
▪ *Atmospheric Pressure*	▪ *Isotropic Wet Etching*
▪ *Plasma Enhanced*	
▪ *Vapour Phase Epitaxy*	**Dry Etching**
	▪ *Vapour Etching*
Physical Vapour Deposition	▪ *Plasma Etching*
▪ *Vacuum Evaporation*	▪ *Reactive Ion Etching*
▪ *Molecular Beam Epitaxy*	▪ *Deep Reactive-Ion Etching*
▪ *Sputtering*	
Electrochemical Deposition	
▪ *Electroplating*	
▪ *Electroless Plating*	
Spin-on Deposition	

Figure 2.2 Thin film deposition and etching processes. (adapted from (Alting et al., 2003)

2.5.1.1.2 LIGA technique

Another manufacturing technique for MEMS is the LIGA process chain (Gad-el-Hak, 2006; Malek and Saile, 2004; Alting et al., 2003; Judy, 2001; Qin, 2010) . LlGA enables the manufacture of structures made of non-silicon materials like plastics, metals and ceramics with almost any kind of lateral geometry and very high aspect ratios (Alting et al., 2003; Malek and Saile, 2004) . The fabrication technique involves a thick layer of X-ray resist , high-energy X-ray radiation exposure through a mask, and development to arrive at a high fidelity resist structure. In most cases, polymethyl methacrylate (PMMA) is used as the resist material. In X-ray-lithography, the almost parallel high energy synchrotron rays enables the fabrication of structures having the following characteristics: depths up to 1000 μm, lateral dimensions down to 0.2 μm, surface quality with Ra 0.3 nm, almost vertical and very smooth side walls, and aspect ratios in the range of 50:1 to 500:1 (Cui, 2005; Jia and Madou, 2006a; Judy, 2001; Alting et al., 2003; Franssila, 2004; Malek and Saile, 2004). If UV light or lasers are used instead of X-rays, lower resolutions and aspect ratios are obtained at a relatively lower cost (Alting et al., 2003).

Some applications require only the tall patterned resist structures themselves, whilst for other applications, the thick resist structures are utilised as plating molds in order to generate metallic microstructures. In particular, material can be quickly deposited into the highly detailed mold by electroplating with different metals like nickel, gold, copper or certain alloys. Subsequently, the resist is dissolved, and freestanding metallic micro structures are left. These metal structures may be the final product or serve as a mould for injection molding or hot embossing (Cui, 2005; Jia and Madou, 2006a; Alting et al., 2003; Giboz et al., 2007; Malek and Saile, 2004; Judy, 2001; Franssila, 2004) .

The most commonly used techniques are the UV and X-ray LIGA while the other variants of this technology, namely, extreme UV LIGA (EUV-LIGA), electron beam LIGA (EB-LIGA)

and ion beam LIGA (IB-LIGA), are considered more efficient however more complex and expensive (Giboz et al., 2007).

2.5.2 Micro Engineering Technologies

2.5.2.1 Mechanical processes

Typical mechanical micro machining methods include micro-drilling, micro-turning, micro-milling, micro-grinding and micro-abrasive jet machining. (Ozel and Thepsonthi, 2011; Rajurkar et al., 2006). Among these technologies, micro-milling is the one most widely applied in the field of master making for microinjection moulding and hot embossing.

2.5.2.1.1 Micromilling

Micromilling (µMilling) is still the most cost effective technology for producing 3D complex micro structures in small batch sizes in a wide range of engineering materials with an acceptable accuracy, precision and surface finish. (Brousseau et al., 2010; Uriarte et al., 2006; Fleischer and Kotschenreuther, 2007; Ozel and Thepsonthi, 2011; Dornfeld et al., 2006; Dhanorker and Ozel, 2008; Filiz et al., 2007; Pham et al., 2009). In order to generate the desired microfeatures, µmilling employs microscale flat-bottom or ball-end-mills, (as small as 10 µm in diameter) at high rotational speeds within high-precision CNC or miniature machine tool platforms. (Filiz et al., 2008). The selection of optimal machining strategies and parameters together with the use of appropriate workpiece materials and monitoring techniques are key factors affecting the µmilling process reliability and performance (Brousseau et al., 2010). The main advantages of µMilling is the possibility of five-axis machining of three-dimensional microstructures that are characterized by high geometric complexity and also the ability to machine tooling grade metals directly, including all kinds of steel up to 62 HRC, and other metals such as Al, Ti, Cu, and brass (Uriarte et al., 2006;

Fleischer and Kotschenreuther, 2007) . In addition, relatively high removal rates can be achieved compared with other micro machining technologies (Fleischer and Kotschenreuther, 2007; Brousseau et al., 2010) and although it is not usually sufficient in most of cases for final part direct manufacturing, it is for tooling production. µMilling is thus a potentially very important component technology in master making process chains. µMilling has been used to manufacture micro-parts for watches, keyhole surgery, housings for microengines, housings and packaging solutions for micro-optical and micro-fluidics and also tooling inserts for microinjection moulding and hot embossing (Brousseau et al., 2010) .

2.5.2.2 Energy assisted processes

Typical energy assisted machining methods are electrochemical micro machining (ECMM) micro-electrical discharge machining (µEDM) , micro-laser machining (µLaser Machining), and Focused Ion Beam (FIB) machining.

2.5.2.2.1 Electrochemical micromachining

In the ECMM process, the shape of the microsized tool electrode is reproduced on the workpiece by a controlled anodic dissolution. The inter-electrode gap size is controlled in the range of a few micrometres and a pulsating power supply is used to produce ultrashort pulses in the order of nanoseconds. The use of such a pulsed current enables the material removal process to be highly localized, thereby allowing submicrometer precision. Furthermore, electrolyte regeneration using microfiltration enables the cleaning of the electrolyte to parts per million levels and can therefore be reused indefinitely. Collectively, these characteristics have made the electrochemical process viable for micromachining applications (Qin, 2010; Joshi and Marla, 2014; Sueptitz et al., 2012) . The ECMM process offers various advantages such as the capability to produce complex 3D shapes, machine structures with high aspect ratios, and to process hard and tough alloys. Other attractive characteristics include excellent

surface finish of the machined surface, burr-free surfaces, no thermal damage, no distortion of the part and no tool wear (Qin, 2010; Joshi and Marla, 2014; Sueptitz et al., 2012). The critical limitation of this technology is its slow machining rate. (Chung et al., 2011) .

A number of variants that are based on the ECMM process described above have also been developed, these include, Microelectrochemical Milling, Electrochemical Drilling for Microholes, and wire-ECMM (Joshi and Marla, 2014; Rajurkar et al., 2006). Apart from the abovementioned process variants, an ECMM mask-based technique can also be employed, which allows complex structures to be easily fabricated with good accuracy. This mask-based technique involves the use of a photo resist pattern that permits selective anodic dissolution along the desired portion of the workpiece (Qin, 2010; Joshi and Marla, 2014; Rajurkar et al., 2006) .

Application areas of the ECMM process include the manufacture of micro nozzles, channels, sensors and actuators in MEMS/NEMS, and also micro molds (Choi et al., 2007).   In addition, various complex internal features such as reverse tapered holes, spherical cavities, internal grooves in microholes and other complex structures have also been fabricated using ECMM techniques (Jo et al., 2009; Yong et al., 2010).

2.5.2.2.2 Micro-electrical discharge machining

μEDM is the process of machining electrically conductive materials by using precisely controlled sparks that occur between an electrode (tool) and a workpiece in the presence of a dielectric fluid (Brousseau et al., 2010; Jahan et al., 2011; Schmidt et al., 2005) . Even though μEDM is based on the same physical principle as conventional EDM, it is not simply an adaptation of the EDM process for machining at the micron level. There are significant differences in the size of the tool used, fabrication method of the micro-sized tools, the power

supply of discharge energy, movement resolution of the axes of the machine tools, gap control and flushing techniques and also in the processing technique (Jahan et al., 2011; Uriarte et al., 2006) . The μEDM process variants are (i) micro-wire EDM (μWEDM), (ii) die sinking micro-EDM (μSEDM), (iii) micro-EDM drilling, (iv) micro-EDM milling and (v) micro-EDM grinding (Brousseau et al., 2010; Fleischer and Kotschenreuther, 2007; Jahan et al., 2011).

The main application areas of μEDM include the manufacture of difficult-to-make features such as fuel injection nozzles and spinnerent holes for synthetic fibres, micro-mechatronic actuator parts; and also tooling inserts for microinjection moulding and hot embossing (Brousseau et al., 2010; Jahan et al., 2011; Fleischer and Kotschenreuther, 2007; Rajurkar et al., 2006; Alting et al., 2003; Kunieda et al., 2005).

One of the principal advantages of the process is its capability to machine hard workpiece materials (Alting et al., 2003) . In addition, the almost negligible machining forces, no burr formation and good repeatability of the process make μEDM very suitable for producing micro-features with high aspect ratios (Pham et al., 2004a; Fleischer and Kotschenreuther, 2007; Cui, 2005). However, there are some specific drawbacks affecting the performance of this process, such as tool/electrode wear, positioning errors, inspection issues and low removal rates (Hansen et al., 2007; Pham et al., 2004a; Fleischer and Kotschenreuther, 2007) . Another drawback is the formation of a recast layer and heat affected zone (HAZ) which affects the properties of the machined surface (Pham et al., 2004a) . In particular, the presence of such a layer and zone may cause problems when the product/ component is in use (Masuzawa, 2000) or for the succeeding processes (Fleischer and Kotschenreuther, 2007) when the component is being fabricated in a process chain. Furthermore, due to the feature sizes and the overall dimensions of micro machined parts, conventional methods such as grinding, or polishing, for recast layer/ HAZ removal and for improving the surface quality of

the µEDMed surfaces are not anymore feasible. All these issues tend to limit µEDM's wider application.

2.5.2.2.3 Micro Laser milling/ ablation

Micro laser milling (also known as micro-laser ablation) involves applying laser energy to remove material through ablation in a layer-by-layer fashion (Pham et al., 2002) . The ablation process causes vaporisation of material due to the interaction between the laser beam and the workpiece. This technology is suitable for machining of a wide range of materials including metals, ceramics, glasses, polymers and semiconductors (Meijer et al., 2002; Ihlemann, 2010) . In particular it is particularly suited for hard materials that are difficult to machine by conventional processes (Dubey and Yadava, 2008; Fleischer and Kotschenreuther, 2007) . This important characteristic is due to the fact that extremely high power can be released within a very short time interval, pulse duration, onto a spot a few micrometres in diameter (Brousseau et al., 2010; Meijer et al., 2002) .

The laser-material interaction and ablation mechanisms are different for pulsed lasers, because of the significantly different pulse durations. In particular, Petkov et al. (2008a) distinguished two main ablation regimes according to the laser pulse length used, namely: ultrashort pulses, femtosecond (fs) and picosecond (ps), and longer pulses, nanosecond (ns) and microsecond (µs). In the former case, the pulse duration is much shorter than the time required to reach thermodynamic equilibrium between the electron system and the atomic lattice; thus, the ablation process can be regarded as a direct solid–vapour transition (sublimation), with negligible thermal conduction into the substrate and almost no heat-affected zone (HAZ). (Petkov et al., 2008a; Cheng et al., 2013; Brown and Arnold, 2010; Fleischer and Kotschenreuther, 2007) . Whilst, in the latter case of the longer pulse lasers, there is enough time for the absorbed energy from the laser pulse to melt the material and a thermal wave to propagate into the material that leads to undesirable effects, such as HAZ,

recast layers, micro-cracks, shock wave surface damage and debris from ejected materials. (Petkov et al., 2008a; Cheng et al., 2013; Brown and Arnold, 2010) . Thus a major advantage of ultrashort laser ablation is its ability to ablate material with a minimal heat affected zone being realised. Furthermore, due to its nature, ultrashort pulse laser ablation is also capable of, precise material removal and thus able to produce accurate small feature sizes, smooth finishing of the surface and flexible structuring (Zheng et al., 2005; Wu and Ozel, 2011; Fleischer and Kotschenreuther, 2007) . All these attractive characteristics make ultrashort pulse laser machining a potentially very important component technology in master making process chains.

Two different methods to pulsed laser ablation/ milling can be applied, namely: (i) direct writing and (ii) mask projection (Gower and Rizvi, 2000; Ihlemann, 2010; Cui, 2005; Stephen and Vollertsen, 2005) . Direct writing is a relatively simple technique and offers great flexibility in the structures that can be produced. However the limitations in the complexity of the features' geometry that can be produced, the small structuring area covered and the fact that it is only suitable for the production of small batches, can be potential drawbacks. On the other hand, the mask projection method is capable of producing many types of structures and is suitable for large batch production. However, the need of a mask makes this technique expensive and time consuming (Alting et al., 2003; Gower and Rizvi, 2000; Cui, 2005; Stephen and Vollertsen, 2005; Meijer et al., 2002) .

Apart from the machining of micro- scale features, laser ablation is increasingly being employed for the processing of advanced materials that cannot be machined by other manufacturing processes and it is also suitable for applications where surface texturing is required (Pham et al., 2002) . In particular, typical application areas, of laser ablation include micro-drilling for microelectronics, micro-lens machining for micro-optics, ablation of micro-actuators, ablation of optical grating structures, machining of microscale features on mold

inserts, machining of microsurgical devices (Pham et al., 2002; Stephen and Vollertsen, 2005; Ihlemann, 2010; Tanaka and Wood, 2010) and surface texturing for tribological and biomedical applications (Fadeeva et al., 2011; Etsion, 2005).

2.5.2.3 Focused ion beam milling

FIB technology has become an important MNM tool and an indispensable technology in semiconductor IC manufacturing and R&D (Tseng, 2004; Cui, 2005; Tseng, 2005; Brousseau et al., 2010; Gierak, 2009; Ali et al., 2010). Two basic working modes, ion beam direct write and ion beam projection have been developed for these applications (Cui, 2005; Tseng, 2004, 2005).   In the direct-write mode, a FIB with a proper beam size, current, and energy is used to remove or add a required amount of material with or without chemical reactions on a predefined location in a controllable manner. In this way, high-precision and complex three-dimensional (3D) micro and nano-structures/ features can be produced (Cui, 2005; Tseng, 2004, 2005).   Whilst for the ion beam projection printing process, a collimated beam of ions passes through a stencil mask to form a pattern that is projected and generated onto the substrate using electromagnetic lens systems. The technology of ion projection printing is also known as ion projection lithography (IPL). It enables the simultaneous production of a large number of devices (Cui, 2005; Tseng, 2004, 2005).

In this research FIB milling has been utilised as a master-making process and thus, in this review, only this direct write approach will be examined further. FIB milling relies on a focused beam of ions which is directed onto the sample. When milling is carried out, the ions sputter atoms from its surface upon hitting the sample. In this way, high precision and complex 3D micro and nano-structures/ features can be created utilising layer-by-layer fabrication methods. The technology enables direct patterning of almost any material with high accuracy and resolution. In particular, it is possible to achieve structures with lateral

dimensions less than 50 nm (Cui, 2005; Tseng, 2004, 2005; Brousseau et al., 2010; Allen et al., 2009; Velkova, 2011; Lalev et al., 2008; Gierak, 2009; Ali et al., 2010).

FIB milling has been improving continuously in terms of processing capabilities and achievable resolution of the patterned structures, particularly in feature lateral dimensions (Gierak, 2009) . In particular, researchers have reported patterning of 2.5D structures like channels/ trenches (Prenitzer et al., 2003; Hopman et al., 2007; Wang et al., 2007a; Ferrara et al., 2014; Velkova et al., 2010) , gratings/ waveguides (Li et al., 2010; Ay et al., 2012) , cantilevers/ beams (Vick et al., 2010) and holes (Kapsa et al., 2004; Hopman et al., 2007) of micron, submicron and nanometer dimensions with relatively low surface roughness (Urbanek et al., 2010) . Furthermore, by implementing layer-based milling combined with specific data preparation techniques, other researchers (Lalev et al., 2009; Svintsov et al., 2009; Velkova et al., 2011) reported the fabrication of 3D microscale structures in fused silica. In addition, using solely FIB, Scholz et al., (Scholz et al., 2011) reported the production of micro lenses in silicon mould inserts and subsequently the machining of nano lenses on their concave surfaces with high shape and positional accuracy.

The FIB milling process's advantages, such as flexibility, high resolution and high surface quality are extremely important for master making (Scholz et al., 2009; Youn et al., 2006) . However, a major limitation of this technology is it's relatively low removal rates (Velkova et al., 2010) which makes it expensive and not feasible to utilise as a stand-alone manufacturing process. Nevertheless, in spite of this disadvantage, there are instances where it is viable to implement FIB within a process chain. In particular, Dimov et al. (Dimov et al., 2006) concluded that although particular component technologies are normally not viable on their own, in specific circumstances their integration with other complementary technologies can lead to the development of novel process chains. The FIB process is an example of this concept (Dimov et al., 2006). More specifically, considering the many advantages this

31

technology has to offer, the FIB process could be employed in novel process chains for fabrication of serial replication tools made from advanced materials, and incorporating micro and nano-scale features. In such a case, FIB milling could be used for fabricating features in the submicron/nano-scale dimensional range on top of micro-features previously produced by employing other technologies.

2.5.3 Replication technologies

Replication technologies can be cost effectively (i) implemented at specific stages within a process chain to suitably structure miniature metallic parts/ components or replication tools and (ii) coupled with master making process chains for serial manufacture of miniature polymer parts (Hansen et al., 2011) . Within this context, an overview of specific processes which can be employed in these two cases is given below.

2.5.3.1 Metal parts / master making based on replication processes

Metallic components and moulds with micro- and nano- scale features can be manufactured by replication processes such as Electroforming and thermoplastic forming (TPF).

2.5.3.1.1 Electroforming

Electroforming is the term used for a replication process involving a master geometry and an electroplated replica. The replica and master may be used as one element or separated for subsequent use. (Hansen et al., 2011; Tang, 2008). Electroplating is used to deposit electroplateable metals using a suitable electrolyte onto the patterned master thus replicating it's geometry. This process requires the master to be electrically conductive and an electrical power supply to deliver the necessary energy. (Tang, 2008) . Due to the nature of the deposition process, the replica is produced ''atom-by-atom'' resulting in an almost perfect copy of the master geometry at virtually all scales. Thus it is possible to replicate complex

shapes accurately and with a good surface finish (Henann et al., 2009; Velkova et al., 2011; Hansen et al., 2011) . It is therefore not surprising that electoforming has been employed in the fabrication of free-standing metallic microstructures (Tang, 2008) and of precision moulds with micro- and nano- scale features (Becker and Gärtner, 2008; Barbero et al., 2007; Ito et al., 2009; Velkova et al., 2011; Azcarate et al., 2006) .

2.5.3.1.2 Thermoplastic forming

Thermoplastic forming (TPF) can be used to fabricate bulk metallic glass (BMG) based miniature components with micro and nano-scale features and is conducted above the glass transition temperature of this material. The BMG softens into a viscous supercooled liquid (SCL) above its glass transition temperature. The fact that the BMG is easily deformable in this state can therefore be used to create a high dimensional accuracy replica of a master having complex geometries at the micro and nano-scales (Schroers, 2010, 2005; Hansen et al., 2011; Kumar et al., 2009a; Henann et al., 2009) . Specific TPF – based fabrication methods suitable for producing micro and nanoscale features on BMG workpieces are blow molding, micro imprinting (HE) and nanoimprinting (Schroers, 2010) . BMGs and the TPF of BMGs will be discussed in more detail in section 2.8

2.5.3.2 Serial replication processes for scale-up manufacture of polymer parts

Replication techniques also allow cost effective manufacturing of polymer parts incorporating features at the micro/sub-micro/nano-scales. Such serial replication technologies include micro-injection moulding (μIM), and hot embossing (HE), together with some of their variations such as compression injection moulding and Roll-to-Roll (R2R) embossing or imprinting (Heckele and Schomburg, 2004; Giboz et al., 2007) . The advantages and disadvantages of these replication processes are discussed next.

2.5.3.2.1 Micro-injection moulding and hot embossing

µIM and HE can be used to produce serially components in any thermoplastic polymer and are considered as the two most important technologies for cost effective scale up manufacture of micro-parts (Giboz et al., 2007; Yao, 2011) . HE is widely used for replicating structures with dimensions in the sub-micron range with high aspect ratios however the cycle times are usually in the range from 5 to 10 minutes. Due to these relatively long cycle times this technology is more suitable for small to medium series production and prototyping (Heckele and Schomburg, 2004; Giboz et al., 2007) . Conversely, the shorter µIM cycle time, which is in the order of seconds, makes it cost effective for high volume production however lead times are much longer, especially to produce the necessary tooling and configure and optimise the process properly. Given that the development of new micro devices is highly dependent on manufacturing systems that can reliably and economically mass produce micro parts, it is clear that µIM represents a more attractive option.

2.5.3.2.2 Compression injection moulding

Compression injection moulding is considered as a hybrid process that combines the capabilities of µIM and HE. This process is widely used in the mass production of CDs, DVDs (Heckele and Schomburg, 2004) and BDs. When comparing it with µIM, the technology offers various advantages when FLSI in replicas has to be achieved because it is a better way to produce different scale features with higher replication quality. This is due to the uniform pressure distribution inside the cavity that is maintained during the compression stage and also because the shrinkage of the polymers can be minimised during the cooling stage (Hansen et al., 2011; Tosello et al., 2010b).

2.5.3.2.3 Roll-to-roll imprinting

Roll-to-roll (R2R) embossing/ imprinting is an established variation of the hot embossing process. R2R embossing has attracted great interest from academia and industry due to its potential for high throughput manufacture of micro/ nano patterned polymer components (Ting et al., 2008; Mäkelä and Haatainen, 2012; Worgull, 2009; Velten et al., 2011; Peng et al., 2014). Using rollers instead of plates, the process is capable of continuous replication of the micro and nano topography on a large substrate area with relatively low cycle times. (Worgull, 2009; Peng et al., 2014; Velten et al., 2010) . Apart from thermal patterning/ structuring of polymers; the R2R embossing technique is also suitable for the structuring of UV-curable materials (Worgull, 2009) . A major difficulty associated with this technology is the structuring of the rollers, particularly at the nano scale (Velkova, 2011) . Nevertheless, this process has been used successfully in the production of microfluidic devices (Yeo et al., 2010) ; optical devices (Mäkelä and Haatainen, 2012; Ting et al., 2008; Chang et al., 2006) and organic electronic devices on flexible substrates (Velkova et al., 2010) .

2.6   BMG Enabled Process Chains for Achieving FLSI

The creation of FLSI replication masters incorporating micro-nano scale structures necessitates the development of cost effective process chains allowing the production of complex 3D shapes in suitable materials, and often using multiple complementary processing technologies. Especially when designing and implementing such master-making process chains, one important consideration is to utilise materials that are compatible with all or the majority of manufacturing processes integrated in them. In particular, it is necessary, to identify material–process combinations for achieving the targeted features' sizes and surface integrity, and then to combine them with other complementary and compatible processes into novel master-making process chains. Thus, the key to successfully apply such a material-

enabled process chain development methodology for achieving FLSI is to first identify suitable candidate materials and processes which can satisfy these requirements.

As discussed in the previous section, the lithography based technologies used in the fabrication of MEMS are able to produce micro and nanoscale structures/ features. However, most of these methods are slow and rather limited in the range of materials which can be processed. Also the MEMS-based methods are typically planar; that is 2.5 D processes that are not capable of fabricating miniature parts that consist of true three-dimensional (3D) features, for example a micro-mold/ insert for injection molding of micro-parts. Moreover, a majority of these processes have long lead times and high costs, and therefore are not economical for small batch size or one-off production. In short, the limitations of the MEMS fabrication methods in terms of cost, lead times, material choices, part / feature shape capability and production run sizes make these processes/ process chains unsuitable for manufacturing of complex miniature parts and replication tools (Dimov et al., 2012; Koc and Ozel, 2011; Bigot et al., 2011; Rajurkar et al., 2006; Uriarte et al., 2006) .

However, as can be observed in Table 2-1, other alternative groups of processes, namely the mechanical and energy assisted processes (e.g. µmilling, µedm, FIB machining, ultra-short pulse laser ablation, etc) could provide the necessary 3D structuring capabilities on a wider range of materials for the fabrication of discrete parts or replication tools incorporating micro and/ or nano-scale features. (Dimov et al., 2012; Koc and Ozel, 2011; Bigot et al., 2011; Rajurkar et al., 2006). Typically, the materials that can be machined by these processes are the same as those used in macro-manufacturing and therefore include an extensive choice of metals, polymers and ceramics and glasses (Dimov et al., 2012; Bigot et al., 2011). However, it is not possible to achieve the required feature resolution and surface quality at all length scales simply by employing "conventional off the shelf" materials (Dimov et al., 2012; Bigot et al., 2011) and therefore "specific materials" are required in order to achieve an optimum

machining response, as was demonstrated in various studies (Popov et al., 2006; Li et al., 2007b; Kettle et al., 2008; Lalev et al., 2009; Quintana et al., 2009) .

Collectively, these investigations show that apart from optimising the specific machining processes (Dimov et al., 2012) , the microstructure and properties of the workpiece material also needs to be controlled / optimised when performing micro/nano structuring in order to achieve high feature resolution and surface integrity. Furthermore, as a consequence, this also means that when developing a process chain and selecting an appropriate workpiece material, it's microstructure should have a favourable response to processing both at the micro and nano scales. In particular, the material microstructure should have specific characteristics, such as being homogeneous and inclusion free at the considered processing scales and thus to minimise uncertainties in micro and nano manufacturing.

Amorphous metallic alloys, in particular Bulk Metallic Glasses (BMGs) possess these characteristics. In particular, taking into account their atomic level homogeneity, these materials can undergo multi-scale patterning successfully (Kawasegi et al., 2006; Loffler et al., 2007) and therefore can be used to design and implement FLSI enabling master-making process chains. Nevertheless, the application of such a BMG-enabled process chain development paradigm still needs to be validated.

Table 2-1 Typical capabilities of various MNM processes --- based on (Azcarate et al., 2006; Uriarte et al., 2006; Fleischer and Kotschenreuther, 2007; Koc and Ozel, 2011; Rajurkar et al., 2006; Velkova et al., 2010; Chung et al., 2011; Joshi and Marla, 2014; Velkova, 2011)**.**

Description	µMilling	ECMM	µWEDM	µSEDM	µLaser Machining	FIB Milling
Minimum Feature Dimension (µm)	50-100	10 -50	20-50	10-50	5	0.005
Feature Shape Constraints (2D/ 2.5 D/ 3D)	3D	3D	2.5D	3D	2.5 D	3D
Accuracy (µm)	3-10	2-8	2	3	1	0.1
Aspect Ratio	2-5	3-10	10-50	3-10	2-50	3
Surface Roughness, Ra (µm)	0.2	0.05-0.4	0.08 – 0.1	0.2 – 0.3	0.3-0.4	0.005
Maximum Structured Area (mm)	100 x 100	20 x 20	200 x 200	200 x 150	200 x 150	0.1 x 0.1
Minimum Tool Size (mm)	< 0.1	0.005-0.05	0.02–0.05	0.05	-	-
Material(s)	Metals/ Polymers/ Ceramics	Conductive materials	Conductive materials	Conductive materials	Almost any material	Almost any material
Material Removal Rate (mm^3/min)	0.02-0.05	6×10^{-6}	0.1	0.01	0.04	5×10^{-10}

2.7   Tooling Requirements and Candidate Tool Materials

When designing mastermaking process chains, it is necessary to utilise materials that not only facilitate the integration of the considered component micro and nano-manufacturing technologies, but at the same time also satisfy the functional and technical requirements of the master. Within this context, a key consideration is that the replication masters have to be robust and capable of producing thousands of parts without any pattern degradations or failures and thus to achieve as high as possible yields. In general terms, the materials used for master making therefore has to satisfy the following requirements: (i) high stiffness; (ii) high strength; (iii) reasonably high fracture toughness; (iv) high surface integrity; (v) good wear and corrosion resistances; (vi) well validated and characterised methods for structuring over a

wide range of length scales and aspect ratios (Henann et al., 2009) and last but not the least (vii) good fatigue properties.

Traditionally a number of different materials have been used for making replication tools with multi scale features for thermo-mechanical forming of polymers. The use of single crystal silicon as a tool material was primarily due to available processing methods, such as deep-reactive-ion etching and wet etching, for making surface patterns on silicon wafers. However, silicon masters are brittle and have a very limited lifespan (Heckele and Schomburg, 2004; Henann et al., 2009; Barbero et al., 2007; Giboz et al., 2007; Guo, 2007) . Electroformed metallic tools such as nickel masters have also been widely used as micro/nano-scale moulds (Becker and Gärtner, 2008; Barbero et al., 2007; Ito et al., 2009; Velkova et al., 2011; Azcarate et al., 2006) due to the dimensional accuracy and excellent surface finish with which the micro and nano scale features can be produced (Henann et al., 2009; Velkova et al., 2011) . Furthermore, such nickel replication tools possess good hardness and wear resistance (Velkova, 2011) . These inserts therefore satisfy most of the abovementioned material requirements; however the electroforming process has several limitations: (i) it is slow and time consuming and thus an expensive process; (ii) it is difficult to produce high-aspect-ratio masters; (iii) electroformed features often fail by delamination from the substrate and (iv) only a limited range of materials can be used for deposition (Heckele and Schomburg, 2004; Henann et al., 2009; Kumar et al., 2009a) . Micro-machined tools from metals such as brass or stainless steel have been widely used, too. They can be produced cost effectively and can withstand a relatively higher number of replication cycles because of their good stiffness, strength, toughness and wear resistance. However, the micro-machining process can be used to produce reliably features with dimensions down to 50 μm only (Becker and Gärtner, 2008; Henann et al., 2009) while any further reduction of feature sizes is limited by the materials' finite grain size (Kumar et al., 2009a) .

BMGs do not have the limitations of these traditional candidate materials for the fabrication of micro and nano-mold tools. Indeed, BMGs, can fulfil the abovementioned requirements for master-making materials and consequently it is not surprising that this group of alloys has recently emerged as a strong candidate for producing replication masters due to their superior mechanical properties and their intrinsic homogeneity down to nanoscale (Kumar et al., 2009a; Kawasegi et al., 2006; Li et al., 2007b; Loffler et al., 2007; Quintana et al., 2009; Browne et al., 2012) .

2.8   Overview of Bulk Metallic Glasses.

The term metallic glass or amorphous alloy describes a class of materials that have no long-range, periodic atomic order (Trexler and Thadhani, 2010) . These amorphous alloys are fabricated through a variety of techniques all of which typically involve rapid solidification from the vapour or liquid phase (Loffler et al., 2007). In particular, the formation of metallic glasses can be realized by solidification of the melt or vapour at cooling rates sufficiently high to suppress the nucleation and growth of crystalline phases (Trexler and Thadhani, 2010; Chen, 2011) .

Bulk metallic glasses are a subset of glass forming multicomponent alloys that can be easily vitrified and formed into fully amorphous sections whose smallest dimensions is at least 1 mm (Schroers, 2010; Schuh et al., 2007) . Due to their chemistry, the amorphous structures of bulk metallic glasses can be realised using moderate cooling rates, e.g. 10 K/s (Chen, 2011; Schroers and Paton, 2006) .

An important feature of BMGs that distinguishes them from general amorphous materials is the glass transition that transforms the supercooled liquids into a glassy state when cooled from high to low temperature and vice versa (Chen, 2011). As will be disclosed in more detail in Section 2.8.2.2, a BMG can be formed in its supercooled liquid region (SCLR) and

this provides a unique processing opportunity to fabricate metallic components/ replication masters incorporating micro and or nano length scale features.

During the last two decades, a wide range of BMG-forming compositions, based on for example, Ti, Cu, Fe, Pd, Zr, Au, and Mg have been developed. These complex multicomponent alloys manifest unique mechanical, thermal and other engineering properties due to their amorphous structures and chemistry. (Schroers, 2010; Schroers et al., 2007b; Schuh et al., 2007; Schroers and Paton, 2006; Suryanarayana and Inoue, 2011). As a result of these unique properties, BMGs are attractive options for use in small-scale devices such as MEMs, biomedical components and masters for injection moulding and hot embossing (Li et al., 2007b; Loffler et al., 2007; Chen, 2011; Schroers et al., 2007a; Zhang et al., 2012a).

2.8.1 Mechanical properties

Apart from the chemistry of the alloy, the amorphous structure defines the mechanical properties of BMGs. In particular, the absence of grain boundaries and dislocations in the amorphous structure of bulk metallic glass results in a homogeneous and isotropic material down to the atomic scale, which displays desirable properties such as very high yield strength, hardness, and corrosion resistance (Trexler and Thadhani, 2010; Schroers et al., 2007b; Kumar et al., 2009a). Furthermore, due to this atomic level homogeneity, BMGs can undergo processing at all length scales down to a few nanometres, and thus they are one of the preferred materials for micro and nano structuring. (Kawasegi et al., 2006; Loffler et al., 2007). Thus bulk metallic glasses are considered as promising candidate materials for producing micro and nano-structured replication masters. (Li et al., 2007b; Quintana et al., 2009; Kumar et al., 2009a).

Two other important characteristics of BMGs are their wear and fatigue properties; however the literature review revealed some contradictory views concerning the effects of introducing

some nano crystallisation on their properties (Greer et al., 2002; Pan et al., 2010; Suryanarayana and Inoue, 2011). In particular, based on these findings, it can be assumed that morphological changes could be controlled to achieve a better wear resistance and fatigue properties whilst simultaneously retaining a satisfactory machining response at the submicron and nano scales. These interesting findings are discussed in more detail in Chapter 5. However at this point it suffices to state that, in spite of the potential advantages such materials can offer in applications such as master making, the literature review revealed that no studies have been carried out to investigate the effects of some partial crystallisation on (i) the robustness of such BMG masters when utilised for serial replication of polymer based FLSI devices and ii) the processing response of BMG workpieces at the micro and nano scales. Both of these issues thus need to be investigated.

2.8.2 Processing techniques for the fabrication of BMG based replication tools/ masters

As stated earlier, BMGs can be used to design and implement FLSI enabling master-making process chains. The key to applying such a BMG-enabled process chain development methodology for achieving FLSI is to identify specific candidate BMG processing methods (i.e. BMG-process combinations) for achieving the targeted features' sizes and surface integrity, and then to combine/ integrate them with other complementary and compatible processes into novel master-making process chains. In order to select the proper BMG processing techniques and sequence them into reliable and cost effective mastermaking process chains, a thorough knowledge of their capabilities and limitations is necessary. Therefore this section will present an overview of the main BMG processing methods considered as viable for implementation in master-making manufacturing routes.

2.8.2.1 Direct casting

Direct casting methods such as suction and die casting have been used as fabrication processes for BMG-based components (Schroers, 2010) . In direct casting of BMGs, fast cooling and forming has to be carried out simultaneously. Thus the process requires a careful balance of the cooling rate to assure satisfactory mold filling while avoiding crystallization during solidification. This can be particularly challenging for components possessing small features (Schroers, 2010; Kumar et al., 2011) and only a careful balance of process parameters has resulted in the fabrication of limited microscale shapes/ features (Zhu et al., 2014; Ishida et al., 2004; Kundig et al., 2003; Nishiyama et al., 2004) .

Furthermore, it has also been reported that casting of BMG based parts incorporating features in the range of 10nm to 10μm is unlikely to be possible due to issues such as (i) the need to fabricate micro/ nano scale featured, high temperature master molds; (ii) the increasing dominance of capillary effects at such small scales, which will resist the liquid alloy flowing into the miniature features; and (iii) the need to be able to separate the cast part from the mold without damaging the miniature features (Browne et al., 2012). In addition, another limitation is that residual internal stresses could reduce the fidelity of the parts produced by the direct casting process (Kumar et al., 2011).

2.8.2.2 Thermoplastic forming technique

Thermoplastic Forming (TPF) is an alternative processing method to direct casting of BMGs, and is unique among metals. In TPF, forming of the part and its subsequent cooling to retain the BMG's amorphous state during solidification are decoupled (Schroers, 2010) .

In particular, as can be observed in Fig 2.3, TPF of a BMG involves heating it into the supercooled liquid region (SCLR) above the glass transition temperature (T_g) of the material but below its crystallization temperature (T_x). In the SCLR , the bulk metallic glass acts as a

highly viscous liquid and can be isothermally formed under an applied pressure to produce intricate micro / nano-scale patterns and subsequently slowly cooled. In this way, features/ structures with complex geometries and a high dimensional accuracy can be successfully produced. The formability is inversely proportional to the viscosity, and therefore increases with increasing temperature. However, BMGs in their supercooled liquid region are metastable and eventually crystallize. This limits the duration the BMGs can be kept at this temperature range, before the onset of crystallisation. The time to reach crystallisation (t_x), is dependent both on the particular alloy being used and the applied processing temperature. Thus, at lower processing temperatures in the SCLR, a longer time is available before the onset of crystallisation, but accompanied by a high viscosity of the BMG. Whilst at higher temperatures, the viscosity of the BMG is significantly lower, but the time available before the onset of crystallisation is shorter. Therefore, the key to successful TPF-based processing is strict control of the temperature and processing time in order to preserve the morphology of the BMG workpiece (Schroers and Paton, 2006; Schroers et al., 2007b; Schroers, 2005, 2010, 2008; Kumar et al., 2011; Henann et al., 2009; Kumar et al., 2009a) .

Suitable TPF – based fabrication methods include: blow molding, micro imprinting (HE) and nanoimprinting. These methods can be used to fabricate BMG components incorporating micro and nano-scale features and structures for various applications, including moulds for subsequent polymer part replication (Kumar et al., 2009a; Henann et al., 2009; Schroers et al., 2007a; Schroers, 2010) .
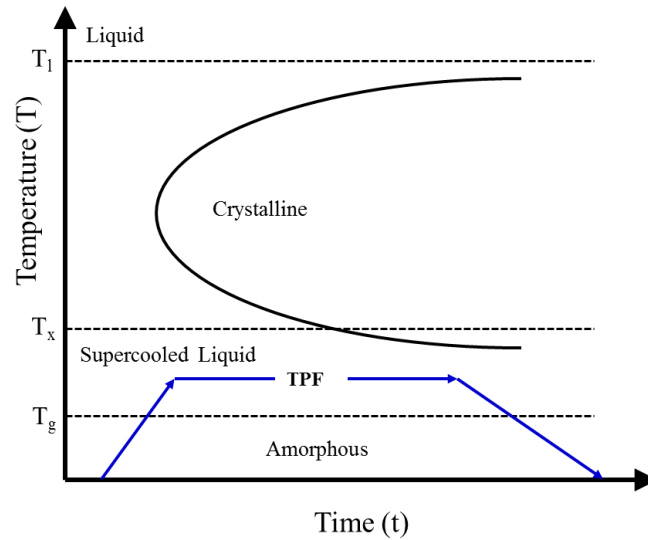
Figure 2.3   A schematic time-temperature-transformation (TTT) diagram for a typical BMG.

The C - shape of the TTT curve is the result of two competition processes of nucleation and growth of new crystalline phase. The nucleation and growth rates are governed by thermodynamic driving force for nucleation defined by degree of undercooling and the movement of atoms defined by atomic mobility, respectively. Hence, at an optimum temperature, both nuclear and growth rates are at maximum values, resulting in a shortest time taken for the transformation of a new crystalline phase.

The diagram denotes the liquid, supercooled liquid, crystalline and amorphous regions. The liquidus, glass transition, and crystallisation temperatures are denoted by T_1, T_g and T_x respectively. The supercooled liquid region (SCLR) is denoted by the temperature interval $Tg < T < Tx$.

2.8.2.3 Direct machining

Direct machining of features onto bulk metallic glass is also a possible manufacturing route for generating components/ replication masters incorporating multiscale features. The following subsections outline some of the direct machining techniques which can be used to structure metallic glasses at the micro and nano-scales.

2.8.2.3.1 Mechanical micromachining

Generally, mechanical machining of BMGs is considered to be expensive due to their high hardness. Furthermore, it is important to note that the literature review has revealed that no studies were conducted on microscale machining of BMGs and only the machining response at the meso- and macro scale, i.e.. by milling, turning and drilling, of Zr- and Pd-based BMGs has been investigated (Bakkal et al., 2005, 2004; Bakkal and Nakşiler, 2009; Fujita et al., 2005) .

2.8.2.3.2 μEDM

Due to the absence of significant machining forces, and it's capability to machine hard and electrically conductive materials, the use of the micro-EDM process to process metallic glasses has also been investigated. In particular, researchers have evaluated the feasibility of using the micro-edm process to drill microholes, and also to machine micro-scale channels and basic 3D microstructures in various BMGs (Yeo et al., 2009; Chen et al., 2008).   The experimental results demonstrated that it is feasible to successfully produce microscale features in the BMG workpieces whilst simultaneously maintaining their amorphous structure. However, the roughness of the surface machined by micro-EDM, tends to be high.

2.8.2.3.3 ECMM

Another technique, namely electrochemical micromachining was also investigated for microstructuring of BMG workpieces. (Sueptitz et al., 2012; Koza et al., 2011) . In both these studies, the production of micro holes in Fe and Zr-based BMGs using a pulsed ECMM technique was demonstrated. However, although pulsed ECMM is a promising method for generating microscale features on BMG surfaces; further research work still needs to be carried out to improve its machining performance (Sueptitz et al., 2012; Koza et al., 2011).

2.8.2.3.4   Laser ablation

Other researchers (Quintana et al., 2009; Lin et al., 2012) have also studied the feasibility of micro-machining BMGs using laser ablation. In summary, these investigations showed that laser processing both with short and ultra-short pulses is a promising technique for cost effective micromachining of Ni- and Mg- based metallic glasses whilst preserving their non-crystalline morphology. Furthermore, another researcher (Chen et al., 2013) also explored the feasibility of surface texturing a Pd-based BMG workpiece using a femtosecond laser This study demonstrated that periodic nanostructures can be patterned on the BMG using a femtosecond laser whilst maintaining its amorphous structure after the laser irradiation process. Thus apart from micro-machining, ultrashort pulse lasers can also be used for surface texturing of bulk metallic glasses.

2.8.2.3.5   FIB

Focused Ion Beam milling allows precise micro, submicron and nano-scale features to be machined on the surface of BMGs (Zhang et al., 2012b; Li et al., 2007b)   with a high level of surface integrity (Li et al., 2007b) .

2.8.2.4 Candidate BMG processing techniques for master-making process chains

Collectively from the discussion above, it can be concluded that TPF, Laser ablation and FIB milling are currently the most promising technologies for micro and nano-scale structuring of metallic glass based workpieces. Consequently these are viable candidate BMG processing methods which can be used to develop master making process chains.

2.8.3 BMG replication tools

BMG based replication tools have been employed for embossing or micro injection moulding or polymer micro components (Henann et al., 2009; Zhang et al., 2012b; Pan et al., 2008; Zhang et al., 2014). However, further studies are required to investigate further their viability as replication tool materials. Furthermore, the literature review has revealed that no studies have been carried out to investigate the viability of using partially crystalline BMGs as a replication tool material, and thus further research is required.

2.9   Factors Affecting the Implementation of Process Chains

When employing a process chain, various factors could lead to an increase in the overall uncertainty associated with the selected manufacturing route. Thus the effective development of a new process chain necessitates that each stage of the manufacturing route be systematically studied in order to:

(i)   identify which are the factors that could compromise the process chain's overall performance.

(ii)   analyse such factors and subsequently identify possible measures for eliminating or reducing their adverse effects and thus minimising the overall uncertainty associated with the process chain's practical implementation.

Based on literature (Velkova et al., 2010, 2011; Tosello and Chiffre, 2004; Joint Committee for Guides in Metrology (JCGM), 2008; United Kingdom Accreditation Service (UKAS), 2007; Hansen et al., 2011) the possible factors affecting the implementation of such process chains can be classified according to the following main sources, namely Process, Equipment, Human and Environment; and are defined in Table 2-2.

Some of these issues are typically specific to the equipment utilised in a given process chain or to the location housing the equipment to implement the given process chain; and therefore only generic issues will be identified in this research.

Table 2-2 Classification of factors affecting the implementation of process chains

Category	Description
Process	These factors are due to the specifics of the process or processes in a given component technology utilised in the process chain and includes the influence of the used parameter settings and also the work-piece's material properties. Such factors could affect the total performance of the technology or cause deviations from the targeted output.
Equipment	These factors are associated with the condition and reliability, of the equipment (both production and inspection) integrated in the process chain, that can affect the particular system setup at different stages, e.g. calibrations and system monitoring during and after the process execution; temperature stability or sensitivity during processing, software used, etc.
Human	These factors are a highly subjective and rather unavoidable source of uncertainty based on the knowledge and experience of the operator; and/or the number of operators involved
Environment	This includes the impact of external factors, e.g. stochastic factors such as noise, oscillations and vibrations, temperature changes, atmospheric conditions, transients in electrical power supply, electromagnetic interference, etc.

2.10 Summary of Open Research Issues

The literature review revealed that the manufacture of micro-products using process chains is still in its infancy, and thus further research is required to characterize existing process chains, and also to develop new ones for the fabrication of novel miniaturized multi-material products. These two underlying requirements prompt the need to look for systematic approaches to assess such process chains at the technology and platform levels. At the technology level, the interfaces between component manufacturing technologies in such process chains should be analyzed in order to assess both their individual and combined capabilities, and also their compatibility and complementarity. While at the platform level, it

is important to develop a tool for evaluating the "maturity" of process chains as potential manufacturing platforms for producing miniaturized products. The combination of these two types of analysis will enable the systematic evaluation of process chains and thus to inform about their further development and design new ones for micro fabrication.

As stated earlier, further research is required to develop new process chains for the fabrication of miniaturized multi-material products. In particular there is a need to develop cost-effective processing capabilities for mass producing polymer-based FLSI devices and components. The demand for mass produced polymer-based FLSI devices and components can be satisfied mainly by the use of replication technologies, such as micro-injection moulding and hot-embossing. Consequently, the quality and performance of micro-parts produced in this way depends on the quality and performance of the respective replication masters. Thus, FLSI enabling process chains should combine the capabilities of novel master-making methods with those of high throughput replication technologies. This is a very active research area and there are constant advances in enabling technologies and new ways for combining their capabilities in process chains are emerging. However, further research is necessary to address many challenges in achieving length-scale integration and 3D patterning simultaneously. Especially, it is necessary to address various specific technology integration issues in developing process chains for producing replication masters. The utilisation of materials that are compatible with all or the majority of manufacturing processes integrated in such process chains is one of important consideration in their development. In particular, it is necessary to identify material–process combinations for achieving the targeted features' sizes and surface integrity, and then to combine them with other complementary and compatible processes into process chains. Thus, when designing a process chain and selecting an appropriate material to address the requirements of the replication master, the processing constraints of its component micro and nano manufacturing technologies should be considered. This means that the

selected material should have a microstructure with a favourable response to processing both at meso/macro and micro/nano scales. To satisfy this requirement, the material should have specific characteristics, such as being homogeneous and inclusion free at the considered processing scales and thus to minimise uncertainties in micro and nano manufacturing.

Amorphous metallic alloys, in particular Bulk Metalic Glasses, are considered promising materials for producing micro and nano- structured replication masters due to their intrinsic homogeneity down to the nanoscale. Due to this atomic level homogeneity, BMGs can undergo multi-scale patterning successfully and therefore can be used to design and implement FLSI enabling master-making process chains. Nevertheless, the viability of such a BMG-enabled process chain development paradigm still needs to be validated.

As already stated, replication technologies are a very important manufacturing solution for serial production of polymer based FLSI devices and components, and the gateway to achieve this is the availability of suitable masters. Consequently the BMG masters produced by master-making process chains need to satisfy specific requirements. Especially, the masters have to be robust and capable of producing thousands of parts without any pattern degradations or failures and thus to achieve as high as possible yields. BMGs can fulfil these requirements and taking into account their intrinsic homogeneity down to nanoscale and unique mechanical and thermal properties they are a very good candidate material for fabricating micro and nano structured replication masters. For such an application, two important characteristics of BMGs are their wear and fatigue properties; however the literature review revealed some contradictory views concerning the effects of introducing some nano crystallisation on their properties. In particular, based on these findings, it can be assumed that morphological changes could be controlled to achieve a better wear resistance and fatigue properties whilst simultaneously retaining a satisfactory machining response at the submicron and nano scales. However the literature review revealed that no studies have been

51

carried to investigate the effects of some partial crystallisation on (i) the wear and fatigue life response of replication masters at micro and nano scale when they are exposed to cyclic thermal and mechanical loads that are typical in the serial replication of polymer based FLSI devices and (ii) the processing response of BMG workpieces when subjected to micro and nano-structuring technologies. Both these issues therefore need to be investigated.

Finally, the open research issues identified for further investigation and discussed here were used to set the research objectives presented in Chapter 1 of this thesis.

CHAPTER 3
TECHNOLOGY MATURITY ASSESSMENT OF MICRO AND NANO MANUFACTURING PROCESSES AND PROCESS CHAINS.

3.1 Introduction

As discussed in chapter 2, there is a need to find a means to assess the 'maturity' of process chains. Therefore, in this chapter, the objective of the research is to develop and validate a systematic approach for assessing the maturity of technologies in the micro and nano manufacturing (MNM) domain. The rest of the chapter is structured as follows. After reviewing a number of maturity assessment techniques, a method for assessing the maturity of MNM processes and process chains is presented. Then, a pilot application of this methodology on a set of MNM processes is described to demonstrate its capabilities. Finally, the results from this pilot application are discussed and conclusions made about the viability of the proposed methodology.

3.2 A Review of Technology Maturity Assessment Approaches.

A popular concept for assessing the maturity of technologies is the Technology Readiness Level (TRL). The TRL concept represents a systematic metric/measurement system that is designed to assess the maturity of a given evolving technology and also to compare the maturity of different technologies (Mankins, 1995) . The assessment is based on a scale from 1 to 9, and generally, if a technology is more developed, the higher is its TRL. The TRL concept and the associated scale were developed over two decades, in particular from mid-1970s to the mid-1990s by the National Aeronautics and Space Administration (NASA) (Mankins, 2002, 2009) . Since their inception, the TRLs have been used within organisations

such as NASA, the United States Department of Defence, the Air Force Research Lab, the European Space Agency and the Turkish defence industry (Altunok and Cakmak, 2010; Mankins, 2002, 2009; Smith, 2005) for measuring the maturity of technologies utilised in military and aerospace systems. In addition, it was proposed to use the TRL concept for monitoring the maturity of emerging technologies (Arman et al., 2006) and also for evaluating the readiness of software products (Smith, 2005) . Recently, Brousseau et al (2009) proposed a methodology inspired by the TRL concept that utilises a common scale composed of seven "maturity phases" for assessing the MNM processes' maturity. This approach was designed to overcome some of the limitations of the TRL concept. Especially, the proposed methodology was developed to simplify the maturity evaluation procedure by combining a large number of inputs from rich and validated knowledge repositories, e.g. in the form of portfolios of R&D projects. Furthermore, Reinhart and Schindler (2010) proposed an approach for evaluating the maturity of a manufacturing technology by combining the technology maturity assessment approach proposed by Brousseau et al (2009) with the technology life cycle concept of Ford & Ryan (1981) . However, these two approaches do not provide a means for assessing the maturity of process chains that integrate more than one constituent manufacturing technology.

Other maturity assessment approaches find their origins in the field of quality management. One of the earliest of these is Crosby's quality management maturity grid (Crosby, 1979) , which was designed to evaluate the status and evolution of an organisation's approach to quality management at five levels of maturity. One of the best-known derivatives from this approach is the capability maturity model (CMM) in software engineering. The software CMM was introduced by Humphrey Watts (1989) and subsequently elaborated further by the Software Engineering Institute (SEI) at Carnegie Mellon University (Paulk et al., 1995). It is a comprehensive model for a continuous software development that describes an evolutionary improvement path for software organizations from an ad hoc, chaotic, and immature process

to a mature and disciplined one. In particular, it classifies processes and organizations into five levels of maturity based on the underlying engineering and management practices that characterize them, namely: (i) Initial, (ii) Repeatable, (iii) Defined, (iv) Managed and (v) Optimized. This SEI CMM has been applied by thousands of organizations (Grant and Pennypacker, 2006) and also has inspired the development of other models that address the specific capabilities required for specialised applications. These multiple models have been consolidated into the Capability Maturity Model Integration (CMMI) approach which is a process improvement maturity model for the development of products and services (Chrissis et al., 2007) . The concepts of process or capability maturity are increasingly being applied to a range of activities, both as a means of assessment and also as part of a framework for improvements. In particular, CMM/CMMI based maturity models were proposed for a diverse range of activities such as assessment of electronic products' reliability, knowledge management, product development collaborations, risk management in complex product development projects and manufacturing engineering, and project management (Berztiss, 2002; Fraser et al., 2003; Hsieh et al., 2009; Ren and Yeo, 2004; Shah et al., 2009; Tiku et al., 2007). However, the existing body of literature reveals that, to date there are no CMM-based maturity models for assessing manufacturing processes and process chains despite the potential benefits that this approach can offer in this domain.

In this context, the focus of this research is to propose and validate a methodology for systematic assessment of the maturity of individual MNM processes and process chains inspired by the CMM approach (Paulk et al., 1995). The proposed methodology can be utilised as a platform for assessing systematically the maturity of both individual micro and nano manufacturing technologies and also their combinations into process chains. Furthermore, the proposed methodology can be used also as a tool for identifying factors

affecting the uncertainty associated with the implementation of MNM processes and process chains in manufacturing platforms and also for defining strategies to manage it.

3.3   Methodology

The proposed methodology represents a combination of top down and bottom up approaches for assessing maturity of technologies/processes as depicted in Fig. 3.1. It is a tool to model the maturity of component technologies and their possible integrations in process pairs and chains. The methodology provides a means to assess such process chains at the technology and platform levels.

At the technology level, the component technologies in process chains are modeled as process pairs as shown in Fig.3.2. The 'process chains', 'individual processes', 'process pairs' and 'technological interface' between individual processes are the four major paradigms of the proposed approach. Each individual process in a pair or a chain executes a specific manufacturing operation and represents a basic "component" technology (e.g. "micro milling") in satisfying the technical requirements of a product. Thus, process chains include a number of process pairs and each pair combines the capabilities of two component technologies, with a specific interface between them. In each process pair, the output of the first process becomes the input of the second one, which creates complex interdependencies that define the so-called technological interface between the component technologies (Denkena et al., 2011, 2006) . By implementing the concept of technological interfaces between two consectutive processes, a link between the processes is established and the effect of their combined set of capability parameters on the performance of a process pair can be modelled and assessed. Thus, at the technology level, the interfaces between component manufacturing technologies in such process chains are systematically analyzed in order to assess both their individual and combined capabilities, and also their compatibility and complementarity. At the same time at the platform level, this modelling approach allows the

"maturity" of process chains to be assessed as potential manufacturing platforms for producing miniaturized products. Finally, the methodology allows informed inputs from MNM process experts to be utilised in assessing the maturity of processes and pairs. A detailed description of the proposed methodology is given in the subsequent sections.
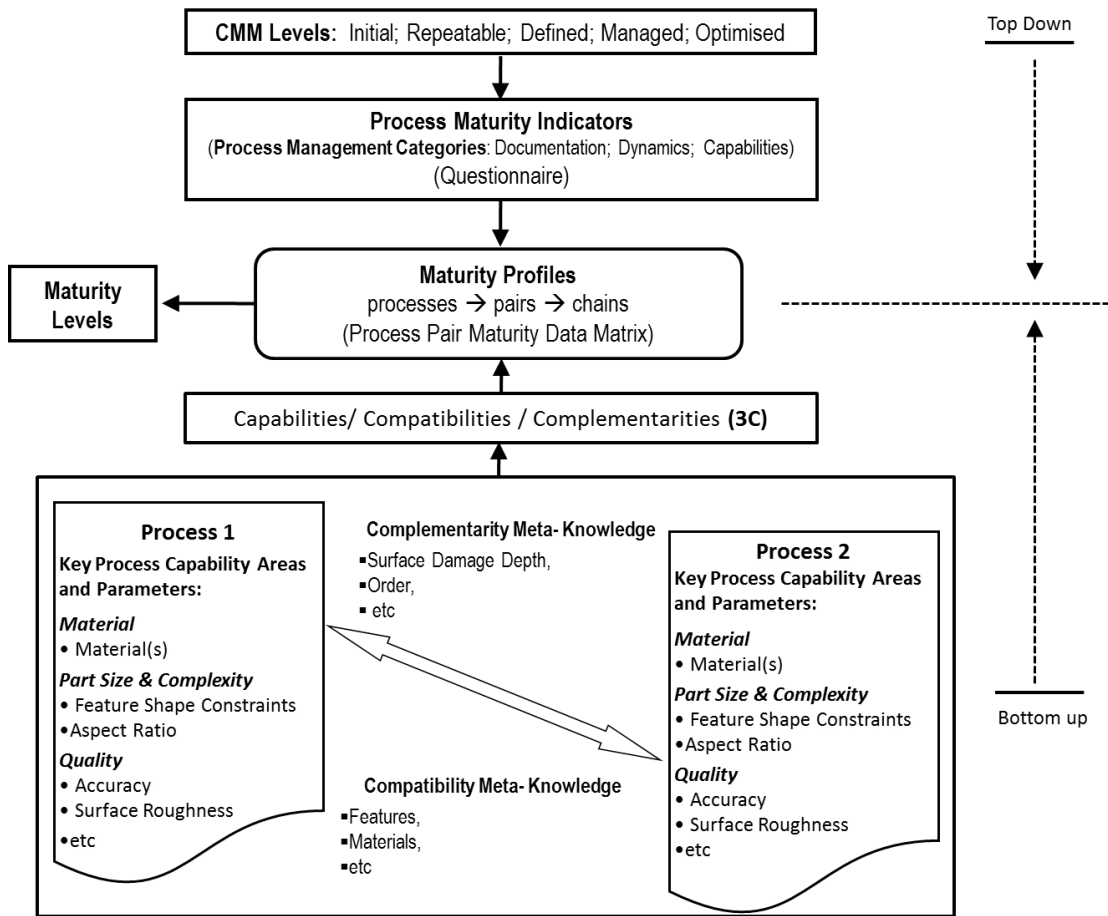
Figure 3.1 Schematic representation of the overall methodology
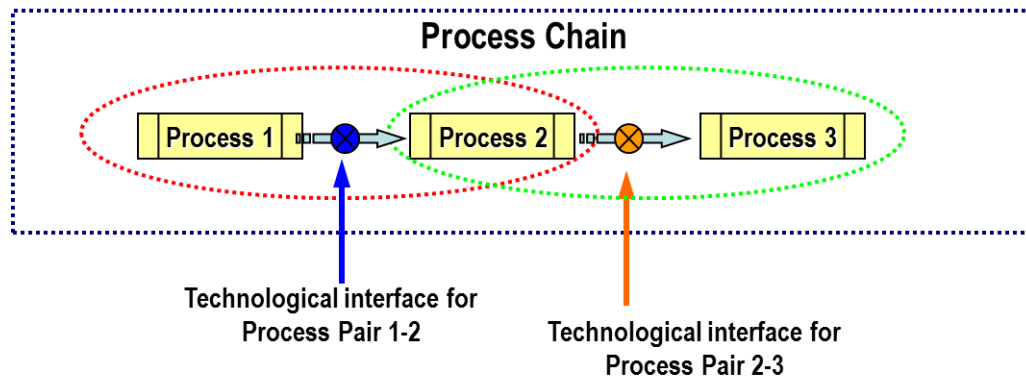
Figure 3.2 Process pairs and process pair technological interfaces

3.3.1 The top down approach

The top down approach for assessing manufacturing processes is based on the CMM in software engineering. Maturity is defined as "a state of being fully grown or developed" (Fraser et al., 2002) . From a manufacturing view point, maturity implies that a process is well understood, documented, and formal training is available while it is consistently applied in practice and is continuously monitored and improved. So, it is possible to state that the performance and the overall behaviour of such a process are highly predictable. Therefore, the maturity assessment of a process or process pair provides a means to estimate the likelihood of achieving particular process outcomes when it is used to fabricate a given part or feature.

This definition of maturity conveys the notion of development from some initial state to some more advanced states as a result of continuous process improvements. Also, implicit in this, is the notion of evolution, suggesting that a manufacturing process or process pair may pass through a number of intermediate states on the way to maturity. Thus, maturity levels are well-defined evolutionary stages towards achieving a mature manufacturing process or process pair. Therefore, the CMM's five level maturity structure was adopted in the proposed methodology. Each maturity level can be scrutinized from abstract summaries down to a more

detailed operational description in the form of Process Maturity Indicators (PMIs) (See Fig 3.1). These are specific indicators which describe typical benchmarking activities, characteristics and performance metrics that a process should achieve or exceed for each maturity level. In addition, PMIs can be associated with process management categories, in particular, documentation, dynamics and capabilities, as they are defined in Table 3-1. An example of a PMI in the context of manufacturing processes is the existence of a good agreement between modelling/simulation results and the actual process performance in a given environment.

Table 3-1 Process management categories

Category	Description
Documentation	This represents the status of the documentation related to a specific manufacturing process. This category describes the type of documentation related activities/ characteristics needed to ensure that the process is established and will endure. Typical documentation items include but are not necessarily limited to scientific papers and internal reports, training material, trade magazine articles, books, guidelines available from equipment manufacturers, standards, procedures, etc.
Dynamics	This defines the level of change related to the capability of a specific manufacturing process. It describes the type of activities and characteristics that lead to changes and improvements in the process performance. For example, are the processing windows for various materials still under development or have they been defined? Obviously in this case, the higher the number of materials with defined processing windows, the higher is the process maturity level.
Capabilities	This defines the level of consistency in achieving the expected outcomes by implementing a specific manufacturing process. It describes the type of activities and characteristics that indicate whether a manufacturing process is consistently achieving the targeted performance and capabilities.

To apply the proposed top down approach it is necessary to identify sets of specific PMIs associated with the three process management categories in Table 3-1. In particular, such sets of PMIs can be identified through brainstorming or Delphi-type workshops with experts in a given manufacturing domain. Then, these sets of PMIs are used to create maturity assessment questionnaires with documentation, dynamics and capabilities subsections that can be used to

obtain expert judgments about the most representative characteristics of processes in any considered manufacturing domain. In particular, the goal of each question in such a survey is to verify whether a specific PMI has been achieved or otherwise and therefore can be used to describe the current process state. Thus, in practice, the maturity level reached by a given process in the top down approach is determined by PMIs characterizing its current state in regards to its overall behaviour, performance and operational environment.

3.3.2 The bottom up approach

In the proposed methodology, the top down approach is complemented by a bottom up approach for assessing component technologies in process chains. More specifically, it is necessary to analyze the compatibility and complementarity of component technologies in such process chains (Brousseau et al., 2010) . In this context, the proposed approach to model the technological interface of a given process pair takes into account the capabilities of its two component technologies, their dependencies and also the overall capabilities of the pair in producing a part with its technical requirements.

To implement the bottom up approach, a new modelling structure (see Fig 3.1) is necessary to represent with sufficient depth the technological interfaces between any two processes. In particular, the structure should store a set of Key Process Capability Parameters (KPCPs) that characterize the component technologies in any process pair. For example in this research 32 KPCPs have been identified as the most important factors in determining the manufacturing capabilities of the MNM processes, namely: (1) positional accuracy; (2) side wall angle; (3) surface roughness; (4) part size; (5) min feature size (channels, ribs & pins); (6) aspect ratio (channels, ribs & pins); (7) minimum feature size (holes); (8) aspect ratio (holes); (9) feature shape constraints; (10) minimum radii; (11) undercuts; (12) metals; (13) polymers; (14) ceramics; (15) glasses; (16) elastomers; (17) composites; (18) cost; (19) removal rate; (20) processing quantity; (21) deposition rate; (22) enabling process or material; (23) surface area

range; (24) burrs/ edge rounding/ debris; (25) surface damage depth; (26) processing directions; (27) direct/ indirect manufacturing ; (28) allowances ; (29) order; (30) manipulation technique; (31) work holding method; and (32) datum requirement . An example of a structure/table to capture these 32 KPCPs is shown in Fig 3.3 where the parameters are grouped under 6 Key Process Capability Areas (KPCAs), namely: Quality & Accuracy; Part Size and Complexity; Material; Efficiency; Processing; and Fixturing & Set-up.

When process pairs are analyzed, in addition to the KPCPs of their component technologies, it is necessary to take into consideration their overall technological capabilities. In the proposed methodology the process pairs' capabilities are referred to as "meta-parameters" due to the combined effects of their two constituent processes in achieving the technical requirements of a given part or product (Dickerhof and Parusel, 2008). In particular, the meta-parameters are additional attributes associated with the process pairs that facilitate the mapping and integration of KPCPs related to the two component technologies in each pair. The values of the meta-parameters are determined by the KPCPs of process pairs, and reflect the level of their compatibility and complementarity. KPCPs and prior experience with the constituent processes in any given pair are used to make a qualitative (expert) judgment about their compatibility and complementarity. In particular, two processes are considered only compatible if they can be combined successfully in a process pair but there is a higher level of overlapping between their capabilities. Thus, the technical requirements of a part or product can be achieved by either of them. For example, if both component technologies in a pair can process the same types of materials and can generate feature sizes within the same length scales, their associated KPCPs are mapped as compatible. Conversely, KPCPs of two processes are mapped as complementary if by using them in a sequence brings added-value or other potential benefits and thus the overall capabilities of a given process pair are enhanced.

For example, the capabilities associated with the achievable "minimum feature sizes" by Pico Second (PS) laser ablation and Focused Ion Beam (FIB) machining are complementary because these two processes can be used for structuring different scale features and thus their associated KPCPs can be mapped as complementary. In particular, the minimum feature sizes achievable with FIB machining are an order of magnitude smaller than those in pico second laser ablation. Thus, it is possible to produce nano scale structures with FIB after the machining of micro scale features with the PS laser, and as a result be able to achieve the so-called length scale integration by pairing these two direct-write technologies. In applying the bottom up approach the compatibility/complementarity meta-parameters of process pairs are created by applying a set of rules. In particular, the left hand side of Table 3-2 depicts the rules which are represented in the form **IF** < KPCP(S) condition/ issue> **AND** < KPCP(S) condition/ issue> **THEN** < KPCP mapping consequence> ; whilst on the right a number provides a cross reference to Table 3-3 for examples of specific applications of the rules. For instance looking at the "part size and complexity" KPCPs sub-set in Table 3-2, the first rule for "minimum feature size" is as follows: if the "minimum feature size" achievable with constituent processes 1 & 2 in a process pair are not of the same order of magnitude, e.g. process 1 has much higher resolution than the follow up process, then this KPCP should be mapped as complementary. So by using this rule to analyze the FIB + PS-Laser process pair, their "minimum feature size (channels, ribs & pins)" KPCPs will be mapped as complementary as their achievable minimum feature sizes are 5nm and 5μm, respectively (See Table 3-3 Example 1). The results of this "meta" analysis of KPCPs associated with process pairs are stored in Process Pair Maturity Matrixes (PPMMs), an example is given in Fig 3.3, that can be used to assess the capability, compatibility and complementarity (3C) of component technologies in process pairs (see Fig. 3.1). Then, these PPMM spreadsheets are required to estimate the maturity levels of process pairs and their constituent process.

The next section presents the five maturity levels considered in the proposed methodology and also how the top down and bottom up approaches described in this section are integrated in a model to assess maturity levels of process pairs and their constituent processes.

Table 3-2 Rules used to perform the "meta" analysis of KPCPs associated with process pairs

Rule Set #	KPCP Description & No.	Rule #	IF P1 KPCP	IF	IF P2 KPCP	AND	THEN Xr	THEN Xb	Example #
1	Positional Accuracy (1); Surface Roughness (3); Part Size (4); Min Feature Size (Channels/ Ribs etc) (5); AR (Channels/ Ribs etc) (6); Min Feature Size (Holes – min dia etc) (7); AR (Holes) (8); Min Radii (10); Cost (18); Material Removal Rate (19), Processing Quantity (20), Deposition Rate (21) Surface Area Range (23)	1.1	V1	>>	V2		X		1
		1.2	V1	<<<	V2		X		
		1.3	V1	≈	V2			X	2
2	Side wall angle (2); Burrs/ Edge Rounding/ Debris (24); Surface Damage Depth (25)	2.1	N	<	N		X		
		2.2	N	<	Y		X		3
		2.3	Y	<	N		X		
		2.4	Y	<	Y			X	4
3	Feature Shape Constraints (9); Processing Directions (1D/ 2D/ 3D) (26)	3.1	V1	>	V2		X		
		3.2	V1	<	V2		X		5
		3.3	V1	o	V2			X	6
4	Undercuts (11); Allowances (28)	4.1	Y	<	Y		X		
		4.2	Y	<	N		X		
		4.4	N	<	N			X	7
		4.4	N	<	Y		X		

Table 3-2 Rules used to perform the "meta" analysis of KPCPs associated with process pairs

Rule Set #	KPCP Description & No.	Rule #	IF			AND	THEN		Example #
			P1 KPCP	<	P2 KPCP		Xr	Xb	
5	Metals (12); Polymers (13); Ceramics (14); Glasses (15); Elastomers (16); Composites (17)	5.1	Y	<	Y	the used processes & material microstructure combination allows satisfactory fabrication of nano / submicron and micro scale features	X		8
		5.2	Y	<	Y	the used processes & material microstructure combination only allows satisfactory fabrication of micro length scale features.		X	9
		5.3	Y	<	N	where process 1 is exclusively used to define the pattern of the structures/ features to be fabricated in material processed by process 2.	X		10
		5.4	N	<	Y	where process 2 is exclusively used to define the pattern of structures/ features to be fabricated in material processed by process 1	X		
		5.5	N	<	N				
6	Enabling Process/ Material (22)	6.1	E	<	E		X		11
		6.2	E	<	Ē		X		
		6.3	Ē	<	Ē			X	
		6.4	Ē	<	E		X		

65

Table 3-2 Rules used to perform the "meta" analysis of KPCPs associated with process pairs

Rule Set #	KPCP Description & No.	Rule #	IF P1 KPCP		P2 KPCP	AND	THEN Xr	Xb	Example #
7	Direct/ Indirect Manufacturing (27)	7.1	D	<	D			X	
		7.2	D	<	ID		X		
		7.3	ID	<	ID			X	
		7.4	ID	<	D		X		12
8	Order (29)	8.1	P1	→|	P2		X		13
		8.2	P1	|↓	P2		X		
		8.3	P1	↕	P2			X	14
9	Manipulation (30)	9.1	H/ NR	<	L		X		
		9.2	L	<	H/ NR		X		
		9.3	NR	<	NR		X		
		9.4	NR	<	H		X		
		9.5	H	<	NR		X		15
		9.6	H	<	H			X	
		9.7	L	<	L			X	
10	Work holding method (31); Datum (32)	10.1	R	<	R			X	16
		10.2	R	<	NR		X		
		10.3	NR	<	R		X		
		10.4	NR	<	NR		X		

Table 3-2 Legend

Generic	Xr = complementary ; Xb = compatibile; V1 = Value of Process 1 (P1) KPCP; V2 = Value of Process 2 (P2) KPCP; ∧ = AND
Rule set 1:	<<< = much worse; or; >>> = much better in comparison to the KPCP of the other process in the pair by at least about one order of magnitude. ≈ = similar / close to the KPCP of the other process in the pair within the same order of magnitude.
Rule set 2:	Y = process generates characteristic N = process does not generate characteristic or minimally generates characteristic.
Rule set 3:	< = worse than; o = same; > = better in comparison to the KPCP of the other process in the pair.
Rule sets 4 & 5:	Y = process generates/ processes/ permits the feature/ material/ characteristic N = process does not generate/ process/ permits the feature/ material/ characteristic
Rule set 6:	∄= No enabling process / material required; ∃= enabling process / material required
Rule set 7:	D = direct manufacturing; ID = indirect manufacturing
Rule set 8:	⇥ = Processing sequence: Process 1 to Process 2; ⇤ = Processing sequence: Process 2 to Process 1; ↔ = Any process sequence
Rule set 9:	L = Low; H = high level in comparison to the KPCP of the other process in the pair. NR = Not required
Rule set 10:	R = Required ; NR = Not required

Table 3-3 Examples of specific applications of the rules

Example #	Description
1	Using this rule to analyse the FIB + PS-Laser process pair, their "minimum feature size (channels, ribs & pins)" KPCPs will be mapped as complementary as their achievable minimum feature sizes are 5nm and 5μm, respectively
2	Using this rule to analyse the Micromilling + PS-Laser process pair, their "surface roughness" KPCPs will be mapped as compatible as their achievable surface roughness values are 0.1μm and 0.3 to 0.4 μm, respectively
3	Using this rule to analyse the Micromilling + PS-Laser process pair, their "surface damage depth" KPCPs will be mapped as complimentary as their values are "No thermal damage" and "20μm depth" ; respectively
4	Using this rule to analyse the Micromilling + PS-Laser process pair, their "Burrs/edge rounding/ debris" KPCPs will be mapped as compatible as both processes generate such defect types.
5	Using this rule to analyse the FIB + Micro injection moulding process pair, their "Processing directions" KPCPs will be mapped as complementary as their processing direction values are 1D and 3D, respectively
6	Using this rule to analyse the Ebeam + DRIE process pair, their "Feature shape constraints" KPCPs will be mapped as compatible as both processes generate 2.5D structures.
7	Using this rule to analyse the Ebeam + DRIE process pair, their "Allowances KPCPs will be mapped as compatible as both processes do not require allowances.
8	Using this rule to analyse the FIB + PS-Laser process pair, their "Glasses" material KPCPs will be mapped as complementary since using both processes, it is possible to satisfactorily machine multi-length scale features on such amorphous materials (e.g. fused silca)
9	Using this rule to analyse the Micromilling + PS-Laser process pair, their "metals" KPCPs will be mapped as compatible as both processes generate single length scale features in crystalline metals (e.g. steel)
10	Using this rule to analyse the X-ray lithography and Electroforming process pair, their "metals" KPCPs will be mapped as complementary as the combination of both processes allows the generation of electroformed metal (e.g. nickel) structures.

Table 3-3 Examples of specific applications of the rules

Example #	Description
11	Using this rule to analyse the Ebeam + DRIE process pair, their "Enabling process or material" KPCPs will be mapped as complementary since both processes require an enabling process. In particular, E beam requires a mask to transfer a geometric pattern onto the "resist," on the substrate. Whilst, the DRIE process requires the patterned resist in order to be able to selectively machine the substrate material. Without these enabling processes/ materials E-beam & DRIE processes cannot be successfully combined together.
12	Using this rule to analyse the X-ray lithography and Electroforming process pair, their "direct/ indirect" KPCPs will be mapped as complementary as first the resist structures/ pattern are fabricated. Then the resist structures are utilised as plating molds. The combination of an indirect & direct process results in the ability to generate metal structures by the electroforming process.
13	Using this rule to analyse a Micro-EDM and Micro-Injection Moulding process pair, their "Order" KPCPs will be mapped as complementary as first the replication tool needs to be structured by EDM before it can be employed in the injection moulding process to fabricate polymer based parts.
14	Using this rule to analyse the Micromilling + PS-Laser process pair, their "Order" KPCPs will be mapped as compatible as no specific process sequence is required.
15	Using this rule to analyse the FIB + HE process pair, their "Manipulation" KPCPs will be mapped as complementary as their manipulation parameters are "5 axes" and "No manipulation required", respectively.
16	Using this rule to analyse the FIB + Micro-Injection Moulding process pair, their "Datum" KPCPs will be mapped as complementary as their parameters are "datum is required" and "No datum is required", respectively.

3C — Maturity Level / Process pair maturity matrix

Key Process Capability Areas	Process 1: FIB — Key Capability Parameters	FIB value	PS Laser value	Process 2: PS Laser — Key Capability Parameters	Key Process Capability Areas
Quality & Accuracy	Positional accuracy	0.1 µm	5µm	Positional accuracy	Quality & Accuracy
	Side wall angle	no	2-5 deg	Side wall angle	
	Surface roughness	5 nm	0.3-0.4 µm	Surface roughness	
Part size and complexity	Size	120 mm	100x100 mm	Size	Part size and complexity
	Min. feature size (Channels, ribs & pins - minimum width)	5 nm	5 µm	Min. feature size (Channels, ribs & pins - minimum width)	
	AR (Channels, ribs & pins)	3:1	5-10:1	AR (Channels, ribs & pins)	
	Min. feature size (Holes - min.dia.)	5 nm	2 µm	Min. feature size (Holes - min.dia.)	
	AR (Holes)	3:1	10:1	AR (Holes)	
	Feature shape constraints 2D/2.5D/3D	3D	3D	Feature shape constraints: 2D/2.5D/3D	
	Min radii	10nm	2 µm	Min radii	
	Undercuts	yes	no	Undercuts	
Material	Metals	yes	yes	Metals	Material
	Polymers	yes	yes	Polymers	
	Ceramics	yes	yes	Ceramics	
	Glasses	yes	yes	Glasses	
	Elastomers	yes	yes	Elastomers	
	Composites	yes	yes	Composites	
Efficiency	Cost	200 £/h	100 £/h	Cost	Efficiency
	Removal rate	0.5 µm^3/min	0.03 mm^3/min	Removal rate	
	Processing Quantity	1	low	Processing Quantity	
	Deposition rate	0.1 µm^3/min	n/a	Deposition rate	
Processing	Enabling process or material	no	no	Enabling process or material	Processing
	Surface area range [mm]	10x10 µm	40x40 µm	Surface area range [mm]	
	Burrs/ edge rounding/ debris	yes – small	yes	Burrs/ edge rounding/ debris	
	Surface damage depth	5 nm	20 µm	Surface damage depth	
	Processing directions (1D/2D/3D)	1D	1D	Processing directions (1D/2D/3D)	
	Direct/indirect manufacturing	direct	direct	Direct/indirect manufacturing	
	Allowances	no	yes	Allowances	
	Order	essential	essential	Order	
Fixturing & set-up	Manipulation	5 axes 102X102X43	5 axes 600x400x250	Manipulation	Fixturing & set-up
	Work holding method	clamps	yes	Work holding method	
	Datum	required	required	Datum	

Figure 3.3 Process pair maturity matrix

3.3.3 Model design

3.3.3.1 Maturity levels.

As stated earlier, maturity levels (MLs) are well-defined evolutionary stages towards achieving mature manufacturing processes or process pairs. The five maturity levels considered in the proposed methodology are provided in Table 3-4. Each level represents a stage in the development and the implementation of any given process pair or its constituent processes.

Table 3-4 Process capability maturity levels

Levels		Description
Initial	**1**	*Introduction of a new process*. Undocumented and dynamically changing. Initial (chaotic, ad hoc) utilization of a new process.
Repeatable	**2**	*A process with a predictable behaviour*. Consistent and repeatable results are achievable if rigorous discipline is applied. The process is used repeatedly with predictable results.
Defined	**3**	*Standard Process.* Subject to improvements. Defined (institutionalized) process. A process approved for given applications or product requirements.
Managed	**4**	*Validated process with a broad usage*. Adaptable to given needs/requirements. Validated process capabilities. Quantified process management and established measurement practices.
Optimized	**5**	*Process with high predictability and performance.* Incremental innovative changes. Defined improvement objectives. Optimized management practices. Planned and well managed process optimization/ improvements.

3.3.3.2 Integration of top down and bottom up approaches

As can be seen in Fig 3.1, the top down and bottom up approaches are applied simultaneously to carry out expert- and KPCP-based assessments of the maturity levels of processes and

process pairs. Fig 3.4 illustrates the four steps required to perform these maturity level assessments.

Step 1: Using output from the questionnaire, generate maturity profiles for processes 1 & 2 across the 6 KPCA in the context of the process management categories →

Process Management Categories Maturity Profiles
1. Quality & Accuracy;
2. Part Size and Complexity;
3. Material;
4. Efficiency;
5. Processing;
6. Fixturing & Set-up

Step 2: Establish overall maturity levels of constituent processes 1 & 2 →

Individual Processes MLs
1. Initial
2. Repeatable
3. Defined
4. Managed
5. Optimised

Step 3: Evaluation of pair 1-2 Complimentarity and Compatibity Scores (Cr & Cb) →

3C Evaluation of Pair 1-2 Interface:
• Capability
• Complementarity
• Compatibility

Step 4: Evaluate overall maturity level of process pair 1-2 →

Process Pair ML:
$ML_{1-2} = f(PML_1, PML_2, \lvert PML_1 - PML_2 \rvert, Cr, Cb)$

Figure 3.4 Individual process and process pair maturity level assessment

The maturity assessment of constituent processes in pairs is carried out in Steps 1 and 2. As discussed earlier, in practice, the maturity level reached by a given process is determined based on experts' judgments through structured questionnaires employing key indicators for each level in the process evolution. The outputs of the questionnaires allow the processes to be positioned objectively on the maturity scale irrespective of their applications. Each 'yes' or 'no' answer given to the maturity assessment questions relates to a specific maturity indicator and thus to determine MLs of the associated KPCAs and process management

categories. For example, an indicator within the "Capabilities" process management category for the maturity of the "Part Size & Complexity", "Material" and "Processing" KPCAs could be the existence of a correlation between modeling/simulation results and actual process performance in a given environment. This approach allows not only the overall maturity of a process to be assessed but also that of its KPCAs and Process Management Categories. The practical implementation of this maturity assessment methodology for a single MNM process is illustrated in Fig 3.5

Next, steps 3 and 4 in Fig 3.4 involve the maturity assessment of process pairs. The ML of a process pair is dependent on ML of its constituent processes, and also it depends on their compatibility and complementarity. Thus, the assessment should reflect the maturity of both technologies in a pair, and accounts for the pair's meta-parameters. The objective is to define a measure to estimate the likelihood of achieving a particular outcome when the pair is used to fabricate a part or a set of features. Such a measure should take into account various factors affecting the Process Pair Maturity Level (PP_ML), in particular: the maturity level of the 1st constituent process (PML_1), the maturity level of the 2nd process (PML_2) and also their complementarity (C_r) and compatibility (C_b).

Indicators (Questionnaire)

Capabilities

Dynamics

Documentation

		Yes	No
1	Are there numerous case studies of commercial implementations of the process?		
2	Are there any standards (national or international) applicable to the process execution or performance?		
3	Do the process equipment manufacturers provide adequate processing manuals and/or instructions?		x
4	Are there numerous scientific (journal, conference) publications and seminars on the process currently		x
5	Are you aware of any reports or surveys on the process performance and capabilities conducted by pro		x
6	Is formal approval needed (e.g. from the equipment producers or menagers) for chaging some process	x	
7	Are there any standard operational procedures?		x
8	Is the process compatible with standard data handling software?		x
9	Does the process require a conversion of standard data files to specific data formats?		x
10	Are there established means for documenting the process in the company's data management system?		x
11	Are there well accepted Design for Manufacture guidelines/rules?	x	
12	Are there many publications available on processing windows for new materials and new applications?		x
13	Are the pocess parameters well described and documented?		x
14	Are there training programmes in place?		x
15	Is the process composed by universal (unified) procedures or steps?	x	

(additional marks: x, x, x, x, x)

Scoring the CMM level

Capabilities

Dynamics

Documentation

INITIAL	REPEATABLE	DEFINED	MANAGED	OPTIMISED
1	1	0	0	0
1	1	1	0	0
1	0	0	0	0
1	1	1	0	0
1	1	0	0	0
1	1	1	0	0
1	1	1	0	0
0	0	1	1	1
0	0	1	1	1
1	1	0	0	0
1	1	0	0	0
0	0	0	0	1
1	1	0	0	0
0	0	0	1	1
1	1	1	1	0
1	1	1	0	0
1	1	1	1	0
0	0	1	1	1

Assessing the key process capability areas

Capabilities

Dynamics

Documentation

Quality & Accuracy	Size & Complexity	Material	Efficiency	Processing	Fixturing & Set-up
			1.5		
2					
	1			1	
2	2	2	2	2	2
1.5	1.5			2	2
2	2	2	2	2	
			2	2	
				4	
4				4	4
	1.5	1.5			1.5
		1.5		1.5	
		5		5	
1.5	1.5	1.5	1.5	1.5	1.5
4.5	4.5	4.5	4.5	4.5	4.5
2.5	2.5	2.5	2.5	2.5	2.5
2					
2.5	2.5	2.5	2.5	2.5	2.5
4	4	4	4	4	4
CMM Level = 2	2	2	2	3	3

CMM profiles of the processes

Mature

Non-mature

Semi-symmetrical

Quality & Accuracy
Fixturing & set-up
Part size and complexity
Processing
Material
Efficiency

1: Initial
2: Repeatable
3: Defined
4: Managed
5: Optimised

Figure 3.5 The methodology for the maturity level evaluation of a single MNM process

C_b is used as an overall metric to assess the input-output compatibility of two processes when they can be combined in a pair and estimates any 'value-added' functional or economic advantages. Thus, if two processes are entirely compatible, they would be just alternative or competing technologies and hence they can have even negative effects on a process chain because without gains leads to increased complexity, higher cost and a likelihood for reliability issues. C_b can be estimated using the following formula:

$$C_b = \sum X_b \qquad (1)$$

where $\Sigma(X_b)$ is the sum of the KPCPs mapped as compatible (meta-parameters) within the overall KPCP set consisting of N capability parameters.

At the same time, C_r of a process pair is a metric for assessing whether by combining two processes, 'value-added' (or synergetic) functional or economic benefits can be gained. Thus, it is an overall measure of the perceived complementarity of two processes in enhancing each other's capabilities. A simple formula for estimating C_r should take into account the whole set of KPCPs (X_r) mapped as complementary (meta-parameters), in particular:

$$C_r = \sum X_r \qquad (2)$$

The methodology was implemented into an excel-based PPMM model. By applying it not only the PP_MLs can be obtained but also the maturity profile across the 6 KPCAs in the context of the Documentation, Dynamics, and Capabilities can be analysed. The pilot application of this model on a set of MNM processes is presented and discussed in the following sections.

3.4   Pilot Implementation

As highlighted earlier, to implement the proposed methodology first it is necessary to identify generic indicators that can be used to characterize the current state of a given manufacturing

process, preferably in the context of the targeted MNM domain. In the proposed modeling approach, expert judgments obtained through a Delphi-type workshop are used to identify them. Then, these indicators are utilized to develop a questionnaire for characterizing and positioning the MNM processes along the adopted maturity scale. The proposed modeling approach was applied to assess the maturity of 10 different state-of-the-art MNM processes integrated within an European Infrastructure program, EUMINAfab (Kautt et al., 2009). The processes considered in this study could be clustered into 4 groups, namely micro and nano patterning, thin film deposition, replication and characterization technologies.

3.4.1 Identification of process maturity indicators and questionnaire design

To identify the process maturity indicators, a workshop was organized that brought together more than 40 MNM experts (See Appendix D for the details of the technology experts who provided the necessary information for the maturity assessment of the individual processes and process pairs reported in this research work) in all four process groups. There were three main steps in defining the questionnaire.

(i) *Identification & Classification of Process Maturity Indicators.* The maturity assessment methodology was presented at the workshop and its objectives was discussed and agreed with the experts. Then, the experts were split in two parallel groups with one moderator each to discuss and then come up with generic indicators in the context of their specific technology areas. The discussion that proceeded was very important in order for the experts to understand what kind of process characteristics could be used as indicators in the context of the whole set of considered MNM technologies and their various possible maturity levels. Then, the participants were asked to provide a set of such generic indicators that were both informative about the current state of a given process and also meaningful across the various considered MNM processes. For

example, one of the key indicators identified by the experts to characterize a given process as 'Managed' (ML 4) was "process yield > 80%".

(ii) Semantic clustering of the process maturity indicators. To be able first to group the indicators and subsequently the structured questionnaire, the experts were asked in a follow-up session to discuss the previously identified indicators and then to group them under the adopted three Common Process Management Categories, 'Documentation', 'Dynamics' and 'Capabilities', while considering their relevance to each of the five MLs along the proposed maturity scale . In particular, for the example given above, the key indicator "process yield > 80%" was classified under the 'Capabilities' category whilst being indicative of ML 4.

(iii) *Development of a Maturity Assessment Questionnaire*. Finally, the identified indicators were used to design the questionnaire and the questions were grouped under the 'Documentation', 'Dynamics' and 'Capabilities' categories as shown in Table 3-5. In addition, as the indicators were also classified along the considered 5 MLs, each question can be used to position the MNM processes, along the adopted maturity scale. When completing the developed questionnaire, the experts have to give a binary answer to each question, and thus the necessary information can be derived for assessing MLs of a given MNM process. Then, the PML for a given MNM process can be obtained by averaging the individual MLs associated with each KPCA under the three semantic categories (Documentation, Dynamics, and Capabilities). Face-to-face type interviews were the preferred mode to complete the questionnaire for the following reasons:

- Some of the questions included complex concepts, which could be difficult to interpret consistently through a self-administered questionnaire (Salant and Dillman, 1994) ;

- The facilitators were able to assess how respondents reacted to the questionnaire and if necessary, they could clarify or explain the meaning of particular questions in order to obtain more accurate and representative responses.

Table 3-5 Questionnaire, subdivided into the three process management categories

Documentation	Dynamics	Capabilities
1. Are there numerous case studies of commercial implementations of the process?	19. Is the process a dynamically changing or an ad-hoc one?	39. Are the process capabilities studied and optimized for structuring various materials?
2. Are there any standards (national /international) applicable to the process execution or performance?	20. Is the process utilized predominantly in laboratory environment (e.g. proof of concept)?	40. Has an analysis to determine process yield and capability (6s, Cp, Cpk, Cm) been performed?
3. Do the process equipment manufacturers provide adequate processing manuals and/or instructions?	21. Are the effects of individual process parameters on its performance still under investigation?	41. Is the commercial impact of the process (revenue generation and/or functionality) studied and known?
4. Are there numerous scientific publications and seminars on the process currently available?	22. Do you consider the process outcomes repeatable in terms of accuracy, throughput yield, surface integrity, etc.?	42. Is the process supported by in-line/in-situ measurement system?
5. Are you aware of any reports or surveys on the process performance and capabilities conducted by professional bodies/organizations?	23. Are the process' characteristics, including the measurable ones, defined and evaluated?	43. Does the process deliver predictable and consistent results at different locations?
6. Is formal approval needed (e.g. from the equipment producers or managers) for changing some process procedures?	24. Are gauge studies performed to understand and minimize the source of measurement errors or process uncertainty?	44. Are the effects of individual process parameters on quality characteristics known?
7. Are there any standard operational procedures?	25. Is the process easily adaptable to particular needs or requirements?	45. Does the process deliver products of acceptable and consistent quality?
8. Is the process compatible with standard data handling software?	26. Do some application specific implementations of the process exist?	46. Do you think that we are at the early stages of establishing the process capabilities (positive trends in the process development)?
9. Does the process require a conversion of standard data files to specific data formats?	27. Is the process already well automated?	47. Does the process deliver products of good quality conforming to specified standards and requirements?
10. Are there established means for documenting the process in the company's data management system?	28. Are the objectives for process improvement / optimization well defined?	48. Are the process outcomes predictable if rigorous discipline is applied?
11. Are there well accepted Design for Manufacture guidelines/rules?	29. Are there continuous process performance improvements through both incremental and innovative technological changes achievable by applying scientific approaches?	49. Is the work-product/production-run known quantitatively?
12. Are there many publications available on processing windows for new materials and new applications?	30. Are the processing windows for various materials still under development?	50. Does the process deliver precise but still not accurate results due to systematic errors?
13. Are the process parameters well described and documented?	31. Is the process performance/ capabilities dependent on the operator's skills/knowledge?	51. Does the process show significant improvement in the yield and capabilities (6s, Cp, Cpk, Cm)?
14. Are there training programmes in place?	32. Is the process universal (unified) and are there more than one/two suppliers/producers of the equipment for the process?	52. Do you consider that analytical modeling/ simulation of the process exists but is not accurately reflecting the actual performance?
15. Is the process composed by universal (unified) procedures or steps?	33. Is the technology commercialized predominantly by technology providers?	53. Do you consider that only relatively accurate correlation between analytical modeling/ simulation and actual process performance is already achieved?
16. Is the process adequately taught at Universities /colleges?	34. Is there high financial (investment) risk associated with the implementation of the process?	54. Are there well accepted and accurate analytical models for simulating the process?
17. Are there established process auditing procedures for quality management purposes?	35. Are there substantial R&D efforts for developing new application areas for the process?	55. Is the performance of the process optimized to meet current & future business needs?
18. Are there only feasibility and/or case studies published on the process capabilities (systematic studies are not available)?	36. Is the equipment downtime relatively low?	
	37. Is this "Off the shelf" technology?	
	38. Does the process reach the maximum of its potential commercial impact in terms of revenue generation and/or functionality?	

3.4.2 Assessment of maturity levels

The proposed methodology was applied also to analyze a set of process pairs that potentially can constitute the building blocks of various process chains. In particular, a maturity assessment of the following eight process pairs and their constituent processes was carried out:

- UV Laser and Projection Mask-Less Ion Beam Patterning (PMLIBP) (Platzgummer et al., 2008) ;

- Focused Ion Beam (FIB) and Pico Second (PS) Laser ablation;

- E-beam Lithography and Deep Reactive Ion Etching (DRIE);

- Micro Milling (µMilling) and PS Laser ablation (PS Laser);

- X-ray lithography and Electroforming;

- FIB and Hot Embossing (HE);

- FIB and Micro-injection Moulding (µIM);

- µMilling and HE.

The individual state-of-the-art MNM processes included in these eight pairs are considered viable technologies within the EUMINAfab infrastructure. Furthermore, based on the discussion in the literature review chapter, some of these eight pairs are considered viable combinations of technologies within both existing and potential new process chains. To assess the maturity levels of these pairs, experts in respective component technologies were asked:

- to complete the Maturity Assessment Questionnaire for the component processes in these pairs, and also

- to provide the required data to complete the PPMMs for the considered process pairs.

In this way the required data was collected to assess MLs of the considered process pairs. It should be stated that the representativeness of such an analysis is highly dependent on the experts' "unbiased" knowledge of the constituent processes in the pairs.

The first step in implementing the methodology was to generate maturity profiles of the constituent processes across the defined KPCAs based on the collected data and thus to create "snap shots" of their current state of development. Next, the PP_ML of each pair was estimated taking into account the factors affecting it as discussed in Section 3.3.3.2. In particular, the maturity level of a process pair (PP_ML(1,2)) could be assessed by accounting for the MLs of its constituent processes (PML_1 and PML_2) and meta-parameters (C_r and C_b). The assessment model is based on the rationale that, the PP_ML increases when:

- the difference in maturity levels ($PML_1 - PML_2$) decreases and is as low as possible;

- the individual maturity levels, PML_1 and PML_2, increase and are as high as possible;

- C_r increases and is as high as possible;

- C_b increases but with a marginal/lower impact in comparison to C_r.

In this pilot implementation, after discussing above interdependences with experts the following formula was adopted:

$$PP\_ML_{(1, 2)} = \frac{1}{6} \left[\sum_{KPCA=1}^{6} \frac{\min(PML_1; PML_2)}{1 + |PML_1 - PML_2|} * C_{cw} \right] \qquad (3)$$

where C_{cw} is the normalised combined complementarity and compatibility weighted score for the respective KPCA. C_{cw} should take into account that a higher C_b means that the two processes in a pair while compatible have a marginal added value. For example, the processes can be considered alternative or competing technologies, and thus one of them could be omitted to reduce the complexity of a process chain and thus the risk and costs associated

with its implementation. At the same time C_r should have a higher impact on C_{cw} because by combining two complementary processes a higher 'value-added' can be gained in a functional and/or economic sense. Therefore, the impact of C_b is marginalized by using the mth root of C_b in the formula for computing C_{cw} while the score increases linearly with the increase of C_r. In this pilot implementation m was set to 10 and thus C_{cw} can increase up to 27% with the increase only of C_b while the impact of C_r on C_{cw} cannot be less than 73% when all KPCPs are mapped as complementary. In particular, the formula for C_{cw} used in this study is as follows:

$$C_{cw} = \frac{C_r + \sqrt[10]{C_b}}{N + \sqrt[10]{N}} \qquad (4)$$

where, C_b is the sum of the KPCPs mapped as compatible and C_r is the sum of the KPCPs mapped as complimentary, within the respective KPCA consisting of an overall KPCP set of N capability parameters.

Based on the obtained PMLs and PP_ML values, the pairs and their constituent processes were positioned along a normalized scale, from 0 to 100%, covering all five maturity levels: (1) Initial, 0 to 20%; (2) Repeatable, 20 to 40%; (3) Defined, 40 to 60%; (4) Managed, 60 to 80%; (5) Optimized, 80 to 100%. Based on this ML assessment, it was possible to conduct:

- a comparison of MLs of the processes in regards to the three process management categories;

- a comparison of MLs of constituent processes in the pairs in regards to their KPCAs;

- the identification of strengths and weaknesses associated with the process pairs taking into account the current state of their constituent processes;

- an assessment of the complementarity and compatibility of technologies with regards

to their respective KPCAs.

3.5   Discussion of Results

MLs of the process pairs and their constituent processes considered in this pilot implementation of the methodology are reported and discussed hereunder to illustrate its analytical potential. Fig. 3.6 presents MLs of the analysed component technologies across the three process management categories. Then, figures 3.7 to 3.14 below present the overall MLs and the ML profiles across the six KPCAs for the considered pairs and their constituent processes.
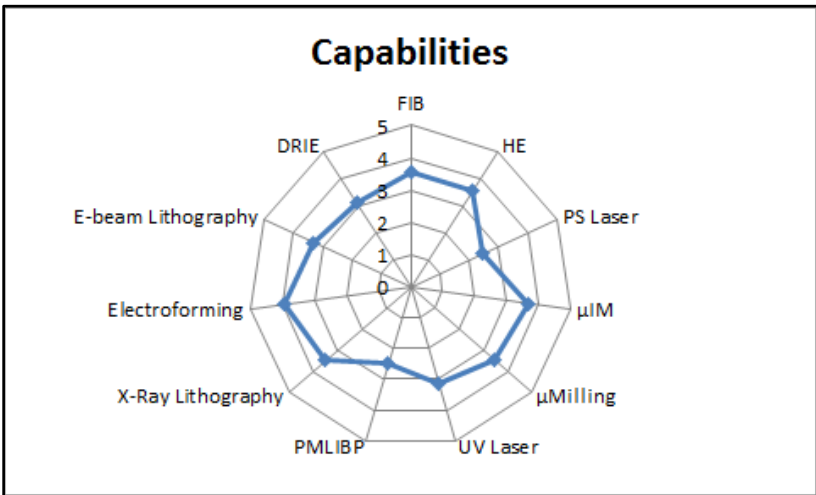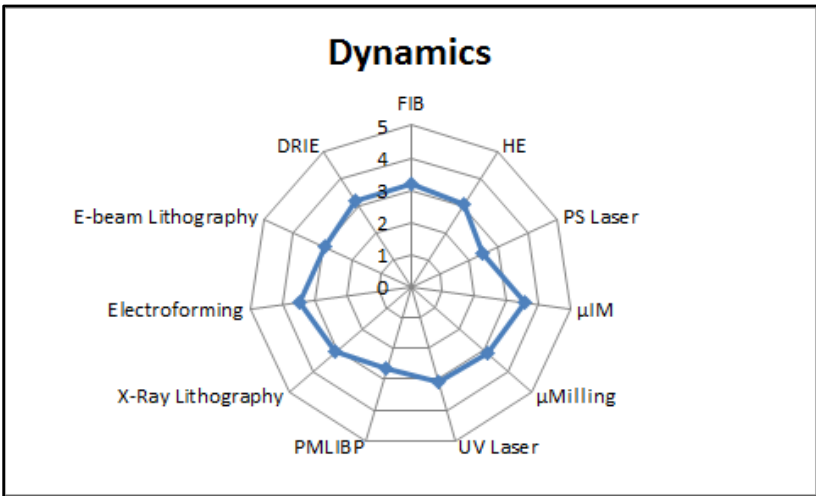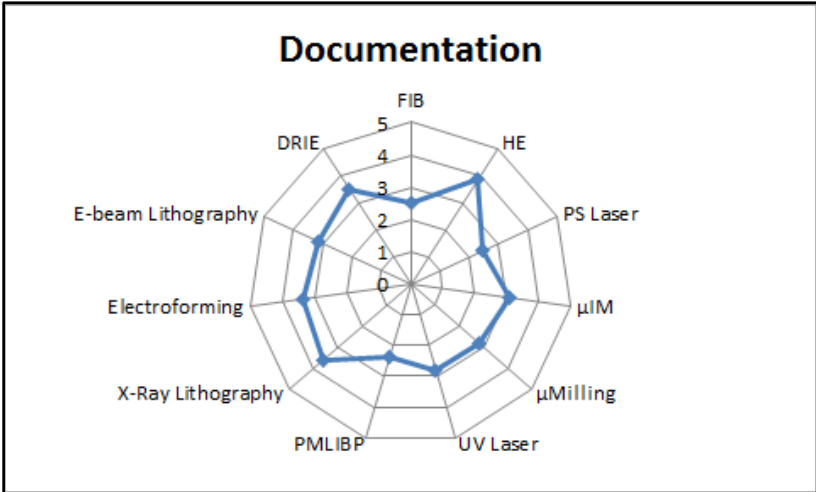
Figure 3.6 Maturity levels of component technologies across the three process management categories
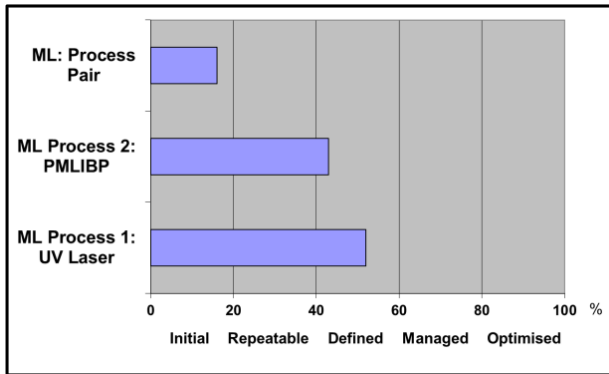
a) Overall MLs of the pair and its constituent processes
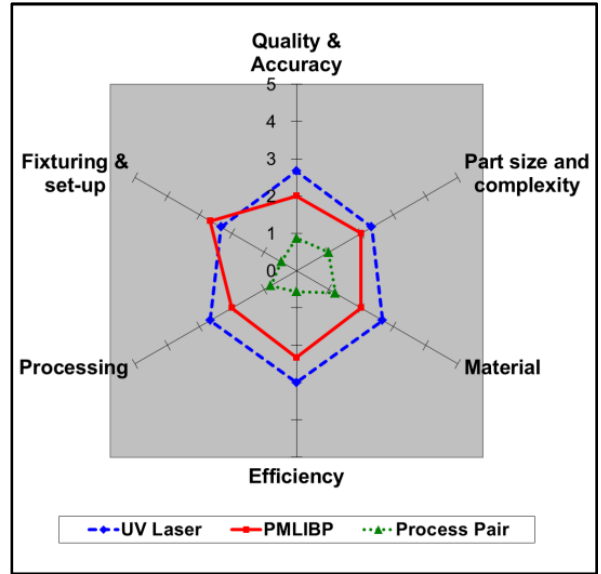
b) KPCA chart of the pair and its constituent processes

Figure 3.7 UV Laser and projection mask-less ion beam patterning
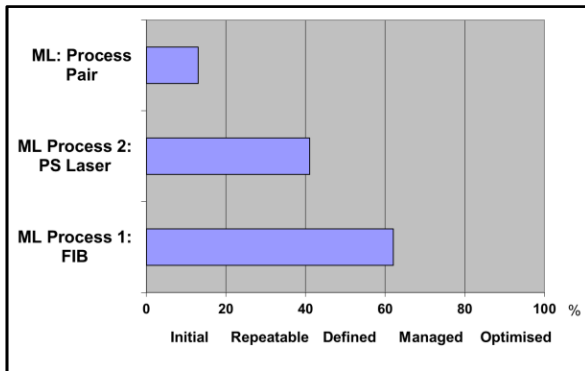
a) Overall MLs of the pair and its constituent processes
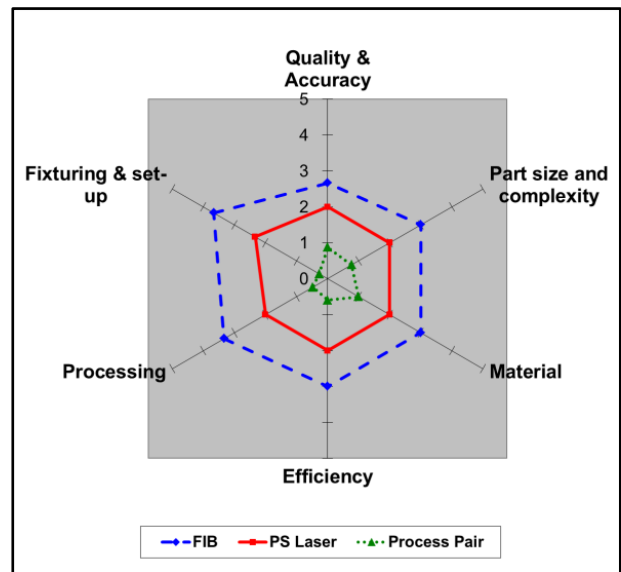
b) KPCA chart of the pair and its constituent processes

Figure 3.8 FIB and PS laser ablation
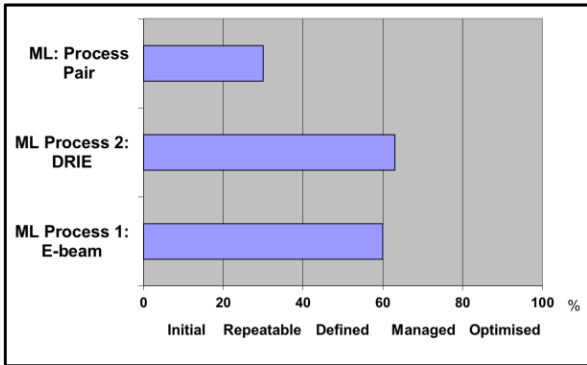
a) Overall MLs of the pair and its constituent processes
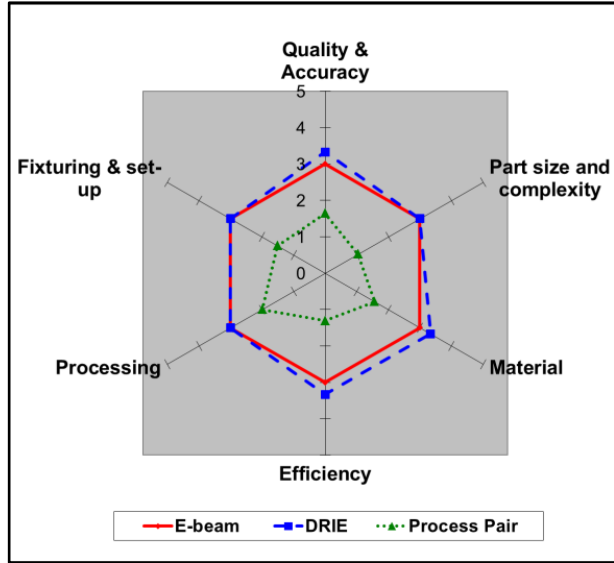
b) KPCA chart of the pair and its constituent processes

Figure 3.9 E-beam lithography and deep reactive ion etching
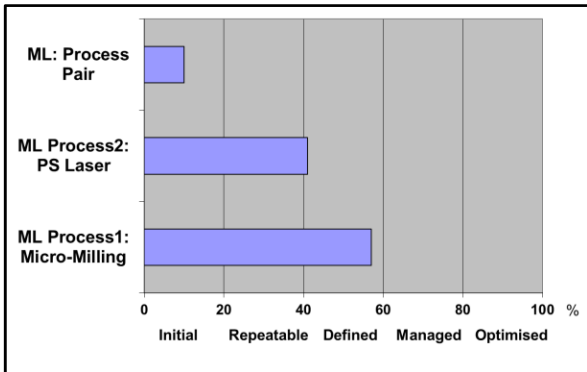
a) Overall MLs of the pair and its constituent processes
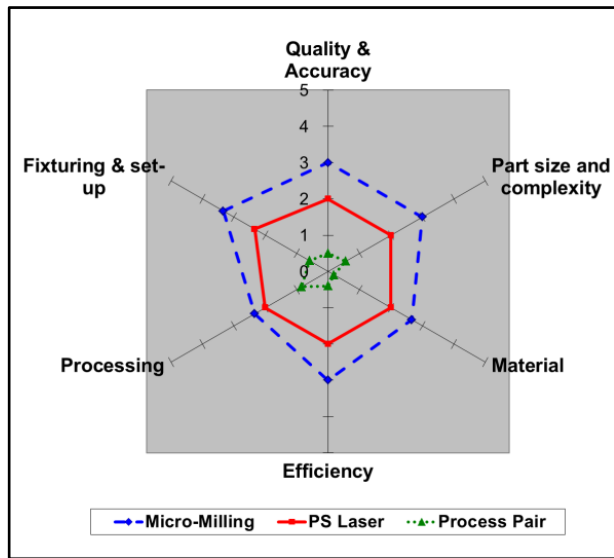
b) KPCA chart of the pair and its constituent processes

Figure 3.10 Micromilling and PS laser ablation
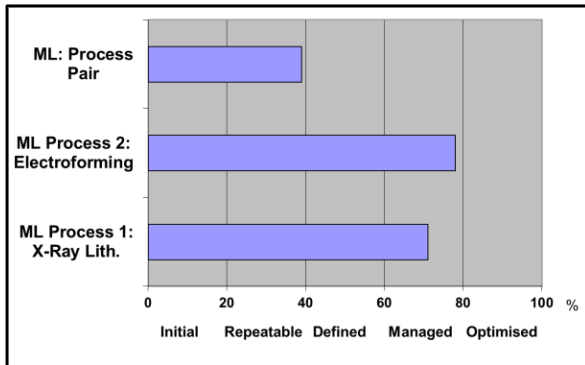
a) Overall MLs of the pair and its constituent processes
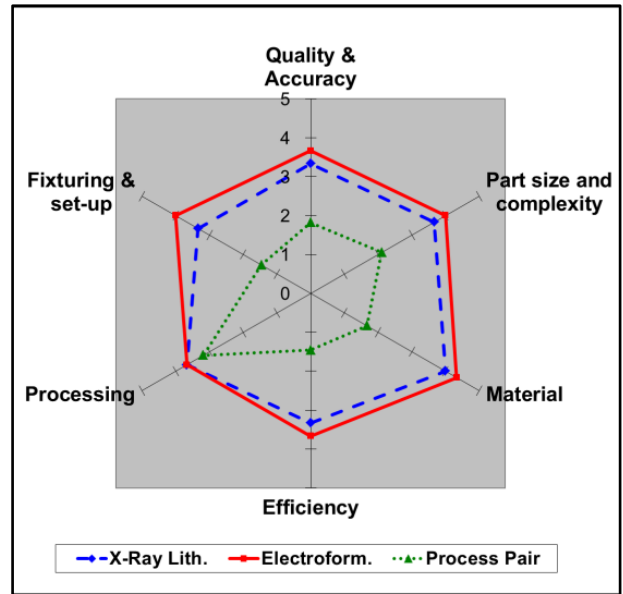
b) KPCA chart of the pair and its constituent processes

Figure 3.11 X-ray lithography and electroforming
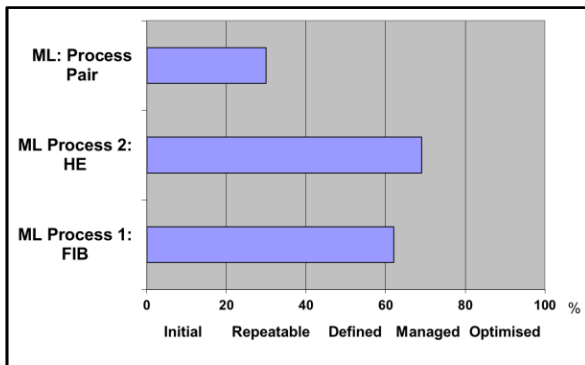
a) Overall MLs of the pair and its constituent processes
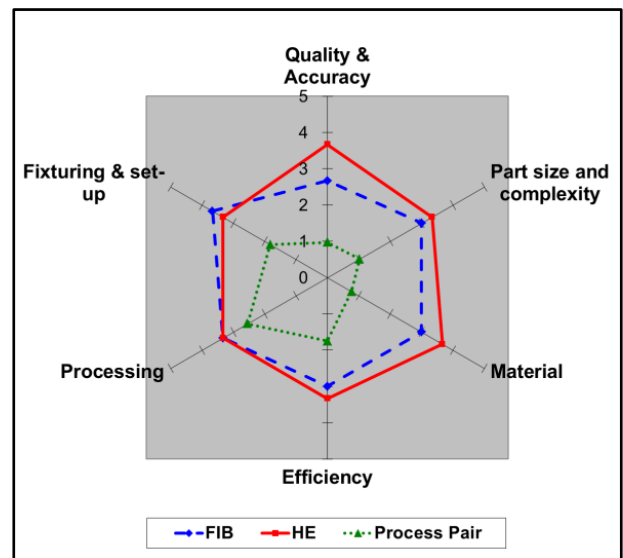
b) KPCA chart of the pair and its constituent processes

Figure 3.12 FIB and hot embossing
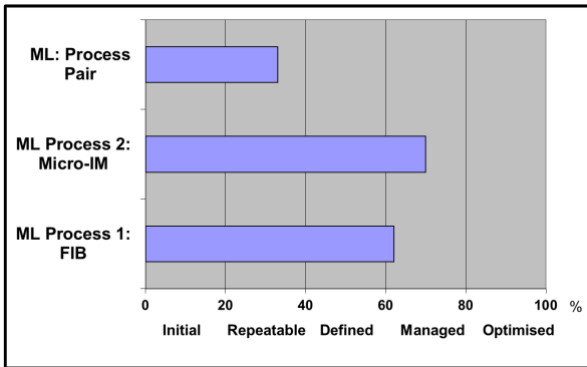
a) Overall MLs of the pair and its constituent processes
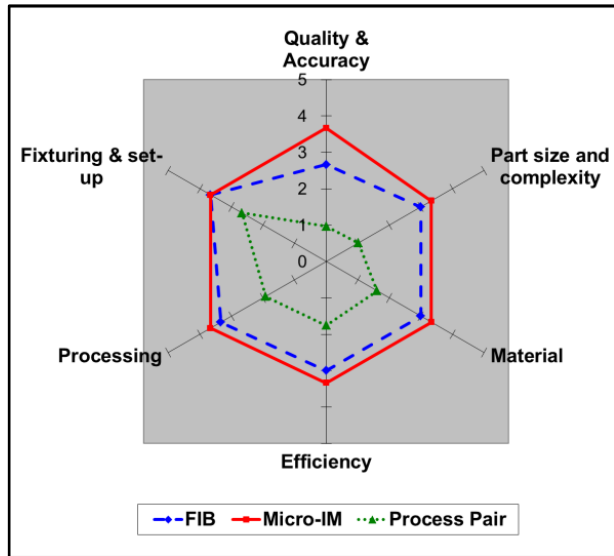
b) KPCA chart of the pair and its constituent processes

Figure 3.13 FIB and micro-injection moulding
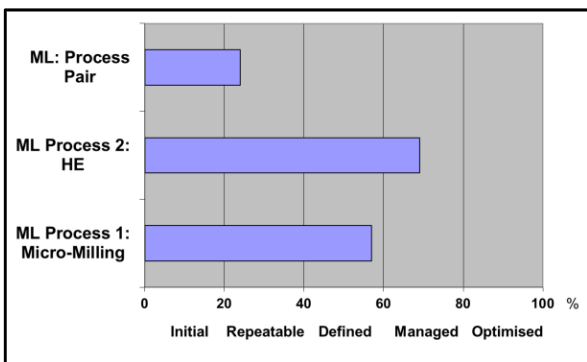
a) Overall MLs of the pair and its constituent processes
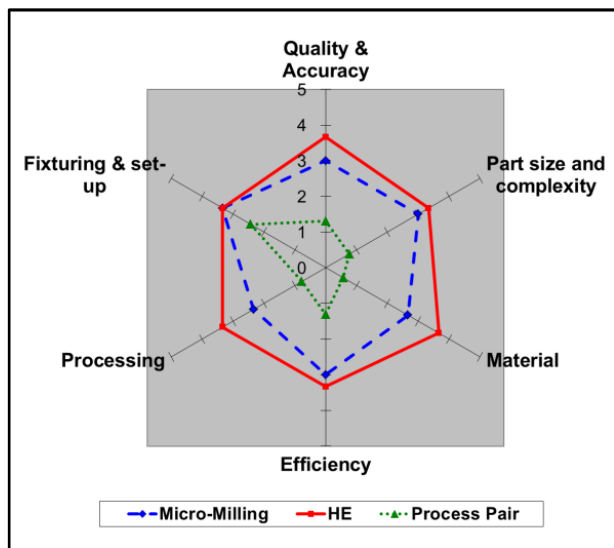
b) KPCA chart of the pair and its constituent processes

Figure 3.14 Micromilling and hot embossing

3.5.1 Component technology maturity levels across the process management categories

Analyzing the component technologies in Fig. 3.6, it can be observed that:

- Any similarities in MLs are reflected in the scale of differentiation between the component technologies' values across the three Process Management Categories. In particular, the Dynamics radar chart depicts less differentiation and thus indicates that the processes are quite similar in their maturity in regards to this process management category.

- Studying the radar chart for the Documentation category, it can be observed that ML of the MNM processes show a higher differentiation and the MLs vary from 'Repeatable' to 'Managed'. HE has the highest ML, whilst PS-Laser and Projection Maskless Ion Beam Patterning (PMLIBP) have the lowest value.

- With regards to the Capabilities radar chart of the considered MNM component technologies the ML are not consistent and they again vary from 'Repeatable' to 'Managed'. The capabilities of Electroforming are judged to be the most validated in comparison with other processes whilst again PS-Laser and PMLIBP are the most underdeveloped.

- In all three categories (Documentation, Dynamics and Capabilities), the overall status of the PMLIBP technology is due to the novelty of the process which is only existing as a proof-of-concept tool. Thus, this process is under development to fulfil the industry's need for a high productivity, flexible and cost-effective structuring technology for large (i.e. over 6 inch) surfaces with a resolution better than 10 nm.

3.5.2 KPCA charts

The results of the analysis of the ML profiles in Figures 3.7b to 3.14b across the six KPCAs of the pairs and their constituent processes are shown in Table 3-6. In particular, the table

depicts the results for the constituent processes on the left and for the pairs to the right, in terms of their overall ML, profiles' consistency and MLs across the 6 KPCAs. At the process level, the MLs of the 6 KPCAs are compared to each other, while the pairs' KPCAs are judged in regards to the average process pair KPCA ML taking into account the specific KPCA's compatibility and complementarity scores. Furthermore, the pairs' overall compatibility and complementarity scores provide another assessment of the constituent processes' suitability for combining them into pairs. Thus the table shows clearly the strengths and weaknesses of the process pairs whilst taking into account the perceived current capabilities of their constituent processes. For example, taking the UV laser + PMLIBP pair, it can be stated for the component processes that the UV laser process has ML 3 while it is borderline between ML 2 and ML 3 for the PMLIBP process. At the same time their capability hexagons are quite symmetrical. With the exception of "Fixturing & set up", the MLs of all the UV laser KPCAs are higher than those for PMLIBP. At the same time, as the pair's MLs are highly dependent on the consistency and magnitude of the constituent process MLs, the magnitude of the difference between the MLs and the compatibility and complementarity scores across all KPCAs (the capability hexagons' symmetricity), the pair has a low ML of 1. It can also be observed that the pair's "Fixturing and Set-up" and "Efficiency" KPCAs have low MLs due to the fact that the considered KPCPs, are predominantly more compatible rather than complimentary. Furthermore, overall the KPCPs of the constituent processes are only marginally more complimentary than compatible. Collectively, the results show that these two processes are alternatives rather than a process sequence that can lead to added-value and thus to broaden the pair's capabilities. A similar analysis of the other pairs can be conducted based on the results in Table 3-6 and thus to make conclusions about their strengths and weaknesses.

Table 3-6 Assessment of the KPCA maturity profiles of the pairs and their constituent processes

Process Pair	ML	ML Profile	(i) Comparison of constituent processes — KPCAs						ML	ML Profile	(ii) Analysis of process pairs — KPCAs						Overall KPCP Cr/Cb Score	Potential as a pair (Y/N)
			Quality and Accuracy	Part Size & Complexity	Material	Efficiency	Processing	Fixturing & Set-up			Quality and Accuracy	Part Size & Complexity	Material	Efficiency	Processing	Fixturing & Set-up		
UV Laser	❸	□	++	+	++	++	++	-	❶	□	≈	←	⇈	→	≈	⇉	(bar)	N
PMLIBP	❷I	□	--	-	-	--	--	+										
FIB	❸I	□	--	-	--	-	0	+	❷	□	→	→	⇉	←	⇇	←	(bar)	Y
HE	❹	■	++	+	++	+	0	-										
FIB	❸I	□	++	++	++	++	++	++	❶	□	←	←	⇇	≈	→	⇉	(bar)	Y
PS Laser	❷I	■	--	--	--	--	--	--										
FIB	❸I	□	--	-	-	-	-	0	❷	□	⇉	⇉	≈	≈	←	⇈	(bar)	Y
μIM	❹	■	++	+	+	+	+	0										

Table 3-6 Assessment of the KPCA maturity profiles of the pairs and their constituent processes

Process Pair	ML	ML Profile	(i) Comparison of constituent processes — KPCAs						ML	ML Profile	(ii) Analysis of process pairs — KPCAs						Overall KPCP Cr/Cb Score	Potential as a pair (Y/N)
			Quality and Accuracy	Part Size & Complexity	Material	Efficiency	Processing	Fixturing & Set-up			Quality and Accuracy	Part Size & Complexity	Material	Efficiency	Processing	Fixturing & Set-up		
μMilling	❸	□	--	-	--	-	--	o	❷	□	←	→	⇉	←	→	⇈		Y
HE	❹	■	++	+	++	+	++	o										
μMilling	❸	□	++	++	++	++	+	++	❶	□	≈	≈	⇉	→	⇈	←		N
PS Laser	❷I	■	--	--	--	--	-	--										
X-Ray Lith.	❹	□	-	-	-	-	o	--	❷	□	≈	←	≈	→	⇈	→		Y
Electroform	❹	□	+	+	+	+	o	++										
E-Beam	❸	■	-	o	-	-	o	o	❷	□	←	⇉	≈	→	⇈	≈		Y
DRIE	❸I	■	+	o	+	+	o	o										

92

Table 3-6 Key

Symmetrical: ■	Quasi-symmetrical: ◻	Asymmetrical: ☐	Cr Level	Cb Level
- - = much worse; - = worse; **o** = same ; + = better; ++ = much better in comparison to the other process in the pair		N = No, **Y** = Yes		
↓↓ = significantly lower ; ↓ = lower; ≈ = similar (close to); ↑ = higher; ↑↑ = significantly higher in regards to the average process pair KPCA ML.		MLs: ❶ ❷ ❸ ❹ ❺		
I = Borderline case between depicted ML value and next higher ML, e.g. ❷I is a borderline ML between ML 2 and ML 3				

93

3.5.3 Overall maturity levels

The overall MLs of the analyzed MNM technologies and their pairs are shown in Figures 3.7a to 3.14a and Table 3-6. Thus, the range of MLs of the individual technologies is from Level 2, 'Repeatable', to Level 4, 'Managed', whilst that of the pairs is from Level 1, 'Initial' to Level 2, 'Repeatable'. The results were discussed with the experts in MNM and it was concluded that they reflect adequately the perceived current MLs of the considered processes and their pairs.

Looking at MLs of the processes, it is not surprising that μMilling is considered a 'Defined' process, ML 3 (57%) , taking into consideration that: (i) a lot of R&D effort was put in its development in recent years, (ii) the technology is currently being exploited commercially by mould and watch making industries, whilst at the same time, (iii) the research community recognizes that further fundamental investigations are still needed to understand and especially to model the machining mechanics at micro scale (Câmara et al., 2012; Dornfeld et al., 2006). Also, μMilling is ranked higher than PS laser ablation and this reflects well the industrial impact of these technologies in context of their use as master-making processes. PS laser ablation is considered as a borderline case between a 'Repeatable' process, ML 2, and a "Defined" process, ML 3, (41%) in spite of the fact that it is currently commercially exploited and significant R&D efforts are put in its development (Wu and Ozel, 2011). However it is generally accepted that various open issues remain with respect to: the modeling & simulation of PS laser-material interactions (Lewis and Perez, 2010; Wu and Ozel, 2011) ; the empirical character of the process optimization; the predictability of the process performance; and the necessity for further optimization of material removal strategies (Petkov, 2011).

Both X-Ray lithography and Electroforming were judged to be 'Managed' processes, ML 4 having normalized values of 71% and 78% respectively. This result was considered representative by the MNM experts and is also supported by the fact that significant efforts

have been placed in the development of these technologies. Furthermore, both processes have been studied extensively in the development of the LIGA process chain that has been widely used to fabricate MEMS, MOEMS and microfluidic devices (Cui, 2005; Malek and Saile, 2004; Worgull, 2009) . In addition, it should also be noted that X-ray Lithography "is still being used as a mature lithography technology for small batch production of VLSI and other micro and nano technology application areas" (Cui, 2005).

E-beam was judged to be 'Defined' process, ML 3 (60%), whilst DRIE with a normalized value of 63% is considered as a borderline case between a "Defined process", ML3 and a "Managed" process, ML 4.These results seems to be on the conservative side when taking into account their application areas and the significant investment in the development of these technologies. In particular, both E-beam lithography and DRIE, have been used in process chains for mass production of ICs and also MEMs (Cui, 2005; Ziaie et al., 2004) whilst DRIE has also been utilised to fabricate silicon based tooling for hot embossing and micro-injection moulding processes (Cui, 2005). Furthermore, in the last decade, substantial work was carried out to improve the performance of these two technologies (Cui, 2005; Grigorescu and Hagen, 2009) .

The FIB process has a normalised maturity level value of 62% and thus is also considered as a borderline case between a "Defined process", ML 3, and a "Managed" process, ML 4. Again this appears to be a realistic judgement when one considers the technology advances in the last two decades to make it an important MNM tool and an indispensable technology in semiconductor IC manufacturing and R&D (Cui, 2005; Tseng, 2004). In particular, recent promising research work concerning the optimisation of the FIB milling process for micromachining applications (Lalev et al., 2008; Svintsov et al., 2009; Velkova, 2011) and the use of the FIB milling process to manufacture replication cavities in various materials (Li et al., 2007b, 2007a; Youn et al., 2007, 2008) has also been published.

Both replication processes, namely HE and μIM were judged to be 'Managed' processes, ML 4 with normalized values of 69% and 70% respectively. These results were judged again representative by the experts and are also supported by the facts that (i) substantial efforts have been aimed at the development of these technologies over the years, and (ii) these processes are utilized by industry successfully for serial production of polymer micro parts in a range of application areas, such as micro/nano optics, precision micromechanics, micro/nano-fluidics, and CD/DVD replication (Attia et al., 2009; Calaon et al., 2013; Giboz et al., 2007; Hansen et al., 2011; Heckele and Schomburg, 2004; Lee et al., 2004; Scholz et al., 2011; Worgull, 2009).

Finally, a close look at MLs of the UV-Laser and PMLIBP processes reveals that PMLIBP is a borderline case residing between a 'Repeatable' process, ML 2, and a "Defined" process, ML 3, (43%) and thus has an equivalent ranking to that of PS-Laser. However, this result should be taken with a certain amount of precaution given that it is based on the experience with only one pilot installation, and thus it is considered premature to judge about the PMLIBP maturity. In contrast, ML 3 (52%) for the UV laser appears to be a conservative judgment when considering its broad use for direct writing or mask based patterning (Bolt et al., 2008; Chen and Darling, 2008; Chiu and Lee, 2011, 2013; Choi et al., 2004; Cui, 2005; Lee et al., 2005; Liu et al., 2012; Mutapcic et al., 2005; Washio, 2010) . Furthermore, it was successfully integrated with other technologies, such as electroforming, μIM and HE, into a LIGA-like process chain called Laser LIGA (Bolt et al., 2008; Cui, 2005; Lee et al., 2005) . Finally, from an application point of view, it was also demonstrated that UV Lasers are suitable to fabricate microstructures for applications in microfluidics, micro-optics and biomedical devices (Chen and Darling, 2008; Chiu and Lee, 2011, 2013; Lee et al., 2005; Liu et al., 2012).

3.5.4 Methodology

The analysis of the results and an evaluation of the proposed methodology revealed both strengths and weaknesses in its implementation.

Strengths:

1) The proposed methodology can be used to unify the maturity assessments of process chains by taking into consideration their constituent manufacturing technologies and by paying special attention to their interfaces through their input-output relationships.

2) The qualitative and quantitative data used for the process pairs and their constituent technologies can be considered representative because they are obtained from experienced process experts.

3) The results provide a valuable insight into the current state of manufacturing technologies and their potential integration into new process chains, and thus to assist in their design and selection taking into account the requirements for any given product.

4) It utilises an expert-based qualitative framework to determine MLs and the results obtained were judged as representative and also reflected well the current state in the development of any given technology.

5) It reveals the 'weaknesses' and 'strengths' of these technologies and their respective process pairs, and thus to make an informed judgment about any open issues on which to focus in their development.

6) It provides ML "snapshots" that can be utilized in follow up studies to judge about the technology advances over given time periods.

7) The methodology can be applied to identify suitable process pairs or their variations in regards to specific product requirements, and ultimately it could be used as a knowledge base for developing new manufacturing solutions. At the same time, it can highlight some open issues associated with process pair/process chains and their constituent technologies.

8) The methodology can be applied to assess not only the manufacturing processes but also systems/equipment for inspection and materials' characterization however it is necessary to modify the maturity indicators accordingly.

Limitations

9) The input of the experts consulted can be biased to given equipment and machines and their specific applications and thus the results may not be sufficiently generic and representative for the capabilities of any particular technology. This could explain the MLs of E-Beam, DRIE and UV laser processes obtained in the methodology's pilot implementation that were on the conservative side. A possible way to address this issue is to rely on a bigger pool of experts.

10) The pilot implementation of the methodology relied on an input from face-to-face type questionnaires that limits the number of the consulted experts. Other techniques such as a self-administered on-line or mail questionnaires can also considered for possible future implementations of the proposed methodology (Salant and Dillman, 1994).

11) The methodology can be used for assessing process pairs and their constituent technologies however further development is necessary to apply it for assessing more complex process chains.

12) It will be beneficial if the proposed expert-based approach can be complemented by empirical assessments of processes and process chains' maturity, e.g. by conducting Round

Robin tests. The results from such research should also be used to find a more evidence-based way for combining complementarity and compatibility scores of pairs.

13) Although the experts in MNM concluded that the ML values of the considered pairs reflect adequately their perceived current level of development and industrial impact, a ML 2 for the X-Ray Lithography + Electroforming pair seems to be somewhat on the conservative side taking into consideration that both technologies have been applied successfully in the LIGA process chain. This result can be attributed to the formula used to calculate the pair's MLs and thus it is necessary to look at and improve it to reflect better the perceived ML of the pairs.

14) The methodology does not adequately take into consideration all implementation related risks. Mankins (2009) states that the maturity of the technology correlates with the technical risks and thus the proposed approach has to be improved further to factor uncertainties associated with the design and implementation of multi-process manufacturing platforms.

3.6 Conclusions

The work reported in this chapter aims at reducing the risks associated with the adoption and integration of manufacturing technologies, e.g. MNM processes, into process chains underpinning existing and emerging miniaturized products. It presents a new instrument for assessing technology maturity of processes and process pairs which: (i) utilizes an approach for modelling output-input dependences of pairs' constituent processes and, (ii) is inspired by a capability maturity model that was applied successfully in the software engineering domain. The main characteristics of the proposed approach for maturity assessment are:

- The methodology provides a systematic and effective way to analyze the interfaces between manufacturing technologies in pairs and process chains and thus to assess their

respective input-output complementarity and compatibility.

- It aims to study the maturity of process pairs, and thus to assess the risks associated with their implementation.

The proposed methodology was tested on eight MNM process pairs to judge about their overall maturity and also about their respective Key Process Capability Areas. The results demonstrate the applicability of the proposed methodology as a means to evaluate the maturity of the MNM pairs and their constituent processes. In addition, it can be stated that this methodology can be employed in the design of new process chains by identifying suitable pairs, and also as a tool to identify weaknesses in pairs related to their KPCAs. The benefits from and advantages of the proposed methodology can be summarized as follows:

- It provides a comprehensive framework for assessing the maturity of processes and process pairs by modeling the interfaces between the component technologies.

- The rationale behind the proposed framework is easy to understand, and it is a systematic and structured approach for conducting studies to determine MLs of individual processes and process pairs

- The methodology utilizes inputs from process experts to assess the maturity of manufacturing processes.

- The ML results can be expressed as: (a) overall values or (b) hexagons across the six KPCAs or (c) polygons for each process management category.

CHAPTER 4
BMG-BASED PROCESS CHAIN FOR PRODUCING REPLICATION MASTERS WITH MICRO AND NANO SCALE FEATURES

4.1   Introduction

In the previous chapter, the systematic study of technological interfaces between a set of micro and nano fabrication technologies revealed that FIB + PS Laser and FIB + µIM are two process pairs deemed suitable to be integrated in process chains.   In this chapter, these complementary technologies are combined into a novel process chain for serial production of polymer based FLSI devices. At the same time, as argued in chapter 2, the workpiece material plays a very important role in their successful integration and also in achieving FLSI in the replication masters. Consequently, this chapter explores the concept that due to their atomic level homogeneity, BMGs can undergo multi-scale patterning successfully and therefore can be used to design and implement FLSI enabling master-making process chains. In addition, due to their unique mechanical and thermal properties, BMGs can also fulfil the specific functional and technical requirements of replication masters.

Therefore within this context, the main objectives of this research are:

- to design and experimentally investigate a new master making process chain that is enabled by the use of a bulk metallic glass (BMG) as a workpiece material, to combine the capabilities of the PS laser ablation and FIB machining technologies in producing replication masters incorporating micro and nano scale structures.

- to validate experimentally such BMG replication masters for serial production of polymer based FLSI devices by employing micro-injection moulding

- to investigate systematically the factors affecting the performance of such masters.

- to experimentally investigate, the capabilities of another laser source, namely NS laser as an alternative candidate for the PS laser step in the abovementioned master-making process chain.

Following this section, the remainder of the chapter is organised as follows. Section 4.2 discusses process and material related issues that have to be considered in achieving length scale integration in master-making process chains. It also provides an overview of the component technologies investigated in this research. Then, Section 4.3 describes the experimental set-up employed to validate the capabilities of the proposed process chain. Finally in sections 4.5 and 4.6 respectively, the obtained results are discussed, and conclusions are made.

4.2 Process Chain Design

As stated in chapter 2, when designing process chains it is necessary to take into account the technical requirements of the product or replication master together with the processing constraints of their component micro and nano manufacturing technologies. Also, it was stated that, the selection of a suitable workpiece material to facilitate the integration of these technologies into a process chain is an important factor in producing parts or replication masters with different length scale functional features. Specifically, the microstructure and properties of a workpiece material need to be considered as one more "variable" in optimising the process chains, and thus to achieve a suitable level of 3C (Capabilities, Compatibilities and Complementarities – See Chapter 3) between the component fabrication technologies. The selected material should have a microstructure that is optimised for performing

processing both at meso/macro and micro/nano scales. In particular, the micro or nano structuring response is favourable if, such a material is homogeneous and inclusion free at the considered processing scales. Thus, the material microstructure and properties of the workpiece are a critical factor affecting the machining results and their consistency in micro and nano manufacturing. Therefore, it is even more important when designing process chains aiming at FLSI in replication masters to identify suitable combinations of complementary structuring technologies and a workpiece material with a favourable machining response to them. In chapter 3, the systematic study of technological interfaces between a set of micro and nano fabrication technologies revealed that the pair of complementary technologies FIB + PS Laser are deemed potentially suitable to be integrated in process chains. The rationale in selecting a suitable workpiece material, to combine their capabilities in producing replication masters incorporating micro and nano scale structures follows.

4.2.1 Process and material Issues

Major advances in material processing technologies and especially in the development of amorphous coatings and alloys have attracted a considerable interest in recent years. This is due to the fact that the high hardness, fracture toughness and fatigue strength of such materials represent important value-added properties in a number of engineering applications (Inoue, 2000; Zhang et al., 2006). For example, amorphous coatings are advantageous for manufacturing micro-electro-mechanical systems (MEMS) and micro-sensor systems (Wang et al., 2007b) . Additionally, due to absence of any long range atomic order, lattice defects and grain boundaries (Kawasegi et al., 2006) , amorphous metallic alloys are considered promising materials for micro and nano- structuring of replication masters (Minev et al., 2010; Quintana et al., 2009) . The absence of grain boundaries in BMG makes them mechanically and chemically homogeneous for processing at all length scales down to a few nanometres. As a result, they are one of the preferred materials for micro- and nano

structuring (Loffler et al., 2007) . However, to benefit from their outstanding properties and employ them successfully in different application areas, it is of prime importance to maintain their non-crystalline morphology during machining, especially when producing parts incorporating micro- and nano-scale features (Quintana et al., 2009) . In a recently conducted feasibility study, it was shown that the processing of an amorphous Nickel-based alloy workpiece with both nano-second (NS) and pico-second (PS) pulsed laser ablation did not trigger phase transitions in the material (Quintana et al., 2009) . In particular, the reported research revealed that machining with both laser ablation regimes did not lead to any crystallisation and long-range atomic ordering of Ni-based metallic glasses. Additionally, there were no signs of crack formation, which indicates a preserved surface integrity after laser machining with short- and ultra-short pulses. Another study reported the effective machining of Mg-based BMG using a 355nm pulsed NS laser. In this study it was demonstrated that by an appropriate adjustment of the laser parameters the non-crystalline morphology of the Mg-based BMG was preserved (Lin et al., 2012) . Hence, both PS and NS laser machining regimes should be considered as very promising methods for the cost effective micro structuring of metallic glasses.

Another study which compared the machining response of an amorphous and polycrystalline Ni alloys when subjected to FIB milling, showed that a higher surface integrity could be achieved when processing the amorphous Ni-based BMG under identical conditions to those used for the polycrystalline Ni alloy (Li et al., 2007b) .

Thus, laser ablation in NS and PS regimes and FIB milling satisfy the 3C prerequisite for their integration in process chains and are promising combinations of complementary technologies for structuring BMGs at micro and sub-micron length scales respectively without introducing any changes in their non-crystalline morphology. In particular, the potential integration of PS laser ablation and FIB machining in a process chain reported in a feasibility study (Scholz et

al., 2009) suggested that PS laser ablation can be used for cost effective micro structuring of large areas on replication masters while FIB milling can be utilised to machine on a pre-existing topography very complex micro and sub-micron 2.5D and 3D structures. The same rationale also applies to the combination of NS laser ablation and FIB milling in a process chain. Thus, the component processes in such process chains can be utilised in their cost effective processing windows and complement each other in achieving FLSI in replication masters. At the same time, it is important to stress that these process chains still need to be validated for producing products or replication masters incorporating micro and nano scale structures.

In the proposed master making process chains (See Fig 4.1) that are enabled by the use of a BMG as a workpiece material, first laser ablation is employed to structure relatively big surface areas with meso and micro scale resolution and acceptable surface integrity, and subsequently FIB milling is applied to achieve high resolution sub-micrometre and nano patterning within a relatively small field. In this manner, by combining the capabilities of these two complementary technologies it is possible to achieve cost effective FLSI in replication masters and benefit from the BMG' s superior mechanical properties for micro injection moulding (µIM) of thermoplastic polymers. A more detailed description of the capabilities of these component technologies in the proposed master making process chains is provided in the following sub-sections.
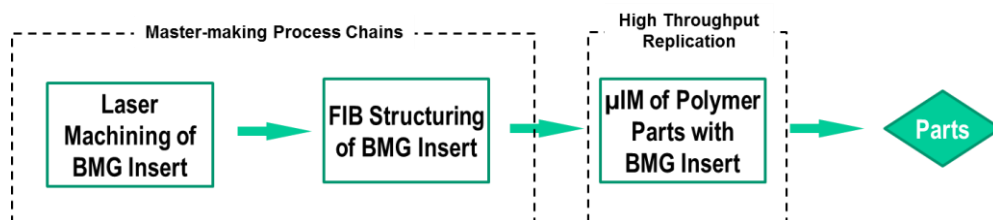
Figure 4.1 Process chain for mass production of polymer parts incorporating different length scale features

4.2.2 Laser machining

Laser micromilling as a technology for manufacturing replication masters has attracted research (Dobrev et al., 2006; Petkov et al., 2008a; Scholz et al., 2011) and industrial interest (Knowles et al., 2007a) . Laser milling can be used to structure parts in a wide range of materials directly from CAD data via a layer by-layer machining strategy (Pham et al., 2004b) . Material removal occurs as a result of laser irradiation and depending on the laser source and the workpiece, the ablation can take place through melting and ejection or sublimation (Petkov et al., 2008a) . The process allows parts with complex shapes to be produced without the need for expensive tooling. Laser milling is mostly used for machining parts from one side only. However, complete laser milling of parts is also possible, but it is necessary to address the accuracy issues associated with the re-positioning of the workpiece, which are common process design concerns when more than one machining setup is necessary (Pham et al., 2004b) .

To set up the laser milling process and achieve the required surface integrity it is usually necessary to take into account a range of factors that can influence the machining outcomes (Pham et al., 2007) . These include laser processing parameters and applied machining strategies (Fleischer and Kotschenreuther, 2007; Lalev et al., 2009; Petkov et al., 2008a; Uriarte et al., 2006; Wu and Ozel, 2011) . Thus, their interdependencies and effects on different output characteristics such as the achievable surface integrity or the material removal rate have to be studied systematically in order to identify optimum processing windows.

Short, NS, and ultra-short laser sources, femtosecond (FS) and PS, have many applications in micro-machining of metals, semiconductors, and dielectrics for the fabrication of electronic, medical, optical and other devices (Wu and Ozel, 2011) . The ultra-short lasers have the advantage of extremely high radiation intensities and thus can ablate almost any material with minimal and sometimes even negligible heat affected zone and therefore they are used for

precise material removal (Brousseau et al., 2010; Wu and Ozel, 2011) . NS laser technology is mature and is widely adopted in industry for micro machining (Knowles et al., 2007b) . This is largely due to their cost-effectiveness and reliability and therefore NS lasers are used in many industrial applications. A major advantage of NS laser ablation is their achievable higher removal rates when compared to lasers with shorter pulses (Quintana et al., 2009) . However, micro machining can be a challenging application for NS lasers. Good quality sidewalls can generally be obtained, but it is usually very difficult to achieve the necessary surface integrity for some applications, e.g. replication masters (Knowles et al., 2007a) . The ultra-short lasers, FS and PS, have a number of advantages in micro machining. The very high repetition rate of the latest generation of FS and PS laser sources together with the advances in the scanning heads' technology allow the resulting surface integrity to be improved substantially while maintaining a higher processing speed (Fleischer and Kotschenreuther, 2007; Petkov et al., 2008a) . However, it is worth noting that such improvements are at the expense of the removal rates when NS and PS laser machining results are compared.

Apart from micro machining, lasers are also used for surface texturing (Bonse et al., 2012; Etsion, 2005) . Especially, they are applied for functionalising surfaces, e.g. to regulate cell-implant interaction for biomedical engineering applications (Vehse et al., 2012) , to reduce the surface friction in mechanical devices (Chen et al., 2012) **,** to modify the wetting properties of the surfaces (Fadeeva et al., 2011; Wu et al., 2011) , or to reduce the surface reflectance (Nayak and Gupta, 2010) . Such applications are also very interesting for master making as laser surface texturing rates are still low for cost effective direct structuring of parts with relatively large surface areas.

In this research, the choice of the laser source requires careful consideration in order to avoid any detrimental effects on the non-crystalline morphology of the BMG workpiece. Such effects are of a particular importance for the proposed process chain as any phase

transformations or crack generation will not only change the material properties of the replication master but can also affect any subsequent sub-micron structuring by FIB milling. Therefore, two alternative laser sources were considered as potential candidates for the first step in this master making process chain. The primary focus of the research is on investigating the feasibility of utilising PS laser machining in the proposed master-making process chain due to its capabilities for machining accurately micro features whilst preserving the mechanical properties and surface integrity of the workpiece material. However, it is also possible to optimise the NS laser ablation process and achieve a relatively good surface integrity while benefiting both from the higher material removal rates and the superior mechanical properties of BMGs as they can also be preserved during the processing with short pulse lasers. Therefore, it was also considered important to investigate the NS laser ablation of BMGs as an alternative component technology in the process chain, in particular what level of surface finish can be achieved without triggering any crystallisation.

4.2.3 FIB milling

The second stage in the process chain is FIB machining of sub-micron and nano-features over the pre-existing topography generated by laser ablation. The FIB milling process offers many advantages, such as flexibility, high resolution and high surface quality that are extremely important for master making (Scholz et al., 2009; Youn et al., 2006) .

The input data for FIB milling can be in a bitmap format when it is necessary to produce simple features like 2.5D channels. In this case, the data can be uploaded into most FIB systems directly. Then, the built-in pattern generator of such systems is used to create directly the 2.5D features. A more sophisticated approach to 2.5D feature generation requires the use of a lithography software and hardware like Elphy Quantum (Raith GmbH) or Nanomaker where various 3D shapes can be designed, duplicated, and if necessary the respective

exposure doses specified. However, the generation of complex 3D shapes like diffractive optical elements, necessitates a different data preparation procedure. Such 3D structures can be designed by employing any 3D CAD package and then, by following a sequence of data translation operations, the 3D geometry is converted into a stack of layers ordered along the vertical axis of the 3D model (Lalev et al., 2008) . After such a 'slicing' step, the model is exported into a GDSII stream file format and each GDSII layer represents a set of exposure pixels defining a slice of the model at a given point along its vertical axis.

The main FIB parameters that should be considered when optimising the process are: ion beam current, ion beam fluence, and exposure time (Lalev et al., 2008; Li et al., 2007b; Minev et al., 2010; Velkova et al., 2010) . An ion beam sputtering simulation software can also be employed to predict and thus reduce some negative effects such as re-deposition of sputtered material and over-etching (Svintsov et al., 2009) . Its use as a data pre-processing step before FIB milling makes it possible to optimise the process parameters and even to modify the model in order to counteract material re-deposition effects (Velkova et al., 2010) .

Another important issue when structuring processes are integrated in process chains is the alignment of new features to any pre-existing features/topography on the workpiece. In the proposed chain, this alignment could be realised either by manually positioning the sample stage while inspecting the specimen in SEM or FIB imaging modes, or automatically, by using the ''feature recognition" option available in some FIB systems to find alignment marks machined in the preceding processing steps.

4.2.4 Micro injection moulding

The proposed master-making process chain can be used to produce masters for scale-up micro replication including µIM and hot embossing (HE) (Heckele and Schomburg, 2004) .

However, given that the development of new micro devices is highly dependent on manufacturing systems that can reliably and economically produce micro parts in large quantities, it is clear from the reviewed literature in Chapter 2, that µIM provides a more attractive option. Therefore, in this study, the structured BMG inserts was used as a master for µIM in order to validate the proposed process chain.

When replicating micro and nano-structures employing µIM, the accuracy of the mould masters is an important prerequisite. Nonetheless, the complex flow and cooling behaviour of the thermoplastic materials can also have a significant influence on achievable product quality. It is therefore usually necessary to optimise the µIM process using design of experiments (DOE) approaches. There are numerous parameters which can influence the process but the most statistically significant factors (Attia et al., 2009; Giboz et al., 2007; Griffiths et al., 2007; Sha et al., 2006; Mani et al., 2013; Zhang et al., 2012b; Huang, 2007; Monkkonen et al., 2002; Tosello et al., 2010a) include: melt temperature; mould temperature; injection speed; holding pressure and duration; mould surface roughness; runner and gate design and venting/ vacuum systems.

Micro-moulding geometries typically have a very high surface to volume ratio when compared with macro scale injection moulded products, which means that polymer solidification can be very rapid, with cooling rates in a fraction of a second in many cases. Such conditions require short filling times to ensure the temperature of the material does not fall below the no-flow temperature before the mould is completely filled. The heat flow during solidification can also have a significant influence on the internal morphology of the part and also on a range of properties affecting its mechanical behaviour. Therefore, the thermal behaviour of the polymer-mould system can have a high impact on the final product's properties and therefore a very accurate control of the melt and mould temperatures is required to achieve a stable process. As a consequence the µIM process windows for quality

components tend to be much smaller than those in conventional injection moulding. In particular, any small changes in the parameter settings can shift the process outside these small windows with detrimental effects on part quality. It is therefore very important to optimise the µIM process for the particular polymer in use and thus to ensure a stable and reliable micro replication process.

4.3   Experimental Setup

4.3.1 Insert material

The BMG used in this study was a Zr-based BMG, namely Vitreloy 1b (Vit1b) (See Appendix E for technical data on Vit 1b alloy samples). The mechanical properties of this alloy are particularly attractive for the fabrication of high wear resistant mould inserts for µIM, especially its high tensile yield strength, 1.9 GPa, and high hardness, 540 Hv. Furthermore, it is expected that micro and nano-structures machined in this material will have a high level of surface integrity due to the fact that crystalline defects, such as dislocation pile-ups, point defect agglomerates and grain boundaries, are not present in the material. Using wire electro discharge machining, the Zr-based BMG sample was cut to produce a circular workpiece with a thickness of 3 mm and a diameter of 10 mm.

4.3.2 Test structure design

The 2D design of a Quick Response (QR) code is used as a test structure.
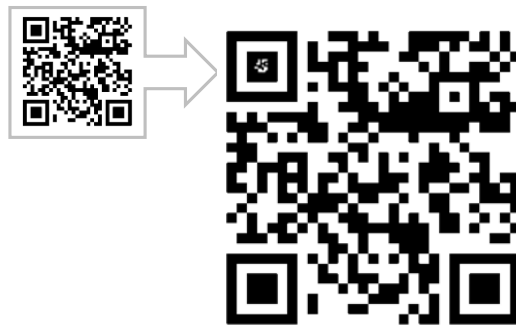
Figure 4.2 Bitmap images of the QR code

The QR code is a specific matrix barcode that consists of square fields in black colour on a white background. The information encoded by such patterns can represent text or other data. The specific QR code used is shown in Fig. 4.2 and it consists of 29 x 29 black or white squares. This pattern was machined at two different length scales on the BMG workpiece. First, a micro scale pattern of the QR code was produced using laser ablation. At this scale, each square has a width of 75 μm and the white squares correspond to pockets with a depth of 10 μm. Next, a nano-scale version of the code was machined on top of a micro-scale black square, as shown in Fig. 4.2, using FIB machining. In this scale, each square has a width of 2.59 μm and the white squares correspond to pockets with a depth of 900 nm. This test structure was selected to demonstrate the feasibility of incorporating different length scale features, micro and sub-micron, cost effectively into replication masters for anti-counterfeiting purposes. In particular, such QR codes could be replicated on the surfaces of macro and meso scale polymer parts.

4.3.3 Laser ablation

As it was stated in Section 4.2.2, PS and NS laser ablation can be used for micro machining of BMGs without triggering any crystallisation. Therefore, in this research two different laser systems were utilised to investigate laser-BMG interactions in these two ablation regimes.

The PS laser ablation is used for machining the features of the micro-scale QR code on the BMG workpiece. To perform laser structuring, first the bitmap file of the QR code was converted into a .dxf (Drawing Interchange Format) format, and then the model was scaled to ensure that the square fields are machined to the specified sizes of 75 μm x 75 μm. Next, this data file was used to generate the laser machining path. A layer-based machining strategy was selected for this study. In particular, the strategy included random "hatching" with a step over of four micrometres between the parallel passes of the laser beam and this was then followed by a border cut for each layer (Petkov et al., 2008b) . The PS laser ablation system used to perform this laser structuring operation incorporates a mode-locked Nd:YVO4 green (532 nm) laser source. The process settings used to carry out the PS laser machining are provided in Table 4-1. The process settings were selected in such a way so that in parallel to the machining of the QR code, the machined fields were also textured with self-organised structures and thus to investigate the μIM capabilities when replicating surfaces with a wide range of micro and sub-micron features/structures.

Table 4-1 PS laser parameters

Pulse duration	8 ps
Repetition rate/ Pulse frequency	50 kHz
Laser beam scanning speed	10 mm/s
Power	25 mW
Fluence	$0.28 J/cm^2$
Pulse energy	0.5 μJ
Hatch distance	4 μm
Beam quality	$M^2 < 1.3$

In addition, an experimental study was carried out to determine whether it would be possible by NS laser ablation to structure Zr-based BMG workpieces with a high surface integrity without triggering any crystallisation. A system that integrates a NS near infrared fibre laser was used to machine fields with depth of approximately 20 μm. Some initial trials were conducted with different processing conditions, in particular by varying scanning speed, pulse duration, repetition rate and fluence, to identify combinations of processing parameters for achieving a high surface integrity with a minimal thermal load. Based on these trials the process settings in Table 4-2 were selected as promising for achieving high surface integrity with minimal thermal damage. Using these settings 10x10 mm fields were laser machined on three Vit 1b samples for a X-ray diffraction (XRD) analysis. After completing the NS laser machining, the three samples were ultrasonically cleaned with a light degreaser to remove any debris without affecting the resulting surface roughness. It should be stressed that this was just a feasibility study to determine whether it will be possible by NS laser ablation to achieve a high surface integrity while retaining the BMG non-crystalline morphology.

Table 4-2 NS-laser parameters

Sample	Pulse Frequency [kHz]	Average Power [W], (measured)	Pulse energy [μJ]	Fluence [J/cm^2] @ 35 micron spot	Pulse duration, [ns]	Scanning speed V [mm/s]	Track distance, [μm]	Layer thickness [μm]	Hatch direction
1	40	0.72	18	1.87	220	600	15	1	cross, 90°
2	250	1.45	5.8	0.60	25	1000	6	0.15	random
3	40	0.72	18	1.87	220	200	5	0.3	random

4.3.4 FIB processing

The next process in the proposed chain was FIB milling of the features with nanometre depth over the micro-topography produced by laser milling. The nano-scale QR code was machined on the BMG workpiece using a Carl Zeiss XB 1540 FIB/SEM system that combines a gallium

ion beam with an electron beam column. As it was mentioned earlier, the FIB milling process can be controlled by utilising a built-in software or an external nanolithography system (Lalev et al., 2008) . Given that the QR code represents a 2D image composed of black and white fields/pixels, the bitmap file of this pattern was processed directly by the built-in software of the FIB system to control the milling operation. The depth and accuracy of the structures fabricated by FIB milling are determined by the processing parameters used. In this study, the process was set up and optimised by conducting trials to find a suitable processing window and thus to achieve the best trade-offs between machining time and feature quality. Especially, in identifying the process parameters it was taken into account that FIB milling with low current results in a better pattern resolution but at the expense of longer milling times. It should also be noted that by increasing the processing time the possibility for quality deterioration and pattern drift also increases. The FIB milling parameters used in this study are provided in Table 4-3. The alignment of the nano-scale QR pattern over the micro-scale code was performed by a manual stage control with the help of the FIB imaging mode of the system.

Table 4-3 FIB parameters

Probe current	200 pA
Accelerating voltage	30kV
Exposure time duration	3 hours
Probe size	40 nm

4.3.5 Micro injection moulding

The machine used to perform the μIM trials was a Battenfeld Microsystem 50 with a 5 mm diameter injection plunger. The BMG insert was integrated into a larger circular cavity mould and installed into a modular tool assembly based on a Hasco 95mm x 95mm standard. The cavity form is a disc with a 17 mm diameter and 0.5 mm depth. The tool is thermoelectrically heated using a cartridge heater array and temperature control was performed using the

integrated control system in the machine. Images in Figure 4.3 depict the assembled mould and one of the replicas.
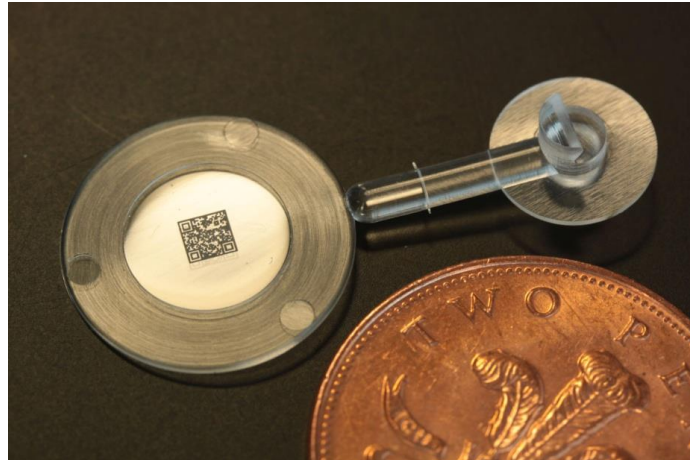
(a) Mould assembly   (a) µIM part

Figure 4.3 Images depicting the assembled mould and one of the replicas.

A material commonly used in injection moulding for optical devices, namely Cyclic Olefin Copolymer (COC) with a trade name Topas 5013S was selected to conduct the replication trials. To fill completely a mould cavity that incorporates micro and sub-micron features it is very important to select the right processing window. Taking into account the results of other experimental studies (Huang, 2007; Monkkonen et al., 2002; Sha et al., 2006; Tosello et al., 2010a) , some preliminary trials were conducted to identify an appropriate combination of parameter settings and thus to produce replicas of required quality. The trials showed that the mould temperature had the highest influence on the replication quality. Therefore, a set of experiments were subsequently performed with the mould temperature settings in Table 4-4 in order to investigate the influence of mould temperature on the replication fidelity in terms of feature width, depth and shape. These settings were selected based on the material manufacturer's data sheets, experimental investigations reported in literature, and the performed trials.

To obtain representative results, the µIM process was first allowed to stabilise for each set of process parameter settings by producing at least 40 components and then a small batch of parts was produced for quality assessments.

Table 4-4 Process settings for micro-injection moulding trials

Parameters \ Trial No	1	2	3	4	5
Melt temp -- T_b [^{o}C]	290	290	290	290	290
Mould Temp -- T_m [^{o}C]	80	110	115	130	140
Holding Pressure -- P_h [Bar]	1300	1300	1300	1300	1300
Injection Speed -- V_i [mm/s]	200	200	200	200	200

4.3.6 Inspection

The surface integrity and dimensional compliance to technical requirements of the tool and subsequently the replicas have to be assessed. Thus, a detailed dimensional analysis was carried out based on five key representative dimensions of both the laser and FIB machined QR codes on the BMG insert and their corresponding polymer replicas. In particular, the widths and the heights/depths of the smallest features and the overall size of the codes were measured. The equipment and the respective inspection procedures employed in this research are described below.

4.3.6.1 Scanning electron microscope

Scanning electron microscope (SEM) images of the QR codes were taken at each stage of the process chain in order to assess lateral (XY) and vertical (Z) dimensions of the produced parts. One BMG master was used for the detailed dimensional analysis. Ten "pixels" located in the corners and the centre of both the "large" and "small" QR codes were measured in X and Y respectively to obtain the width values of the smallest features. Whilst to obtain the

values of the overall QR codes' dimensions, five measurements were conducted along the X and Y axes. All X and Y measurements were carried out using the SEM. For the height/depth measurements of the smallest features, 10 "pixels" of the "large" QR code were measured. These Z measurements were carried out at an angle of 54° between the electron beam and the sample holder. The tilt compensation option of the SmartSEM software was used to calculate the actual values of the vertical dimensions. For the polymer parts' analysis, five replicated Topas samples were selected and each part was measured in the same way as the BMG insert.

4.3.6.2 Atomic force microscope

A representative area of the FIB milled and replicated small scale QR code was inspected with an atomic force microscope (AFM), Asylum Research MFP 3D, to judge about the FIB structuring and the μIM replication quality. The measurement was carried out when the instrument was in its tapping mode configuration. The probe used was parabolic in shape, with an apical tip radius of 15nm and a half cone angle (a) of 30°, from the vertical plane. The profiles of the features were obtained at the same place on the FIB milled insert and all μIM parts. For the mouldings, three samples were randomly selected from each batch of Topas 5013X parts. The dimensions of the scanned area were 50 x 50 μm. After the measurement, the data sets were processed using IGOR Pro 6 software in order to generate the average line profiles of the features and carry out on them depth and width measurements. Finally, the average profiles for each batch produced were compared to decide which combination of process parameters gave the best replication results.

4.3.6.3 Confocal microscopy

The laser and FIB patterns on both the insert and mouldings were inspected using an Olympus LEXT 4000 laser scanning confocal microscope. Two modes of operation were used, in

particular, a 20x objective with a 25 image stitched dataset (5 horizontal, 5 vertical) for the large-scale QR code pattern and a single 100x image for the FIB structures. The resolution of each image was 1024 x 1024 pixels and the overlap area for the stitching was 20%.

The surface roughness of the textured surfaces of the large scale QR-code on both the insert and the replicas together with the pixel step height measurements of the insert's "small" QR code were carried out using this confocal microscope. In particular, in order to determine the step heights, the integrated Olympus software was employed to obtain histograms of the height distributions. Average step heights of the scan areas were determined by computing the difference between the individual mean heights of the histograms' two peaks as shown in Fig 4.4. For the polymer parts' dimensional analysis, five Topas replicas were measured in the same way as the BMG insert.
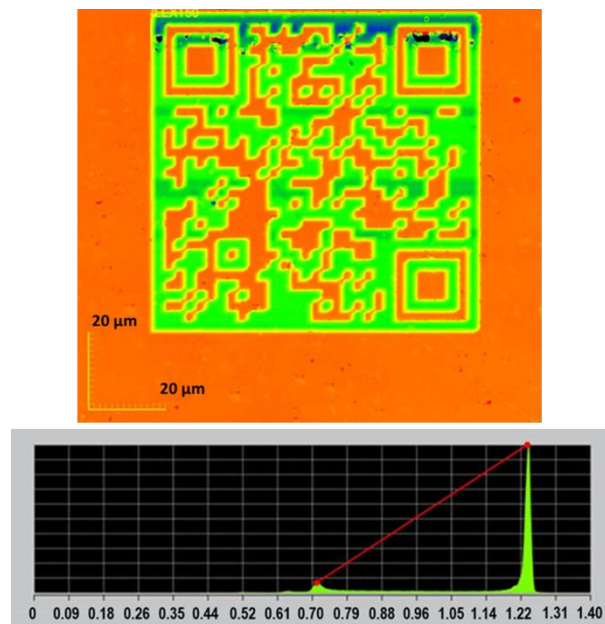
Figure 4.4 Step height measurement using Olympus software

This method for evaluating average step heights was validated using a Veeco SHV2119 step height calibration artefact where 5 measurements were performed at various locations on the

sample using the magnification parameters adopted for each scan. The results fell within the ranges defined by the calibration certificate so it was accepted as a valid technique.

For assessing the replication quality of the FIB structures on the BMG insert and five Topas replicas from each mould temperature setting, three methods were used:

i) *Volume ratio.* The volume of the features and cavities was determined using the LEXT software by considering the volume enclosed by the measured surface and a plane coincident with the original (pre-machined) surface. A ratio of the volume of the moulded feature relative to the original cavity volume was used as a measure of the replication quality.

ii) *Sa ratio*. The Sa parameter is the arithmetic mean of the absolute value of the height within the sampling area. The Sa parameter of both the features and cavities was determined using the LEXT software. The ratio between Sa of the moulded feature relative to the original cavity Sa was used as a measure of replication quality.

iii) *Average step height ratio*. As described earlier, the average step height was determined for the insert and each of the moulded specimens by using histogram information as shown in Fig 4.4. The ratio between the average step height of the moulded feature relative to the original cavity step height was used as a measure of replication quality.

4.3.6.4 XRD

The focus of the NS laser machining trials was to achieve as high as possible surface integrity without triggering any crystallisation and thus to preserve the attractive mechanical properties of Zr-based BMGs. Therefore, a XRD analysis of Vit 1b samples before and after laser machining to form 10x10 mm fields, was carried out using a Bruker D8 Advance' X-Ray Diffractometer with Ni filtered CuKa radiation to verify the amorphicity or otherwise of the four samples.

4.3.6.5 Talysurf 120L

The roughness measurements for the three NS laser machined samples were taken using a Talysurf 120 L surface texture measurement instrument. The sizes of the sampling/evaluation lengths were chosen according to ISO 4288: 1997 (ISO4288, 1997). The parameter used to evaluate the surface roughness was the arithmetic mean roughness (Ra) because relative heights in microtopographies are more representative, especially when measuring flat surfaces. (Popov et al., 2006).

4.3.6.6 Dimensional and surface roughness measurements uncertainty

The average values of dimensional measurements were calculated and where deemed applicable are also provided with their associated expanded uncertainty, U, (at 95% confidence level) which was determined, following an established procedure (Joint Committee for Guides in Metrology (JCGM), 2008; Kirkup and Frenkel, 2006; United Kingdom Accreditation Service (UKAS), 2007).

The error sources for the SEM and confocal microscope were identified by adapting the recommendations given in literature for SEM and other non-contact measuring systems (Tosello and Chiffre, 2004; Tosello et al., 2009b, 2012; Tosello, 2008; Velkova, 2011). In the case of the SEM, to account for the worst-case scenario the measurement uncertainty u(P) of the SEM measurements was calculated as 3% of the measurand's average value (Velkova, 2011). The reported average surface roughness measurements are also provided with their associated expanded uncertainty, U, (at 95% confidence level) which was determined by following an established procedure (Leach, 2001) and by adapting recommendations given for surface roughness measurements in a separate study (Tosello et al., 2012).

Additional data on the carried out uncertainty analysis and calculations is provided in Appendix A.

4.4   Results and Discussion

This section discusses the results obtained after each process step and includes the detailed dimensional analysis of the QR codes' micro and sub-micron structures.

4.4.1 Laser milling

4.4.1.1 PS laser milling

Fig. 4.5 shows the micro-scale QR code generated by PS laser ablation. As the PS laser machined features had tapered side walls, the measurements of their widths were taken at the bottom of the protrusions representing the black squares/pixels in the QR code.

The average depths and widths of one pixel in the bitmap image of the "large" QR code are provided in Table 4-5. The table also includes the mean of the overall size of the QR code.

Table 4-5 "Large" QR code dimensions

Pixel Width (X) (µm)	Pixel Width (Y) (µm)	Pixel Height (µm)	Overall QR Code Width (X) (µm)	Overall QR Code Width (Y) (µm)
98.62 ± 6.12	98.83 ± 6.06	13.92 ± 1.06	2769.65 ± 167.26	2771.83 ± 166.78
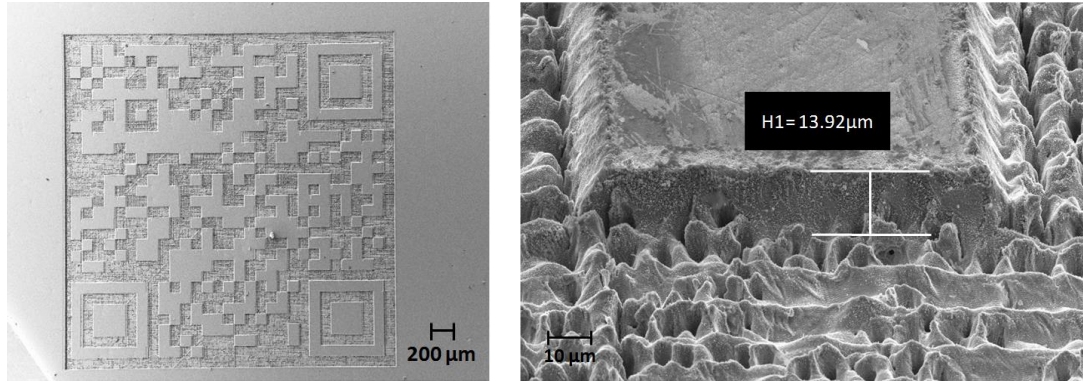
a) Overall view of micro-scale QR code   b) A magnified image of the micro-scale QR Code

Figure 4.5 Micro-scale QR code generated by PS laser ablation

It can be seen in Fig. 4.5 that the QR pattern was milled according to the scaled bitmap image and each pixel was textured with self-organised patterns. The average height of the PS laser milled fields, the white pixels of the QR-code, was estimated to be 13.92 μm (see Table 4-5) which differs from the targeted value of 10 μm, and also there was a draft angle on their walls. The functionality of the structured pattern, the QR code, can be affected by the dimensional accuracy of the milled square pockets but not by the depth variations and the surface texturing effects. However, the surface texturing might adversely affect the μIM process, in particular the part demoulding, if the textured fields represent a substantial part of the part surface area but this is not the case in the anti-counterfeiting applications.

The average widths at the top and the bottom of the measured QR pixels were 83.07 and 98.62 μm in the X direction and 83.04 and 98.83 μm in the Y direction, respectively (Table 4-5). The average pixel widths both at the top and bottom are considerably larger than the targeted values of 75 μm. Also, the overall average dimensions of the "large" QR code are bigger, 2.770 and 2.772 mm in X and Y directions respectively as stated in Table 4-5. These discrepancies are mostly due to not introducing a compensation of the beam diameter, 15 μm, in the laser milling strategies and also to some extent could be attributed to measurement errors as the edges of the QR code pixels are not well defined. It can also be seen in Fig 4.5
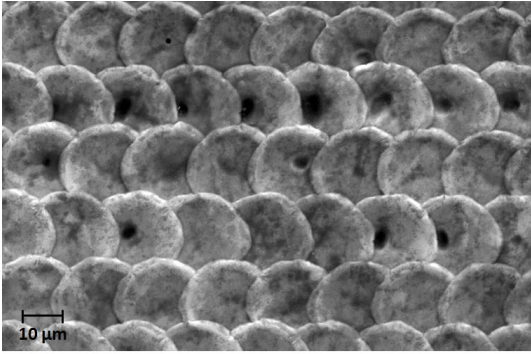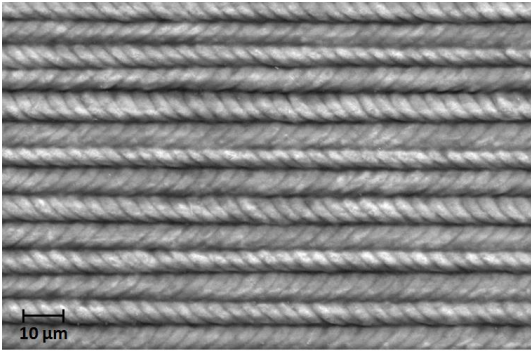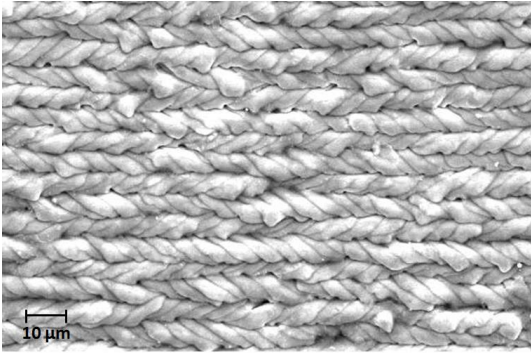
that some of the ablated material was re-deposited on the edges of the pockets/ pixels of the QR code that can lead to a further increase of the measurement uncertainty. Overall, these results are encouraging but they also show that further work is required to optimise the laser milling process and thus to improve the quality of the machined structures.

Finally in Fig 4.5b it can be observed that the pockets/pixels of the QR code were successfully textured with self-organised structures consisting of an array of relatively high aspect ratio micro holes with approximately 4.89 μm diameter. In addition, surface roughness measurements of the bottom / floor of the machined pockets were carried out using the Confocal Microscope and the Ra roughness value is 1.462 ± 0.06 μm.

4.4.1.2 NS laser milling

Table 4-6 reports the results of the surface roughness measurements after the NS laser machining of the 10x10 mm fields on samples 1, 2 and 3 that were measured using a sampling length of 0.8 mm and an evaluation length of 4 mm respectively in accordance with ISO 4288: 1997 (ISO 4288, 1997) . Measurements were carried out diagonally across the machined fields to give the most accurate roughness measurement. The obtained average roughness values and the corresponding SEM images of the laser machined fields on samples 1, 2 and 3 are provided in Table 4-6.

Table 4-6 Average surface roughness measurements of NS laser machined fields.

Sample	Ra (µm)	Image of machined surface
1	0.22 ± 0.03	
2	0.16 ± 0.01	
3	0.26 ± 0.03	

A comparison of the results in Table 4-6 shows that the best surface roughness, R_a value of 0.16 µm, is achieved on Sample 2. However, the surface roughness of all samples is comparable to that achievable after micro milling and thus can be considered acceptable for producing µIM tooling inserts. Thus, it is necessary to analyse the XRD results to determine whether NS laser ablation can be used as an alternative component technology to the PS laser ablation in the proposed process chain. Fig 4.6 shows the X-ray diffraction results of the as-

received Vit 1b sample workpiece, sample 4, and after the NS laser machining of samples 1, 2 and 3. The typical broad diffraction maxima in the XRD pattern can be observed in Fig 4.6a that depicts the fully amorphous characteristics of the as-received Vit 1b sample. This is as expected and the XRD results are identical to those reported by other investigations of amorphous Zr-Ti-Ni-Cu-Be alloys (Waniuk et al., 2003) .

a)   As-received workpiece

b)   sample 1
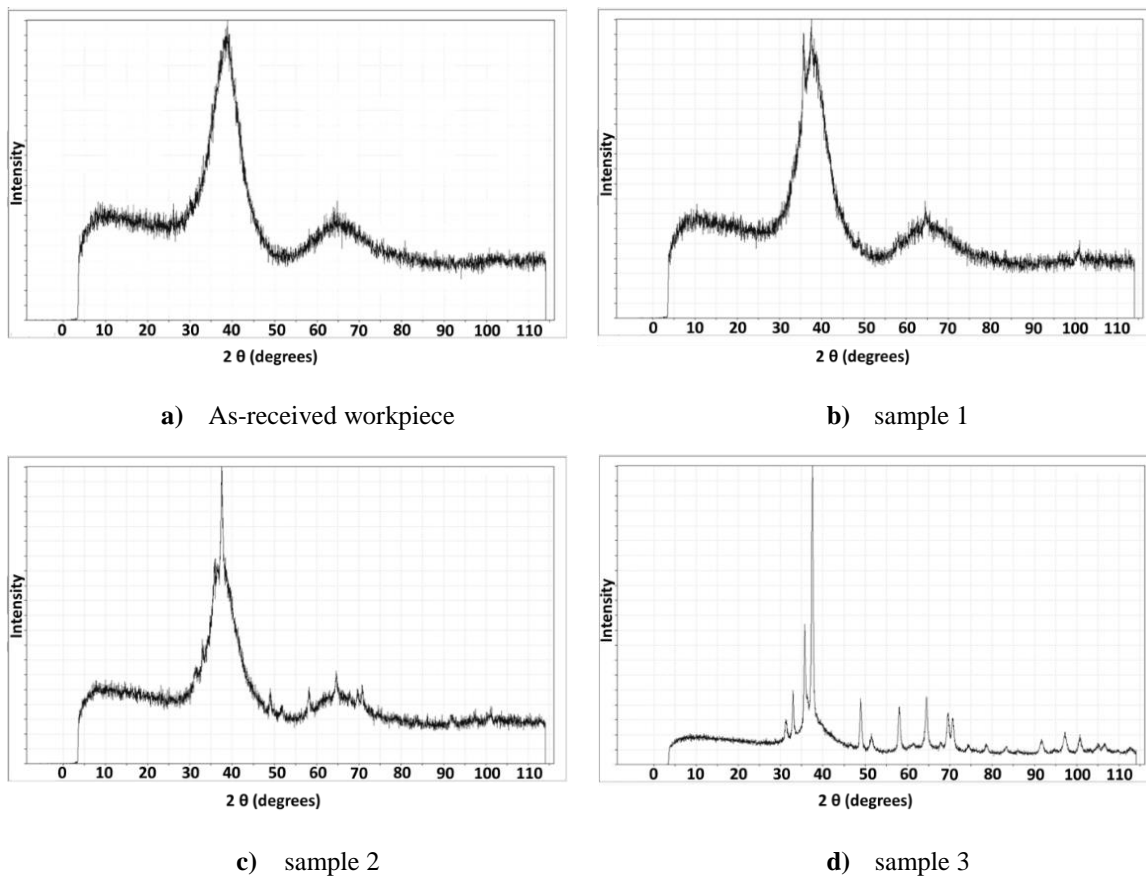
c)   sample 2

d)   sample 3

Figure 4.6 XRD Results for the as-received and laser machined samples

In Figs 4.6b and 4.6c it can be observed that there are a few weak but sharp crystalline peaks superposing on the broad humps meaning that they are still predominantly amorphous. Whereas for the sample 3 in Fig 4.6d there is a substantial increase in sharp crystalline peaks that indicates a substantial increase of the crystalline phase in the Vit 1b material. These

results concur with those reported in another investigation where it was demonstrated that the non-crystalline morphology of a Mg-based BMG could be retained after optimising the NS laser ablation process (Lin et al., 2012). Thus, taking into account the surface roughness and XRD results obtained on the Vit 1b samples it can considered that after some further optimisation of the NS laser ablation process it will be possible to achieve the necessary micro machining response to potentially replace PS laser ablation in the proposed master making process chain.

4.4.2 FIB milling

a) Overall view of Nano-scale QR code b) A magnified image of the nano-scale QR code
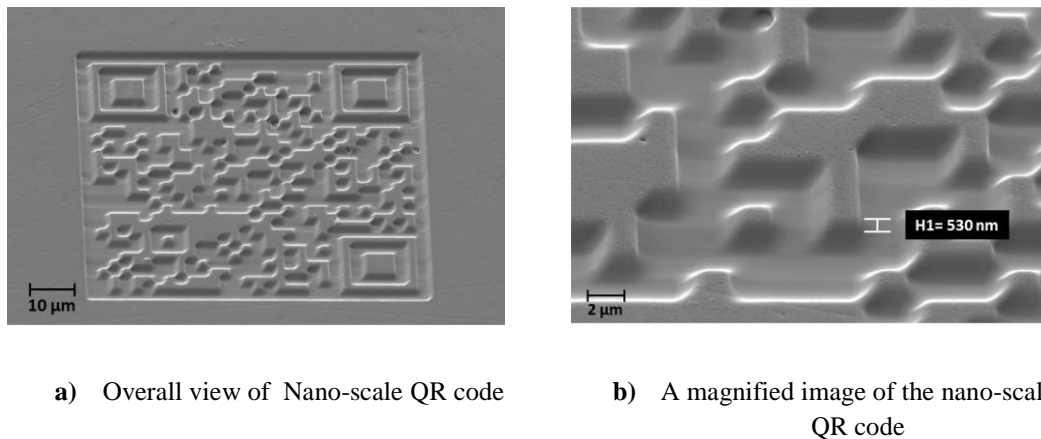
Figure 4.7 Nano-scale QR code generated by FIB milling

Fig. 4.7 shows the nano-scale QR code structure fabricated by FIB milling. It can be judged from this figure that the structure was milled satisfactorily on the BMG workpiece. Similarly to the results reported in the previous section, Table 4-7 presents the average values for the measured heights and widths of the smallest features. Also, Table 4-7 includes the average values of the QR code overall size.

From these measurement results it can also be seen that the average widths in the X and Y directions at the bottom of protrusions are larger than the nominal value of 2.59 μm. Again, this difference could be due to both not introducing a compensation for the beam diameter, 40nm during the FIB machining and also due to measurement errors as the pixels' edges are rounded and difficult to locate precisely. Besides these two factors, the discrepancies could also be the result of calibration and set-up issues associated with the FIB system used. The table also includes the overall average width of the nano-scale QR code, 76.63 and 78.11 μm in X and Y directions, respectively. Taking into consideration these values and also that each side includes 29 pixels, it can be calculated that the average widths of the pixels in X and Y directions are 2.64 and 2.69 μm, respectively. These two values are very close to the nominal pixel size of 2.59 μm. Again, as it was the case with the bigger QR code, through some process optimisation, the FIB machining accuracy can be improved but nevertheless as it is, the nano-scale QR code has the required resolution to fulfil its functional requirements.

Table 4-7 "Small" QR code dimensions

Pixel Protrusion Width (X) (μm))	Pixel Protrusion Width (Y) (μm)	Pixel Height (nm)	Overall QR Code Width (X) (μm)	Overall QR Code Width (Y) (μm)
2.98 ± 0.21	3.09 ± 0.20	530.0 ± 12.6	76.63 ± 4.60	78.11 ± 4.69

The height measurements of the BMG insert are given in Table 4-7. It can be observed in Fig. 4.7b and Table 4-7, that the average height of the structures was estimated to be 530 nm while the specified target value was 900nm. Again, this result could be explained both with not calibrating the sputtering process, in particular the sputtering rate for the selected FIB milling parameters in Table 4-3, and also with the measurement errors associated with the quality of the "pixel" edges. An investigation of different factors that affect the accuracy of the FIB

milling process was carried out in another research (Velkova, 2011) . The findings of this study showed that the deviations in sizes of complex 3D structures could be kept within 2 to 5 % of their nominal dimensions by employing a specially developed methodology for optimising the layer-based FIB milling process. As this research reports a feasibility study, the process settings were not optimised using this methodology. Thus, through such optimisation it will be possible to improve substantially the accuracy of the FIB milling process.

Finally, Fig. 4.7b shows that there is a draft angle on the vertical walls of the milled pockets. This phenomenon is due to the positional drift of the pattern during the FIB milling process that is caused by relatively long machining times. As it can be judged from Fig. 4.8, the nano-scale QR code was successfully structured over the pre-existing micro topography created by PS laser milling. The alignment of the nano-scale pattern was performed using the approach described in the previous section and the positional error was estimated to be less than 2μm.
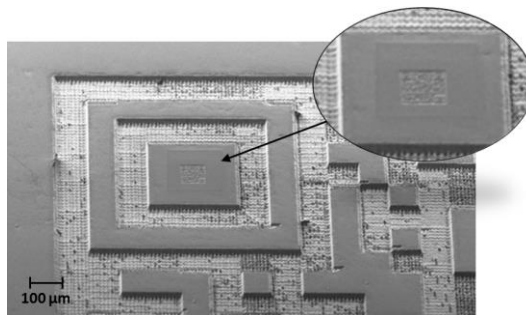
Figure 4.8 Nano-scale QR code produced on the top of the micro-scale QR pattern

4.4.3 Micro-injection moulding

Utilising the BMG insert for µIM, polymer replicas in TOPAS 5013X (COC) were produced. Since the "small" QR code posed the greatest challenge, the replicated depths of the pattern were measured and compared for the five process settings in Table 4-4 and thus to determine the set of parameters which gave the best replication results. The surface topography was inspected using the SEM, whilst the instruments used to compare the QR code pattern depths were the AFM and the confocal microscope.

Figs 4.9a to 4.9f depict the SEM images of the polymer replicas produced with the five µIM process settings in Table 4-4, together with the corresponding AFM and confocal microscope surface inspection results. Studying the SEM images in Fig 4.9, it can be judged that the "small" QR code with sub-micron features was replicated satisfactorily. The best replication results were obtained with the higher mould temperatures of 130°C and 140°C. This is as expected because by increasing the mould temperature, the bulk temperature of the polymer can be kept sufficiently high to ensure the complete filling of the sub-micron surface structures (Griffiths et al., 2007; Tosello et al., 2010a) .
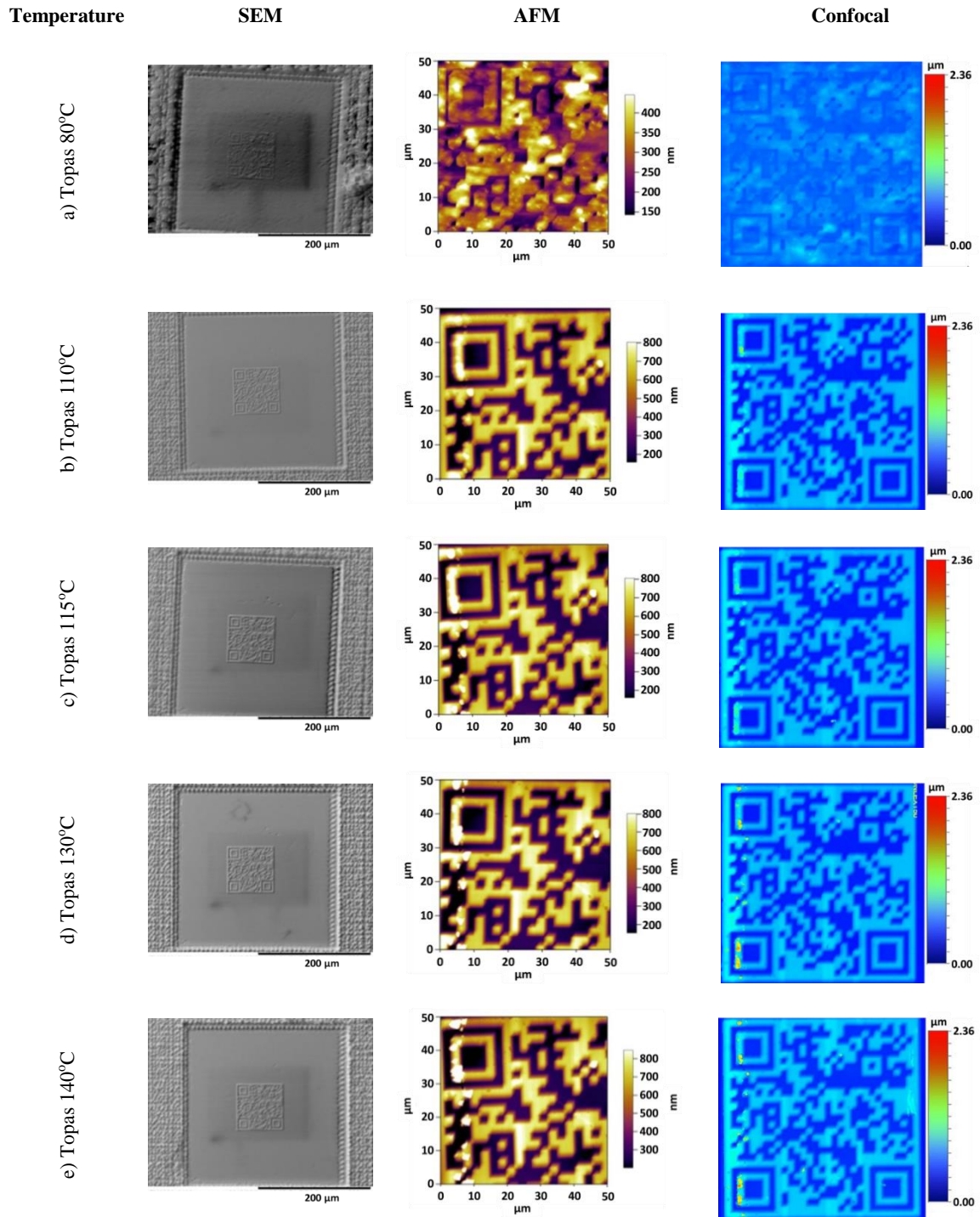
Figure 4.9 SEM images of µIM parts together with the AFM and confocal microscope surface inspection results

A histo-distribution generated from the AFM measurements of the inspected samples is presented in Fig 4.10 and concurs with the SEM surface analysis results. As can be observed in the figure the pattern height is much lower at the mould temperature of 80°C. This is

because the bulk temperature of the polymer cannot be kept sufficiently high and so the viscosity of the Topas 5013 melt remains relatively high, too. Consequently, the complete filling of the "small" QR code pattern cannot be achieved and thus resulting in premature solidification and incomplete filling of the small QR code features. From Fig. 4.10, it can also be observed that as the mould temperature increases progressively the polymer viscosity gets sufficiently low to fill the sub-micro features, and thus the cavities are filled much better. The best height replication results were obtained for the 130°C and 140°C mould temperature settings.
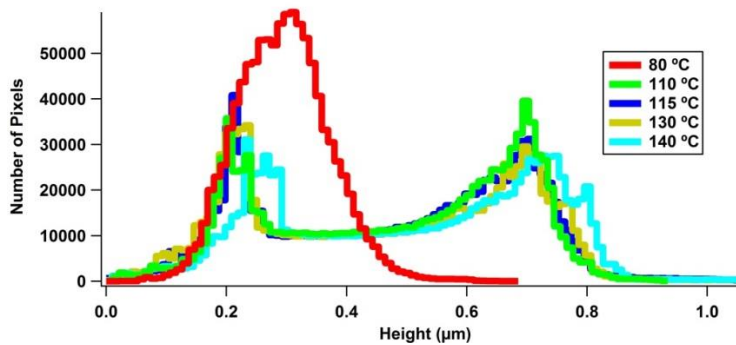
Figure 4.10 AFM Histo-distribution for the analysed polymer samples
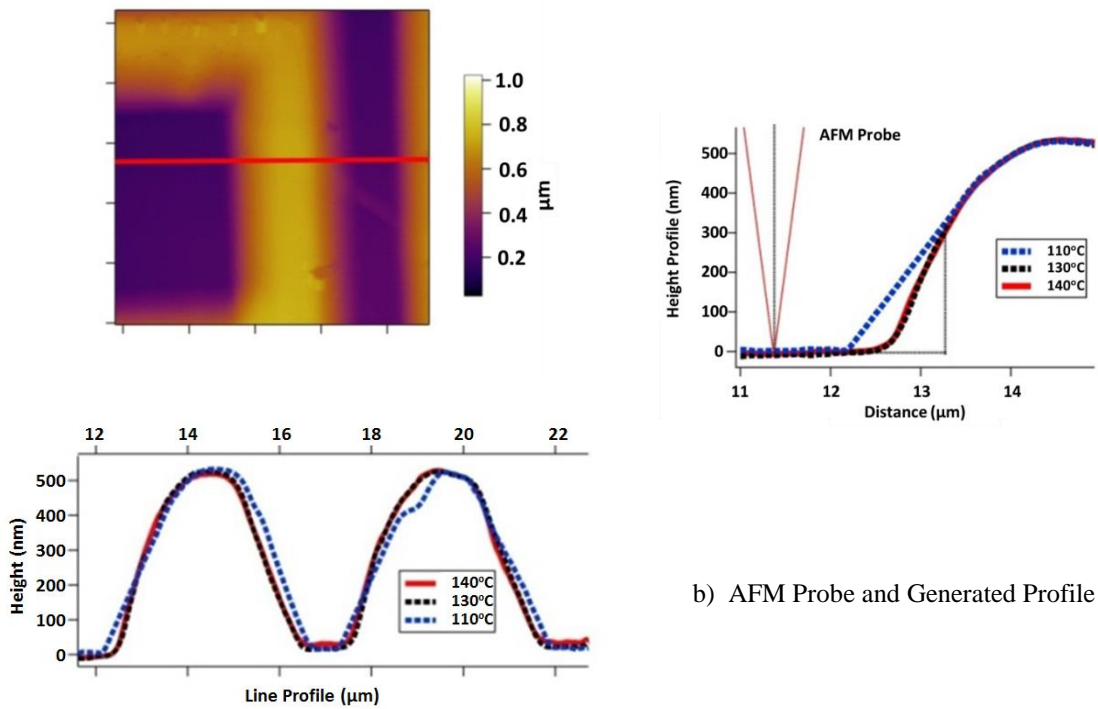
b) AFM Probe and Generated Profile

a) AFM Profiles of the top left feature

Figure 4.11 Profiles of the top left feature of the "small" QR code

Based on the AFM scan data, a profile of the top left feature of the "small" QR code was generated. The profile is presented in Fig 4.11 and shows that the 130° and 140° C samples have sharper "pixel" edges then those at 110^oC. In addition, it can be observed that the feature depth is approximately 500 nm and this is in agreement with the confocal microscope results, below. The wall side angles of the QR grid are $37.2°$, $37.2°$ and $16.6°$ for the samples produced at 140^oC, 130^oC and 110^oC, respectively. Figure 4.11b depicts the geometry of the AFM probe in relation to the line section of the QR grids for the 140^oC, 130^oC and 110^oC trials, respectively. As the angles are less than $60°$ the probe geometry did not affect the results. This shows again that the samples made at 130 and 140^oC are of better quality than

those produced at 110°C. Whilst the profiles of the 130°C and 140°C samples are virtually identical and steeper than the 110°C sample, they still cannot be considered as edge-like. This is most likely due to the draft angle on the vertical walls of the FIB milled fields on the BMG insert and also possibly due to some trapped air in the mould (Zhang et al., 2012b; Heckele and Schomburg, 2004) . As suggested in literature the latter problem could potentially be minimised by air evacuation from the mould just before injection (Attia et al., 2009; Giboz et al., 2007; Heckele and Schomburg, 2004) .

An additional analysis to one of selected line sections of the insert and the polymer replicas for each of the 140°C, 130°C 115 ^{o}C, 110°C and 80°C µIM trials was carried out by using the confocal microscope data sets. In particular, the replication quality of the FIB structures on the replicas at these temperature settings was assessed by applying the methods for the Volume, Sa and Average Step height ratios as detailed in Section 4.3.6.3. The results are shown in Table 4-8.

Table 4-8 Results of volume , Sa and average step ratios for µIM trials.

			Volume ratio	Sa ratio	Step ratio
Insert			1.000	1.000	1.000
Polymer replicas	Mould Temp (°C)	80	0.165	0.271	0.160
		110	0.821	0.921	0.928
		115	0.806	0.941	0.934
		130	0.913	0.956	0.945
		140	0.970	0.956	0.947

The best average step height ratios are 0.945 and 0.947 respectively, and they indicate that the 140°C mouldings are marginally better than the ones produced at the mould temperature of

130°C. Collectively, the best replication accuracy was obtained for the 130° C and 140°C mould temperature settings and this is in agreement with the results from the AFM inspection. It can also be observed in Table 4-8 that the Sa Ratio for both the 130° C and 140°C mould temperature trials is the same. Whilst, the volume ratios are 0.913 and 0.970 for the the130^o C and 140°C mould temperature trials, respectively. The latter Volume Ratio indicates that a slightly better fill has been achieved for the 140°C mould temperature setting than that obtained for the 130°C trials. This analysis has showed clearly that the surface quality and the profiles of the replicated "small" QR codes were satisfactory for the considered application. Therefore, given that the replication quality for 140°C mould temperature setting are slightly better than that obtained at 130°C, only the parts from the 140° C trials were used to investigate further the replication fidelity for both the "large" and "small" QR codes.

4.4.3.1 "Large" QR code

The "large" QR code produced by PS laser milling on the BMG insert was replicated well as far as it can be judged by comparing the image of the replica in Fig. 4.12 with the insert in Fig. 4.5.

(a)   (b)
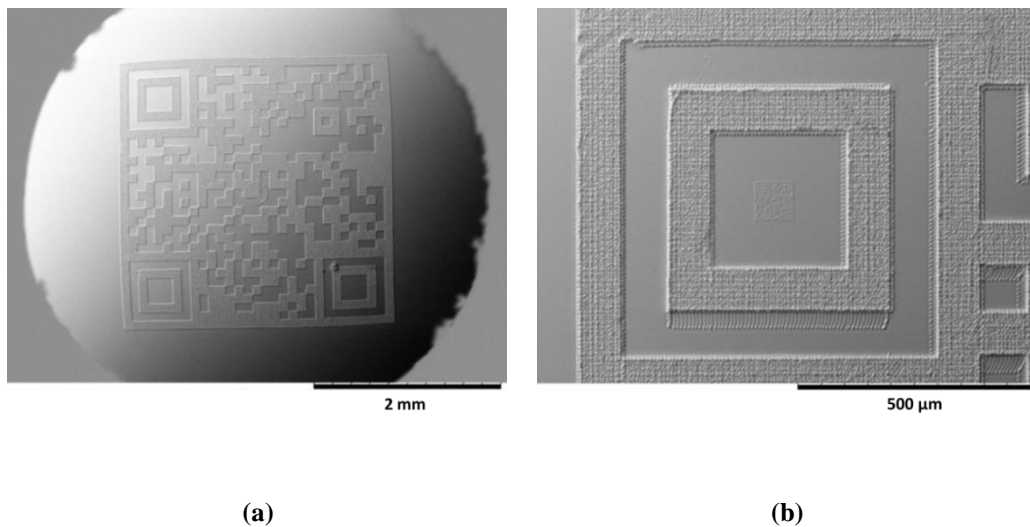
Figure 4.12 Replicated "large" QR Code (a) overall view (b) top left features of the code

The PS laser texturing of the "large" QR code white pixels was replicated successfully on the polymer parts as can be seen clearly in Fig 4.13 and "nub" structures with relatively high aspect ratio and an average diameter of 4.09 μm were created. This average value was calculated based on the confocal microscope inspections of three Topas parts. In addition, the average Ra surface roughness of the parts' textured surfaces is 1.843 ± 0.25 μm. Comparing the diameters of the micro-holes and Ra values of the PS laser textured surfaces on the BMG insert with the diameters and Ra values of the replicated "nub" structures on the Topas parts, it can be judged that the texturing was replicated with relatively good fidelity. The use of BMG inserts for replicating such texturing effects on surfaces is very important due to their very high wear resistance and thus being capable of retaining the surface functionality for more μIM cycles.
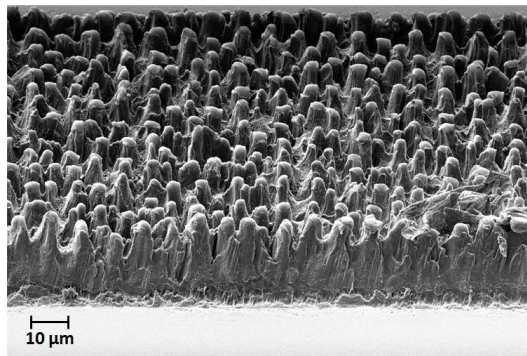
Figure 4.13 Surface texturing of the "large" QR Code replica

The results from the inspection of the smallest micro scale features of the "large" QR code replicas together with the average overall size of the code are provided in Table 4-9. If the dimensions of the pixels on the COC replicas and the BMG insert are compared in Tables 4-5 and 4-9 the deviation of the height is 3.52 % while for the width is 1.58% and 1.22% in the X

and Y directions, respectively. These deviations are higher than the expected typical shrinkage values of 0.4 to 0.7% for this material but they could be explained both with some measurement errors and also the used injection moulding parameters which were not fully optimised.

The average width dimensions of the 29 "large" QR pattern's pixels can also be calculated based on the overall size of the code in Tables 4-5 and 4-9. As stated before, these dimensions are likely to be more accurate estimates of the pixel sizes because the measurement error is "shared" between the pixels constituting the QR code. Thus, the average widths can be estimated to be 95.51 and 91.73 μm in the X direction and 95.58 and 91.64 μm in the Y direction for the BMG insert and the COC replicas, respectively. For the COC replicas, there is an average 5.7 μm difference with the as-measured pixel cavity values reported in Table 4-9 in particular 97.06 μm and 97.62 μm. This again can be explained with the measurement errors incurred whilst inspecting the individual pixels. Similarly, for the BMG insert, the average error between the estimated and the actual pixel sizes reported in Table 4-5 is approximately 3.18 μm. This means that the estimated average errors incurred when measuring the overall size of the "large" QR code on the BMG insert and COC replicas are 3.18 μm and 5.7 μm respectively. If these two error values are taken into account in the shrinkage calculation, the average percentage difference between the overall side lengths of the replicated large QR code and the laser milled BMG QR code is approximately 4.13%. From a statistical point of view, using the paired-sample t test, it can be stated with 99% confidence that the difference between the means of the BMG insert and the five COC parts is significant and they can be predominantly attributed to shrinkage. In this case, the actual shrinkage is higher than the expected typical shrinkage values reported for this material. However, it should be noted that by subjecting the COC material to a high holding pressure should help minimise material shrinkage. In particular, one of the techniques that have been

suggested to decrease the effect of shrinkage is to increase the holding pressure however this increases also the stresses inside the mouldings (Giboz et al., 2007) . Thus, the results were not expected taking into account that a high holding pressure was used, 1300 bar, that is much higher than the recommended packing pressure for COC of 600 bar.

Overall, considering that this is only a feasibility study, and none of the component processes in the proposed chain have been fully optimised it can be stated that the "large" QR code was replicated with a relatively good fidelity. Also, it is clear that in order to produce a product with higher accuracy the laser machining and the micro-injection moulding stages in the process chain have to be optimised further and thus to improve the quality of replicated micro features. The analysis of the replication stage shows that the results can be affected significantly by the outcome of the preceding stages in the process chain, in particular the laser milling. Also, this feasibility study reveals some of the challenges in performing an effective dimensional quality control and reliable manufacturing when precise micro structures have to be produced.

Table 4-9 Replicated "large" QR code dimensions

Pixel Width (X) [μm]	Pixel Width (Y) [μm]	Pixel Height [μm]	Overall Width (X) [μm]	Overall Width (Y) [μm]
97.06 ± 6.09	97.62 ± 5.94	13.43 ± 0.93	2660.03 ± 167.46	2657.65 ± 161.95

4.4.3.2 "Small" QR code

Fig. 4.14 shows that the "small" QR code was replicated successfully on the COC parts. The average heights and widths of the smallest features together with the average overall size of the "small" QR code are provided in Table 4-10. If the dimensions of the smallest features on the COC replicas and the BMG insert are compared in Tables 4-7 and 4-10 the deviation of the height is 6.72 % while for the width is 3.36% and 6.15% in X and Y directions,

respectively. Again, this is higher than the expected typical shrinkage values of $0.4 - 0.7\%$ for this material. The average dimensions of the 29 "small" pixels was also calculated based on the overall size of the QR code in Tables 4-7 and 4-10, in particular the average widths were approximately 2.64 μm in the X direction and 2.69 μm in the Y directions for both the BMG insert and the COC replicas. Thus, the average errors incurred when measuring the overall size of the "small" QR code on the BMG insert and COC replicas is 0.37 μm and 0.225 μm respectively and it is mostly due to the edge definition as it is shown in Fig 4.15. If these two error values are taken into account in the shrinkage calculation, the measurement errors are much smaller, and the average percentage difference between the overall side lengths of the replicated "small" QR code and the FIB milled QR code on the BMG insert is approximately 0.05%.
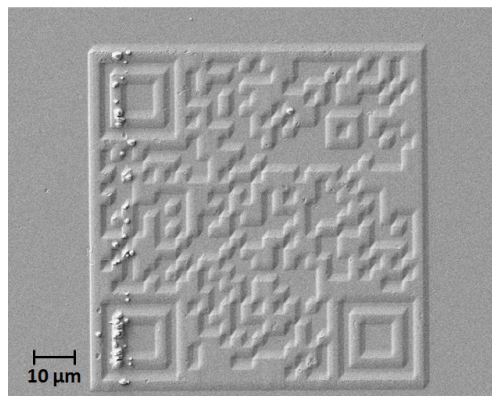
Figure 4.14 Replicated small scale QR code.

From a statistical point of view, using the paired-sample t test, it can be judged with 80% confidence that there is a significant difference between the means of the small QR code overall side length of the BMG insert and the five COC replicas. Therefore, it is not possible to state unequivocally if the observed difference is significant or whether it may be attributed to stochastic factors. This is reinforced even further when the magnitude of the measurement

uncertainty is also taken into consideration with respect to the estimated percentage difference and the number of samples available.
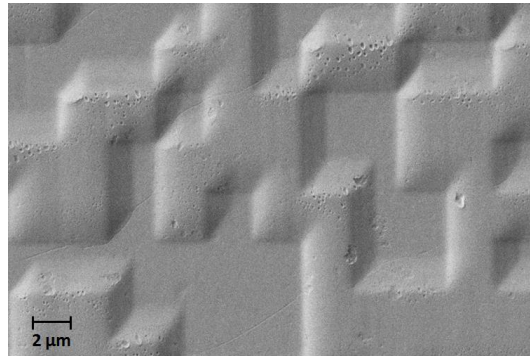
Figure 4.15 Feature edge quality of the replicated "small" QR code.

As stated above, in Tables 4-7 and 4-10, there is also a 6.72 % difference between the average height of the insert and the replicas that again could be attributed to the measurement errors, material shrinkage and not fully optimised replication process. Also, the research had revealed potential challenges in performing an effective dimensional quality control and reliable manufacturing at sub-micron scale.

Table 4-10 Replicated "small" QR code dimensions

Pixel Width (X) (μm)	Pixel Width (Y) (μm)	Pixel Height (nm)	Overall Width (X) (μm)	Overall Width (Y) (μm)
2.88 ± 0.18	2.90 ± 0.18	494.4 ± 12.6	76.53 ± 4.60	78.00 ± 4.69

4.5   Conclusions

A cost effective process chain for achieving FLSI in mass produced miniaturised devices was investigated in this feasibility study. It integrates compatible and complementary structuring and replication technologies by utilising a Zr-based BMG with very attractive mechanical properties. The capabilities of laser machining as a micro structuring technology were

combined with those of the FIB milling to fabricate replication inserts incorporating micro and sub-micron structures. Then, to demonstrate the viability of the proposed master making process chain, the Zr-based BMG insert was integrated into a tool to produce a batch of thermoplastic parts by µIM.

The following conclusions about the proposed master making process chain and its component technologies could be drawn from this research.

- The NS laser machining showed that it is possible by proper selection of the processing settings to machine successfully Zr-based BMG workpieces with an acceptable surface integrity for µIM without triggering significant changes in the BMG short range atom arrangements. The results demonstrated that the required surface quality for successful replication can be achieved.

- With the selected PS laser processing parameters, it was possible to satisfactorily texture the BMG insert surface with high aspect ratio self-organised structures. Despite the fact that the selected PS laser machining parameters showed limitations with respect to the resulting structuring quality, it can be concluded that the PS laser process is a promising component technology for master making and also for achieving FLSI in replication tools.

- The viability of using Zr-based BMG masters to enable integration of compatible and complementary micro and sub-micron structuring and replication technologies for serial fabrication of FLSI thermoplastics components was demonstrated.

- The experimental investigation identified the factors affecting the performance of the proposed PS-FIB-µIM process chain. In particular, the following factors are considered to have the highest impact: the used process settings for its different component technologies, the Zr-based response to structuring technologies, e.g. PS Laser and FIB milling, with different specific processing energies and the metrology issue in inspecting

multi-scale structures. However, it was difficult to quantify their effects on the overall performance of the proposed process chain.

Collectively, the results demonstrate that there is good process compatibility and complementarity between the component technologies in the proposed process chain, especially for the length scale ranges aimed at this research. Such a process combination can therefore be used for the mass production of polymer parts incorporating different length scale features in one step.

CHAPTER 5
PROCESS CHAIN DESIGN FOR ACHIEVING LENGTH SCALE INTEGRATION IN BMG INJECTION MOULDING INSERTS

5.1 Introduction

In this chapter, another novel process chain for serial production of polymer based FLSI devices is proposed. In the previous chapter, the capabilities of PS laser machining as a micro-structuring technology were successfully combined with those of the FIB milling to fabricate BMG replication inserts incorporating multi-scale structures. At the same time, it should be noted that the optimisation of the laser processing parameters will not be enough to produce sufficiently smooth surfaces on the microscale features for direct follow up FIB sub-micron and nano structuring. Thus in this chapter an alternative novel BMG enabled master-making process chain was investigated in order to overcome this issue and also to develop cost effective manufacturing capabilities for achieving FLSI in products incorporating 3D features. In particular, in the proposed process chain, the PS Laser + FIB milling pair of processes was replaced by the μMilling + HE and HE + FIB process pairs, which were also identified in Chapter 3 as being suitable to be integrated in process chains. Furthermore, as outlined in Chapter 2, partially crystalline BMGs with their enhanced wear and fatigue properties, can offer potential advantages when utilised to fabricate replication tooling. Thus this research also explores the concept that the morphology of the BMG workpiece could be controlled to achieve a better wear resistance and fatigue properties whilst simultaneously retaining a satisfactory machining response at the submicron and nano scales.

Within this context, the objectives of the research presented in this chapter are:

- to design and experimentally validate a process chain, composed of three complementary technologies, namely μMilling, HE, and FIB, for the production of partially crystalline Zr-based BMG inserts incorporating micro and nano length scale functional features.

- to validate the replication capabilities of the produced Zr-based BMG inserts' for serial fabrication of thermoplastic polymer FLSI parts by injection moulding.

- to investigate systematically the factors affecting the performance of such masters

- to study the machining response of a partially crystalline BMG workpiece in order to investigate the robustness of the proposed process chain and its effects on the master's properties, especially when utilized for micro-injection moulding.

The rest of the chapter is organised as follows. Section 5.2 presents the rationale behind the design of the proposed master-making process chain. The component technologies utilised to achieve FLSI in the fabricated BMG masters and polymer parts are also described. Then, Section 5.3 describes the experimental set-up employed to validate the capabilities of the proposed process chain. Finally, in sections 5.4 and 5.5 respectively, the obtained results are presented and discussed, and conclusions are made.

5.2   Process Chain Design

The sequence of component technologies in the proposed process chain is shown in Fig. 5.1. In particular, three technologies, namely micromilling (μMilling), thermoplastic forming (TPF) and focused ion beam (FIB), are integrated to fabricate Zr-based BMG inserts. Then, the inserts are used for micro injection moulding (μIM) of microfluidic devices in a commonly used polymer material to assess the capabilities of the proposed process chain.

The process chain starts with an indirect tooling step due to two main considerations. First, it is much easier to machine Al alloys than BMGs with high accuracy and surface integrity and also the tool wear is expected to be much less. Secondly, it is often faster to machine "negative" structures, e.g. channels in the Al alloy, than their respective "positive" protrusions as much less material has to be removed (Tang et al., 2006). Also, it is important to note that the literature review has revealed that no studies were conducted on μMilling of Zr-based BMGs and only their machining response at the meso- and macro scale, i.e. by milling, turning and drilling, has been investigated (Bakkal et al., 2005, 2004; Bakkal and Nakşiler, 2009; Fujita et al., 2005) . The results from the meso-end milling investigation showed that the required cutting forces for the Zr-based BMG were higher than those for the aluminium for all feed rates (Bakkal and Nakşiler, 2009) . Furthermore, the macro-scale turning and drilling studies concluded that tool wear is expected to be a problem for machining of BMGs. (Bakkal et al., 2005, 2004) . Taking these considerations into account the machining of an Al master is the first step in the proposed process chain.

The TPF process is the next technology in the process chain and it is used as an intermediate step to produce a BMG replica of the Al plate with its micro structures fabricated by μMilling. The replication is performed above the BMG glass transition temperature and therefore the material flows readily into the small features and asperities of the Al master. Whilst this is very important for replicating structured surfaces, it can make the non-destructive separation of the BMG insert from the Al master difficult and even impossible due to the frictional and mechanical interlocking between them. So, it may be necessary to dissolve the Al plate and thus to safeguard the replicated micro structures. This is one more reason to select a tooling grade Al for fabricating the TPF plate. In this research, the Al master was selectively dissolved in an alkaline solution, in particular sodium hydroxide, in order to release the BMG replica. In selecting the TPF process settings it was important to find a

processing window that allows the morphology of the Zr-based BMG to be maintained and thus to benefit from the material's attractive mechanical and physical properties. This is even more important when FLSI has to be achieved in the replication master as any follow up structuring step at sub-micron and nano scale can be affected by any material inhomogeneity.

The third step employs FIB milling to produce sub-micron structures on top of a pre-existing micro features. This technology can be applied for patterning accurately and cost effectively only relatively small areas, e.g. up to 100 X 100 µm without stitching, due to its low material removal rates. Therefore, less demanding meso and micro structures have to be produced using other technologies, e.g. µMilling and TPF in the proposed process chain, to define the insert's overall geometry and thus to prepare it for the subsequent FIB milling.

Finally, to demonstrate and also to assess the replication capabilities of the produced micro- and nano- structured BMG inserts, they were integrated into an injection moulding tool to produce small batches of thermoplastic microfluidic devices that required FLSI in the polymer replicas to be achieved in a single step. The capabilities of the above component technologies together with some specific considerations in integrating them in the proposed process chain are discussed in the following sub-sections.
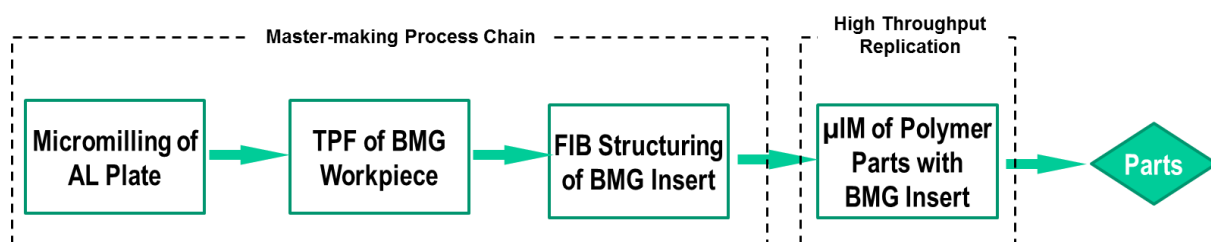
Figure 5.1 Overall process chain design

5.2.1 Micromilling

μMilling is the most cost effective technology for producing 3D complex micro structures (Uriarte et al., 2006; Brousseau et al., 2010; Fleischer and Kotschenreuther, 2007) . In particular, relatively high removal rates can be achieved compared with other micro machining technologies (Brousseau et al., 2010; Fleischer and Kotschenreuther, 2007) and tooling inserts from a wide range of metals can be produced cost effectively. Furthermore, the resulting surface quality is usually better than that achieved by μEDM or laser machining. (Fleischer and Kotschenreuther, 2007) . So, production quality tools can be produced to withstand a large number of replication cycles (Fleischer and Kotschenreuther, 2007; Dirckx et al., 2006) . The use of μMilling to machine Al and steel tools has been extensively investigated by researchers (Tang et al., 2006; Aramcharoen and Mativenga, 2009; Bissacco et al., 2005; Schaller et al., 1999; Schmidt and Tritschler, 2004) . Collectively, it is evident from these studies that it is more cost effective to machine tooling grade Al alloys when there is a need to produce parts with micro features with a higher dimensional accuracy. This is very important in the context of the specific application in this research, namely the machining of TPF plates. In particular, high surface finish, high accuracy and minimum burrs become essential requirements for the machined Al TPF masters. It is important to point out that due to the feature sizes and the overall dimensions of micro machined parts conventional finishing methods such as grinding or polishing for burr removal and for improving the surface quality of the μMilled parts are not anymore feasible. Thus, in the context of the proposed process chain, two potential problems in employing μMilling have to be considered, particularly the presence of burrs and relatively inferior surface finish compared with inserts produced by etching and electroforming. Burr generation in μMilling was also investigated by researchers (Tang et al., 2006; Aramcharoen and Mativenga, 2009; Bissacco et al., 2005) . The research results show that it is possible to minimise or even prevent the burr formation

and improve the resulting surface quality by optimising the cutting parameters and machining strategies (Dimov et al., 2004) . Thus, it is possible to avoid any post processing finishing steps that are difficult or impossible to perform due to the feature sizes.

The mechanism of surface roughness formation is also very complex and process dependent. In μMilling, the ways in which the side step and step over movements are realized in tool paths could lead to inconsistencies in the cutting conditions and hence affects negatively the resultant surface finish. In part programs, these two issues can be addressed by selecting appropriate machining strategies. Other factors that have a direct or indirect effects on the resultant surface integrity during machining include: depth of cut, feed rate per tooth, cutting speed, cutting tool wear, use of cutting fluid/air/oil mist, (Dimov et al., 2004; Cardoso and Davim, 2012, 2011) and last but not the least the workpiece material microstructure (Bissacco et al., 2005; Popov et al., 2006; Vázquez et al., 2010) . Thus, it is possible to optimise the cutting parameters and machining strategies in order to improve the surface integrity and also to minimise burr formation for the particular workpiece material in use. Investigations of the above mentioned factors were reported by a number of researchers (Dimov et al., 2004; Cardoso and Davim, 2011) . In addition, Popov et al (Popov et al., 2006) investigated the machining response of a metallurgically and mechanically modified Al, and concluded that through a refinement of material microstructure it is possible to improve significantly the surface integrity of the micro components and tooling cavities produced by μMilling.

Overall, it can be stated that by utilising the correct combination of workpiece material, namely tooling grade Al alloys, machining parameters and strategies it is possible to minimise burr formation and achieve an acceptable surface finish. These considerations together with the capability to produce 3D complex micro structures and relatively high material removal

rates, were the main reasons for selecting μMilling for producing the TPF plates and thus to use this technology as the first step in the proposed master-making process chain.

5.2.2 Thermoplastic forming

The TPF process is a net-shape processing method for replicating micro-scale features into BMG substrates in their supercooled liquid state, in particular at temperatures above their glass transition temperature (T_g) but below their crystallisation temperature (T_x). Since very big elongations can be achieved with this process at temperatures above T_g this forming technology is also called superplastic forming (SPF) (Henann et al., 2009; Kumar et al., 2009a; Schroers et al., 2007b) . A typical time-temperature-transformation (TTT) diagram of the TPF process when forming BMGs is shown schematically in Fig 5.2.
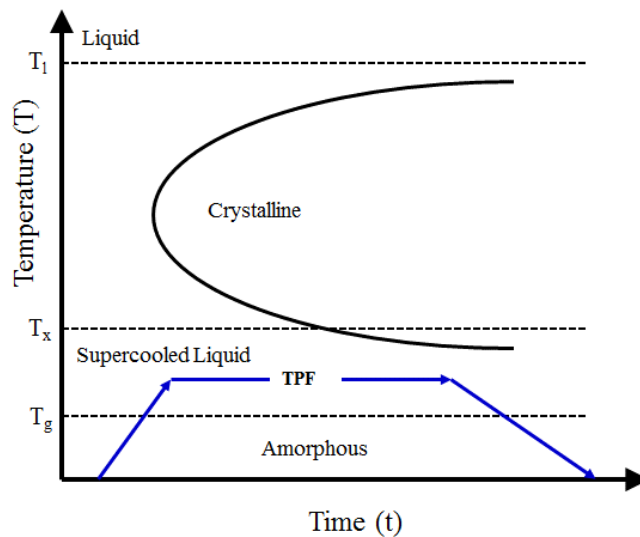
Figure 5.2 A schematic time-temperature-transformation (TTT) diagram for a typical BMG.

149

The TPF processing of BMGs includes first, heating of the workpiece/blank to a set temperature in the supercooled liquid region (SCLR), where it can be isothermally formed under a pressure, and then subsequently cooled down while the material is metastable (Henann et al., 2009; Schroers et al., 2007b) . It is reported that the BMG crystallisation during the TPF process has to be avoided, since it degrades their mechanical properties (Henann et al., 2009; Schroers, 2005) and thus can subsequently have an adverse effect on the wear and fatigue properties of the replicas. However, as it was mentioned in Chapter 2, literature reviews on wear and fatigue properties of BMGs revealed conflicting opinions when a mixed amorphous – nanocrystalline structure exists (Greer et al., 2002; Pan et al., 2010; Suryanarayana and Inoue, 2011) . With regards to wear, some researchers reported that metallic glasses could have a better wear property than the fully or partially crystalline alloys with same compositions (Gong et al., 2002; Tam and Shek, 2004) while others advocated the opposite, especially that partially crystalline metallic glasses can have a higher wear resistance than in their fully amorphous state (Anis et al., 1994; Gloriant, 2003; Liang et al., 2004; Wang et al., 2000) . In particular, Gloriant (2003) investigated the microhardness and abrasive wear resistance of zirconium-based, lanthanum-based, palladium-based metallic glasses and aluminum-based amorphous alloys and concluded that the hardness and wear resistance are both observed to be enhanced by nanocrystallization in a residual amorphous matrix. Whilst Liang et al. (2004) studied the nano scratching behaviour of a Zr-based metallic glass and the results showed that partial crystallization led to a better wear property . With regards to fatigue, Wang et al (2008a) reported that BMG composites with nano crystalline phases exhibit poorer fatigue behaviour than the fully-amorphous BMGs, while Suryanarayana and Inoue, (2011) argued that the presence of nano crystalline phases in small quantities might not have a detrimental effect. It was suggested that the metallic glasses' plasticity could be improved by incorporating a discontinuous crystalline phase into their

homogeneous glass matrix and thus to enhance their ductility and consequently their fatigue properties, too. The latter effect was observed by other researchers, too. In particular, Flores and Dauskardt (2004) reported that a Zr- based BMG matrix composite exhibited improvements in both fracture resistance and fatigue lifetime when compared with its fully amorphous counterpart while Fujita et al (2008) reported that nanocrystal dispersed Ti based BMGs with no micro-defects had a higher fatigue strength than their respective high strength crystalline alloys. Thus, a number of studies collectively suggest that the presence of some controlled partial crystallisation could provide an effective way to optimise the wear and fatigue properties of the BMG mould insert. However, the effect of such partial crystallisation on the material's FIB milling response was not investigated and this is important in the context of the proposed process chain. Therefore, the potential detrimental effects of some partial crystallisation on the resulting surface integrity after FIB milling are studied in this research, too.

The crystallisation kinetics of BMGs is sluggish and this results in a relatively large processing window in which the BMGs do not crystallise. Therefore, TPF can be judiciously "tuned" either to avoid the BMG's crystallisation (Henann et al., 2009; Schroers et al., 2007b) or possibly to trigger a controlled partial crystallisation of the workpiece. Also, since TPF is performed isothermally with subsequent low cooling rates, consequently residual stresses and part distortions can be minimized (Henann et al., 2009; Schroers, 2005) . These considerations are very important when producing BMG inserts by applying the proposed master making process chain.

Micro Hot Embossing is a specific implementation of the TPF process that is suitable for replicating microscale and high aspect ratio features on metallic glass substrates (Henann et al., 2009) . The process has been used for producing BMG components for various applications, such as mould making for fabricating micro- and nano scale features or

structures (Henann et al., 2009; Kumar et al., 2009a; He et al., 2012; Pan et al., 2008; Saotome et al., 2001) , MEMS/ NEMS (Schroers et al., 2007b, 2007a; Sharma et al., 2007) , optical gratings (Chu et al., 2007; Saotome et al., 2007) and other metallic micro components (Bardt and Sawyer, 2007) . As it is the case with all micro replication processes, the accuracy of the used masters is a very important pre-condition for any successful implementation of the TPF technology, and together with the selection of correct process settings determine the overall process performance.

The most important process parameters for forming BMGs satisfactorily in their supercooled liquid state are the embossing temperature, applied pressure and the maximum processing time (Henann et al., 2009; Schroers et al., 2007b; Schroers, 2005) . The optimum processing settings depend on the used BMG and also on the feature sizes being replicated. Collectively, the literature review suggests that the processing temperature should be selected as high as possible to obtain the best formability conditions, as long as full crystallisation can be avoided. Therefore, the process settings have to be judiciously selected and optimised for the particular BMG in use and thus to find a processing window that can ensure a stable and reliable replication whilst simultaneously controlling the morphology of the BMG workpiece during the TPF step.

5.2.3 FIB milling

The FIB milling process offers flexibility, high resolution and high surface quality which are extremely important for master making (Scholz et al., 2009; Youn et al., 2006) . Therefore, FIB machining is included in the proposed process chain, particularly to produce sub-micron and nano-features over the pre-existing micro-scale topography created by the TPF process. The FIB technology can be used to produce complex 3D micro features and also nano-scale structures in a range of materials by sputtering atoms in layer-by-layer fashion with high

accuracy and resolution, especially lateral dimensions of less than 50 nm can be achieved (Brousseau et al., 2010) .

The FIB milling process has been used to manufacture replication cavities in materials such as amorphous Ni- and Zr-based alloys (Zhang et al., 2012b; Li et al., 2007b) , Silicon (Youn et al., 2008) glassy carbon (Youn et al., 2007) and fused silica (Li et al., 2007a) . All these studies demonstrated that the FIB milling process could be used as an alternative technology to lithography-based pattern transfer techniques to produce replication masters directly. At the same time no studies on the FIB machining response of partially crystalline BMGs were reported in spite of the potential advantages such materials can offer in master making. Therefore, it should be investigated whether sub-micron and nano-scale structures with the required resolution and surface integrity can be satisfactorily produced when the FIB milling process is used on partially crystalline BMGs.

To produce simple features like 2.5D channels, the input data for performing FIB milling can be in a bitmap format that can be processed directly by the built-in pattern generators in most FIB systems. A more sophisticated approach for 3D patterning is required that involves the use of a lithography software and hardware like Elphy Quantum (Raith GmbH) or Nanomaker to design and duplicate various shapes, and if necessary to specify the respective exposure doses. To execute such 3D FIB milling it is necessary to have a seamless data flow between the CAD software used to create the 3D models and the FIB machine control system. In particular, first the 3D structures are designed employing a 3D CAD package and then a specially designed post-processer is utilised to convert the 3D geometry into a stack of layers ordered along the vertical axis of the 3D model (Lalev et al., 2008) . Then, the "sliced" model can be exported into a GDSII stream file format that is the interface between the CAD package and the follow-up FIB process.

The main FIB parameters that have to be considered when optimising the milling process are: ion beam current, ion beam fluence, and exposure time (Velkova et al., 2010; Li et al., 2007b; Lalev et al., 2008; Minev et al., 2010). In addition, an ion beam sputtering simulation software can also be employed to predict and thus minimise some negative effects such as re-depositioning of sputtered material and over-etching (Svintsov et al., 2009). The use of such data pre-processing step makes possible the optimisation of the FIB milling settings and if necessary even to modify the model in order to counteract some material re-depositioning effects (Velkova et al., 2010).

Another important issue when structuring processes are integrated into process chains is the alignment of new additional features to any pre-existing features/topography on the workpiece. This alignment can be either realised by manually positioning the sample stage while inspecting the specimen in SEM or FIB imaging modes, or automatically, by using the ''feature recognition'' option available in some FIB systems, and thus to locate alignment marks machined in the previous processing steps.

The main shortcoming of the FIB milling technology is its relatively low removal rates. To address this issue and thus to be able to structure bigger areas, a multi-ion beam concept was proposed that combines the high resolution capabilities of the FIB technology with the high throughput that parallel lithography systems can offer. In particular, a projection maskless nano-patterning (PMLP) system was developed (Platzgummer et al., 2008) to satisfy the requirements for high productivity. Its pilot implementation demonstrated a significant increase of the removal rates and improved resolution compared to conventional single FIB systems. By utilizing such a multi-beam system together with the data preparation technique outlined above it is possible to produce larger areas with complex 3D surface structures requiring nanometre precision within a reasonable time scale (Lalev et al., 2008).

5.2.4 Serial replication

The proposed process chain can be used to produce masters for scale-up micro replication, e.g. µIM and hot embossing (HE). As discussed in Chapter 2, given that the development of new micro devices is highly dependent on manufacturing systems that can reliably and economically mass produce micro parts, it is clear that µIM represents a more attractive option. Thus, in this study, the BMG masters were used for µIM as it is a viable technology for serial production of micro parts for a wide range of applications, such as micro/nano optics, precision micromechanics and micro/nano-fluidics (Scholz et al., 2011; Hansen et al., 2011; Attia et al., 2009; Calaon et al., 2013; Lee et al., 2004) . At the same time, the use of this technology for achieving FLSI in products poses big challenges with regards to the available master making process chains and the products' geometrical complexity and accuracy requirements at different length scales. Thus, the successful implementation of a process chain for scale up manufacture of thermoplastic parts with micro and nano-scale features depends on: (a) the satisfactory fabrication of mould insert cavities with high accuracy and surface finish; and also on (b) the successful execution of an optimised and repeatable injection moulding process to obtain high replication fidelity with satisfactory part quality. This latter aspect is directly related to the moulding process, in particular to find an optimum processing window for the selected polymer material. There are many parameters which can influence the process but the most statistically significant factors include (Giboz et al., 2007; Attia et al., 2009; Griffiths et al., 2008b, 2008a, 2007; Huang, 2007; Monkkonen et al., 2002; Sha et al., 2006; Tosello et al., 2010a; Zhang et al., 2012b; Mani et al., 2013)   : melt temperature; mould temperature; injection speed; holding pressure and duration; mould surface roughness; runner and gate design and the used venting/ vacuum systems. Thus, an optimisation of these process settings is necessary for the particular polymer in use and thus to ensure a stable and reliable micro replication process that is capable of achieving FLSI in high quality parts.

5.3 Experimental Setup

5.3.1 Tool insert material

The material has to satisfy the functional and technical requirements of the replication master and at the same time to facilitate the integration of all necessary master-making technologies. Therefore, a workpiece material suitable for both the TPF and FIB processing has to be selected while taking into account their respective constraints in producing different length scale features with the required surface integrity. Based on these considerations the BMG material selected to implement the proposed master-making process chain is the commercially available Vitreloy 1b alloy (Vit1b). The mechanical properties of Vit1b are very attractive for producing high wear resistant mould inserts for μIM, in particular its tensile yield strength is 1.9 GPa while its hardness is 540 Hv.

Vit 1b has excellent thermoplastic formability in the SCLR to replicate micro and nano features (Schroers, 2010) by TPF. At the same time due to the material homogeneity down to atomic scale it is expected to have a very favourable machining response to FIB milling as other BMGs (Li et al., 2007b) and thus to produce masters with nano scale resolution and high surface integrity. Also, it is important to note that Vit 1b is resistant to most acids and bases and thus it is possible to dissolve selectively the Al master after the TPF step in the process chain (Schroers et al., 2007b) .

5.3.2 Test structure design

Microfluidic devices use channels with dimensions in the range of tens to hundreds of micrometres, and even extend to the submicron and nanometer scale (Abgrall and Gue, 2007; Craighead, 2006; Nguyen and Wu, 2005; Whitesides, 2006) . The functionalities of these devices can be enhanced by employing structured functional surfaces. These include, hydrophobic / superhydrophobic surfaces and optical elements which have surface features in

the micro/nano scales (Scholz et al., 2011; Hainberger et al., 2010; Kalima et al., 2007; Saarikoski et al., 2009; Yoo et al., 2009). Therefore, a microfluidic structure that incorporates both micro and nano scale features was selected to validate the capabilities of the proposed BMG enabled master making process chain for achieving FLSI in thermoplastic parts. In particular, this test structure was selected to demonstrate the feasibility of adding sub-micron and nano scale structures directly onto already pre-existing micro-scale features of a Vit1b master, and then to replicate them in a single step. A schematic view of the simple micro-mixer used in this study is given in Fig 5.3 that also shows the dimensions of its channel and reservoir features. In addition, the locations of three sub-micron and nano scale gratings in the larger reservoir are also shown in the figure. Each grating is a pattern of 20 x 20 black or white fields and the white fields are pockets. The dimensions of these three grating structures are given in Fig 5.4. The smallest pixel dimensions in X, Y and Z directions for gratings 1, 2 and 3 are 1µm, 600nm and 200nm, respectively.
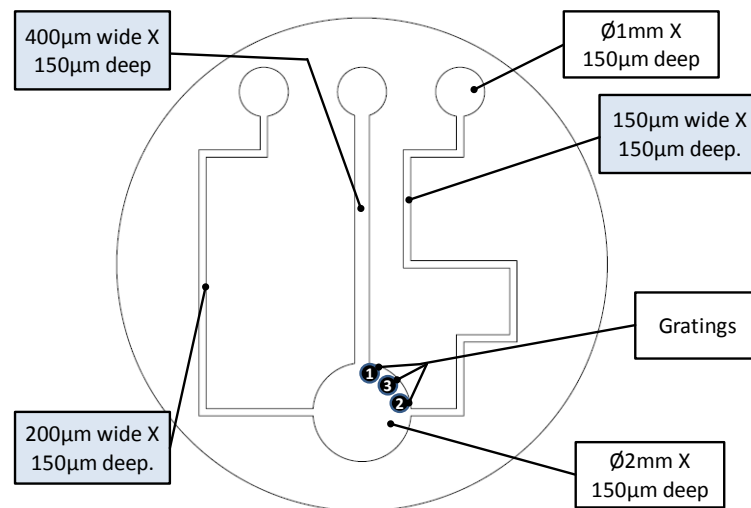
Figure 5.3   A Schematic of the micro-mixer design and the locations of the sub-micron grating structures

Structure No	X (μm)	Y (μm)
1	20	20
2	12	12
3	4	4
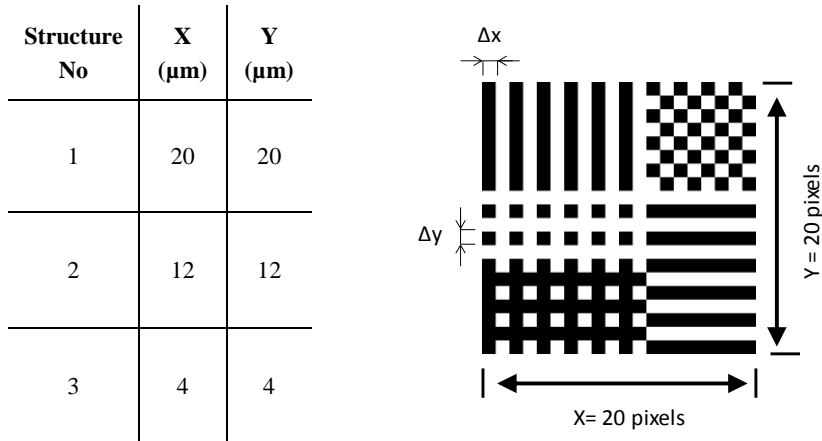
Figure 5.4 Grating structures

5.3.3 Micro milling of Al masters

The μMilling technology was employed in the proposed process chain to machine the micro-mixer features onto the Al workpiece. A tooling grade Al was used, in particular AL5083. This Al alloy was selected because of its machinability (Popov et al., 2006) and the requirement to dissolve it after completing the TPF step. The machining of the Al master was carried out on a KERN HSPC 2216 micro-machining centre and a 150 μm nominal diameter end-mill was used to mill the channels and the reservoirs. The factors affecting the performance of μMilling operations investigated in a previous study (Dimov et al., 2004) were taken into account in selecting the machining parameters for producing the Al master. This included: (i) the use of a cutting depth that would keep milling forces within predefined limits along the machining path and (ii) spindle speeds and feed rates that reflected the chosen workpiece – tool-material combination. The used machining parameters were as follows: feed rate 250 mm/min; spindle speed 40,000 rpm; depth of cut 2 μm; and step over 50μm. The channels and reservoirs were machined to their full depth of 150 μm by applying reciprocating plunge-cut cycles.

5.3.4 TPF of BMG insert

In this research, a hot embossing machine based on a Zwick universal testing machine with short cycle times was employed to fabricate the Vit1b master. The forming is performed by a displacement and force controlled embossing step, which is executed by a high precision load cell. To ensure homogenous temperature and pressure distribution during the TPF process, the force and temperature were kept constant for a pre-set time that was selected taking into account the structure design, and thermal conductivity and flow ranges of the Vit1b (Kolew et al., 2010).

A circular flat Vit1b workpiece having a diameter of 15mm with an approximate thickness of 2mm was placed together with the micro-mixer patterned Al master between the parallel heated compression platens. Subsequently, the Vit1b specimen was aligned with the Al master. The Vit1b workpiece-Al master combination was then heated to a temperature above the Vit1b's T_g and then a pre-defined pressure was applied over a set time. After that, the pressure was gradually reduced and the Al master-BMG insert assembly was cooled down.

To fill completely the Al master micro features it is very important to select a right processing window for the BMG in use. At the same time, it is important to stress that after a certain amount of time at a given temperature above T_g, the Vit1b will start crystallising. As discussed earlier, the material morphology should be controlled because it affects the Vit1b homogeneity, and consequently, it will have a negative effect on the Vit1b's machining response to the FIB process. Therefore, it is imperative to consider this time constraint when selecting appropriate temperature–time settings for the TPF process. The mechanical behaviour of BMGs is highly temperature dependent above their T_g, 350° C for the used Vit 1b alloy, as their viscosity decreases dramatically as the temperature increases. Therefore, in order to maximise formability it is very important to choose a temperature setting as high as

possible for the respective processing time (Henann et al., 2009; Schroers et al., 2007b) whilst simultaneously controlling the material morphology. All the above mentioned factors need to be considered in selecting the TPF process window, given that the main objective for the HE trials was to control and maintain the Vit1b's morphology while achieving high replication fidelity with regards to micro mixer feature widths, depths and shape. As the focus of this research was on the design and validation of the proposed master making process chain, a systematic optimisation of the TPF process was outside its scope. Therefore, only five tests were carried out and the TPF processing window for the trials was determined taking into account the available material data, experimental investigations reported in literature (Henann et al., 2009; Schroers et al., 2007b; Schroers, 2005; Waniuk et al., 2003) and the specific micro mixer geometry. From these five trials the Vit1b insert with the best feature resolution and surface integrity was selected for further FIB structuring and injection moulding trials. In particular, the process settings used in this TPF trial were as follows: processing temperature (Tp) 450 ^{o}C, applied force 5 kN and an overall process time 230 s.

Following the TPF step, the Vit 1b substrate and Al insert were mechanically interlocked together and therefore it was necessary to dissolve the Al master in a heated NaOH bath. The NaOH (60 gr/l) solution was heated at a constant temperature of 65°C using a hotplate set-up, whilst simultaneously mechanical agitation of the solution was applied, to enhance the dissolution process and also to ensure homogeneity of the solution temperature. Subsequently, the Vit 1b insert was machined by wire EDM to the required overall size for integrating it into an injection moulding tool.

5.3.5 FIB processing

The next step in the process chain was the FIB machining of the three grating structures (See Figs 5.3 and 5.4) over the TPF micro-mixer reservoir. These three structures were machined

onto the Vit 1b insert using a Carl Zeiss XB 1540 FIB/SEM system. Given that the gratings represented 2D images composed of black and white fields/pixels, the bitmap file of these patterns was used directly by the built-in software of the system to control the FIB milling operation. The depth and accuracy of the structures fabricated by FIB milling were determined by the processing parameters used. They were selected by taking into account that FIB milling with a low current results in better quality patterns but at the expense of longer machining times and hence potential focus losses and pattern drifts. Some machining trials were carried out to identify a suitable processing window, whilst also achieving the best trade-offs between machining time and resulting surface integrity. The processing parameters selected in this experimental study are provided in Table 5-1. The alignment of the gratings over the micro mixer reservoir was performed manually using the FIB imaging mode of the system.

Table 5-1 FIB milling parameters

Structure No.	1	2	3
Probe current	2nA	200 pA	10 pA
Accelerating voltage	30kV	30kV	30kV
Exposure time duration	489s	963s	1070s
Probe width	150nm	40nm	14 nm

5.3.6 Micro-injection moulding

The machine used to perform the micro injection moulding tests was a Battenfeld Microsystem 50. The Vit1b insert was integrated into the primary mould by using a secondary insert holder as shown in Fig 5.5. The overall cavity design included a circular main body with dimensions of Ø11 mm x 2 mm and four "wing" features to assist demoulding. In

addition, a gate and a runner were machined into the secondary mould insert holder to allow the plastic to flow from the injection nozzle into the Vit1b insert.
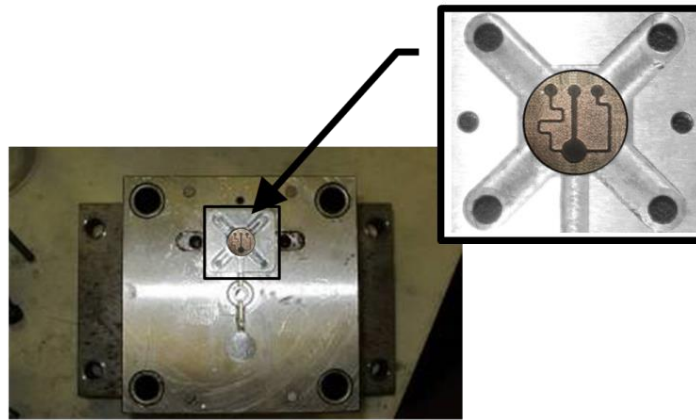
Figure 5.5 BMG insert and secondary insert holder assembly fitted into the primary mould

A commonly used material in injection moulding, namely Polypropylene (PP), was selected to conduct the replication trials and thus to demonstrate the feasibility of this process chain for replicating satisfactorily both the micro and nano scale structures. As discussed earlier, the filling performance of micro and nanoscale features relies heavily on selecting correctly the melt temperature (T_b), mould temperature (T_m), holding pressure (P_h), holding pressure duration (t_h), and injection speed (V_i). Again, since the main objective of this research was to design and demonstrate the feasibility of the proposed master making process chain an optimisation of the μIM process was not conducted and the process settings were selected based on results reported in other experimental studies (Scholz et al., 2011; Tosello et al., 2007) . The process settings used in this feasibility study to produce a small batch of PP parts were as follows: Tb 220° C, Tm 60°C, P_h On, t_h 5s and V_i 150mm/s.

5.3.7 Inspection

The surface roughness and feature dimensions of the relevant machined or replicated features were inspected by employing the equipment and measurement procedures described below.

5.3.7.1 Linear dimensions

The micro mixer channel/protrusion width measurements of the Al master, Vit1b insert and three PP replicas were performed with a Leica DMLM optical microscope using the instrument's built-in software. In addition, a Mitutoyo QV Accel 404 Measuring System (optical coordinate measuring machine) was used to determine the depths and heights of the micro mixer channel and protrusion features. The height and depth measurements were performed using the QV PAK software provided by the instrument manufacturer. The widths or depths of the protrusions and channels were obtained by inspecting them in three predefined positions along the channels and protrusions. For each channel, the values recorded are the average ones from these three measurements.

Scanning Electron Microscope (SEM) images of the grating structures of the Vit1b insert and three PP replicas were used to assess their lateral and vertical (XY) dimensions. The images were taken on the system where the FIB machining was performed, in particular the Carl Zeiss XB 1540 FIB/SEM system. Depth and height (Z) measurements were carried out at an angle of 54°. The tilt compensation option of the SmartSEM software was used to calculate the actual values of the vertical dimensions. After a calibration with a reference sample, the measurement uncertainty of the instrument in the lateral and vertical directions was assessed to be in the range of 1%−3% of the nominal dimensions (Velkova, 2011) . For each grating, three measurements were conducted along their overall lengths in both the X and Y directions and thus to obtain the overall widths of the gratings. At the same time, measurements were conducted across 10 different field/pixels in X, Y and Z to get their widths and depths/ heights, respectively. Again, the values reported are the average ones of these measurements.

Finally, all of the linear dimensions reported in the chapter are provided with their associated expanded uncertainty, U, (at 95% confidence level) which was determined, following an established procedure (Joint Committee for Guides in Metrology (JCGM), 2008; Kirkup and Frenkel, 2006; United Kingdom Accreditation Service (UKAS), 2007) . The error sources for the optical measuring microscope, optical coordinate measuring machine (OCMM) , and SEM were identified by applying the measurement recommendations given in literature (Velkova, 2011; Tosello and Chiffre, 2004; Tosello et al., 2009b, 2012; Tosello, 2008) . In the case of the SEM, to account for the worst-case scenario the measurement uncertainty u(P) of the SEM was calculated as 3% of the measurand's average value (Velkova, 2011) . Additional data on the carried out uncertainty analysis and calculations is provided in Appendix B.

5.3.7.2 Surface roughness

Surface roughness measurements of the bottom and top surfaces of the micro mixers' 400 μm channels and protrusions of both the Al and Vit1b samples, respectively were performed using a Talysurf 120 L Surface Texture Measurement instrument. The samples' evaluation lengths were chosen according to ISO 4288: 1997 (ISO4288, 1997; Leach, 2001) . The parameter used to inspect the surface roughness was the arithmetic mean roughness (Ra) because relative heights in micro topographies are more representative, especially when measuring flat surfaces (Popov et al., 2006) . The reported surface roughness measurements are also provided with their associated expanded uncertainty, U, (at 95% confidence level) which was again calculated by following an established procedure (Leach, 2001) and also by adapting recommendations given for surface roughness measurements in a separate study (Tosello et al., 2012) . Again, additional data on the carried out uncertainty budget calculations is provided in Appendix B.

5.4   Results and Discussion

The experimental results obtained after each process chain step are presented and discussed in detail in the subsections below. The values of the X & Y lateral measurements and the Z heights of the machined and replicated features, and the achieved surface roughness are used to quantitatively compare the results after each step of the proposed master making process chain.

5.4.1 Micro milling

As it can be judged from Fig. 5.6, the micro mixer was successfully machined. Table 5-2 presents the average channel widths and depths of the Al master. The measurements were taken at the top of the channels. From this table it can be judged that there is a relatively constant deviation from the target channel widths of 200µm, 400µm and 150µm respectively and the channels were consistently slightly bigger. The average 13.48 µm deviation could be due to: (i) not introducing sufficient compensation for the actual tool radius; (ii) the spindle/tool radial runouts during machining; and (iii) some measurement errors as the channel edges were difficult to detect precisely. This deviation is significant and indicates that the µMilling set-up was not optimised. Also, there is a small average deviation of 2.24 µm from the target channel depths of 150µm (see Table 5-2). This can be due to both the spindle growth and also for not introducing a correct compensation for the tool axial runouts during machining. Another contributing factor could be the measurement errors associated with the automated focussing of the Mitutoyo QV system. This deviation is not significant and it should be possible by optimising the µMilling process to minimise it and increase the machining accuracy. As far as the deviations from the targeted dimensions are known they will not affect the analysis of the follow up steps in the process chain.
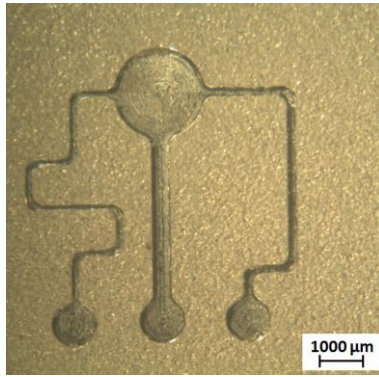
Figure 5.6 Al master with micro-scale features produced by micro milling

To evaluate the surface integrity of the micro channels, the surface roughness measurements at the bottom of the 400μm micro-channels were taken using Talysurf 120 L. The average Ra value for the Al master is 0.3378 ± 0.0565 μm. This value is higher than expected and is due to some μMilling texture on the machined surfaces. As can be seen in Fig 5.7, an examination of the Al master revealed that the material morphology is not homogenous and includes relatively large grains. This affected the resulting surface integrity as materials with a coarse grain structure have a less "favourable" machining response (Popov et al., 2006; Koc and Ozel, 2011) . However, despite this relatively high surface roughness, it was possible to identify sufficiently smooth regions and thus to add sub-micron and nano-scale features by FIB milling on the Vit1b insert after the TPF step.

As the research reported in this chapter is only a feasibility study the Al master was considered adequate to proceed with the analysis of the follow up steps in the process chain.
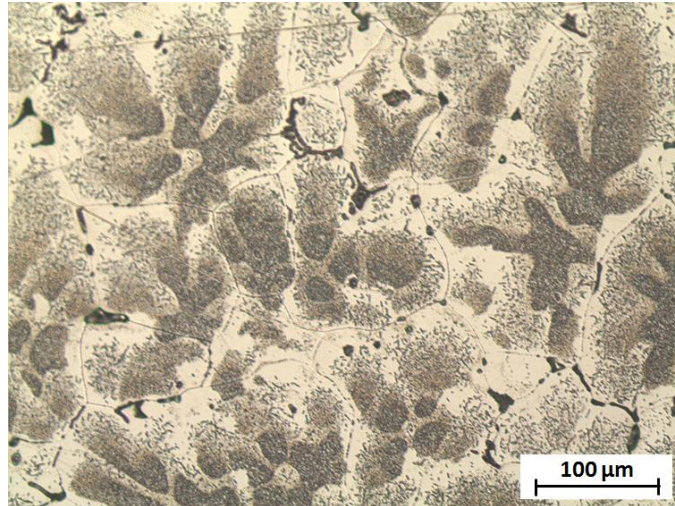
Figure 5.7 Microstructure of Al master

5.4.2 Thermo plastic forming

Prior to executing the TPF step, a XRD analysis of the as-received Vit 1b plates was performed with a Rigaku™ Ultima IV X- Ray diffractometer having a monochromated CuKa$_1$ radiation source and using the θ / 2θ Bragg-Brentano configuration. The results are shown in Figure 5.8. The broad diffraction maxima of the XRD spectra depicts typical amorphous characteristics that are similar to those reported for Vit 1b (Waniuk et al., 2003) . These results verified that the as-received Vit 1b sample was fully amorphous and thus any changes in the material morphology should be attributed to the TPF step in the proposed master making process chain.
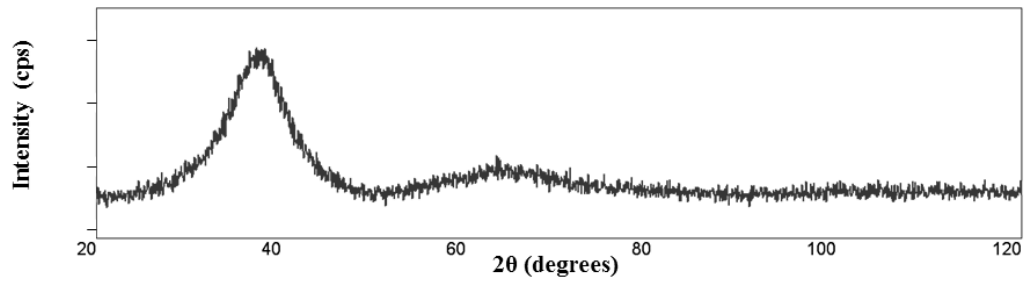
Figure 5.8 XRD spectra taken on the polished Vit 1b sample

As it was already stated the best Vit 1b insert (See Fig 5.9) from the five tests was selected for further analysis. Table 5-2 presents the average depths/heights and widths of the micro scale features of both the Al TPF master and it's corresponding Vit 1b replica. Comparing the average results for the protrusions' and channels' widths of the Vit 1b insert and the Al master respectively, it is not difficult to see that they concur closely for all three channels sizes.
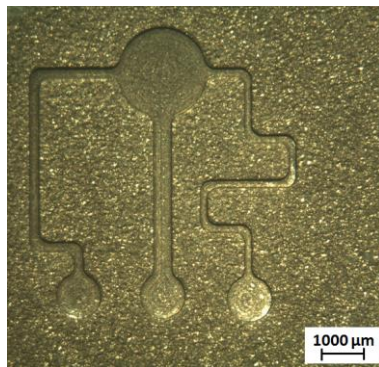
Figure 5.9 Vit 1b workpiece with micro-scale features produced by TPF

Table 5-2 Comparison of average depths & widths of hot embossed BMG insert with corresponding Al master.

Al Master						Hot Embossed BMG Insert					
Channel 1 (200)		Channel 2 (400)		Channel 3 (150)		Protrusion 1 (200)		Protrusion 2 (400)		Protrusion 3 (150)	
Width (μm)	Depth (μm)	Width (μm)	Depth (μm)	Width (μm)	Depth (μm)	Width (μm)	Depth (μm)	Width (μm)	Depth (μm)	Width (μm)	Depth (μm)
212.63 ± 1.79	151.63 ± 3.68	414.50 ± 1.72	152.25 ± 3.77	163.31 ± 2.47	152.85 ± 5.50	215.57 ± 2.22	151.70 ± 6.22	417.40 ± 1.68	151.60 ± 5.01	165.46 ± 2.91	150.75 ± 7.11

The results show that the average Vit 1b insert protrusion widths are marginally bigger than the corresponding Al master channel in the range from 2.15 to 2.94 μm. This is as expected and can be explained both with some measurement errors and dimensional changes of the Al master and the Vit 1b insert due to the underwent heating and cooling cycles during the TPF step. The shrinkage/expansion S of the TPF Vit 1b insert features can be calculated using the following equation:

$$S = \frac{l_m - l_{mr}}{l_m} \times 100\% \quad (1)$$

where: l_m is any specific feature dimension (length or depth) of the Al masters and l_{mr} is the corresponding dimension on the replicated part. Thus, by applying equation 1 to the data in Table 5-2, the S values of the considered Al master channels and Vit 1b insert protrusions are -1.3%, -1.4% and -0.7% off from their nominal values of 150μm, 200μm and 400μm, respectively. There is a consistent negative S trend, in particular the Vit 1b feature widths are consistently larger than the corresponding Al master feature widths. Also, it is not difficult to see that there is a tendency for the S values to decrease with the increase of the protrusion width. This tendency could be due to the increase of the relative measurement error with the decrease of the nominal dimensions. Nevertheless, the results are very close and therefore the Vit 1b insert can be considered an accurate replica of the Al master with regards to the widths

of the micro fluidics channels. The deviations from the pattern design are as expected, and as stated earlier they can be attributed to the shrinkage/expansion of the Vit 1b features during the TPF cycles, and also again to some measurement errors. The magnitude of S is determined by the Al alloy and Vit 1b properties together with the applied TPF process settings whereas the measurement errors could be explained with the relatively poor edge definition of the channels.

The deviations between the Vit 1b insert protrusion heights and the corresponding Al master channel depths in Table 5-2 are 2.1μm, -0.07μm and 0.65 μm (for the 150μm, 200μm and 400μm micro mixer channels respectively) from their nominal value of 150μm. It is evident that whilst the average heights of the Vit 1b protrusions concur closely with the corresponding Al masters' channel depths, the deviations are not consistent and vary in the range from -0.05 to 1.4 %. These deviations cannot be due to the TPF process settings because as it can be seen in Fig 5.10 the milling marks in the Al master were faithfully replicated in the Vit 1b insert and thus the Al master was completely filled during the TPF step. Therefore, this deviation can be attributed again to the underwent expansion/shrinkage during the TPF heating/cooling cycles and measurement errors. The surface conditions of both the top and bottom planes of the Vit 1b and Al parts could explain these errors during the QV system measurements. Overall, it is evident that the TPF step was executed satisfactorily.

Prior to the FIB milling step, it should be ascertained that (i) the morphology of the Vit 1b has been retained with only minimal changes after the TPF step and (ii) the surface roughness is sufficiently low such that the FIB milling can be performed. Therefore, the surface integrity of the embossed features was investigated using the SEM and Talysurf 120L whilst X-ray diffraction was used to confirm the amorphicity or otherwise of the Vit 1b insert after the TPF step. A SEM image of the Vit 1b replica is given in Fig 5.10 while the average Ra roughness value of the 400 μm protrusion is 0.2866 ± 0.0099 μm .
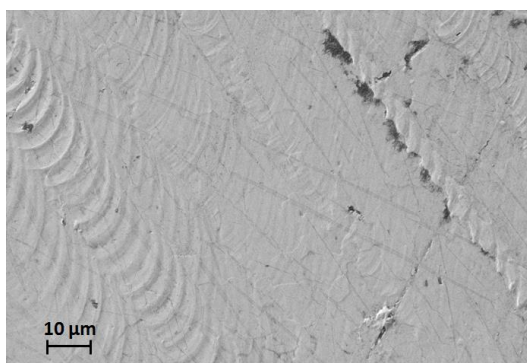
Figure 5.10 SEM images of the Vit 1b insert

It is evident from the SEM image that the embossing temperature of 450 ^{o}C was sufficiently high to replicate clearly the µMilling surface texture on the Vit 1b insert and also its roughness was only marginally better, Ra 0.29 µm than Ra 0.34 µm on the corresponding Al master (see section 5.4.1). While this surface roughness is relatively high, the Vit 1b insert has sufficiently smooth areas, e.g. on the large reservoir feature, where the follow up FIB milling step can be carried out. As this is just a feasibility study the produced Vit 1b insert can provide sufficient evidences about the capabilities of both the component technologies and the proposed process chain as a whole.

The unstructured bottom surface of the Vit 1b insert was polished and subsequently investigated by X-ray diffraction using the same instrument. Fig 5.11 depicts the XRD pattern of the selected Vit 1b sample from the carried out five trials.
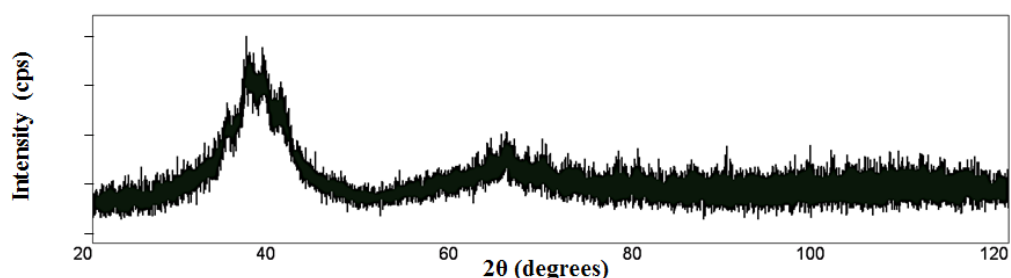
Figure 5.11 XRD analysis of the BMG insert after the HE step

It can be seen in Fig 5.11 that there are a few weak but sharp crystalline peaks superimposed on the broad humps, which means that full amorphicity was not retained at the used TPF settings. This was not expected since the set temperature (450° C) and time (230 s) were within the constraints of the processing window discussed in section 5.3.4. In particular, the embossing temperature and processing time did not exceed the crystallisation thresholds of 460° C and 255 s, respectively. This could be explained with a combination of two factors, a lower T_x for the Vit 1b plates used and their likely shorter onset time, that led to some morphological changes. However, TPF is a controllable process and with judicious selection of the process parameters it is possible to control such changes. These initial results are encouraging and demonstrate that Vit 1b inserts with the required material morphology, resolution and surface integrity can be produced by employing the TPF process.

5.4.3 FIB milling

Regions with the required surface integrity for further FIB processing were identified on the surface of the large reservoir and as the Vit 1b insert underwent minimal morphological changes the possibility to add nanoscale gratings was investigated and thus to benefit from the, better fatigue and wear resistance properties of partially crystalline BMGs. Three nano-scale gratings were machined by FIB milling following the experimental plan discussed in Section 5.3.5. The three nano-scale grating structures were milled satisfactorily on the Vit 1b insert as can be seen in Fig 5.12 in spite of the partial crystallisation.
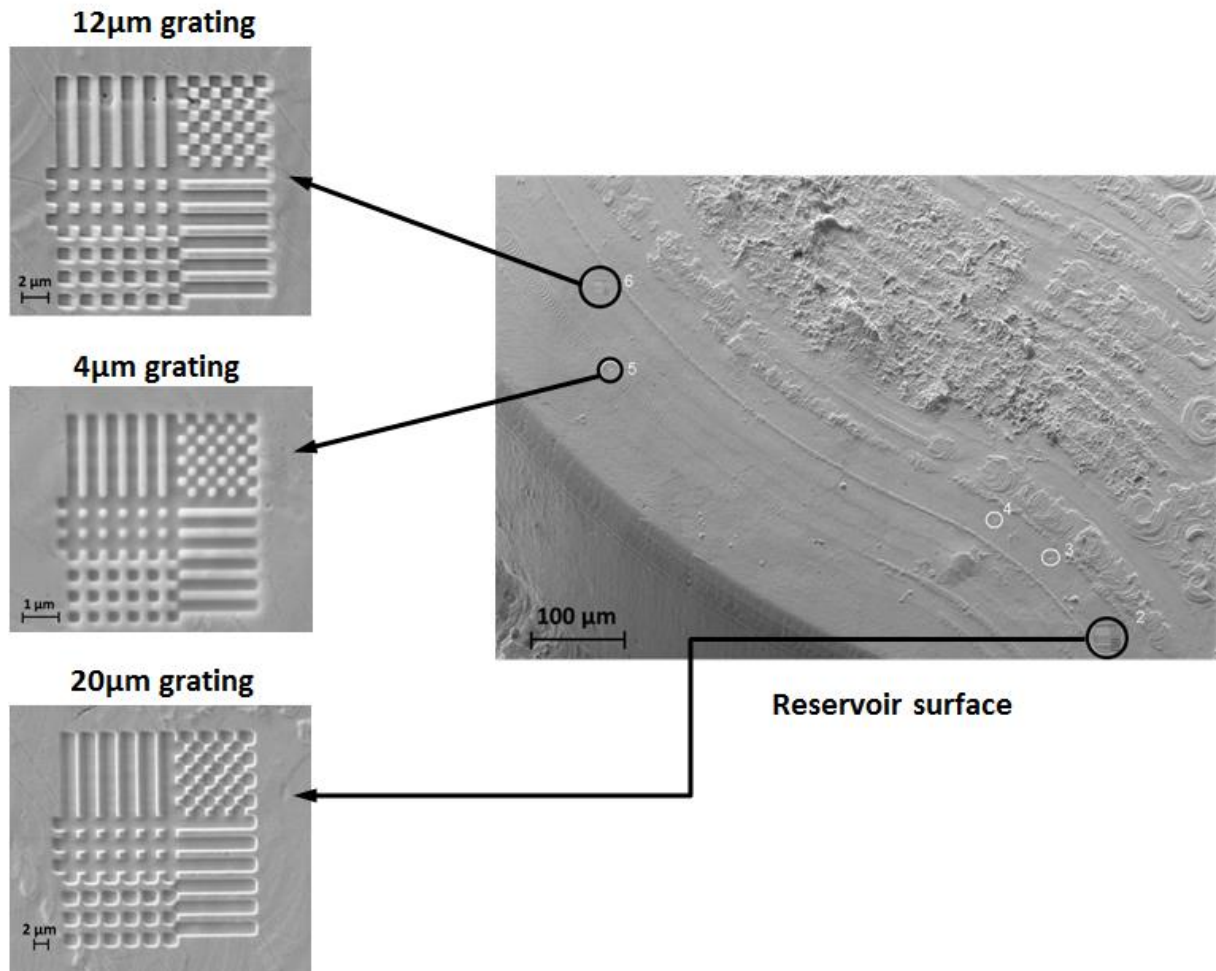
Figure 5.12 Nano-scale gratings FIB milled onto microfluidic device reservoir feature

Table 5-3 Micro and nano - scale feature dimensions of the gratings

Grating Structure No.	Pixel Width (X) (μm))	Pixel Width (Y) (μm)	Pixel Height (nm)	Overall Width (X) (μm)	Overall Width (Y) (μm)
1 (20μm)	1.46 ± 0.11	1.47 ± 0.11	651.7 ± 72.4	28.53 ± 1.72	28.59 ± 1.72
2 (12μm)	0.88 ± 0.06	0.88 ± 0.05	420.0 ± 51.8	17.26 ± 1.04	17.35 ± 1.05
3 (4μm)	0.28 ± 0.02	0.29 ± 0.03	159.9 ± 16.3	5.62 ± 0.34	5.78 ± 0.35

The average heights and widths of the gratings' smallest features together with their average overall sizes are provided in Table 5-3. The table also includes the associated expanded uncertainty of these measurements at 95% confidence level. For all three gratings, the

average pixel widths in the X and Y directions at the bottom of the protrusions are larger than the targeted values of 1 µm, 600nm and 200nm. However, the average pixel sizes of the three gratings calculated based on their overall XY widths are 1.428 µm, 0.866 µm and 0.285 µm respectively; and concur closely with the as-measured pixel widths. This allows us to attribute the systematic error during the FIB milling to some process calibration and setting-up issues.

At the same time, the average heights in Table 5-3 are smaller than the targeted values of 1 µm, 600nm and 200nm, which can be explained again with some systematic error during the layer-based FIB milling process. In another research it was shown that this error can be reduced to 2 to 5 % of features' nominal dimensions by employing a specially developed methodology for optimising the FIB milling process (Velkova, 2011) . As this chapter reports a feasibility study, the process settings were not optimised and it was just assumed that it would be possible to improve substantially the accuracy of the FIB milling process if this methodology is applied. In summary, it can be stated that the submicron and nano-scale gratings were successfully created over the pre-existing micro topography in spite of the Vit 1b partial crystallisation. There were some deviations from the targeted dimensions but they were predominantly due to systematic errors. Thus, FLSI in masters could be achieved by optimising the FIB machining process as a component technology in the proposed process chain. The results also show that nano-scale features with the required resolution and surface integrity could be achieved when processing the partially crystalline BMG. Thus, it can be stated that the partial crystallisation did not have a detrimental effect on the Vit 1 B response to FIB milling at submicron and nano scales.

5.4.4 Micro-injection moulding

The micro mixer was replicated well as can be judged by comparing the images of the replicas in Fig. 5.13 with the Vit 1b insert in Fig. 5.9. The results from the measurements of the PP replicas are provided in Table 5-4.
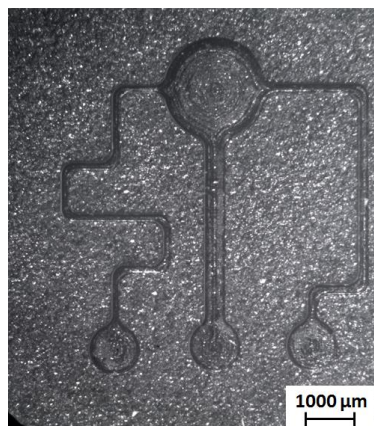
Figure 5.13 Overall view of PP replicated microfluidic device

Table 5-4 PP-based microfluidic device channels dimensions

Microfluidic Device Features					
Channel 1 (200)		Channel 2 (400)		Channel 3 (150)	
Width (µm)	Depth (µm)	Width (µm)	Depth (µm)	Width (µm)	Depth (µm)
204.03 ± 2.65	148.0 ± 2.92	405.40 ± 2.50	149.00 ± 2.47	152.16 ± 2.28	148.67 ± 1.82

Comparing the average protrusion width of the Vit 1b insert (Table 5-2) with the corresponding average channel width of the PP parts in Table 5-4 it is clear that they concur closely. The average PP channel widths are slightly smaller than the corresponding Vit 1b insert protrusion widths by 8.0 %, 5.4 %, and 2.9% for the 150µm, 200µm and 400µm channels, respectively. These deviations can be explained with the PP shrinkage, usually in

the region of 1 to 2%, and also with potential measurement errors due to not well defined channel edges of the micro mixer channels. The shrinkage could be higher because the µIM parameters were not optimised, in particular the packing pressure and time, and also due to cooling rates effects on the shrinkage of semi crystalline materials such as PP. The mould temperature was set towards the higher end within the material's recommended range in order to replicate fully the nano structures. However this caused the PP replicas to cool down more slowly and led to a higher crystallinity and shrinkage (Beaumont et al., 2002; Osswald et al., 2008). The opposite effect can be achieved by increasing the cooling rate and thus to reduce the shrinkage accordingly.

The insert protrusions' heights (Table 5-2) are on average 1.8% bigger than their corresponding PP channel depths (Table 5-4). As expected, this difference is less than that for the channels' widths because the shrinkage is higher in the direction of the polymer flow (Osswald et al., 2008). Again, this can be explained with the µIM settings, which were not optimised together with the effects of lower cooling rates on the PP shrinkage. Another contributing factor can be the QV measurement errors due to the different surface conditions of the top and bottom focusing planes of the PP parts. In addition, it can be seen in Fig 5.14 that the milling texture replicated first into the Vit 1b insert was again faithfully reproduced into the PP parts. This is further evidence that the Vit 1b insert was completely filled and thus the height deviations were not due to incomplete filling.
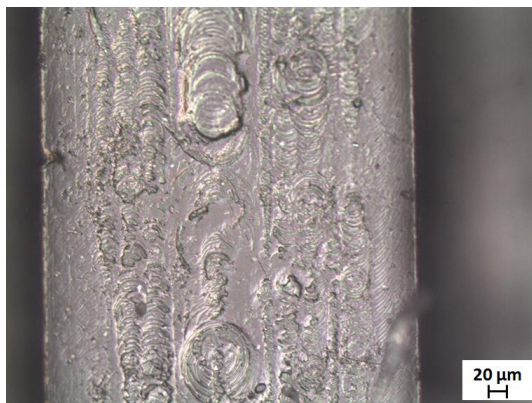
Figure 5.14 Image of surface topography of 400 µm channel floor

Looking at the fidelity of the different sub-micron features achieved with the used µIM settings, only the 20 µm and 12 µm gratings were replicated successfully. Therefore, only the replication results for these structures are presented in Fig. 5.15 and are discussed further.
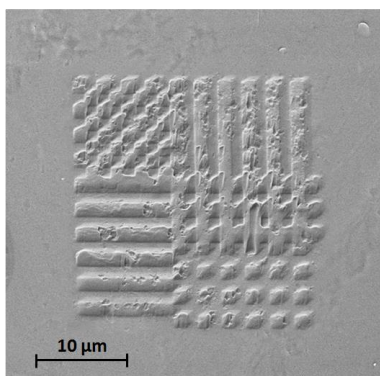
a) PP Structure 1
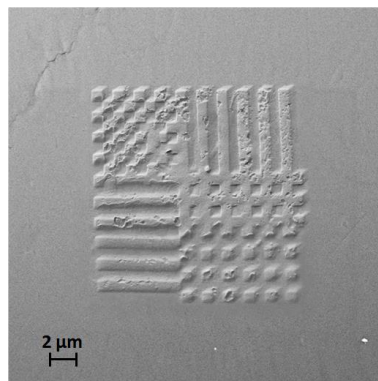
b) PP Structure 2

Figure 5.15 Replicated grating structures.

Table 5-5 shows the average heights and widths of the smallest gratings' features. The table also provides the average overall sizes of these gratings. Comparing the average pixel widths of these two gratings in Table 5-5 with the corresponding ones on the Vit 1b insert (Table 5-3), it can be concluded that they concur closely and the deviation is in the range from 2.84 % to 3.1 %. These differences can be due to both measurement errors associated with the quality of the "pixel" edges and also the PP's higher shrinkage as it was the case with the micro mixer dimensions.

Table 5-5 PP gratings micro and nano - scale feature dimensions

Grating Structure No.	Pixel Width (X) (µm))	Pixel Width (Y) (µm)	Pixel Height (nm)	Overall Grating Structure Width (X) (µm)	Overall Grating Structure Width (Y) (µm)
1 (20µm)	1.43 ± 0.11	1.41 ± 0.11	583.6 ± 43.0	27.29 ± 1.64	27.57 ± 1.66
2 (12µm)	0.86 ± 0.07	0.85 ± 0.07	372.6 ± 27.5	16.33 ± 0.98	16.69 ± 1.01

The comparison of the height values of the Vit 1b and the PP gratings in Tables 5-3 and 5-5 revealed deviations of 10.45% and 11.3% for the 20µm and 12µm structures, respectively and again they are higher than the expected typical shrinkage values of 1 to 2%. Again, this can be explained with the µIM settings, which were not optimised together with the effects of the lower cooling rates of the sub-micron features on the PP shrinkage and the overall SEM measurement error. It can be seen in Fig. 5.15 that some of the 20µm grating's pixels incurred some distortion that have directional characteristics. This can be explained by: (i) a positional misalignment of the replicated pattern with respect to the grating structures on the BMG insert during the demoulding process and (ii) the existence of imbalanced and localised ejection forces due to the part overall geometry (Griffiths et al., 2009), variations in the surface finish

across the Vit 1b insert and possible pressure and temperature gradients across the moulded part during the injection moulding step (Attia et al., 2009) .

Finally, as it was already stated the µIM settings were not fully optimised and therefore it could be concluded that the 20µm and 12µm gratings had been replicated successfully. Overall, the results show that relatively good fidelity of different scale features can be achieved with the µIM process and it can enables FLSI in thermoplastic components. It should be also noted that the research has revealed potential challenges in performing an effective dimensional quality control and reliable manufacturing at sub-micron scale that should be addressed. At the same time, as it was stated in Chapter 2 , it can be expected that the replication performance would have improved if compression injection moulding had been used, especially the 20µm and 12µm would have been moulded better and potentially the 4µm grating could have been replicated, too (Hansen et al., 2011; Tosello et al., 2010b) . Thus, the proposed master making process chain could benefit from applying it in conjunction with the compression injection moulding technology to achieve a better FLSI in polymer parts.

5.5   Conclusions

A cost effective master making process chain for achieving FLSI in mould inserts was proposed that integrates compatible and complementary structuring and replication technologies while utilising a Zr-based BMG workpiece with its attractive mechanical properties. In particular, the proposed master-making process chain integrates three different technologies, namely µMilling, TPF and FIB milling for micro structuring and sub-micron patterning, and thus to fabricate inserts incorporating different length scale functional features. Subsequently, the produced inserts' replication capabilities are validated by employing one of them for injection moulding a small batch of polymer parts. Based on the

analysis carried out after each step of this process chain the following conclusions can be made:

1. It was demonstrated that the process chain could be a viable route for producing BMG replication masters. In particular, it is a promising manufacturing solution for producing micro injection moulding inserts with complex 3D structures that incorporate different length scale features. The process chain could be a viable fabrication route for serial production of polymer based FLSI devices by replicating both micro and sub-micron structures simultaneously.

2. The use of BMGs enables the integration of complementary manufacturing technologies in the proposed master making process chain whilst satisfying the functional and technical requirements for producing mould inserts, an imperative consideration when designing such chains.

3. The analysis of micro and sub-micron structures produced after each process revealed that they were transferred sufficiently well through the four steps of the proposed process chain. Collectively, the results demonstrate that there is good process compatibility and complementarity between the component technologies in the proposed process chain, especially for the targeted length scales.

4. It was demonstrated that TPF is a "tuneable" process and through a judicious selection of the process settings it is possible to minimise the BMG's morphological changes and produce inserts with required surface integrity. The follow up FIB milling also showed that sub-micron features could be successfully added on such BMG inserts with the required resolution and surface integrity and thus to benefit from their better wear and fatigue properties.

5. The experimental investigation identified the factors affecting the accuracy and surface integrity of a replication master produced by applying the proposed master-making process chain. However, it is difficult to quantify fully the effects of all these factors at each processing step on its overall performance. Nevertheless, the factors that are considered to have the highest impact are: the workpiece microstructure both for producing the Al masters and then the BMG inserts; the machine set-ups and processing conditions used for all component technologies and the BMG's response to TPF and FIB processing.

CHAPTER 6
OPTIMISATION ISSUES IN SERIAL MANUFACTURE OF POLYMER COMPONENTS WITH MICRO- AND NANO-SCALE FEATURES

6.1 Introduction

In the previous chapter, a cost effective master making process chain for achieving FLSI in mould inserts was designed and implemented. It employed a Zr-based BMG workpiece to integrate µMilling, Hot Embossing and FIB machining technologies in producing a replication master incorporating micro and nano scale structures. Subsequently, this FLSI enabling master-making process chain was validated by integrating the micro- and nano-structured Zr-based BMG insert into an injection moulding tool to produce small batches of thermoplastic devices. The results provided sufficient evidences about the viability of this master making process chain as a fabrication route for serial production of polymer based FLSI devices. However, this was just a feasibility study and all component technologies in the proposed process chain have to undergo further optimisation in the context of any specific application, and also their capabilities have to be studied systematically and potentially developed further. This chapter therefore reports follow-up research work to investigate the component technologies of this FLSI enabling master-making process chain. In particular, supplementary trials to investigate potential improvements to the surface integrity of the Al masters generated by the µMilling process are presented. Also, an experimental study of the TPF process is carried out to investigate its constraints in regards to the achievable replication quality. The FIB machining response of a fully amorphous Zr-based BMG insert is also systematically studied and subsequently compared with the previously reported results for partially crystalline Zr-based BMG inserts and thus to determine whether there are any

differences in the achievable nanoscale feature resolution and surface integrity. Finally, μIM trials are carried out to understand the broader applicability of the proposed FLSI enabling master-making process chain. The effects of BMG partial crystallisation on the insert's wear and fatigue life response is also studied in the context of the proposed process chain. The rest of the chapter is organized as follows. Next section outlines the experimental set-up utilised to carry out the above mentioned investigations. Then, the obtained results are discussed, and conclusions are made.

6.2   Experimental Setup

6.2.1 Insert material

For the reasons outlined in the previous chapter, the particular BMG used in this study is the commercially available Vitreloy 1b (Vit1b)

6.2.2 Test structure design

A schematic view of the simple micro-mixer used in this study is shown in Fig 6.1. Its channel and reservoir features are of micro scale while it also integrates three gratings that are of sub micron and nano scales. As it is depicted in Fig 6.2, each grating consists of a pattern of 20 x 20 black or white fields and all white fields are pockets. The smallest pixel dimensions in X, Y and Z directions of Gratings 1, 2 and 3 are 1μm, 600nm and 200nm respectively.

Furthermore, from Fig 6.1 it can be observed that the grating structures were placed in a specific position on top of the large reservoir. This was done so that when the BMG insert was placed in the mould cavity, the gratings would be in a location, where abrasion from the polymer during the injection moulding trials is expected to be most severe.
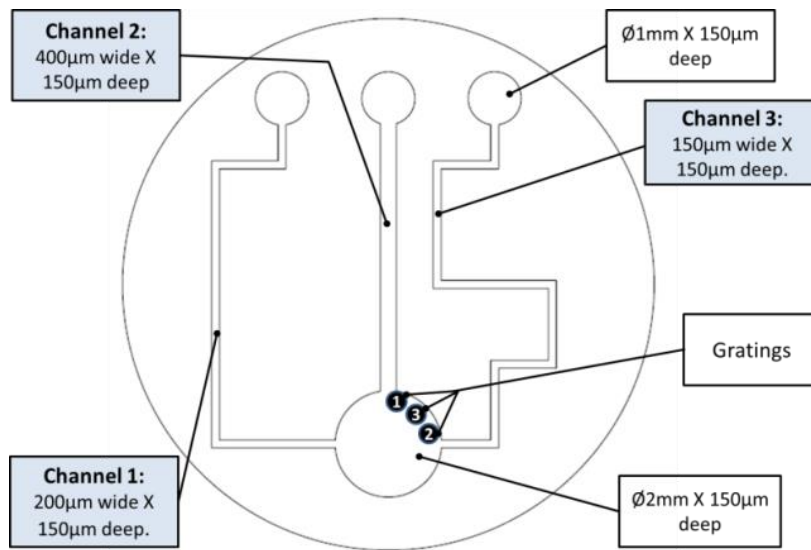
Figure 6.1 The micro-mixer design

Structure No	X (μm)	Y (μm)
1	20	20
2	12	12
3	4	4
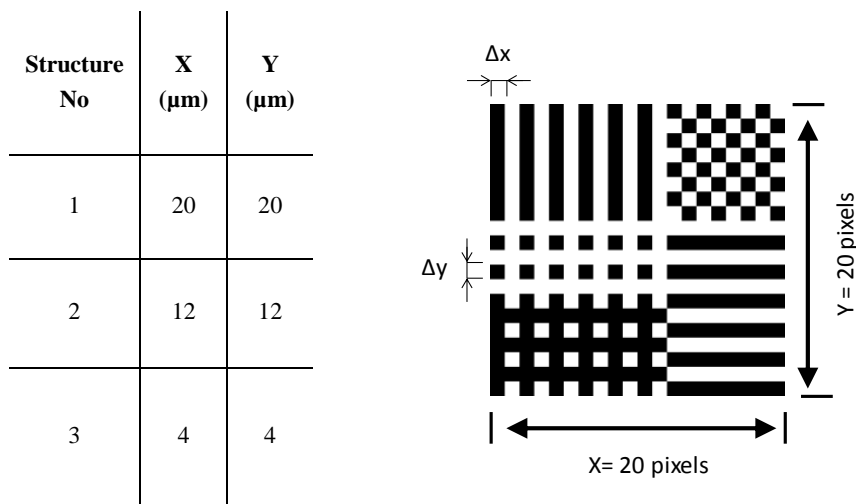
Figure 6.2 Grating structures

6.2.3 Micromilling of aluminium masters

The μMilling technology was employed to machine the micro-mixer features onto the Al workpieces. A tooling grade Al was used, in particular AL5083. This Al alloy was selected

because of its machinability (Popov et al., 2006) and the requirement to dissolve it after completing the TPF stage.

Samples from two different grades of Al 5083 blanks with different grain sizes were machined on a KERN HSPC 2216 micro-machining centre. The factors affecting the performance of μMilling operations investigated in a previous study (Dimov et al., 2004) were taken into account in selecting the machining parameters for producing the Al master. This included (i) the selection of cutting depth that would keep milling forces within predefined limits along the machining path; and (ii) spindle speeds and feed rates were optimised for the workpiece − the cutting tool - material combination. The used machining parameters were as follows: feed rate 250 mm/min; spindle speed 40,000 rpm; depth of cut 2 μm; and step over 50μm. The channels and reservoirs were machined to their full depth of 150 μm by applying reciprocating plunge-cut cycles. A 150 μm nominal diameter end-mill was used to mill the channels and the reservoirs.

6.2.4 TPF of BMG inserts

A hot embossing machine based on a Zwick universal testing machine with short cycle times was employed to produce the Zr-based BMG master. For each trial, a circular/ rectangular flat Vit 1b workpiece having a diameter/ side lengths of 15mm with an approximate thickness of 2mm was placed together with the Al master between parallel heated compression platens. The workpiece and Al master combination was then heated to a temperature above the Vit1b T_g, and then a pre-defined pressure was applied over a set time. After that, the load was gradually removed and the Al master-BMG insert "sandwiched" structure was cooled down.

To fill completely the Al master micro features it is essential to select a high processing temperature as the viscosity of the BMG decreases dramatically as the temperature increases.

However, it is important to stress that after a certain time at a given temperature above T_g, the Zr-based BMG will start crystallising. Thus, the material morphology should also be controlled because it affects the Vit1b homogeneity, and consequently, it will have a negative effect on the Vit1b's machining response to the FIB process. Therefore, it is very important to choose a temperature setting as high as possible for the respective processing time in order to maximise formability (Henann et al., 2009; Schroers et al., 2007b) whilst simultaneously controlling the material morphology. All these factors need to be considered in selecting the TPF process windows, given that an important objective for the HE trials was to control and maintain the Vit1b's morphology while achieving high replication fidelity with regards to micro mixer feature widths, depths and shape. As the focus of this research was to investigate the TPF process's replication constraints with regards to the achievable replication quality for both partially crystallised and fully amorphous workpieces, a systematic optimisation of the process was outside its scope. Consequently, only five tests were carried out with different processing temperatures, applied forces and overall process times that depended on the set temperature and cooling water flow rate. The parameter settings for each of these trials are presented in Table 6-1. These process settings were selected based on the available Vit 1b data, experimental investigations reported in literature (Henann et al., 2009; Schroers et al., 2007b; Schroers, 2005; Waniuk et al., 2003) and the specific micro-mixer test structure.

Table 6-1 Process settings for the TPF trials

Parameters	Trial No				
	1	**2**	**3**	**4**	**5**
Processing temp – T_p [°C]	435	420	440	440	450
Applied Force F_p [N]	4000	6000	4000	5000	5000
Overall Process Time - t_p [s]	180	185	340	198	230

Following the embossing stage, the Vit 1b inserts were separated from the Al masters by dissolving it in a heated NaOH bath. The BMG inserts were then inspected using SEM to select the inserts with the best feature resolution and surface integrity to undergo the follow up FIB structuring and subsequent injection moulding trials. Prior to FIB structuring, the selected Vit 1b inserts were also machined by wire EDM to the required overall size to integrate them into an injection moulding tool.

6.2.5 FIB processing

Two inserts, one partially crystallised and one fully amorphous Vit 1b metallic glass were each FIB milled with the three grating structures in Figure 6.2, in order to evaluate their machining response and thus to determine whether there are any differences in the achievable feature resolution and surface integrity. The three structures were machined onto the BMG workpieces using a Carl Zeiss XB 1540 FIB/SEM system that combines a gallium ion beam with an electron beam column. Given that the three gratings represent a 2D image composed of black and white fields/pixels, the bitmap file of this pattern was used directly by the FIB system's built-in software to control the milling operation. The depth and accuracy of the structures fabricated by FIB milling are determined by the processing parameters used. In this research, the process was set up by conducting the necessary machining trials on a fully amorphous workpiece to find out quickly a suitable processing window, whilst also achieving the best trade-offs between machining time and resulting surface quality. Both inserts were milled using the same set of process parameters in order to compare their FIB machining response. The processing parameters used in this experimental study are provided in Table 6-2.

Table 6-2 FIB milling parameters

Parameters	Structure No.		
	1	**2**	**3**
Probe current	2nA	200 pA	10 pA
Accelerating voltage	30kV	30kV	30kV
Exposure time duration	489s	963s	1070s
Probe width	150nm	40nm	14 nm

6.2.6 Micro-injection moulding

The machine used to perform the micro injection moulding tests was a Battenfeld Microsystem 50. The BMG insert was integrated into the primary mould using a secondary insert holder as seen in Fig 6.3. Three commonly used materials in injection moulding, namely Polypropylene (PP), Polycarbonate (PC) and Polyamide filled with 20% Glass fibre (PA+20%GF) were selected to conduct the replication trials. The first two materials were used to demonstrate the validity of this process chain for replicating satisfactorily both the micro and nano scale structures while the third one was primarily selected to investigate the durability of the partially crystalline BMG insert. The PA+20%GF material used in this research was Grivory GV-2 FWA Black 9225 and the technical data for this material are provided in Appendix F.
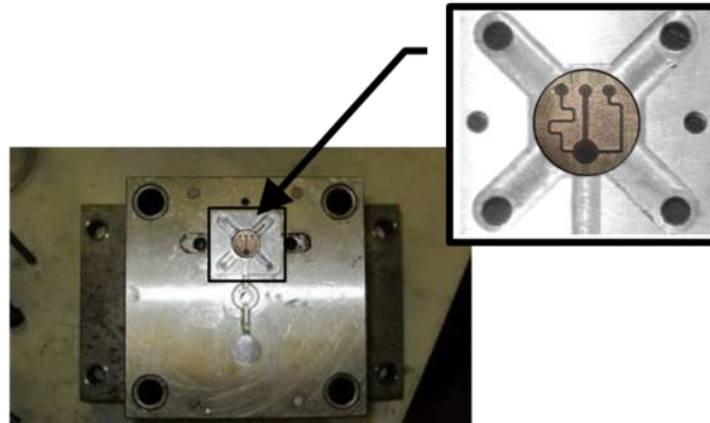
Figure 6.3 BMG insert and secondary insert holder assembly fitted into the primary mould

To replicate completely a mould cavity that incorporates micro and sub-micron features it is very important to select the right processing window. Many studies have been carried out to investigate how the process parameters influence the quality of the replicated parts, and the role and the consequences on the tool in achieving this (Mani et al., 2013; Huang, 2007; Monkkonen et al., 2002; Sha et al., 2006; Tosello et al., 2010a) . Since the main objective of this research was to investigate the component technologies of the proposed master making process chain an optimisation of the µIM process was not conducted and the process settings were selected based on results reported in other experimental studies. The moulding trials were carried out in two stages. In the first stage, the process settings were selected based on the material manufacturer's data sheets and results reported in other experimental studies for PP and PC (Scholz et al., 2011; Tosello et al., 2007) .   For both materials the initial trials showed that the process parameters needed to be optimised further in order to improve the replication quality of the nanoscale structures. Thus, the main objective of the second set of trials was to demonstrate that it was feasible to replicate nanoscale structures with a satisfactory dimensional quality. Therefore, the parameter settings were based mostly on experimental investigations into the filling performance of micro moulds with micro and sub-

micrometer features reported in literature (Huang, 2007; Monkkonen et al., 2002; Sha et al., 2006; Tosello et al., 2010a; Chen et al., 2010) , and thus to achieve as high as possible nano-scale gratings replication fidelity in terms of feature width, depth and shape. The process settings used for trials 1 and 2 for both PP and PC are presented in Table 6-3.

As it was mentioned above the third material was used to investigate the durability of the partially crystalline BMG insert by conducting 1000 replication cycles with a highly abrasive thermoplastic, namely PA+20%GF. The process settings given in Table 6-3 were selected based on the manufacturer's material data and experimental investigations reported in literature for a similar glass fibre filled polyamide (Tosello, 2008) . In addition, the partially crystallised Vit 1b insert was specifically orientated inside the cavity so that the large reservoir was in line with the gate as depicted in Fig 6.3, since this was the position where maximum wear on the reservoir top edge and nano-gratings was expected.

To obtain representative results about the Vit 1b insert performance, the micro injection moulding process was first allowed to stabilise for each set of process parameter settings by producing at least 20 components and only then batches of parts were produced for quality assessment.

Table 6-3 Micro-injection moulding process settings

Material:	PP (PPH 5042)		PC (Lexan HPS1-1124)		PA+GF20% (Grivory)
	Trial 1	Trial 2	Trial 1	Trial 2	Trial 1
Melt temp -- T_b (^{o}C)	220	240	260	290	270
Mould Temp -- T_m (^{o}C)	60	90	70	90	80
Holding Pressure -- P_h	ON	ON	ON	ON	ON
t_h (s)	5	8	5	8	7
Injection Speed -- V_i (mm/s)	150	200	200	400	400

6.2.7 Inspection

6.2.7.1 Dimensional measurements of microfluidic device

All the Al and BMG masters produced by μMilling and TPF, and also five replicas selected from the batches of the PP, PC and PA +20% GF polymer parts were inspected to analyse their dimensional accuracy. The microfluidic device channel/protrusion width inspections were performed with a Leica DMLM optical measuring microscope having an integrated PixeLink camera to capture images for further digital processing using the instrument's built-in software. Whereas the depth/height of the microfluidic device channel / protrusion features were inspected using an optical coordinate measuring machine (OCMM), namely a Mitutoyo QV Accel 404 Measuring System. The height/depth measurements were performed using the QV PAK software provided by the instrument manufacturer. As it was not possible to inspect exactly the same position of the channel features on the Al masters, BMG inserts' and polymer replicas' width and height/depth measurements in three predefined positions were conducted along each of the channel/ protrusion lengths and the average values were recorded.

6.2.7.2 Lateral measurements of grating structures.

Scanning Electron Microscope (SEM) images of the grating structures/features were taken first on the BMG inserts after the FIB milling stage and then on three PP and PC replicas to assess their lateral and vertical (XY) dimensions. These images were taken on the same system where the FIB machining was performed, in particular the Carl Zeiss XB 1540 FIB/SEM system. On each sample, three measurements for each grating were conducted in both the X and Y directions to obtain their overall widths. At the same time, 10 different

pixels in X and Y directions were also measured to obtain their widths and the average values are reported.

6.2.7.3 Depth measurements of grating structures

The three gratings on the Vit 1b inserts, and also on three PP and PC replicas were inspected with a Park Systems XE-100 atomic force microscope (AFM) in its non-contact mode configuration. The dimensions of the scanned areas were 35 x 35 μm, 22 x 22 μm and 7 x 7 μm for the 20 X 20 μm, 12 x 12 μm and 4 x 4 μm gratings, respectively. After the measurement, the data sets were processed using Park Systems XEI Data Processing and Analysis software to obtain the average line profiles of the features at specific locations in the scanned areas. In addition, the XEI software was used to create histograms and their two peaks corresponding to the height distributions of the original and the machined surfaces were used to determine average step heights. This method for evaluating average step heights was previously validated in chapter 4.

6.2.7.4 Surface roughness measurement

The surface quality of the Al masters and their Vit 1b replicas after the micromilling and TPF steps respectively was investigated. In particular, roughness measurements of the bottom/top surfaces of their 400 μm channels and protrusions respectively were performed using the Talysurf 120 L Surface Texture Measurement instrument. Furthermore, to quantitatively assess the wear of the partially crystalline Vit 1b insert after 1000 μIM cycles with PA +20% GF, the surface roughness of the top surface of the 400 μm protrusion was also measured before and after the μIM trial. The samples' evaluation lengths were chosen according to ISO 4288: 1997 (ISO4288, 1997; Leach, 2001) . The parameter used to inspect the surface roughness was the arithmetic mean roughness (Ra) because relative heights in micro

topographies are more representative, especially when measuring flat surfaces (Popov et al., 2006) . The surface texture measurements obtained were analysed using the instrument's built-in software. Three measurements were conducted along the channels/protrusions' lengths to calculate the average values of their surface roughness.

6.2.7.5 XRD

The thermal loads during the TPF and µIM process steps can trigger crystallisation of the Vit 1b BMG. Therefore, XRD analysis of the Vit 1b workpieces in the as-received condition and subsequently after the TPF operation and 1000 µIM cycles trial were carried out. A Rigaku™ Ultima IV X- Ray diffractometer having a monochromated CuKa$_1$ radiation source and using the θ / 2θ Bragg-Brentano configuration was employed for this analysis. The setup allowed the verification of the amorphicity or partial crystallinity of the BMG samples through the identification of characteristic peak developments which result on the onset of crystallisation.

6.2.7.6 Micro hardness measurements

Micro-hardness indentation measurements were carried out on the as received BMG material, and the partially crystallized Vit 1b insert after the TPF process step and 1000 µIM cycles. They were conducted using a Mitutoyo MVK-H2 Hardness testing machine fitted with a Vickers micro-indenter. The applied maximum load was 500gf. For each sample, 5 indentations were performed and the average hardness values of their measurements are reported.

6.2.7.7 Nano indentation hardness measurements

Nanoindentation experiments were carried out using a Micromaterials™ Nano Test 600 equipped with a Berkovich indenter. All the experiments were carried in an isolated chamber maintained at room temperature. Prior to nanoindentation, the samples were carefully polished to a mirror-like finish using 3 µm diamond paste. The indentation routine consisted of a loading segment of 40 s up to a load of 500 mN, this was followed by a load holding

segment of 30 s. The unloading segment was kept fixed at 40 s. Values for the reduced modulus as well as the material hardness were obtained from the unloading curve for which correction for the diamond area function and in- test thermal drift was done using the in- built software. For each sample, groups of 4 X 5 indents (20) were performed allowing a distance between indents of approximately 25µm in order to avoid interactions between each indent. Following the indentation experiments, the residual impressions of the indents were examined under a Carl Zeiss™ Merlin Field Emission SEM to observe and record the surface deformation characteristics.

6.2.7.8 Measurement uncertainty assessment

The linear dimensional measurements are reported with their associated expanded uncertainty, U, at 95% confidence level, which was determined by applying an established procedure (Joint Committee for Guides in Metrology (JCGM), 2008; Kirkup and Frenkel, 2006; United Kingdom Accreditation Service (UKAS), 2007) . For the AFM, the error contributors typical of AFM instruments (Tosello, 2008; Marinello et al., 2009; Tosello et al., 2009a, 2010b) were considered in the uncertainty budget. Whilst, the error sources for the optical measuring microscope, OCMM and SEM were identified by applying the recommendations for such measurements (Tosello, 2008; Tosello and Chiffre, 2004; Tosello et al., 2009b, 2012; Velkova, 2011) . In the case of the SEM, to account for the worst-case scenario the measurement uncertainty u(P) of the SEM was calculated as 3% of the measurand's average value (Velkova, 2011) . The reported surface roughness measurements are also provided with their associated expanded uncertainty, U, at 95% confidence level that was determined by following an established procedure (Leach, 2001) and by adopting recommendations given for surface roughness measurements in another study (Tosello et al., 2012) .

Finally, the reported hardness measurements are also provided with their associated expanded uncertainty, U, at 95% confidence level that was again determined by following an

established procedure and taking into consideration recommendations given for the estimation of hardness measurement uncertainty in the ISO-GUM standard (Joint Committee for Guides in Metrology (JCGM), 2008) and BS EN ISO 14577−1:2002 (BS EN ISO 14577, 2002) .

Additional data on the carried out uncertainty analysis and calculations is provided in Appendix C.

6.3 Results and Discussion

The experimental results obtained after each process chain step are presented in this section.

6.3.1 Micro milling step

Seven Al masters were produced in total using two grades of AL 5083 material. In particular, the Al 5083 samples 1 to 4 had a finer grain size to those of samples 5 to 7, respectively.

6.3.1.1 Dimensional accuracy

Table 6-4 presents the average channel widths and depths of the Al 5083, 1 to 4 and 5 to 7 masters, respectively. The measurements of the widths were taken at the top of the channels. As expected both sets of average widths and depths values concur very closely. Table 6-4 also presents the average channel widths and depths of all seven Al 5083 masters. There is a consistent deviation of the channel widths from their nominal values of 200μm, 400μm and 150μm respectively and thus it can be judged that the channels were cut oversized. This deviation is significant and is in the range between 13.3 μm and 14.5 μm and could be due to: (i) not introducing sufficient compensation for the actual tool radius; (ii) spindle/tool radial runout during machining; and (iii) measurement errors as the channel edges had some burrs and thus it was difficult to detect the edge location precisely.

Table 6-4 The average dimensions of the Al 5083 masters' micro features.

Samples		Channel 1 (200 µm)	Channel 2 (400µm)	Channel 3 (150 µm)
1 to 4	Width	213.2 ± 1.7	414.4 ± 1.6	163.6 ± 1.7
1 to 4	Depth	156.6 ± 2.0	155.4 ± 2.6	153.1 ± 2.2
5 to 7	Width	213.4 ± 1.7	414.7 ± 1.7	163.8 ± 1.8
5 to 7	Depth	153.2 ± 2.2	153.3 ± 1.9	152.1 ± 3.4
All	Width	213.3 ± 1.6	414.5 ± 1.6	163.7 ± 1.7
All	Depth	155.1 ± 1.6	154.5 ± 1.7	152.7 ± 1.8

It can be seen in Table 6-4 that there is also a consistent deviation between the channel depths and their nominal values of 150µm. Again, some systematic error is present though it is not so evident, being in the range of 2.7 to 5.1 µm. This deviation is not significant and could be due to both the spindle growth and the tool axial runouts during machining. Another contributing factor can be the measurement errors associated with the automated focussing process in detecting the top and bottom surfaces of the Al 5083 masters' channels. It should be possible to reduce both the width and depth deviations by carefully setting up the µMilling process but anyway these results are adequate taking into account the objective of this research, in particular to investigate the capabilities of the proposed master making process chain.

6.3.1.2 Surface roughness

Two average surface roughness values were obtained that correspond to samples being machined from the two different grades of Al 5083 workpieces, namely Ra 0.06 ± 0.012 and 0.34 ± 0.022 µm for samples 1 to 4 and 5 to 7, respectively. The significant difference of an almost 6 times better surface roughness can be explained with the refined microstructure of the Al 5083 samples 1 to 4 that has a direct "favourable effect on the" machining response (Popov et al., 2006; Koc and Ozel, 2011) . This surface finish can be considered adequate for TPF of the micro fluidic structures onto the BMG insert and then to add the sub-micron and

nano gratings by FIB milling in the follow up step. As FLSI is targeted in this research, especially nano scale structures are to be added on top of the pre-existing micro structures, the µMilled Al 5083 masters should have the best possible surface finish. Thus, to achieve this it is important to utilise workpieces with refined microstructures, e.g. ultrafine grained (UFG) Al alloys.

As the research reported in this chapter is only a pilot implementation of the proposed master making process chain, and also taking into consideration that the µMilling process and tooling set-up strategy were not fully optimised, it can be concluded that the Al 5083 masters were successfully fabricated. Collectively, it can be stated that the machining results are very promising and demonstrate that Al TPF masters with the required surface quality and dimensional accuracy can be fabricated successfully by µMilling when the right grade of Al alloys is utilised.

6.3.2 TPF step

Out of the 5 TPF trials performed, due to a set-up error and machine related malfunction, only three completely filled Vit 1b masters were produced. Consequently, in the following sections, only the results for these masters are presented.

6.3.2.1 Dimensional analysis

Table 6-5 presents the average depths/ heights and widths of the microscale features of both the Al 5083 TPF masters and their corresponding fully filled Vit 1b replicas. Comparing the average results for the protrusions' and channels' widths it is not difficult to see that for the three trials, they concur closely.

Table 6-5 Comparison of average depths & widths of hot embossed BMG inserts with corresponding aluminium masters.

		Aluminium Master					Hot Embossed BMG Insert					
		Channel 1 (200 μm)		Channel 2 (400 μm)		Channel 3 (150 μm)		Protrusion 1 (200 μm)		Protrusion 2 (400 μm)		Protrusion 3 (150 μm)	
Trial No		Width (μm)	Depth (μm)	Width (μm)	Depth (μm)	Width (μm)	Depth (μm)	Width (μm)	Depth (μm)	Width (μm)	Depth (μm)	Width (μm)	Depth (μm)
RTN 2		213.3 ± 2.4	152.0 ± 4.1	414.8 ± 1.7	150.5 ± 1.4	163.7 ± 1.9	151.0 ± 7.6	216.6 ± 3.9	152.1 ± 4.4	416.2 ± 1.7	151.7 ± 5.1	166.8 ± 5.6	150.7 ± 2.5
RTN 4		214.3 ± 1.8	151.8 ± 2.0	414.5 ± 1.9	153.8 ± 5.5	164.4 ± 2.8	154.9 ± 6.5	217.3 ± 2.1	151.5 ± 5.4	419.2 ± 2.3	149.1 ± 4.8	166.0 ± 1.9	151.9 ± 5.9
RTN 5		212.6 ± 1.8	151.6 ± 3.7	414.5 ± 1.7	152.3 ± 3.8	163.3 ± 2.5	152.9 ± 5.5	215.6 ± 2.2	151.7 ± 6.2	417.4 ± 1.7	151.6 ± 5.0	165.5 ± 2.9	150.8 ± 7.1

Thus, based on the data in Table 6-5, the percentage difference (S) values are provided in Fig 6.4. There is a consistent negative S trend; in particular the Vit 1b feature widths are consistently larger than the corresponding Al master feature widths. This is as expected and is due to both measurement errors and the dimensional changes of the Al 5083 master / Vit 1b insert micro scale features caused by the expansion/shrinkage effects of the heating/cooling cycles during the TPF step. Also, it is not difficult to see that for the three trials there is a tendency for the S values to decrease with an increase of the protrusion width, especially the 150μm protrusion 3 has the highest S value with a maximum difference of 1.9%.
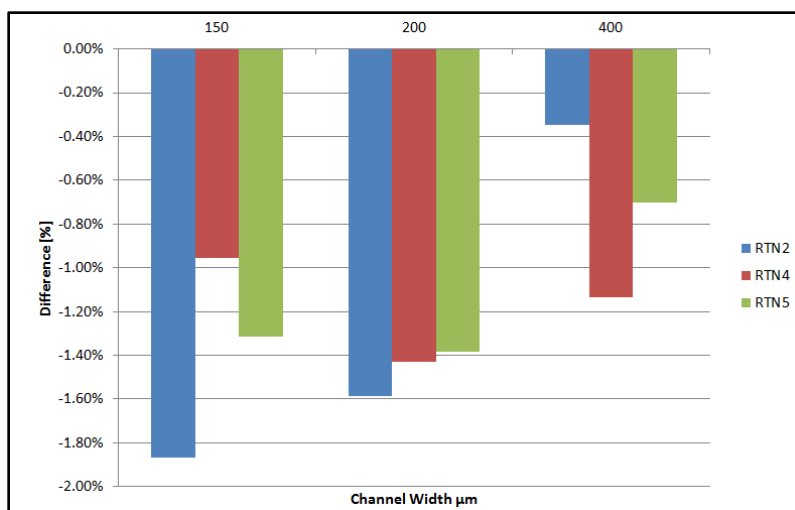
Figure 6.4 The percentage difference between the as-measured widths of the Al 5083 masters channels and Vit 1b inserts protrusions.

Nevertheless, the results for the three trials are very close and therefore the Vit 1b inserts can be considered accurate replicas of the Al 5083 masters in regards to the widths of the micro fluidics channels. The deviations from the pattern design is as expected, and as stated earlier they can be attributed to the expansion/shrinkage of the TPF Vit 1b insert features during the TPF heating/cooling cycles and also to some extent to measurement errors. The expansion/shrinkage magnitude is influenced by the Al 5083 alloy and Vit 1b properties in combination with the applied TPF process settings. Whereas the measurement errors are due to feature edges' definition and therefore there is an accumulation of measurement errors during feature measurements after each step in the process chain.
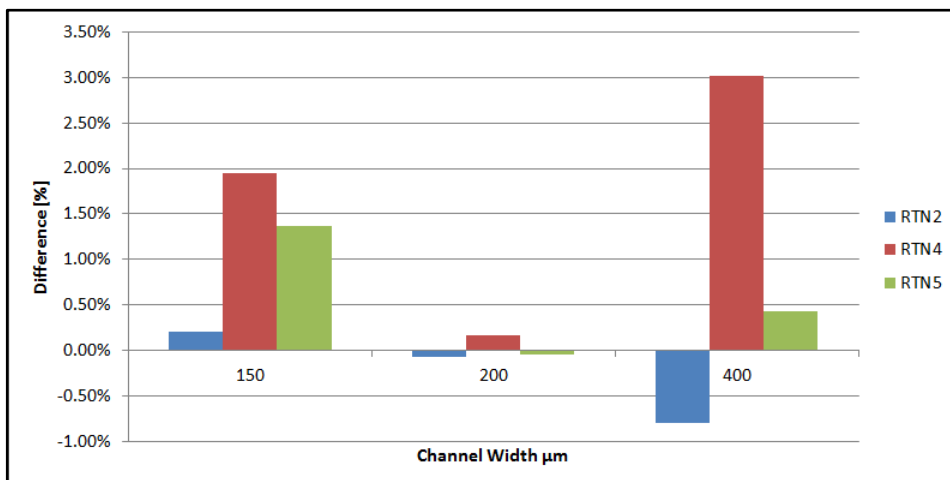
Figure 6.5 The percentage difference between the as-measured depths of the Al master channel features and the corresponding Vit 1b insert protrusions heights

From Table 6-5 and Fig 6.5, it is evident that that the average heights of the Vit 1b protrusions concur with the corresponding Al 5083 masters' channel depths. The negative and positive values indicate that the Vit 1b insert features are respectively larger or smaller than their corresponding Al master features. Again, they can be explained by the expansion/ shrinkage during the TPF heating/cooling cycles and the errors' accumulation when measuring the

channel depths and protrusion heights of the Al 5083 masters and Vit 1b inserts, respectively. Another contributing factor to these deviations is the focusing error during the QV system measurements.

Overall it is evident from the results that the TPF performance is adequate considering the small number of trials, only three, and the specific length scales.

6.3.2.2 Surface quality and XRD analysis of Vit 1b inserts.

Before proceeding to the FIB milling step, it is necessary to ascertain that: (i) the material has remained amorphous or has partially crystallised after the TPF step and (ii) the surface roughness is sufficiently low such that the FIB milling can be performed satisfactorily. Therefore, the surface integrity of the embossed features was investigated using the SEM and Talysurf 120L. At the same time X-ray diffraction was used to confirm the amorphicity or otherwise of the Vit 1b inserts both before and after the TPF step.

The roughness measurements of the 400 μm channels and protrusions of the Al 5083 and Vit 1b samples used in each TPF trial are provided in Table 6-6. In addition, the SEM images of one as-received Vit 1b plate and the three Vit 1b inserts after the TPF trials are shown in Figure 6.6.

Table 6-6 Comparison of 400 μm protrusions'/ channels' surface roughness of Vit 1b inserts with their corresponding Al 5083 masters.

Trial No	Al 5083 Master Channel 2 (Ra) (μm)	Vit 1b Insert Protrusion 2 (Ra) (μm)
RTN 2	0.0752± 0.0053	0.4478± 0.0117
RTN 4	0.3490± 0.0505	0.4953± 0.0167
RTN 5	0.3378± 0.0565	0.2866 ± 0.0099
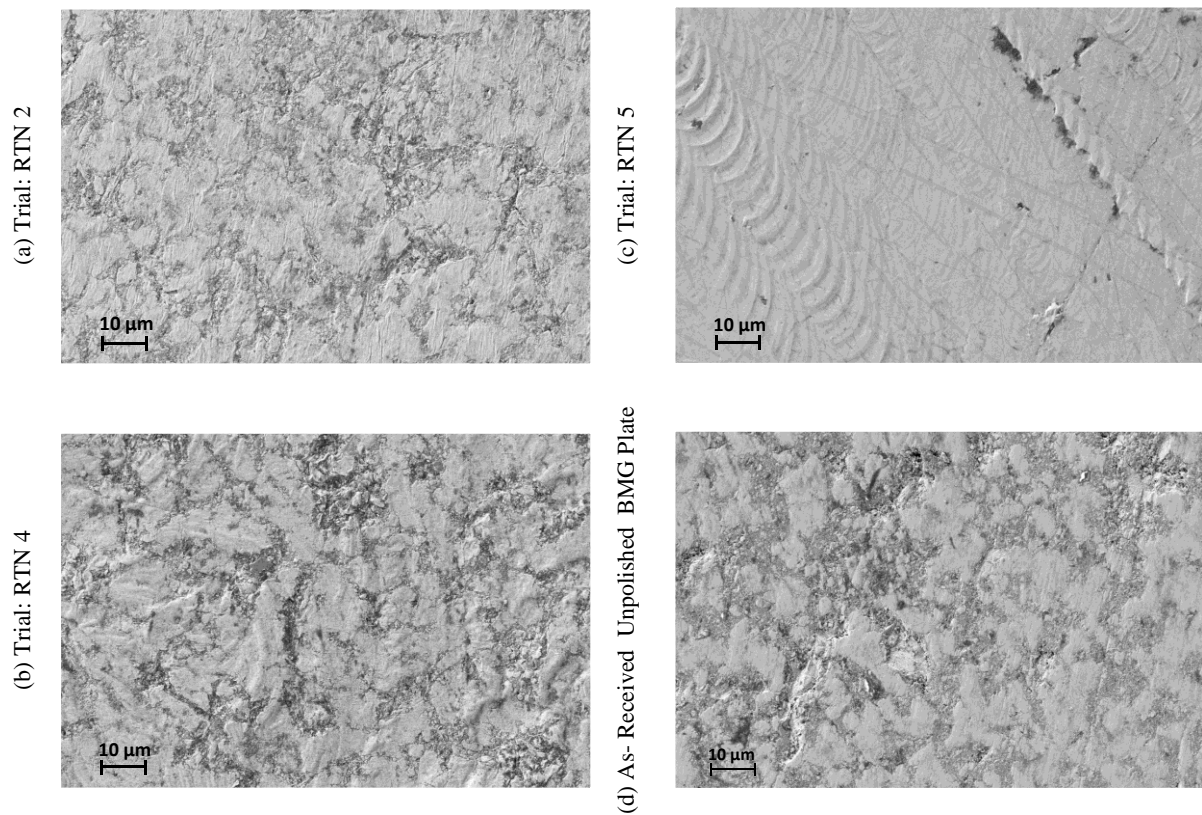
Figure 6.6 SEM images of the Vit 1b inserts after TPF and as received unpolished BMG plate

An initial examination of the results in Table 6-6 and Fig 6.6 reveals that the surface roughness of RTN 2 and 4 inserts are substantially higher than that of the RTN 5 insert. As it is discussed in the following section, this high surface roughness appears to originate from some initial surface contamination of the as-received Vit 1b workpieces prior to the TPF step. In particular, in the RTN 2 & 4 trials an as-received unpolished BMG plate was used, whilst in RTN 5 a polished one was used. Quantitatively, the average Ra values of the unpolished and polished Vit 1b plates before the TPF step were 0.48 and 0.01 µm respectively. Analysing the results in Table 6-6 and the images in Fig 6.6 (a) and (b) and Fig 6.6 (d) it is clear that both the Al masters' and the as-received Vit 1b plates' roughness contribute to the resulting surface roughness after the TPF step. In particular, it can be seen that for RTN 2 the surface

roughness after the TPF step is marginally better than that of the as-received unpolished Vit 1b plate. Whilst for RTN 4 it is slightly worse than the roughness of the unpolished Vit 1b plate before the TPF step. Overall, these results demonstrate that the TPF process did not reduce the surface imperfections on the as-received Vit 1b plates. These results were not expected, since a recent study (Kumar et al., 2010) revealed that the TPF surfaces are two orders of magnitude smoother than the polished surface of the same alloy. Thus, the TPF process is capable of generating atomically smooth surfaces and also to replicate closely the surface topography of the Al masters. A potential contamination of the as-received Vit 1b plates prior to the TPF step together with the used embossing process settings could explain the outcomes of RTN 2 and 4. Therefore, an Energy Dispersive Spectroscopy (EDS) analysis of the as received unpolished and polished Vit 1b plates was carried out. The EDS analysis showed that the unpolished Vit 1b plates in addition to a large amount of Vit 1b elements also contain traces of aluminium and oxygen. Whilst for the polished plate these traces are substantially smaller. These results confirmed the hypothesis for a prior contamination of the as-received unpolished BMG plates with aluminium oxide (alumina) that was substantially reduced by mechanically polishing them. The alumina traces cannot be TPF at the applied embossing temperature settings and this explains the resultant high surface roughness. Such surface contamination could have originated from the Vit 1b casting process. A similar problem was reported by Bardt and Sawyer (2007) where a crystalline layer was found at the interface between a silicon mould and a Zr-based BMG component. Collectively, the results and the discussion above stipulate that although the surface roughness of the as-cast Vit 1b plates are relatively low, they still need to be polished prior to the TPF step in order to remove any surface contaminants, and thus to assure excellent imprintability at the applied embossing temperature settings.

Regarding the applied TPF processing settings, the analysis of Figs 6.6 (a) and 6.6 (b) shows that the µMilling texturing of the Al masters is not evident on the Vit 1b insert in RTN 2 when it is compared with the insert in RTN 4. This can be explained by the applied process settings, especially the higher embossing temperature, 440 ^{o}C in comparison with 420 ^{o}C in RTN 2. A further increase of the embossing temperature to 450 ^{o}C together with the use of the polished plate in RTN 5 led to a much clearer replication of the µMilling texturing onto the Vit 1b insert and also the insert roughness is marginally better, Ra 0.29 µm than Ra 0.34 µm on the corresponding Al 5083 master (see Table 6-6 and Fig 6.6 (c)). These improvements in the replication performance can be attributed clearly to the lowering of the Vit 1b viscosity with the increase of the embossing temperature, and thus to facilitate the Vit 1b viscous flow and reproduce fully the surface texture of the Al master. This is as expected since the 'viscosity' of BMG decreases dramatically as the temperature increases, and also concurs with other studies which suggest that, selecting a temperature as high as possible (Henann et al., 2009; Schroers et al., 2007b) whilst simultaneously controlling the material morphology is the most important consideration in identifying the optimum TPF processing window.

It can be stated that with the use of polished Vit 1b plates and proper TPF process settings it is possible to replicate accurately the Al master's surface topography even at nano scale , as the results in RTN 5 showed. The entire top surface of the Vit 1b insert's microfluidic pattern cannot be used for follow-up sub-micron and nano structuring, however adequately smooth areas can be located to carry out FIB milling. The TPF results are encouraging but they also show that further work is required to optimise the embossing process, and thus to improve both the surface integrity and the replication quality of the produced Vit 1b inserts. The analysis of the TPF step also shows that the results can be affected significantly by the outcomes of the preceding stages in the process chain, in particular the µMilling step and also by the cross-contamination of the as-received BMG material.

The BMG inserts were analysed both before and after the TPF step to verify either their amorphicity or partial crystallinity. In particular, one as-received BMG plate and the unstructured bottom surface of each Vit 1b insert after TPF was polished and subsequently analysed by X-ray diffraction. Fig 6.7 depicts the XRD patterns of one as-received polished BMG plate before the TPF step, and the three Vit 1b samples after the TPF step. In Fig 6.7 (d) the broad diffraction maxima of the XRD spectra shows typical amorphous characteristics that are similar to those obtained for a fully amorphous Vit 1b in another study (Waniuk et al., 2003) and thus can be used to validate the TPF step.
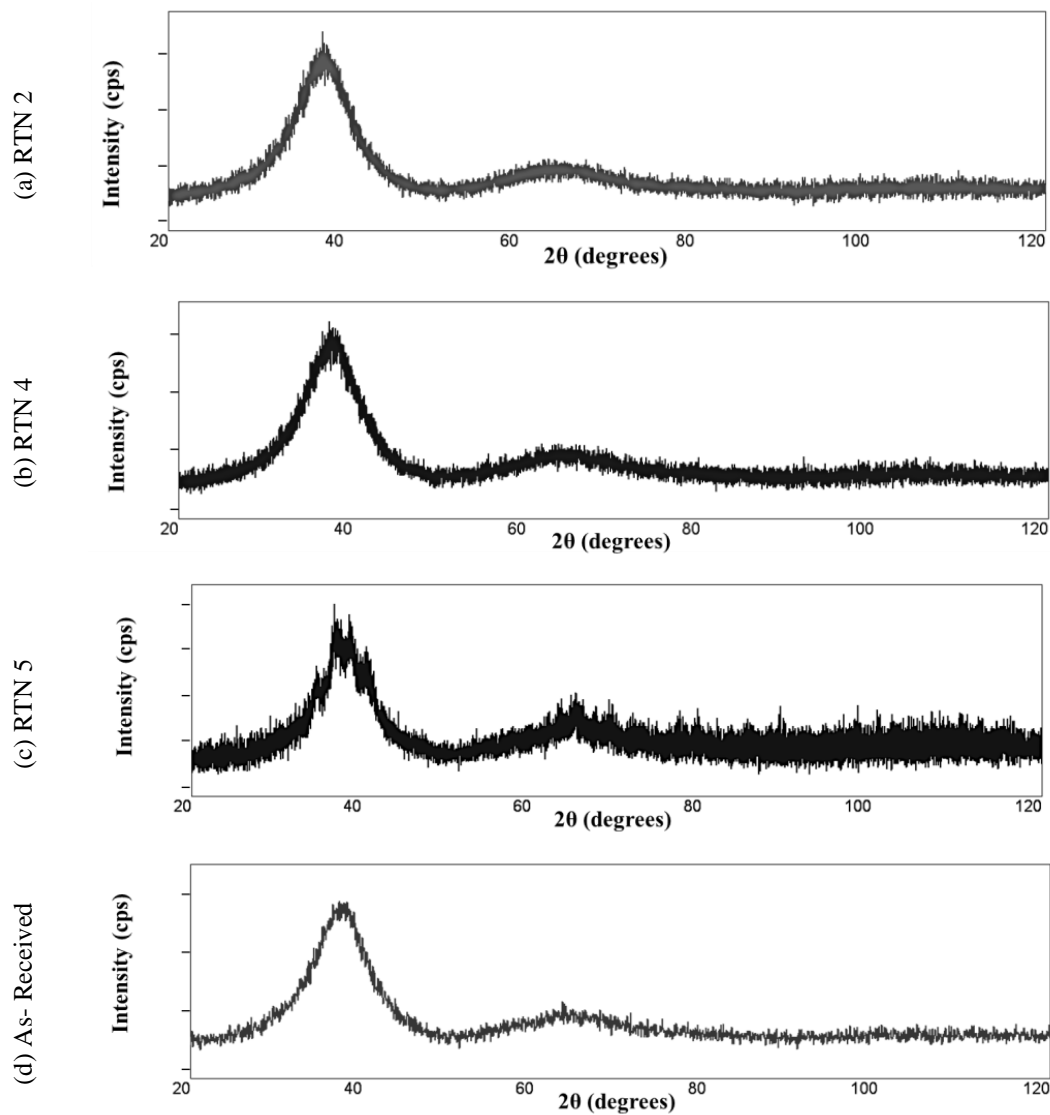
Figure 6.7 XRD analysis of the BMG inserts after the HE step and the polished as received Vit 1b plate

In Figs 6.7 (a) and (b), the typical broad diffraction maxima of the XRD patterns also confirms the fully amorphous characteristics of the Vit 1b inserts in RTN 2 and 4. For both inserts, no crystalline peaks were found within the XRD detection limit and thus their amorphicity was retained at the respective TPF parameter settings. However in Fig 6.7 (c) for RTN 5 it can be seen that there are a few weak but sharp crystalline peaks superimposed on the broad humps meaning that the full amorphicity was not retained at the respective TPF settings and elapsed processing time. Nonetheless, as shown in chapter 5, since the produced Vit 1b insert is still predominantly amorphous, it is possible to create nanoscale gratings onto the top of pre-existing functional micro structures during the FIB milling step. As also discussed in the previous chapter, this partial crystallisation was not expected at the used processing conditions since the processing temperature and time were within the processing constraints discussed earlier, in particular the embossing temperature and time have not exceeded the crystallisation thresholds of 460° C and 255 s, respectively (Waniuk et al., 2003). This can be attributed to a combination of two factors, a lower T_x for the Vit 1b plates used that is close to the embossing temperature together with a likely shorter crystallisation onset time.

It is apparent from these XRD results that TPF is a highly sensitive but "tuneable" process and that with judicious selection of the process settings it is possible to generate both fully amorphous and/or partially crystallised BMG inserts. It is also clear that although the XRD results are within the technical requirements for producing such functional structures further improvements are possible by optimising the TPF process, especially the embossing temperature and time.

Collectively, in spite of the limited optimisation efforts in this study these results are encouraging and demonstrate that both fully amorphous and partially crystallised Vit 1b inserts with the required resolution and surface integrity can be produced by TPF.

6.3.3 FIB milling step

The partially crystallised Vit 1b insert produced in RTN 5 had the required surface quality on the reservoir surface to carry out the follow up FIB milling step. The results are compared with the same grating structures FIB milled onto a polished as-received fully amorphous Vit 1b blank.

Figs 6.8 and 6.10 depict the three nano scale gratings milled onto the fully amorphous and partially crystallised Vit 1 B inserts. Comparing the images, it can be judged that for all the three grating structures, the pixel features milled on both inserts are well produced and very similar in terms of resolution and surface integrity.

Structure 1   Structure 2   Structure 3
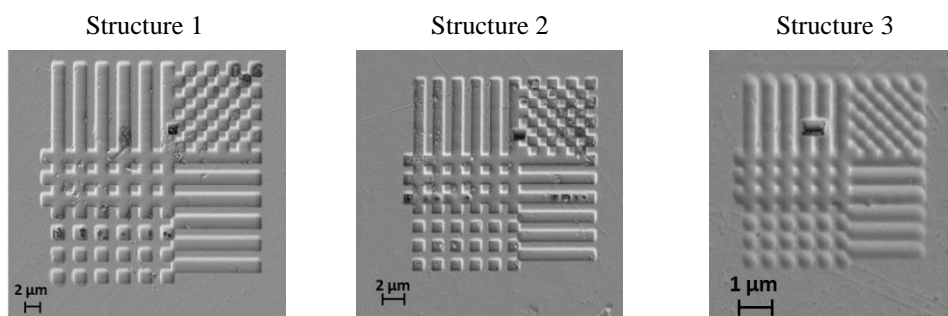
Figure 6.8 Nano-scale gratings FIB milled onto a fully amorphous Vit 1b insert
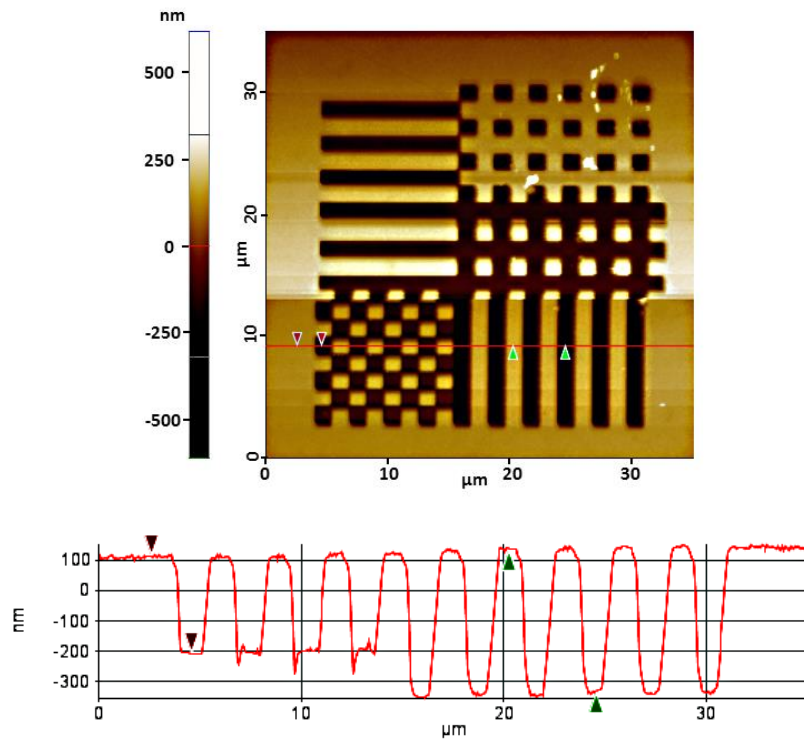
Cursor		ΔY (nm)
■	Red	-319.826
■	Green	-465.199

Figure 6.9 Grating structure 1 profile of the fully amorphous BMG insert
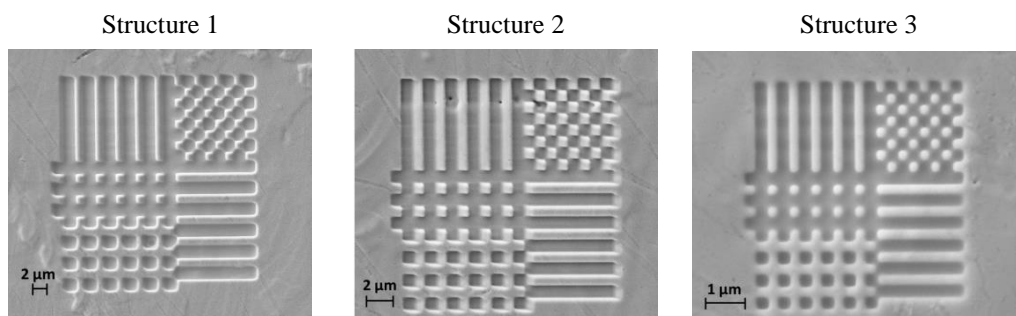
Figure 6.10 Nano-scale gratings FIB milled onto the partially crystallised Vit 1b insert.

The average AFM line profiles of the three grating structures at pre-defined locations were analysed. In particular, Figures 6.9 and 6.11 depict the average AFM line profiles of the 20µm gratings on the fully amorphous and partially crystallised Vit 1b inserts, respectively. It can be observed that although the same FIB parameters were used on both inserts, the pixel structures on the partially crystallised BMG exhibit a higher degree of sidewall tapering. Similar results were also observed for grating structure 2, whilst for grating structure 3 both inserts exhibited the same degree of pixel sidewall tapering. The tapering of grating structures 1 and 2 could be explained with the used FIB process parameters that were not optimised for processing partially crystallised Vit 1b BMG substrates (Li et al., 2007b) or possibly some setting up issues as the processing of the fully amorphous sample was carried out with different system calibration. It should be noted that such tapering could be even beneficial for replicating sub-micron structures.

Tables 6-7 and 6-8 present the average heights and widths of the gratings' smallest features of both inserts, respectively. The average step heights of the pixels were determined using the histo-distributions generated from the AFM height measurements of the gratings. The tables also include the average values of the gratings' overall sizes.

Table 6-7 The gratings dimensions of the fully amorphous Vit 1b insert

Grating Structure No.	Pixel Width (µm)		Pixel Height (nm)	Overall Width (X) (µm)	Overall Width (Y) (µm)
	X	Y			
1 (20µm)	1.46 ± 0.10	1.46 ± 0.10	381.18 ± 4.64	28.83 ± 1.73	28.95 ± 1.75
2 (12µm)	0.87 ± 0.05	0.87 ± 0.06	319.73 ± 4.44	17.34 ± 1.04	17.31 ± 1.04
3 (4µm)	0.30 ± 0.03	0.31 ± 0.04	84.30 ± 4.01	5.84 ± 0.35	5.88 ± 0.36

Table 6-8 The gratings dimensions of partially crystalline Vit 1b insert

Grating Structure No.	Pixel Width (µm)		Pixel Height (nm)	Overall Width (X) (µm)	Overall Width (Y) (µm)
	X	Y			
1 (20µm)	1.46 ± 0.11	1.47 ± 0.11	461.90 ± 9.37	28.53 ± 1.72	28.59 ± 1.72
2 (12µm)	0.88 ± 0.06	0.88 ± 0.05	289.22 ± 5.74	17.26 ± 1.04	17.35 ± 1.05
3 (4µm)	0.28 ± 0.02	0.29 ± 0.03	92.03 ± 4.12	5.62 ± 0.34	5.78 ± 0.35

The comparison of the lateral dimensions shows that the values for both workpieces concur very closely. Also, it can be observed for both inserts that the average pixel widths in the X and Y directions at the bottom of the protrusions are larger than their nominal values of 1 µm, 600nm and 200nm. This difference could be due to not introducing adequate compensation for the used FIB diameters of 150nm, 40nm and 14nm, respectively and also due to measurement errors as the pixels' edges are rounded thus making their precise detection more difficult. Besides these two factors the discrepancies could also be the result of calibration and set-up issues associated with the FIB system used.

From Tables 6-7 and 6-8 it is also evident that that the average step heights of the gratings milled on the fully amorphous Vit 1b workpiece do not concur so closely with those milled on the partially crystallised counterpart. In particular, the average step height deviations are approximately 80.72 nm, -30.51 nm, and 7.73nm for the 20µm, 12µm and 4µm gratings, respectively. At this point, taking into account the limited number of inserts and the inconsistencies of these small deviations, it is not possible to state unequivocally if they are significant and due to differences in the milling FIB response of the two inserts or whether they may be attributed to stochastic factors.
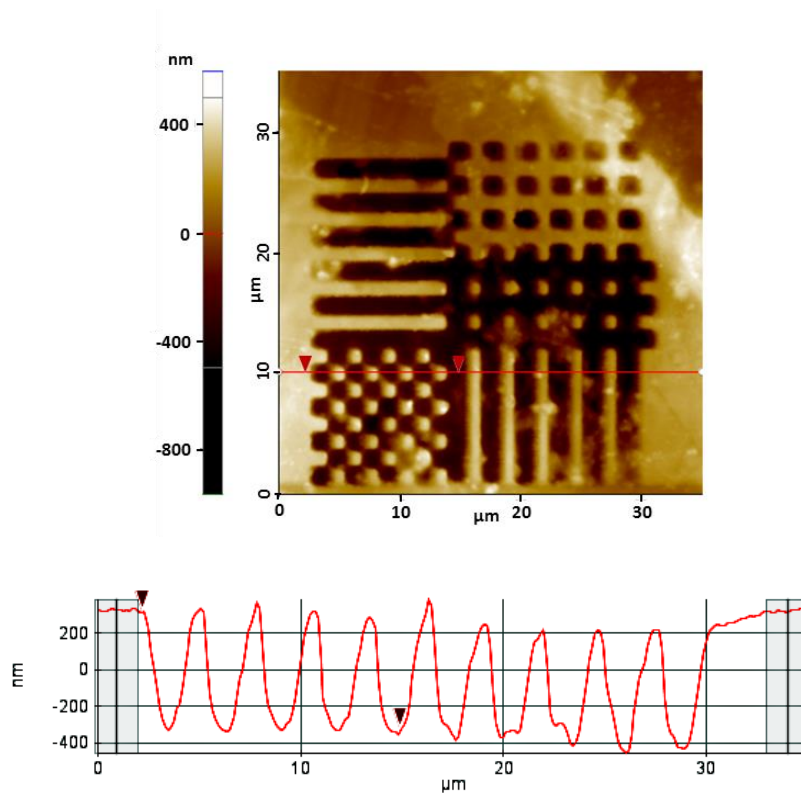
Cursor	ΔY(nm)
■ Red	-643.564

Figure 6.11 Grating structure 1 profile of the partially crystallised BMG insert

The step height results for the three grating structures also show that for both inserts the average heights are substantially smaller than their nominal values of 1 μm, 600nm and 200nm, respectively. In addition, examining Figures 6.9 and 6.11 it can also be judged that the FIB milling depths are also not uniform across the grating structure 1 on both inserts. Similar results were obtained for the other two gratings. Again, these results could be explained both with the measurement errors associated with the quality of the pixel edges and also with not properly calibrating the layer-based FIB milling process, in particular the sputtering rates for the selected FIB milling settings in Table 6-2. If such a calibration is

carried out the form deviations of complex 3D structures could be kept within 2 to 5 % of their nominal dimensions (Velkova, 2011) .

In spite of the limited optimisation efforts, the results show that the geometrical accuracy and surface integrity of the nano-scale grating features on the partially crystallised Vit 1b insert are similar to those obtained on the fully amorphous workpiece. There were some deviations from the nominal dimensions and shape but the FIB milling process can be optimised to meet the requirements of the proposed FLSI enabling master making process chain.

6.3.4 µIM process step

6.3.4.1 Replication of microfluidic device pattern

Figure 6.12 shows the microfluidic device pattern (see Figure 6.1) that was replicated well using the three materials, PP, PC and PA+20% GF, investigated in this research.

a) PP Microfluidic Device.   b) PC Microfluidic Device   c) PA+20% GF Microfluidic Device.
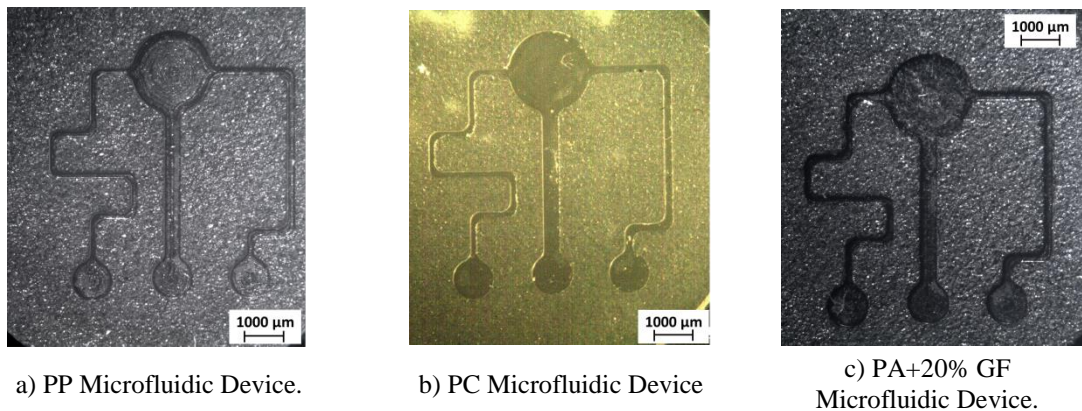
Figure 6.12 Replicated microfluidic patterns in PP, PC and PA+20% GF

The average channel heights and widths of the PP, PC and PA+20%GF micro-mixer replicas generated using the Trial 1 process parameter settings (see Table 6-3) are provided in Table 6-9.

Comparing the partially crystallised RTN 5 insert's average protrusion width in Table 6-5 with the corresponding channel width of the replicas in Table 6-9, it can be judged that they concur closely.

Table 6-9 The dimensions of the replicated microfluidic devices

Trial No	Channel 1 (200 µm)		Channel 2 (400 µm)		Channel 3 (150 µm)	
	Width (µm)	Depth (µm)	Width (µm)	Depth (µm)	Width (µm)	Depth (µm)
PP Parts	203.5± 2.1	148.0± 1.7	404.2± 2.1	148.2± 1.6	153.7 ± 2.4	147.4± 1.3
PC Parts	211.6± 2.8	149.7± 1.6	414.9± 2.6	150.2± 1.6	158.9± 2.4	149.4± 2.0
PA + 20%GF Parts	212.1± 2.9	150.3± 2.2	414.3± 2.1	149.9± 2.4	157.2± 2.9	150.7± 2.3

The average percentage difference for the channels is around 5.3%, 2.1 % and 2.5% for the PP, PC and PA + 20% GF materials respectively. These deviations are higher than the expected typical shrinkage values of 1 to 2% for PP, 0.5 to 0.7 % PC and 0.15 to 0.75 % for the PA+20% GF. Again, measurement errors due to not well defined channel and protrusion edges together with the used injection moulding parameters, in particular the packing pressure and time, could be the reasons for this. PP parts exhibit the highest percentage difference, which can be attributed to the cooling rates that affect the shrinkage of a semi crystalline material. In particular, the mould temperature was set towards the maximum recommended value in order to replicate fully the sub-micron structures. However, this caused the PP replicas to cool down more slowly and led to a higher crystallinity and shrinkage (Beaumont et al., 2002; Osswald et al., 2008) . This problem can be overcome by increasing the cooling rate and consequently the shrinkage can be reduced. As expected the average shrinkages of

PC and the glass filled PA replicas are significantly lower than that of the PP replicas. In particular, they are more accurate replicas of the BMG insert's microfluidic pattern with average width deviations of 2.1 % and 2.5 %, respectively. Again, a higher than typical shrinkage of the glass filled PA replicas can be explained with the material's semi crystallinity, however, the negative effects are mitigated by the presence of glass fibres.

The insert's protrusion height (see Table 6-5) concurs quite closely with the corresponding channel depths of the replicas in Table 6-9. The average difference for all channels is around 2.3%; 1.04 % and 0.70% for the PP, PC and PA + 20% GF replicas, respectively. As expected, this difference is less than that for the channel widths because the shrinkage is higher in the direction of the polymer flow (Osswald et al., 2008) . However, the differences are again small and therefore all the polymer parts can be considered accurate replicas of the BMG insert microfluidic pattern despite the fact that the process parameters were not fully optimised.

6.3.4.2 Replication of nano-scale gratings

Fig. 6.13 shows that the grating structures were replicated successfully on the polymer parts when using the fully amorphous Vit 1b mould insert and the Trial 2 μIM parameter settings in Table 6-3. There are some localised voids in the grating structures on both the PP and PC replicas due to some trapped air in the microcavity (Heckele and Schomburg, 2004; Zhang et al., 2012b) . This can be minimised by introducing air evacuation from the cavity prior to injection (Giboz et al., 2007; Sha et al., 2006; Attia et al., 2009; Griffiths et al., 2011; Heckele and Schomburg, 2004) and thus to improve further the replication quality of the nanoscale structures.

| a) PP Structure 1 | b) PC Structure 2 | c) PP Structure 3 |
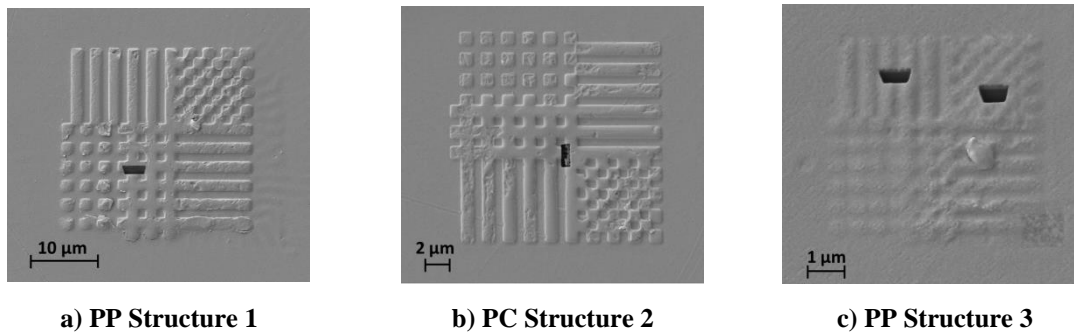
Figure 6.13 Replicated grating structures.

Tables 6-10 and 6-11 show the average heights and widths of the smallest gratings' features from the samples replicated in PP and PC, respectively. Also, the tables show the average overall sizes of the gratings in the X & Y directions. The dimensions of the three gratings concur closely with the corresponding ones in Table 6-7 for the fully amorphous Vit 1b insert. In particular, the pixel width deviations vary between 0.7 to - 6.3 % and 0 to -3.5 % for the PP and PC replicas, respectively, but there is no consistent percentage difference trend. The average width dimensions of the "small" pixels were also calculated based on the overall sizes of the individual gratings in Tables 6-7, 6-10 and 6-11 and the number of pixels (20) in order to minimise the effects of the accumulated measurement errors associated with the quality of the "pixel" edges. If the shrinkage is calculated based on these more realistic width values the differences are reduced to 2.1 - 3.3 % and 0.9 - 2.6 % for the PP and PC replicas, respectively. For both polymers, these deviations are still higher than the expected typical shrinkage values and again they can be explained with the injection moulding settings that were not fully optimised and also the semi crystallinity in the case of PP.

Table 6-10 PP Gratings micro and nano - scale feature dimensions

Grating Structure No.	Pixel Width (μm)		Pixel Height (nm)	Overall Grating Structure Width (X) (μm)	Overall Grating Structure Width (Y) (μm)
	X	Y			
1 (20μm)	1.46 ± 0.10	1.45 ± 0.09	369.02 ± 8.16	28.32 ± 1.70	28.30 ± 1.70
2 (12μm)	0.91 ± 0.06	0.92 ± 0.07	306.23 ± 6.72	16.86 ± 1.01	16.97 ± 1.02
3 (4μm)	0.32 ± 0.03	0.32 ± 0.03	74.72 ± 4.10	5.65 ± 0.34	5.74 ± 0.35

Table 6-11 PC Gratings micro and nano - scale feature dimensions

Grating Structure No.	Pixel Width (μm)		Pixel Height (nm)	Overall Grating Structure Width (X) (μm)	Overall Grating Structure Width (Y) (μm)
	X	Y			
1 (20μm)	1.5 ± 0.09	1.5 ± 0.10	360.50 ± 11.69	28.72 ± 1.73	28.67 ± 1.72
2 (12μm)	0.90 ± 0.06	0.90 ± 0.06	316.78 ± 9.28	16.99 ± 1.02	16.91 ± 1.02
3 (4μm)	0.30 ± 0.02	0.31 ± 0.02	78.67 ± 4.21	5.70 ± 0.34	5.73 ± 0.34

The gratings' step heights of the PP and PC replicas in Tables 6-10 and 6-11 respectively were also determined by considering the histo-distributions generated from the AFM scans. Comparing them with their corresponding heights for the fully amorphous Vit 1b insert in Table 6-7, it can be observed that they are consistently slightly smaller. In particular, the average depth difference for all three gratings varies between 3.2 - 11.4 % and 0.9 - 6.7 % for the PP and PC parts, respectively and again they are higher than the expected typical shrinkage values due to the same reasons as those for the width deviations. Fig 6.14 depicts a typical average line profile of the 20μm grating replicated on one of the PP parts. The pixel depths are not uniform and similar results were obtained for the other two gratings on the PP replicas and also for the three gratings on the PC replicas. These results can be attributed both to some non-uniformity of the gratings in the Vit 1b insert and again with some trapped air.

Thus, it can be judged that the 20µm, 12µm and 4µm gratings were replicated successfully on the PP and PC mouldings in this feasibility study but the quality can be improved further by optimising the µIM settings systematically. Also, the research has revealed potential challenges in performing an effective quality control and reliable manufacturing at sub-micron scale that should be addressed, too.
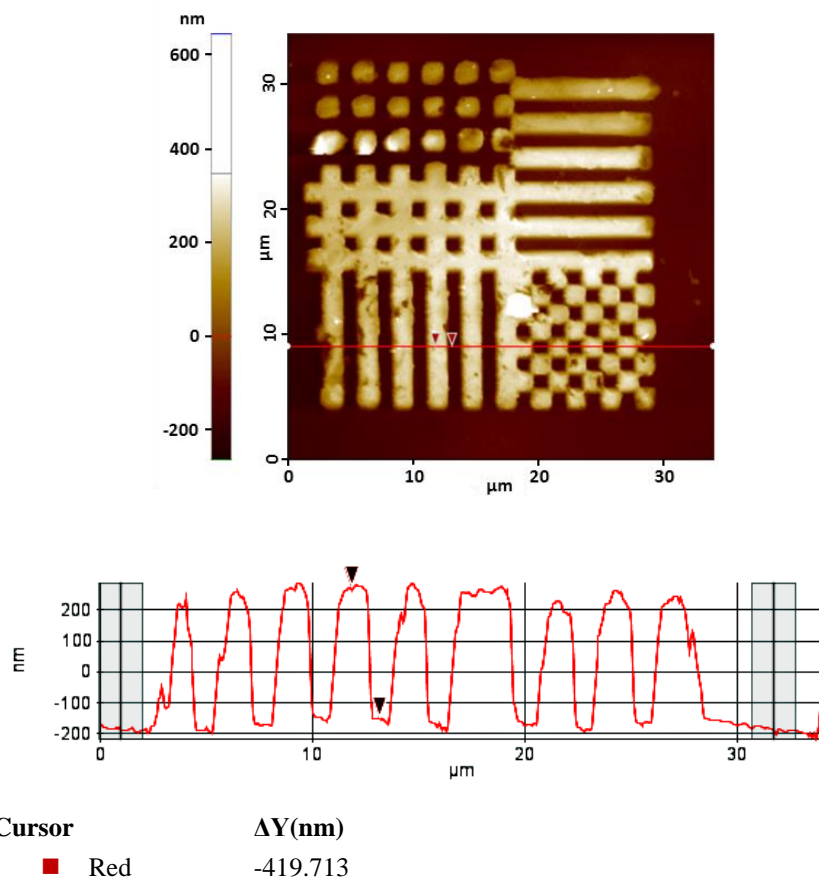
Figure 6.14 PP grating structure 1 AFM profile of the features

6.3.5 Tooling performance evaluation.

In this section the performance of the partially crystalline BMG insert is evaluated by studying it's condition after enduring 1000 injection moulding cycles with the highly abrasive PA+20% GF thermoplastic.

6.3.5.1 Insert wear

SEM images of the Vit 1b insert's surface before and after the 1000 injection cycles are used for a qualitative wear assessment. Figure 6.15 shows SEM images of the large reservoir side wall in a selected location at progressively increasing magnifications: (a) before the µIM trials, 0 shots, (b) after 167 cycles and (c) after 1000 cycles. The smoothening effect on the reservoir edge and the µMilling surface texture with the increase of µIM cycles is very small in spite of fact that the imaged area was situated directly in front of the gate and as consequence of this there was some glass fibre impingement erosion. Furthermore, the glass fibres seem to leave scratches on the reservoir's top surface and upper part of the side wall due to the sustained strain during the µIM cycles. The reason for this is that the reservoir's surface is not only strained during the polymer injection step but also during the demoulding of the solidified replicas.
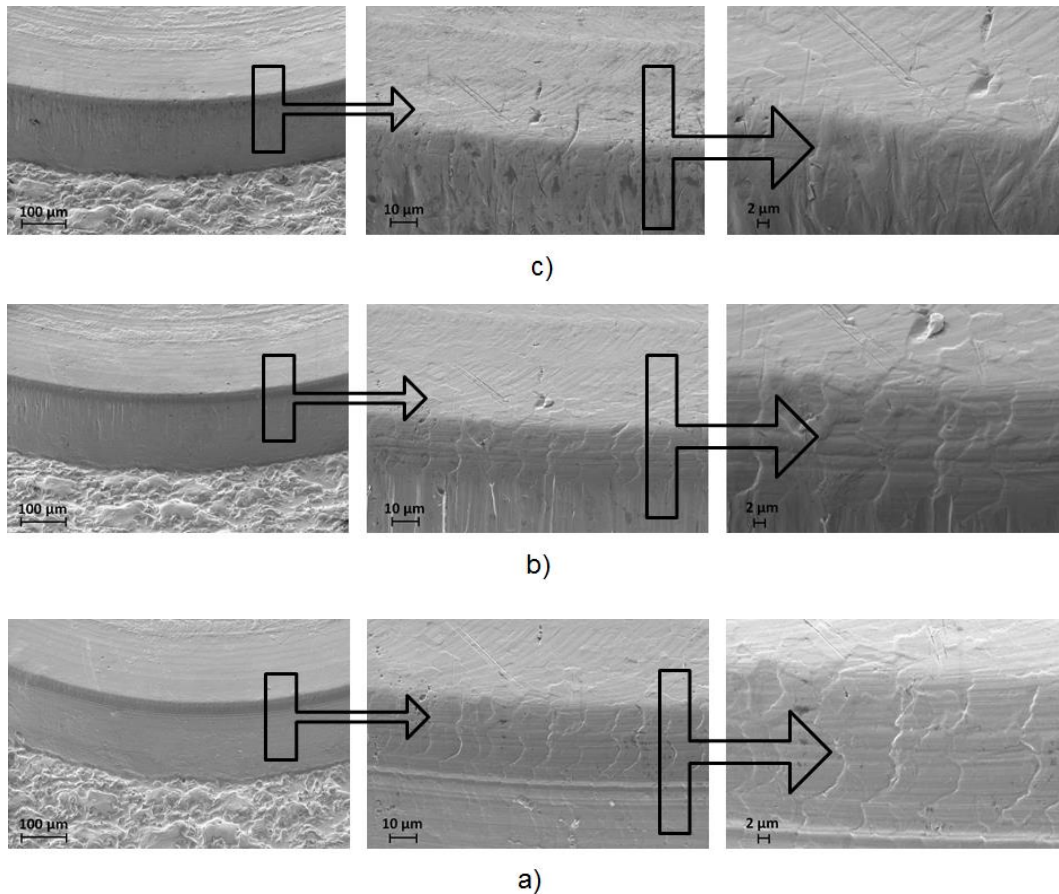
Figure 6.15 SEM images of the Vit 1b insert reservoir side wall: (a) before the µIM trials, (b) after 167, and (c) 1000 injection cycles.

20 µm grating   12 µm grating   4 µm grating
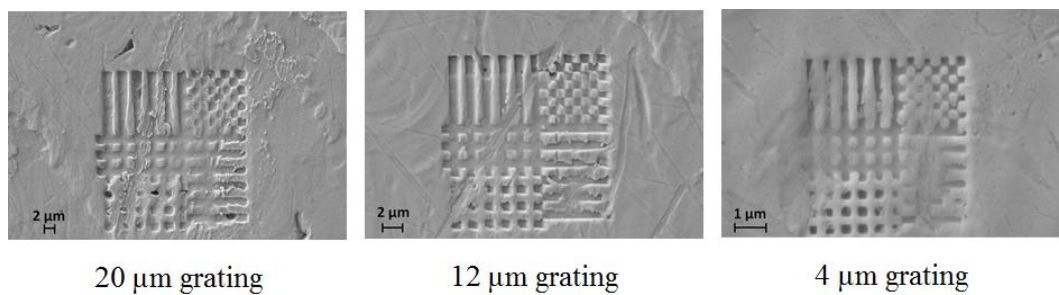
Figure 6.16 SEM images of the Vit 1b insert gratings after 1000 injection cycles

Figure 6.16 shows SEM images of the three grating structures and their surrounding areas on the large reservoir after 1000 injection cycles. Comparing Figures 6.10 and 6.16, it can be seen that the three structures show varying degrees of wear and also some plastic deformation of the pixel structures. Some indentation like marks can also be observed. Depending on the

angle on impingement, the glass fibre endings seem to either leave traces of scratches when the polymer is flowing over the surface or indentation, impact or deformation marks when hitting the surface. Considering that all three gratings, especially the 4 µm one, are still relatively intact and the µMilling marks are also still clearly visible after the exposure to 1000 µIM cycles with the highly abrasive PA +20%GF thermoplastic it can be judged that the wear on these structures is relatively small.

The surface roughness of the 400µm protrusion before and after the 1000 µIM cycles was Ra 0.3 ± 0.01µm and 0.8 ± 0.02µm, respectively, which represented an increase of approximately 500 nm. Although this appears to be a significant increase, the wear effects can be considered relatively small if the aggressive abrasive conditions during the µIM cycles are taken into account, in particular the used temperature settings in combination with the e-glass's hardness that is approximately 64% higher than that of the partially crystallised Vit 1b insert. This estimation was based on the measured average Vickers micro-hardness value, Hv 597 of the partially crystallised Vit 1b insert after the TPF process step. Thus, it can be judged that the surface degradation of the Vit 1b insert is mainly due to sustained strain during the µIM cycles, in particular as a result of the inflow of the polymer and ejection of the solidified polymer parts from the mould (Kumar et al., 2009b) . It is also evident that the mechanism and degree of surface degradation depend mainly on the mould geometry, the type of thermoplastic and filler material used, the volume fraction of filler materials, the filler (fibre) inclination angle, injection conditions and the response of the mould material (Kumar et al., 2009b; Bergstrom et al., 2001) .

With respect to the material's response, it should be noted that there is a general correlation between the hardness and the BMGs' wear resistance (Eckert and Das, 2007; Gloriant, 2003; Huang et al., 2010; Liang et al., 2004; Wang et al., 2000) . In particular, a lower hardness produces a lower wear resistance; and also that hardness and wear resistance are both

observed to be enhanced by partial crystallization of the BMG. Therefore, the micro- and nano- hardness of the as-received, and the partially crystallised Vit 1b insert after the TPF step and 1000 µIM cycles were measured and the results are shown in Table 6-12.

Table 6-12 Micro and nano-hardness of Vit 1b insert after processing steps

Sample	Micro-Hardness HV (GPa)	Nano-Hardness GPa
As Received Vit 1b	534.4 ± 27.7 (5.24 ± 0.27)	6.05 ± 0.23
Vit 1 B after TPF	596.7 ± 26.4 (5.85 ± 0.26)	6.89 ± 0.24
Vit 1 B after 1000 injection moulding cycles	597.3 ± 27.0 (5.86 ± 0.26)	7.03 ± 0.23

Similar Hv micro-hardness values were reported for amorphous to fully crystallised Zr-based BMG alloys with compositions similar to that of the Vit1B alloy. (Greer et al., 2002; Löffler, 2003) . It can also be observed that the nano-hardness values are about 15.5 – 20.0% higher than the microhardness values, and is well within the expected deviation range of 10–30% reported in another study (Qian et al., 2005) . As expected the micro and nano-hardness values of the Vit 1b insert after the TPF process step increased by 11.7 and 13.9 % respectively and this provides initial evidence that the wear resistance of the partially crystallised Vit 1b should have improved, too. However, although hardness is usually regarded as a primary material property which determines the wear resistance, the elastic modulus can also have a significant impact on wear behaviour. Therefore, ratios between hardness (H) and elastic modulus (E) can be used to predict wear resistance rather than hardness alone (Leyland and Matthews, 2000) . In particular, the ratio H/E can be used to evaluate wear behaviour (Leyland and Matthews, 2000) and thus to assess wear resistance for various materials (Dao et al., 2007; Fornell et al., 2010; Fox-Rabinovich et al., 2006; González et al., 2012; Leyland and Matthews, 2000) . In this study, the value of E was

estimated using the procedure described by Zorzi and Perottoni (2013).   The results are provided in Table 6-13 and reveal that the H/E ratio increases after the TPF process step when nanocrystallites become embedded in the amorphous matrix. Similar results were reported for other Zr-based BMGs (Wang et al., 2000) and families of metallic glasses, for example for FE- based BMGs (Fornell et al., 2010) where again an amorphous matrix with dispersed nanocrystalline particles exhibited the best wear performance.

Another parameter related to the wear characteristics is H^3/E^2 (Dao et al., 2007; Fornell et al., 2010; González et al., 2012; Leyland and Matthews, 2000; Musil et al., 2002) . The H^3/E^2 ratio was calculated, too in this research and the results are provided in Table 6-13. Again, they indicate that the partially crystallised Vit 1b should have an improved wear performance after the TPF step.

Finally, the results in Tables 6-12 and 6-13 show that all three parameters, the nano indentation hardness, H and the H/E and H^3/E^2 ratios, increased after 1000 injection moulding cycles indicating a further wear performance improvement. This can be due to some micro-structural changes in the insert as a result of the injection moulding cycles but it will be premature to make any conclusions and further investigations are necessary.

Table 6-13 Summary of values of E, H/E and H^3/E^2

Sample Description	Young's Modulus, E (GPa)	H/E	H^3/E^2
Fully Amorphous As-Received Vit 1b	106.64	0.0567	0.0195
Partially Crystallised Vit 1 B after TPF Process Step	120.70	0.0571	0.0225
Partially Crystallised Vit 1 B after 1000 Injection Moulding Cycles	121.15	0.0580	0.0237

Overall, the results from the carried out in-situ wear trials in combination with the results from the micro and nano indentation tests are very encouraging. The wear resistance of the Vit 1b insert can be judged to be satisfactory while the introduction of the crystalline nano phases in the monolithic-amorphous Vit 1b appears to be an effective means of improving the wear resistance.

6.3.5.2 Failure mechanism

After approximately 1150 injection moulding cycles, the partially crystallised Vit 1b insert showed signs of cracking. This premature failure was not expected and therefore a further analysis of the insert was carried out to identify the probable mechanism leading to this. The Vit 1b insert was constrained within the mould base and consequently it experienced complex repeated stress cycles due to both temperature and pressure variations during the μIM trials. Thus, the insert failure could be due to material fatigue as a result of underwent dynamic and cyclic stress that led to the initiation of cracks and then their propagation and final fast fracture (Suryanarayana and Inoue, 2011) . To confirm this, the insert's surface was examined by SEM.

(a) A Top view of fractured BMG insert

(b) A top view of a fracture surface

(c) Region 1 at higher magnification and coarse striations in Region 2

(d) Magnified image of region 2 showing fine within coarse striations

(e) Region 3

(f) Magnified Image of Region 3
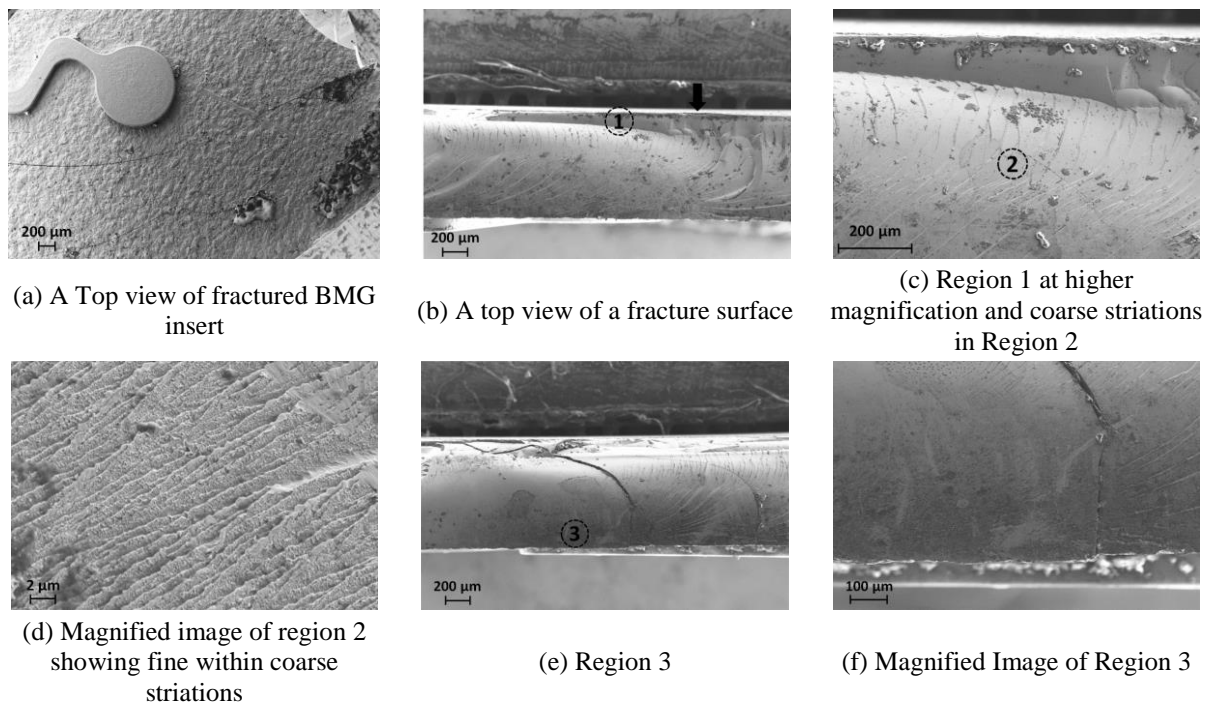
Figure 6.17 SEM images of fractured BMG insert

Representative SEM images of the examined fractures are shown in Figures 6.17a to 6.17f. Fig 6.17a shows a plan view of the Vit 1b insert with various cracks running across the insert top surface while Figures 6.17b to 6.17f depict the fracture surfaces that are normal to the insert surface. Three distinct regions can be observed, namely: (i) region 1 near the top surface, where the fracture is smooth and flat (Figures 6.17b and 6.17c); (ii) region 2 exhibiting a striation-type fracture that covers most of the surface (Figures 6.17c and 6.17d); and (iii) region 3, which is very rough and demonstrates a dimple-type morphology (Figures 6.17e and 6.17f). It is evident that the µIM trials generated complex stress states and thus it is difficult to directly correlate the insert's fracture morphology with that obtained in conventional fatigue tests. However, similar fracture morphology to that in regions 1, 2 and 3 was reported in other studies on the fatigue behaviour of both fully amorphous and partially crystallised BMGs where their differences were associated with the crack initiation site, propagation area and final fast fracture surface respectively (Hess and Dauskardt, 2004; Wang

and Liaw, 2007; Wang et al., 2008b) . This suggests that the insert failure is caused by fatigue and the following factors could have affected the fracture mechanism: surface quality, insert size, and microstructure related effects (Suryanarayana and Inoue, 2011; Wang et al., 2008a, 2011; Wang and Liaw, 2010) .

It should be noted that no microstructural defects were observed on the fractured surfaces. However, it can be seen in Figure 6.17a that the top surface of the insert is relatively rough. The fatigue behaviour is sensitive to the insert's structural quality and surface flaws/ irregularities (Wang et al., 2008a; Wang and Liaw, 2010) that can lead to stress amplification and initiation of cracks (Suryanarayana and Inoue, 2011) . Thus, the Vit 1b surface quality after the TPF process step (the replicated μMilling texture and also the burrs), and during the μIM cycles (glass fibre induced scratches and indentations during the μIM cycles); could have all adversely affected the insert fatigue behaviour.

Another contributing factor could have been the relatively small size of the insert as the fatigue lifetimes and endurance limits of the large-size samples are greater (Wang et al., 2011).

Furthermore, changes in the microstructure brought about by the thermal processing steps could also have modified its plasticity and consequently its fatigue behaviour, too. Therefore, the nanoindentation tests in conjunction with an additional XRD analysis were also carried out to investigate whether the thermo-mechanical steps in the process chain led to any changes in the Vit 1b's microstructure and thus affected adversely the BMG plasticity. The SEM images of the residual nano-indentation impressions on the as-received BMG, and the Vit 1b insert after the TPF step and 1000 injection moulding cycles are shown in Figs 6.18 (a), (b) and (c) respectively. All the indents inspected indicated the formation of characteristic semicircular shear bands along the edges of the impression. Also, it can be observed in Fig 6.18 that the three samples possess the same amount of concentric shear bands surrounding

the respective indents, thus indicating that the plasticity of all three samples is similar. These types of bands are similar to those reported by Vaidyanathan et al. (2001)   and Van Steenberge et al (2008) in Zr-based BMGs that were also subjected to Berkovich indentations. They were attributed to a pile-up of the material around the indents due to plastic flow (Basu et al., 2003) . Based on these results it can be stated that the partially crystallised BMG insert after the TPF step did not exhibit improvements in plasticity with respect to the as received Vit 1b BMG. In particular, the nanoindentation results together with the premature failure of the insert suggest that the Vit 1b insert ability to deform plastically has not been optimised. This is not as expected and can be explained with the relative effects of nanocrystallisation and free volume. In particular, it has been suggested in literature (Schuh et al., 2007; Suryanarayana and Inoue, 2011) that the BMGs plasticity could be improved by incorporating a discontinuous crystalline phase into their homogeneous glass matrix and thus to enhance their ductility and fatigue properties, too   (Suryanarayana and Inoue, 2011; Flores and Dauskardt, 2004; Fujita et al., 2008) . Furthermore, other studies indicate that a specific small volume fraction of nano crystallisation is necessary to enhance the BMGs plasticity (Nagahama et al., 2005; Ohkubo et al., 2007) . At the same time it was reported that apart from nanocrystallisation, free volume is also necessary for improved plasticity (Ohkubo et al., 2007) and can enhance the fatigue behaviour of BMGs. (Gu et al., 2009; Murali and Ramamurty, 2005; Xu et al., 2010; Yokoyama et al., 2006) . In addition, Concustell et al (2005) concluded that a critical amount of free volume is necessary for sufficient plastic deformation.
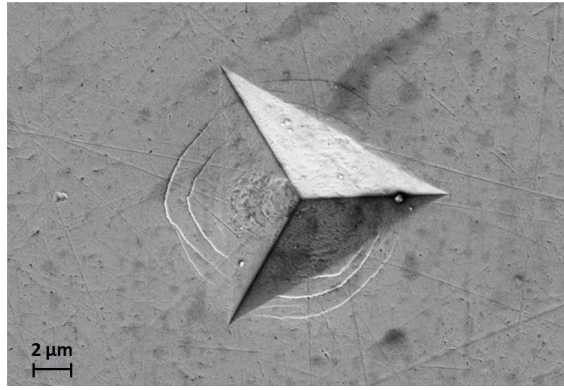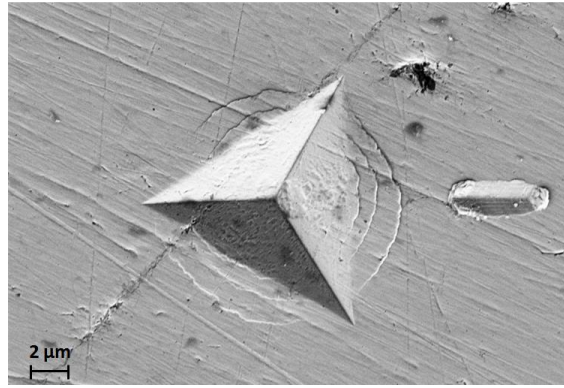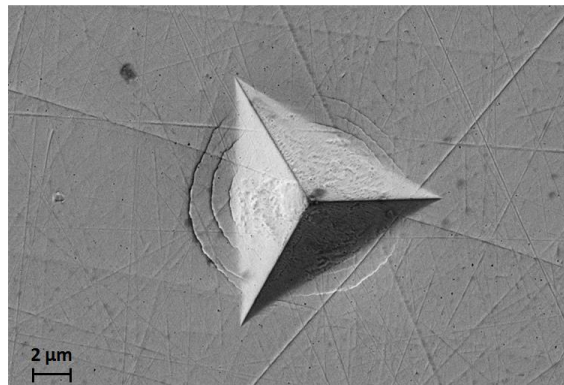
Figure 6.18 SEM images of residual nano indentations

Thus, the relative effects of nanocrystallisation and free volume determine the overall plasticity of the insert material (Mondal et al., 2008; Ohkubo et al., 2007) and consequently its fatigue behaviour. In this context, the fact that the partially crystallised BMG insert does not exhibit an improvement in plasticity with respect to the as received Vit 1b BMG can be explained by the decrease of free volume in the residual amorphous phase during the thermo-mechanical processing step that counteracted the presence of nanocrytsallisation. In

particular, the resultant volume fraction nanocrystallisation and the degree of free volume within the partially crystallised BMG are determined by its thermal history, i.e. the TPF step and also the casting of the as-received Vit 1b. Thus, the degree of free volume and volume fraction of nanocrystallization have to be optimised, as suggested in other studies (Mondal et al., 2008; Ohkubo et al., 2007) , which should enhance plasticity of BMGs and also to improve their fatigue behaviour.
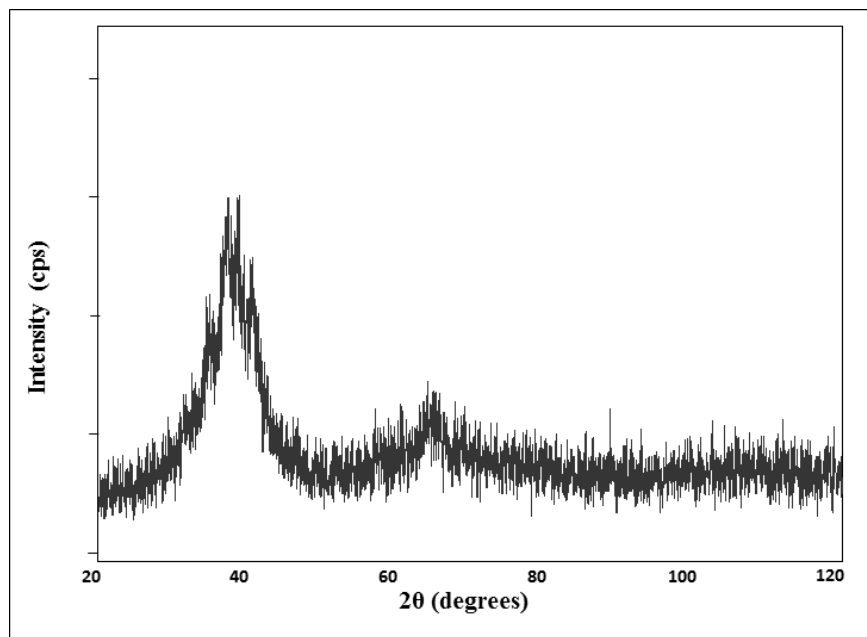
Figure 6.19 XRD spectra of partially crystallised Vit 1b insert after the µIM step

In addition, based on the SEM analysis of the residual nano-indentation impressions, it can be stated that no change in insert's plasticity after the injection moulding cycles. Furthermore, Figure 6.19 shows that the XRD pattern of the polished Vit 1b sample after the injection moulding cycles is similar to that obtained for the same insert just after the TPF step (See Fig 6.7c). Thus, there are no evidences of any changes in nanocrystallisation in the Vit 1b insert after the µIM step. Collectively, the results of both the nano-indentation impressions and XRD analyses suggest that the momentary repetitive annealing cycles below the Vit 1b's T_g

did not trigger any noticeable microstructural changes in the BMG insert with the used injection moulding parameters. This is beneficial, however, due to the observed marginal increase in nano-indentation hardness after the 1000 µIM cycles, as it was discussed in the previous section, this matter requires further investigation in order to ascertain that no additional microstructural changes occur in the Vit 1b insert during the injection moulding step.

Overall, when taking into consideration the limited number of experiments carried out and the contributing factors discussed above it is apparent that this fatigue issue requires further investigation.

6.4 Conclusions

This chapter presents an experimental investigation of a master making process chain for achieving FLSI in devices. The research demonstrated that the process chain can be a viable fabrication route for both fully amorphous and partially crystalline Zr-based BMG inserts that incorporates different length scale features. The results show that relatively good fidelity of the different scales' features can be achieved with the µIM process and it can enable FLSI in thermoplastic components. Collectively, there is good process compatibility and complementarity between the component technologies in the process chain and thus to enable FLSI in masters and ultimately in thermoplastic replicas. In particular, the masters and/or replicas after each processing step, were analysed and the factors that are considered to have the highest impact on the overall performance of the process chain are: (i) workpiece microstructure both for producing the Al masters and then the BMG inserts; (ii) the optimisation of the set-ups and processing conditions for the component technologies; and (iii) the Zr-based BMG response to TPF and FIB processing. In addition, the following

conclusions regarding the component technologies and their contributions to the process chain overall performance were made:

- The analysis of the TPF and FIB steps shows that their results can be affected significantly by the preceding component technologies in the process chain, in particular the Al masters produced by μMilling and then both μMilling and TPF steps, respectively. Therefore, additional surface conditioning and post processing should be considered to improve the resulting surface quality after the μMilling and TPF steps.

- The analysis of the complex features' profiles revealed that the feature geometry was accurately transferred through the three steps of the master-making process chain to the Zr-based BMG insert and also that a careful selection of inspection strategies is required in order to minimise measurement uncertainty.

- The surface contamination of Zr-based BMG workpieces adversely affects the surface integrity of the inserts after the TPF step. The study has shown that it is essential to polish the as-received workpieces prior to the TPF step to eliminate any surface contamination. The use of workpieces with some surface contamination limits the replication performance of the TPF step.

- Nano-scale grating structures were successfully produced using the FIB process on both the fully amorphous Zr-based workpiece and also on the micro features of a partially crystalline insert after the TPF step. In particular, the geometrical accuracy and surface integrity of the nano-scale grating features on the partially crystallised BMG insert are similar to those obtained on the fully amorphous workpiece, thus confirming that their response to FIB machining is similar.

- The analysis of thermoplastic replicas shows that the nanoscale replication results can be significantly affected by the FIB milling step and the μIM process settings.

- The in-situ wear tests in combination with the micro- and nano-indentation hardness test results (i.e. the increase in micro and nano-hardness values, and also the H/E and H^3/E^2 ratios after the TPF process step) provided evidences that the wear resistance of the insert was improved by introducing crystalline nano phases in the monolithic-amorphous Zr-based BMG and thus the use of such inserts could extend the tool life, especially when replicating micro and sub-micron features. At the same time it should be noted that the fatigue performance of the insert can be affected significantly by the preceding stages in the process chain, in particular the µMilling, and potentially the TPF and µIM steps and also the initial casting process of the as-received Vit 1b BMG.

CHAPTER 7
CONTRIBUTIONS, CONCLUSIONS AND FUTURE WORK

7.1 Overview

This chapter presents the main contributions and the conclusions reached in this research work. It also provides suggestions for future work.

7.2 Contributions

The overall aims of this research were to develop a systematic approach for assessing the maturity of MNM technologies and to investigate cost-effective implementations of BMG enabled master-making process chains for serial replication of thermoplastic polymer based FLSI devices. To accomplish these goals the following research tasks were carried out:

1. Development and validation of a systematic approach for assessing the maturity of MNM technologies. **(Chapter 3)**

2. Design and experimental investigation of new BMG enabled master making process chains for producing micro and nano scale structures. **(Chapters 4 and 5 & 6)**.

3. Experimental validation of BMG replication masters for serial production of polymer based FLSI devices and the systematic investigation of the factors affecting the performance of such masters. **(Chapters 4 & 5 & 6)**

4. Investigation of the effects that partial crystallisation of BMG workpieces has both on MN structuring technologies and the robustness of such BMG masters when utilized for serial replication of polymer based FLSI devices. **(Chapters 5 & 6)**

5. Investigation of the key component technologies in BMG-enabled master making process chains to systematically study, optimise and develop further their capabilities. **(Chapters 4 & 6)**

The main research findings and contributions to existing knowledge in micro and nano manufacturing technologies domain are presented in the subsections below.

7.2.1 A systematic approach for assessing the maturity of MNM technologies.

A new methodology for assessing technology maturity of processes and process pairs was developed and validated in this research. The most important characteristics of the proposed methodology are:

- a set of PMIs are used to assess the ML of a process by characterising its current state in regards to its overall behaviour, performance and operational environment.
- output-input dependencies of process pairs are modelled; and
- a set of rules are proposed to assess such dependencies.

Collectively, the methodology provides a comprehensive framework for assessing the maturity of processes and process pairs by modelling the interfaces between their component technologies. The pilot implementation of the proposed methodology demonstrated its applicability as a means to evaluate the maturity of MNM pairs and their constituent processes. In addition, it was also shown that the methodology can be employed as a tool to identify process pairs that are potentially suitable for integration in process chains, and the weaknesses of pairs in relation to their KPCAs.

An effective graphical representation of the maturity analysis outputs was devised for identifying and providing an overall view of the pairs' strengths and weaknesses in relation to their KPCAs.

7.2.2 Design and experimental investigation of new BMG enabled master making process chains.

Two novel Zr-based BMG enabled master making process chains, PS Laser ablation + FIB Milling and μMilling + HE + FIB Milling, were developed and experimentally validated for the fabrication of BMG replication tools incorporating features and patterns of different length scales. The produced tools were also validated as inserts for injection moulding of thermoplastic parts. Based on the analysis of the workpieces after each master-making component technology of these two process chains the following conclusions were made:

- BMG-enabled master-making process chains can be successfully applied for producing replication inserts incorporating different length scale 2.5D and 3D structures.

- The use of BMG workpieces with their intrinsic homogeneity at micro, sub-micron and nano-scale scales enables the integration of compatible and complementary micro- and sub-micron/nano- structuring and replication technologies for achieving FLSI in μIM inserts.

- The accurate transfer of micro, sub-micron and nanoscale structures through the steps of both manufacturing routes to the BMG inserts also confirmed that there is good process compatibility and complementarity between the component technologies in the proposed process chains, especially for the targeted length scales' ranges.

- The PS laser machining regime is a very promising method for the cost-effective micro-structuring of BMGs.

7.2.3 Experimental validation of BMG replication masters for serial production of polymer based FLSI devices and systematic investigation of the factors affecting the performance of such masters.

The replication capabilities of the inserts' produced by the two master making process chains were experimentally validated by injection moulding small batches of thermoplastic polymer parts. Based on the analysis carried out on the Zr-based BMG inserts and polymer replicas after the injection moulding step of both chains, the following conclusions were made:

- Both process chains can be used for the mass production of polymer parts incorporating different length scale features.

- The dimensional analysis of the produced thermoplastic replicas revealed that good fidelity of the different scales' features can be achieved. Thus, the FLSI achieved on the BMG masters can be transferred reproducibly on the thermoplastic replicas in one step.

- The replication of microscale and in particular the submicron/nanoscale features can be significantly affected by the preceding master-making technologies in the process chains. Furthermore an optimisation of the μIM process settings has to be carried out in order to guarantee an optimal simultaneous replication of the different length scale features.

- The main factors affecting the accuracy and surface integrity of the BMG replication masters produced by the PS + FIB process chain are: the used process settings for its different component technologies, and the BMG response to structuring technologies, i.e. PS Laser and FIB milling, with different specific processing energies.

- For the BMG masters produced by the μMilling + HE + FIB process chain, the main factors affecting its performance are: the workpiece microstructure both for producing the Al masters and then the BMG inserts; the machine set-ups and processing

conditions used for all component technologies and the BMG's response to TPF and FIB processing.

7.2.4 Investigation on the effects of partially crystalline BMG workpieces on the MN structuring technologies and their robustness as masters for replication of polymer FLSI devices.

The μMilling + HE + FIB milling mastermaking process chain was experimentally validated for the production of partially crystalline Zr-based BMG inserts incorporating different length scale functional features for the serial fabrication of thermoplastic polymer FLSI parts. The main findings are:

- The process chain can be a viable fabrication route for producing partially crystalline BMG inserts that incorporate different length scale features.

- Micro HE, a specific implementation of the TPF process, is a "tuneable" process, and through a judicious selection of the process settings it is possible to minimise the BMG's morphological changes and simultaneously produce partially crystalline inserts incorporating microscale features with the required resolution and surface integrity.

- Nano-scale grating structures with the required resolution and surface integrity can be successfully produced using the FIB process on top of the micro features of the partially crystalline BMG inserts after the TPF step.

- Partially crystalline BMG inserts can be successfully applied for injection moulding of thermoplastic FLSI devices that incorporate micro and submicron structures simultaneously and also such replication masters are robust and capable of producing batches of parts without any pattern degradations or failures.

The effects of the Zr-BMG's partial crystallisation on the insert's wear and fatigue life response was also experimentally studied in the context of the overall μMilling + HE + FIB milling + μIM process chain. The conclusions from this investigation are:

- The micro and nano-hardness values, and also the H/E and H^3/E^2 ratios of the Zr-based BMG insert increased after the TPF process step. These results are evidences that the wear resistance of the insert was improved by introducing crystalline nano phases in the monolithic-amorphous Zr-based BMG and thus the use of such inserts could extend the tool's life, especially when replicating micro and sub-micron features.

- The fatigue performance of the insert can be affected significantly by the preceding stages in the master-making process chain, in particular the μMilling, and potentially the TPF and μIM steps.

7.2.5 Investigation of the key component technologies in BMG-enabled master making process chains.

In the experimental investigation of the PS laser ablation + FIB milling master-making process chain, the capabilities of another laser source, namely NS laser was also experimentally investigated as an alternative candidate for the first step in this master-making process chain. The main conclusion is that it is possible to optimise the NS laser ablation process to machine successfully Zr-based BMG inserts with an acceptable surface integrity for μIM without triggering changes in the BMG short range atom arrangements. Consequently the superior mechanical properties of BMGs properties can also be preserved during the NS laser processing, whilst benefiting from their higher material removal rates. Thus the NS laser machining regime is also a very promising method for the cost-effective

micro-structuring of the Zr-based BMGs and can therefore replace PS laser in the abovementioned process chain.

The key component technologies in the μMilling + HE + FIB milling master-making process chain were also experimentally investigated to systematically study, optimise and potentially develop further their capabilities. The investigations led to the following main conclusions:

- Nano-scale grating structures with the required resolution and surface integrity can be successfully produced using the FIB process on both the fully amorphous Zr-based workpieces and also on the partially crystalline ones. In particular, the geometrical accuracy and surface integrity of the nano-scale grating features on the partially crystallised BMG insert are similar to those obtained on the fully amorphous workpiece, thus confirming that their response to FIB machining is similar.

- The analysis of the TPF and FIB steps shows that their results can be affected significantly by the preceding component technologies in the process chain, in particular the Al masters produced by μMilling and then both μMilling and HE steps, respectively. Thus the overall performance of this master manufacturing route can be substantially improved by utilising material(s) having the most suitable microstructure in conjunction with optimised processing parameters and set-ups. Furthermore, additional surface conditioning and post processing should be considered to improve the resulting surface quality after the μMilling and TPF steps.

- Any surface contamination of Zr-based BMG workpieces adversely affects the surface integrity of the inserts after the TPF step. Thus the study has shown that it is essential to polish the as-received workpieces prior to the TPF step to eliminate any surface contamination and consequently maximise the replication and structuring performance of the TPF and FIB steps respectively.

7.3   Conclusion

Finally, it can be concluded that, the results of this research confirmed the two main hypotheses followed in this research. In particular, with respect to the first hypothesis, it is concluded that a systematic approach for assessing the maturity of micro and nano-manufacturing (MNM) technologies and their interfaces in process chains enables the analysis and evaluation of such manufacturing routes, and thus provides an objective means to inform about the further development of existing process chains and also to design new ones for the fabrication of novel miniaturized products. Furthermore, with respect to the second hypothesis, it is concluded that BMGs can be used to design and implement FLSI enabling master-making process chains.

7.4   Future Work

Based on the work presented here, some areas of future research efforts have been identified as follows:

1. The analysis of the results and the evaluation of the proposed methodology for assessing the maturity of MNM processes and process chains in chapter 3 revealed a number of weaknesses in its implementation. Thus further research is necessary to address the following specific shortcomings/ aspects:

   - The methodology can be used for assessing process pairs and their constituent technologies however further development is necessary to apply it for assessing more complex process chains.

   - It will be beneficial if the proposed expert-based approach can be complemented by empirical assessments of processes and process chains' maturity, e.g. by conducting Round Robin tests. The results from such research should also be used to find a more evidence-based way for combining complementarity and compatibility scores of pairs.

- It is necessary to review and improve the formula currently used to calculate the process pair's MLs and thus to reflect better the perceived ML of the pairs.

- The methodology does not adequately take into consideration all implementation related risks. Mankins (2009) states that the maturity of the technology correlates with the technical risks and thus the proposed approach has to be improved further to factor uncertainties associated with the design and implementation of multi-process manufacturing platforms.

2. The experimental studies reported in chapters 4, 5 & 6 highlighted that all component technologies in both of the proposed process chains have to undergo further optimisation. Such process optimisation can be achieved either by employing specially developed methodologies such as that reported earlier for optimising the layer-based FIB milling process or through the use of DOE methodology (Clark et al., 1995; Montgomery, 2009; Telford, 2007) .

3. In addition, these experimental studies also highlighted that further research is necessary to address specific issues in the two proposed process chains as follows:

PS Laser + FIB Milling + µIM Process Chain

- The NS laser machining results are very promising and demonstrate that the required surface quality for successful replication can be achieved. Taking into account the ablation mechanism when laser processing with ultra-short pulses is performed, it can be expected that an even better surface integrity than that reported for the NS laser ablation could be obtained after PS laser machining in terms of surface roughness without changes in the non-crystalline morphology of the BMG workpiece. At the

same time, it should be noted that the optimisation of the laser processing parameters will not be enough to produce sufficiently smooth surfaces for follow up FIB sub-micron and nano structuring. This implies that additional surface conditioning and smoothening after the laser processing will be required. Recent results reported in the literature have shown that micro and nano scale features imprinted on Pt based BMGs may be erased by subsequent annealing in the BMG supercooled liquid region (Kumar and Schroers, 2008; Packard et al., 2009) and thus to smooth the surface. However, such a post processing step for the surface smoothening of Zr-based BMG masters has not been fully investigated (Pavey, 2013).

µMilling + TPF + FIB Milling + µIM Process Chain

- The fabrication of Al TPF masters employing the µMilling process shows real promise when an ultrafine grained Al alloys are utilised. However, it was also clear that process optimisation will not be solely sufficient to completely eliminate the burrs on the top edges of the microfluidic channels and achieve the required surface finish for the follow up FIB machining. Therefore, additional surface conditioning and post processing should be considered to eliminate the burrs and improve the surface quality after the µMilling step.

- Another possible way to improve the surface quality of the Vit 1b inserts is to have some additional surface conditioning and smoothening after the TPF step. However, as stated earlier a post processing step for surface smoothening Zr-based BMG masters by subsequent annealing at a set temperature in the material's SCLR needs to be investigated further.

- The wear resistance of the Vit 1b insert requires further study. In particular the wear performance of partially crystallised Zr-based BMG inserts under injection moulding

conditions should be investigated further and compared with that of fully amorphous BMG and tool steel inserts.

- The nanoindentation results showed a marginal increase of the BMG insert hardness after µIM cycles. Thus, further research is required to investigate whether µIM momentary but repetitive thermal cycles below the BMG Tg lead to further changes in the microstructure of partially crystallised BMG inserts.

- It is suggested that plasticity and consequently the fatigue properties of the partially crystalline Vit 1b inserts can be improved by optimising their free volume and volume fraction of nanocrystallization. However, this has to be investigated experimentally and only then conclusions can be made. In addition, various other aspects of the second (i.e. crystalline) phase such as its composition, size, shape, and its distribution in the amorphous matrix (Schuh et al., 2007; Suryanarayana and Inoue, 2011; Zhu et al., 2008) have to be taken into consideration as they also affect the resultant plasticity of the Vit 1b insert and thus its fatigue behaviour, too.

- Another important factor that could affect the fatigue life of BMG inserts is the thermal load exercised on them (Suryanarayana and Inoue, 2011; Wang and Liaw, 2010). Based on the carried out literature review, there was only one study on the temperature effects on the BMGs' fatigue behaviour (Hess and Dauskardt, 2004). In addition the literature review also revealed that no studies were carried out on the effects of temperature on the fatigue behaviour of partially crystalline BMGs. Therefore, more research is required to understand the effect of temperature on the fatigue behaviour of both the fully amorphous and partially crystalline BMGs.

APPENDIX A

UNCERTAINTY ANALYSIS AND CALCULATIONS FOR DIMENSIONAL AND SURFACE ROUGHNESS MEASUREMENTS IN CHAPTER 4

Table A.1 Uncertainty analysis and calculation for SEM based QR Code dimensional values at various stages of the process chain

Measurand	Mean Value (μm)	u(rep) (μm)	u(proc) (μm)	u(P) (μm)	u_c (μm)	v_{eff}	k	U (μm)
PS Laser milling: "Large" QR Code on BMG workpiece								
Pixel Width (X)	98.62	0.334	0.709	2.959	3.061	2809	2	6.12
Pixel Width (Y)	98.83	0.206	0.588	2.965	3.029	6150	2	6.06
Pixel Height	13.92	0.029	0.307	0.418	0.519	73	2.05	1.06
Overall QR Code Width (X)	2769.65	9.384	1.337	83.089	83.628	25217	2	167.26
Overall QR Code Width (Y)	2771.83	5.771	2.442	83.155	83.391	168963	2	166.78
FIB milling: "Small" QR Code on BMG workpiece								
Pixel Width (X)	2.98	0.002	0.055	0.089	0.105	120	2	0.21
Pixel Width (Y)	3.09	0.003	0.036	0.093	0.100	504	2	0.20
Overall QR Code Width (X)	76.63	0.060	0.104	2.299	2.302	870966	2	4.60
Overall QR Code Width (Y)	78.11	0.076	0.101	2.343	2.347	876494	2	4.69
Injection Moulding: "Large" QR Code on COC parts								
Pixel Width (X)	97.06	0.879	0.154	2.912	3.046	575	2	6.09
Pixel Width (Y)	97.62	0.446	0.213	2.929	2.970	7805	2	5.94
Pixel Height	13.43	0.061	0.222	0.403	0.464	872	2	0.93
Overall QR Code Width (X)	2660.03	24.101	7.848	79.801	83.730	581	2	167.46
Overall QR Code Width (Y)	2657.65	12.153	7.216	79.730	80.973	7722	2	161.95
Injection Moulding: "Small" QR Code on COC parts								
Pixel Width (X)	2.88	0.003	0.026	0.086	0.090	6867	2	0.18
Pixel Width (Y)	2.90	0.005	0.020	0.087	0.090	18724	2	0.18
Overall QR Code Width (X)	76.53	0.072	0.048	2.296	2.298	4124727	2	4.60
Overall QR Code Width (Y)	78.00	0.142	0.064	2.340	2.345	291621	2	4.69

Table A.2 Uncertainty analysis and calculation for confocal microscope based QR code height values at various stages of the process chain

Measurand	Mean Value (nm)	u(art) (nm)	u(cal) (nm)	u(res) (nm)	u(step) (nm)	u(rep) (nm)	u(proc) (nm)	u(temp) (nm)	u_c (nm)	v_{eff}	k	U (nm)
FIB milling: "Small" QR Code on BMG workpiece												
Pixel Height	530.0	5.25	1.71	2.89	0.44	0.61	0.14	0.01	6.28	713	2	12.6
Injection Moulding: "Small" QR Code on COC parts												
Pixel Height	494.4	5.25	1.71	2.89	0.41	0.61	0.09	0.08	6.28	713	2	12.6

Table A.3 Uncertainty analysis and calculation for confocal microscope based surface roughness values at various stages of the process chain

Measurand	Mean Value (µm)	u(rep) (µm)	u(proc) (µm)	u_c (µm)	v_{eff}	k	U (µm)
PS Laser milling: "Large" QR Code on BMG workpiece							
Textured surface Ra	1.462	0.0010	0.0132	0.0132	2	4.53	0.06
Injection Moulding: "Large" QR Code on COC parts							
Textured Surface Ra	1.843	0.0013	0.1053	0.1053	8	2.37	0.25

Table A.4 Uncertainty analysis and calculation for stylus instrument based surface roughness values of the three NS laser machined samples

Measurand	Mean Value (µm)	u(rep) (µm)	u(proc) (µm)	u_c (µm)	v_{eff}	k	U (µm)
Sample 1 surface Ra	0.22	0.0020	0.0060	0.0064	2	4.53	0.03
Sample 2 surface Ra	0.16	0.0014	0.0027	0.0030	3	3.31	0.01
Sample 3 surface Ra	0.26	0.0023	0.0067	0.0071	2	4.53	0.03

The equations used to calculate the combined standard uncertainty (u_c), the effective degrees of freedom (ν_{eff}) and the expanded uncertainty (U) are listed below:

$$u_c = \sqrt{\sum_{i=1}^{N} u_i^2} \qquad\qquad (1)$$

$$\nu_{eff} = \frac{u_c^4}{\sum_{i=1}^{N} \frac{u_i^4}{\nu_i}} \qquad\qquad (2)$$

$$U = k.u_c \qquad\qquad (3)$$

where,

u_i = individual standard uncertainty due to measurement variation contributor i

$N = N^{th}$ measurement variation contributor.

ν_i = degrees of freedom of standard uncertainty u_i

k = coverage factor determined at a level of confidence (i.e. 95 %) for a given number of degrees of freedom (i.e. ν_{eff})

APPENDIX B

UNCERTAINTY ANALYSIS AND CALCULATIONS FOR DIMENSIONAL AND SURFACE ROUGHNESS MEASUREMENTS IN CHAPTER 5

Table B.1 Uncertainty analysis and calculation for optical microscope based microfluidic device feature width values at various stages of the process chain

Measurand	Mean Value (μm)	u(art) (μm)	u(cal) (μm)	u(res) (μm)	u(rep) (μm)	u(proc) (μm)	u(temp) (μm)	u_c (μm)	v_{eff}	k	U (μm)
Micromilling: AL Master microfluidic device features											
Channel 3 Width (150 μm)	163.31	0.577	0.447	0.087	0.232	0.701	0.019	1.043	8	2.37	2.47
Channel 1 Width (200 μm)	212.63	0.577	0.447	0.087	0.232	0.363	0.025	0.853	27	2.102	1.79
Channel 2 Width (400 μm)	414.5	0.577	0.447	0.087	0.232	0.289	0.048	0.825	32	2.082	1.72
TPF: BMG Insert microfluidic device features											
Channel 3 Width (150 μm)	165.46	0.577	0.447	0.087	0.298	0.837	0.008	1.153	6	2.52	2.91
Channel 1 Width (200 μm)	215.57	0.577	0.447	0.087	0.298	0.602	0.011	0.996	12	2.23	2.22
Channel 2 Width (400 μm)	417.40	0.577	0.447	0.087	0.298	0.169	0.021	0.812	35	2.07	1.68
Micro-Injection Moulding: PP parts microfluidic device features											
Channel 3 Width (150 μm)	152.16	0.577	0.447	0.087	0.339	0.718	0.151	1.093	30	2.09	2.28
Channel 1 Width (200 μm)	204.03	0.577	0.447	0.087	0.339	0.930	0.202	1.250	22	2.12	2.65
Channel 2 Width (400 μm)	405.40	0.577	0.447	0.087	0.339	0.798	0.401	1.205	33	2.08	2.50

Table B.2 Uncertainty analysis and calculation for optical co-ordinate measuring machine (OCMM) based microfluidic device feature depth values at various stages of the process chain

Measurand	Mean Value (μm)	u(art) (μm)	u(cal) (μm)	u(res) (μm)	u(rep) (μm)	u(proc) (μm)	u(temp) (μm)	u_c (μm)	v_{eff}	k	U (μm)
Micromilling: AL Master microfluidic device features											
Channel 3 Depth (150 μm)	152.85	0.115	0.212	0.029	0.459	1.098	0.018	1.214	2	4.53	5.50
Channel 1 Depth (200 μm)	151.63	0.115	0.212	0.029	0.459	0.982	0.018	1.112	3	3.31	3.68
Channel 2 Depth (400 μm)	152.25	0.115	0.212	0.029	0.459	1.014	0.018	1.139	3	3.31	3.77
TPF: BMG Insert microfluidic device features											
Channel 3 Depth (150 μm)	150.75	0.115	0.212	0.029	0.347	1.510	0.007	1.569	2	4.53	7.11
Channel 1 Depth (200 μm)	151.70	0.115	0.212	0.029	0.347	1.306	0.008	1.374	2	4.53	6.22
Channel 2 Depth (400 μm)	151.60	0.115	0.212	0.029	0.347	1.021	0.008	1.105	2	4.53	5.01
Micro-Injection Moulding: PP parts microfluidic device features											
Channel 3 Depth (150 μm)	148.67	0.115	0.212	0.029	0.345	0.694	0.147	0.826	14	2.20	1.82
Channel 1 Depth (200 μm)	148.00	0.115	0.212	0.029	0.345	1.202	0.147	1.282	10	2.28	2.92
Channel 2 Depth (400 μm)	149.00	0.115	0.212	0.029	0.345	1.000	0.148	1.096	11	2.25	2.47

Table B.3 Uncertainty analysis and calculation for SEM based gratings width values at various stages of the process chain

Measurand	Mean Value (µm)	u(rep) (µm)	u(proc) (µm)	u(P) (µm)	u$_c$ (µm)	v_{eff}	k	U (µm)
FIB milling: BMG Grating structure 1 (20 µm)								
Pixel Width (X)	1.46	0.002	0.030	0.044	0.053	86	2.032	0.11
Pixel Width (Y)	1.47	0.002	0.034	0.044	0.056	65	2.043	0.11
Overall Width (X)	28.53	0.043	0.043	0.856	0.858	208510	2	1.72
Overall Width (Y)	28.59	0.032	0.040	0.858	0.859	356977	2	1.72
FIB milling: BMG Grating structure 2 (12 µm)								
Pixel Width (X)	0.88	0.001	0.012	0.026	0.029	294	2	0.06
Pixel Width (Y)	0.88	0.001	0.006	0.026	0.027	2852	2	0.05
Overall Width (X)	17.26	0.023	0.023	0.518	0.519	326036	2	1.04
Overall Width (Y)	17.35	0.016	0.047	0.521	0.523	31294	2	1.05
FIB milling: BMG Grating structure 3 (4 µm)								
Pixel Width (X)	0.28	0.001	0.003	0.008	0.009	547	2	0.02
Pixel Width (Y)	0.29	0.001	0.009	0.009	0.012	35	2.07	0.03
Overall Width (X)	5.62	0.015	0.009	0.169	0.169	51054	2	0.34
Overall Width (Y)	5.78	0.012	0.009	0.173	0.174	119493	2	0.35
Micro-Injection Moulding: PP Grating structure 1 (20 µm)								
Pixel Width (X)	1.43	0.002	0.035	0.043	0.055	181	2	0.11
Pixel Width (Y)	1.41	0.003	0.033	0.042	0.054	197	2	0.11
Overall Width (X)	27.29	0.040	0.019	0.819	0.820	698405	2	1.64
Overall Width (Y)	27.57	0.049	0.040	0.827	0.830	261739	2	1.66
Micro-Injection Moulding: PP Grating structure 2 (12 µm)								
Pixel Width (X)	0.86	0.001	0.021	0.026	0.033	180	2	0.07
Pixel Width (Y)	0.85	0.002	0.020	0.026	0.033	198	2	0.07
Overall Width (X)	16.33	0.025	0.012	0.490	0.491	551159	2	0.98
Overall Width (Y)	16.69	0.036	0.024	0.501	0.503	133201	2	1.01

Table B.4 Uncertainty analysis and calculation for SEM based gratings depth values at various stages of the process chain

Measurand	Mean Value (nm)	u(rep) (nm)	u(proc) (nm)	u(P) (nm)	u_c (nm)	v_{eff}	k	U (nm)
FIB milling: BMG Grating structures								
Grating 1 (20 μm) Pixel height	651.7	0.72	27.81	19.55	34.01	20	2.13	72.43
Grating 2 (12 μm) Pixel height	420.0	0.40	20.42	12.60	24.00	17	2.16	51.84
Grating 3 (4 μm) Pixel height	159.9	0.32	5.98	4.80	7.68	24	2.12	16.27
Micro-Injection Moulding: PP Grating structures								
Grating 1 (20 μm) Pixel height	583.62	1.047	12.429	17.509	21.497	258	2	42.99
Grating 2 (12 μm) Pixel height	372.62	0.81	7.94	11.18	13.73	260	2	27.47

Table B.5 Uncertainty analysis and calculation for stylus instrument based surface roughness values of the BMG and AL workpieces at different stages of the process chain

Measurand	Mean Value (μm)	u(rep) (μm)	u(proc) (μm)	u_c (μm)	v_{eff}	k	U (μm)
Micromilling: Microfluidic device on AL master Channel 2 (400 μm)							
Bottom surface Ra	0.3378	0.0044	0.0117	0.0125	2	4.53	0.0565
TPF: Microfluidic device on BMG insert Protrusion 2 (400 μm)							
Top surface Ra	0.2866	0.0025	0.0028	0.0038	5	2.65	0.0099

The equations used to calculate the combined standard uncertainty (u_c), the effective degrees of freedom (v_{eff}) and the expanded uncertainty (U) are listed below:

$$u_c = \sqrt{\sum_{i=1}^{N} u_i^2} \qquad (1)$$

$$v_{eff} = \frac{u_c^4}{\sum_{i=1}^{N} \frac{u_i^4}{v_i}} \qquad (2)$$

$$U = k.u_c \qquad\qquad\qquad (3)$$

where,

u_i = individual standard uncertainty due to measurement variation contributor i

$N = N^{th}$ measurement variation contributor.

v_i = degrees of freedom of standard uncertainty u_i

k = coverage factor determined at a level of confidence (i.e. 95 %) for a given number of degrees of freedom (i.e. v_{eff})

APPENDIX C

UNCERTAINTY ANALYSIS AND CALCULATIONS FOR DIMENSIONAL, SURFACE ROUGHNESS AND HARDNESS MEASUREMENTS IN CHAPTER 6

Table C.1 Uncertainty analysis and calculation for optical microscope based microfluidic device feature width values at µMilling stage of the process chain

Measurand	Mean Value (µm)	u(art) (µm)	u(cal) (µm)	u(res) (µm)	u(rep) (µm)	u(proc) (µm)	u(temp) (µm)	u_c (µm)	v_{eff}	k	U (µm)
AL 5083 masters 1 to 4 microfluidic device features											
Channel 3 Width (150 µm)	163.63	0.577	0.447	0.087	0.232	0.220	0.019	0.802	37	2.066	1.66
Channel 1 Width (200 µm)	213.19	0.577	0.447	0.087	0.232	0.252	0.025	0.812	39	2.062	1.67
Channel 2 Width (400 µm)	414.44	0.577	0.447	0.087	0.232	0.143	0.048	0.786	35	2.07	1.63
AL 5083 masters 5 to 7 microfluidic device features											
Channel 3 Width (150 µm)	163.81	0.577	0.447	0.087	0.232	0.434	0.019	0.885	40	2.06	1.82
Channel 1 Width (200 µm)	213.42	0.577	0.447	0.087	0.232	0.300	0.025	0.828	40	2.06	1.71
Channel 2 Width (400 µm)	414.67	0.577	0.447	0.087	0.232	0.202	0.048	0.799	37	2.066	1.65
ALL AL 5083 masters microfluidic device features											
Channel 3 Width (150 µm)	163.71	0.577	0.447	0.087	0.232	0.223	0.019	0.803	38	2.064	1.66
Channel 1 Width (200 µm)	213.29	0.577	0.447	0.087	0.232	0.191	0.025	0.795	36	2.068	1.64
Channel 2 Width (400 µm)	414.54	0.577	0.447	0.087	0.232	0.117	0.048	0.782	34	2.074	1.62
RTN 5 AL master microfluidic device features											
Channel 3 Width (150 µm)	163.31	0.577	0.447	0.087	0.232	0.701	0.019	1.043	8	2.37	2.47
Channel 1 Width (200 µm)	212.63	0.577	0.447	0.087	0.232	0.363	0.025	0.853	27	2.102	1.79
Channel 2 Width (400 µm)	414.50	0.577	0.447	0.087	0.232	0.289	0.048	0.825	32	2.082	1.72

Table C.1 Uncertainty analysis and calculation for optical microscope based microfluidic device feature width values at μMilling stage of the process chain cont'd

Measurand	Mean Value (μm)	u(art) (μm)	u(cal) (μm)	u(res) (μm)	u(rep) (μm)	u(proc) (μm)	u(temp) (μm)	u_c (μm)	v_{eff}	k	U (μm)
RTN 4 AL master microfluidic device features											
Channel 3 Width (150 μm)	164.38	0.577	0.447	0.087	0.232	0.807	0.019	1.116	6	2.52	2.81
Channel 1 Width (200 μm)	214.25	0.577	0.447	0.087	0.232	0.373	0.025	0.857	26	2.106	1.80
Channel 2 Width (400 μm)	414.50	0.577	0.447	0.087	0.232	0.441	0.048	0.890	21	2.126	1.89
RTN 2 AL master microfluidic device features											
Channel 3 Width (150 μm)	163.69	0.577	0.447	0.087	0.232	0.406	0.019	0.872	23	2.118	1.85
Channel 1 Width (200 μm)	213.25	0.577	0.447	0.087	0.232	0.667	0.025	1.020	9	2.32	2.37
Channel 2 Width (400 μm)	414.75	0.577	0.447	0.087	0.232	0.289	0.048	0.825	32	2.082	1.72

Table C.2 Uncertainty analysis and calculation for OCMM based microfluidic device feature depth values at μMilling stage of the process chain

Measurand	Mean Value (μm)	u(art) (μm)	u(cal) (μm)	u(res) (μm)	u(rep) (μm)	u(proc) (μm)	u(temp) (μm)	u_c (μm)	v_{eff}	k	U (μm)
AL 5083 masters 1 to 4 microfluidic device features											
Channel 3 Depth (150 μm)	153.05	0.115	0.212	0.029	0.293	0.916	0.018	0.992	14	2.21	2.19
Channel 1 Depth (200 μm)	156.56	0.115	0.212	0.029	0.293	0.833	0.018	0.916	15	2.20	2.02
Channel 2 Depth (400 μm)	155.38	0.115	0.212	0.029	0.293	1.104	0.018	1.168	13	2.23	2.60
AL 5083 masters 5 to 7 microfluidic device features											
Channel 3 Depth (150 μm)	152.13	0.115	0.212	0.029	0.459	1.387	0.018	1.481	10	2.28	3.38
Channel 1 Depth (200 μm)	153.21	0.115	0.212	0.029	0.459	0.839	0.018	0.987	12	2.23	2.20
Channel 2 Depth (400 μm)	153.33	0.115	0.212	0.029	0.459	0.672	0.018	0.850	14	2.21	1.88
ALL AL 5083 masters microfluidic device features											
Channel 3 Depth (150 μm)	152.65	0.115	0.212	0.029	0.266	0.791	0.018	0.869	28	2.102	1.83
Channel 1 Depth (200 μm)	155.13	0.115	0.212	0.029	0.266	0.692	0.018	0.781	30	2.09	1.63
Channel 2 Depth (400 μm)	154.50	0.115	0.212	0.029	0.266	0.708	0.018	0.795	30	2.09	1.66
RTN 5 AL master microfluidic device features											
Channel 3 Depth (150 μm)	152.85	0.115	0.212	0.029	0.459	1.098	0.018	1.214	2	4.53	5.50
Channel 1 Depth (200 μm)	151.63	0.115	0.212	0.029	0.459	0.982	0.018	1.112	3	3.31	3.68
Channel 2 Depth (400 μm)	152.25	0.115	0.212	0.029	0.459	1.014	0.018	1.139	3	3.31	3.77
RTN 4 AL master microfluidic device features											
Channel 3 Depth (150 μm)	154.90	0.115	0.212	0.029	0.459	1.332	0.018	1.430	2	4.53	6.48
Channel 1 Depth (200 μm)	151.75	0.115	0.212	0.029	0.459	0.553	0.018	0.759	5	2.65	2.01
Channel 2 Depth (400 μm)	153.75	0.115	0.212	0.029	0.459	1.093	0.018	1.210	2	4.53	5.48
RTN 2 AL master microfluidic device features											
Channel 3 Depth (150 μm)	151.00	0.115	0.212	0.029	0.293	1.633	0.017	1.677	2	4.53	7.60
Channel 1 Depth (200 μm)	152.00	0.115	0.212	0.029	0.293	0.816	0.018	0.901	2	4.53	4.08
Channel 2 Depth (400 μm)	150.50	0.115	0.212	0.029	0.293	0.408	0.017	0.558	6	2.52	1.41

Table C.3 Uncertainty analysis and calculation for optical microscope based microfluidic device feature width values at TPF stage of the process chain

Measurand	Mean Value (μm)	u(art) (μm)	u(cal) (μm)	u(res) (μm)	u(rep) (μm)	u(proc) (μm)	u(temp) (μm)	u_c (μm)	v_{eff}	k	U (μm)
RTN 5 BMG insert microfluidic device features											
Channel 3 Width (150 μm)	165.46	0.577	0.447	0.087	0.298	0.837	0.008	1.153	6	2.52	2.91
Channel 1 Width (200 μm)	215.57	0.577	0.447	0.087	0.298	0.602	0.011	0.996	12	2.23	2.22
Channel 2 Width (400 μm)	417.40	0.577	0.447	0.087	0.298	0.169	0.021	0.812	35	2.07	1.68
RTN 4 BMG insert microfluidic device features											
Channel 3 Width (150 μm)	165.95	0.577	0.447	0.087	0.298	0.419	0.008	0.897	23	2.118	1.90
Channel 1 Width (200 μm)	217.31	0.577	0.447	0.087	0.298	0.560	0.011	0.971	14	2.20	2.14
Channel 2 Width (400 μm)	419.20	0.577	0.447	0.087	0.298	0.625	0.021	1.010	11	2.25	2.27
RTN 2 BMG insert microfluidic device features											
Channel 3 Width (150 μm)	166.75	0.577	0.447	0.087	0.298	1.503	0.008	1.700	3	3.31	5.63
Channel 1 Width (200 μm)	216.63	0.577	0.447	0.087	0.298	1.099	0.011	1.355	4	2.87	3.89
Channel 2 Width (400 μm)	416.18	0.577	0.447	0.087	0.298	0.249	0.021	0.832	34	2.074	1.73

Table C.4 Uncertainty analysis and calculation for OCMM based microfluidic device feature depth values at TPF stage of the process chain

Measurand	Mean Value (µm)	u(art) (µm)	u(cal) (µm)	u(res) (µm)	u(rep) (µm)	u(proc) (µm)	u(temp) (µm)	u_c (µm)	v_{eff}	k	U (µm)
RTN 5 BMG Insert microfluidic device features											
Channel 3 Depth (150 µm)	150.75	0.115	0.212	0.029	0.347	1.510	0.007	1.569	2	4.53	7.11
Channel 1 Depth (200 µm)	151.70	0.115	0.212	0.029	0.347	1.306	0.008	1.374	2	4.53	6.22
Channel 2 Depth (400 µm)	151.60	0.115	0.212	0.029	0.347	1.021	0.008	1.105	2	4.53	5.01
RTN 4 BMG Insert microfluidic device features											
Channel 3 Depth (150 µm)	151.88	0.115	0.212	0.029	0.298	1.245	0.008	1.303	2	4.53	5.90
Channel 1 Depth (200 µm)	151.50	0.115	0.212	0.029	0.298	1.137	0.007	1.201	2	4.53	5.44
Channel 2 Depth (400 µm)	149.10	0.115	0.212	0.029	0.298	0.984	0.007	1.056	2	4.53	4.78
RTN 2 BMG Insert microfluidic device features											
Channel 3 Depth (150 µm)	150.68	0.115	0.212	0.029	0.249	0.664	0.007	0.750	3	3.31	2.48
Channel 1 Depth (200 µm)	152.10	0.115	0.212	0.029	0.249	0.898	0.008	0.963	2	4.53	4.36
Channel 2 Depth (400 µm)	151.70	0.115	0.212	0.029	0.249	1.061	0.008	1.117	2	4.53	5.06

Table C.5 Uncertainty analysis and calculation for stylus instrument based surface roughness values of the BMG and AL workpieces at Micromilling and TPF stages of the process chain

Measurand	Mean Value (µm)	u(rep) (µm)	u(proc) (µm)	u_c (µm)	v_{eff}	k	U (µm)
Micromilling: AL masters microfluidic device channel 2 (400 µm) bottom surface							
RTN 5 AL Channel 2 Ra	0.3378	0.0044	0.0117	0.0125	2	4.53	0.0565
RTN 4 AL Channel 2 Ra	0.3490	0.0046	0.0102	0.0111	2	4.53	0.0505
RTN 2 AL Channel 2 Ra	0.0752	0.0017	0.0006	0.0018	4	2.87	0.0053
TPF: BMG inserts microfluidic device protrusion 2 (400 µm) top surface							
RTN 5 BMG Protrusion 2 Ra	0.2866	0.0025	0.0028	0.0038	5	2.65	0.0099
RTN 4 BMG Protrusion 2 Ra	0.4953	0.0044	0.0045	0.0063	5	2.65	0.0167
RTN 2 BMG Protrusion 2 Ra	0.4478	0.0040	0.0008	0.0041	4	2.87	0.0117

Table C.6 Uncertainty analysis and calculation for SEM based gratings width values at FIB Milling stage of the process chain

Measurand	Mean Value (µm)	u(rep) (µm)	u(proc) (µm)	u(P) (µm)	u_c (µm)	v_{eff}	k	U (µm)
Partially Crystalline BMG Grating structure 1 (20 µm)								
Pixel Width (X)	1.46	0.002	0.030	0.044	0.053	86	2.032	0.11
Pixel Width (Y)	1.47	0.002	0.034	0.044	0.056	65	2.043	0.11
Overall Width (X)	28.53	0.043	0.043	0.856	0.858	208510	2	1.72
Overall Width (Y)	28.59	0.032	0.040	0.858	0.859	356977	2	1.72
Partially Crystalline BMG Grating structure 2 (12 µm)								
Pixel Width (X)	0.88	0.001	0.012	0.026	0.029	294	2	0.06
Pixel Width (Y)	0.88	0.001	0.006	0.026	0.027	2852	2	0.05
Overall Width (X)	17.26	0.023	0.023	0.518	0.519	326036	2	1.04
Overall Width (Y)	17.35	0.016	0.047	0.521	0.523	31294	2	1.05
Partially Crystalline BMG Grating structure 3 (4 µm)								
Pixel Width (X)	0.28	0.001	0.003	0.008	0.009	547	2	0.02
Pixel Width (Y)	0.29	0.001	0.009	0.009	0.012	35	2.07	0.03
Overall Width (X)	5.62	0.015	0.009	0.169	0.169	51054	2	0.34
Overall Width (Y)	5.78	0.012	0.009	0.173	0.174	119493	2	0.35
Fully Amorphous BMG Grating structure 1 (20 µm)								
Pixel Width (X)	1.46	0.002	0.020	0.044	0.048	297	2	0.10
Pixel Width (Y)	1.46	0.001	0.018	0.044	0.048	401	2	0.10
Overall Width (X)	28.83	0.035	0.037	0.865	0.866	446476	2	1.73
Overall Width (Y)	28.95	0.029	0.081	0.869	0.873	26163	2	1.75
Fully Amorphous BMG Grating structure 2 (12 µm)								
Pixel Width (X)	0.87	0.001	0.007	0.026	0.027	1708	2	0.05
Pixel Width (Y)	0.87	0.002	0.009	0.026	0.028	889	2	0.06
Overall Width (X)	17.34	0.013	0.035	0.520	0.521	94692	2	1.04
Overall Width (Y)	17.31	0.034	0.023	0.519	0.521	149296	2	1.04
Fully Amorphous BMG Grating structure 3 (4 µm)								
Pixel Width (X)	0.30	0.001	0.009	0.009	0.013	39	2.07	0.03
Pixel Width (Y)	0.31	0.001	0.014	0.009	0.016	19	2.14	0.04
Overall Width (X)	5.84	0.015	0.018	0.175	0.177	15961	2	0.35
Overall Width (Y)	5.88	0.015	0.017	0.176	0.178	17845	2	0.36

Table C.7 Uncertainty analysis and calculation for AFM based gratings height values at FIB milling stage of the process chain

Measurand	Mean Value (nm)	u(cal) (nm)	u(art) (nm)	u(noise) (nm)	u(rep) (nm)	u(res) (nm)	u(proc) (nm)	u(temp) (nm)	u_c (nm)	v_{eff}	k	U (nm)
Partially Crystalline BMG Grating structure 1 (20 μm)												
Pixel height	461.90	1.163	1.501	0.008	2.596	0.058	0.562	0.023	3.266	4	2.87	9.37
Partially Crystalline BMG Grating structure 2 (12 μm)												
Pixel height	289.22	1.163	1.501	0.008	1.626	0.058	0.304	0.014	2.519	10	2.28	5.74
Partially Crystalline BMG Grating structure 3 (4 μm)												
Pixel height	92.03	1.163	1.501	0.008	0.517	0.058	0.091	0.005	1.971	30	2.09	4.12
Fully Amorphous BMG Grating structure 1 (20 μm)												
Pixel height	381.18	1.163	1.501	0.008	1.056	0.058	0.108	0.019	2.176	20	2.13	4.64
Fully Amorphous BMG Grating structure 2 (12 μm)												
Pixel height	319.73	1.163	1.501	0.008	0.886	0.058	0.161	0.016	2.102	25	2.11	4.44
Fully Amorphous BMG Grating structure 3 (4 μm)												
Pixel height	84.30	1.163	1.501	0.008	0.234	0.058	0.082	0.004	1.916	29	2.094	4.01

Table C.8 Uncertainty analysis and calculation for optical microscope based microfluidic device feature width values at µIM stage of the process chain

Measurand	Mean Value (µm)	u(art) (µm)	u(cal) (µm)	u(res) (µm)	u(rep) (µm)	u(proc) (µm)	u(temp) (µm)	u_c (µm)	v_{eff}	k	U (µm)
PP microfluidic device features											
Channel 3 Width (150 µm)	153.71	0.577	0.447	0.087	0.339	0.794	0.152	1.144	41	2.06	2.36
Channel 1 Width (200 µm)	203.54	0.577	0.447	0.087	0.339	0.558	0.201	1.004	50	2.05	2.06
Channel 2 Width (400 µm)	404.17	0.577	0.447	0.087	0.339	0.487	0.400	1.026	64	2.043	2.10
PC microfluidic device features											
Channel 3 Width (150 µm)	158.91	0.577	0.447	0.087	0.429	0.815	0.055	1.180	38	2.064	2.44
Channel 1 Width (200 µm)	211.59	0.577	0.447	0.087	0.429	1.062	0.074	1.363	31	2.086	2.84
Channel 2 Width (400 µm)	414.90	0.577	0.447	0.087	0.429	0.935	0.144	1.273	35	2.07	2.63
PA + 20% GF microfluidic device features											
Channel 3 Width (150 µm)	157.15	0.577	0.447	0.087	0.477	1.098	0.078	1.407	30	2.09	2.94
Channel 1 Width (200 µm)	212.09	0.577	0.447	0.087	0.477	1.084	0.105	1.398	31	2.086	2.92
Channel 2 Width (400 µm)	414.33	0.577	0.447	0.087	0.477	0.461	0.205	1.011	40	2.06	2.08

Table C.9 Uncertainty analysis and calculation for OCMM based microfluidic device feature depth values at μIM stage of the process chain

Measurand	Mean Value (μm)	u(art) (μm)	u(cal) (μm)	u(res) (μm)	u(rep) (μm)	u(proc) (μm)	u(temp) (μm)	u_c (μm)	v_{eff}	k	U (μm)
PP microfluidic device features											
Channel 3 Depth (150 μm)	147.44	0.115	0.212	0.029	0.345	0.449	0.146	0.634	24	2.114	1.34
Channel 1 Depth (200 μm)	148.00	0.115	0.212	0.029	0.345	0.658	0.147	0.796	23	2.118	1.69
Channel 2 Depth (400 μm)	148.22	0.115	0.212	0.029	0.345	0.630	0.147	0.772	23	2.118	1.64
PC microfluidic device features											
Channel 3 Depth (150 μm)	149.44	0.115	0.212	0.029	0.498	0.732	0.052	0.919	19	2.14	1.97
Channel 1 Depth (200 μm)	149.67	0.115	0.212	0.029	0.498	0.465	0.052	0.726	14	2.20	1.60
Channel 2 Depth (400 μm)	150.22	0.115	0.212	0.029	0.498	0.513	0.052	0.757	16	2.17	1.64
PA + 20% GF microfluidic device features											
Channel 3 Depth (150 μm)	150.67	0.115	0.212	0.029	0.763	0.645	0.075	1.031	11	2.25	2.32
Channel 1 Depth (200 μm)	150.33	0.115	0.212	0.029	0.763	0.516	0.074	0.956	9	2.32	2.22
Channel 2 Depth (400 μm)	149.89	0.115	0.212	0.029	0.763	0.724	0.074	1.082	13	2.21	2.39

Table C.10 Uncertainty analysis and calculation for SEM based gratings width values at μIM stage of the process chain

Measurand	Mean Value (μm)	u(rep) (μm)	u(proc) (μm)	u(P) (μm)	u_c (μm)	v_{eff}	k	U (μm)
PP Grating structure 1 (20 μm)								
Pixel Width (X)	1.46	0.002	0.026	0.044	0.051	435	2	0.10
Pixel Width (Y)	1.45	0.002	0.019	0.044	0.047	1225	2	0.09
Overall Width (X)	28.32	0.030	0.022	0.850	0.851	2338929	2	1.70
Overall Width (Y)	28.30	0.030	0.022	0.849	0.850	2211137	2	1.70
PP Grating structure 2 (12 μm)								
Pixel Width (X)	0.91	0.001	0.010	0.027	0.029	2370	2	0.06
Pixel Width (Y)	0.92	0.001	0.018	0.027	0.033	347	2	0.07
Overall Width (X)	16.86	0.017	0.013	0.506	0.506	2688097	2	1.01
Overall Width (Y)	16.97	0.023	0.020	0.509	0.510	770850	2	1.02
PP Grating structure 3 (4 μm)								
Pixel Width (X)	0.32	0.001	0.009	0.010	0.013	134	2	0.03
Pixel Width (Y)	0.32	0.001	0.010	0.010	0.014	112	2	0.03
Overall Width (X)	5.65	0.009	0.005	0.169	0.170	500369	2	0.34
Overall Width (Y)	5.74	0.023	0.013	0.172	0.174	11788	2	0.35
PC Grating structure 1 (20 μm)								
Pixel Width (X)	1.50	0.002	0.015	0.045	0.047	2969	2	0.09
Pixel Width (Y)	1.50	0.001	0.015	0.045	0.048	2751	2	0.10
Overall Width (X)	28.72	0.030	0.025	0.862	0.863	2240320	2	1.73
Overall Width (Y)	28.67	0.024	0.029	0.860	0.861	3263378	2	1.72
PC Grating structure 2 (12 μm)								
Pixel Width (X)	0.90	0.001	0.010	0.027	0.029	2275	2	0.06
Pixel Width (Y)	0.90	0.001	0.008	0.027	0.028	5426	2	0.06
Overall Width (X)	16.99	0.010	0.020	0.510	0.510	2847859	2	1.02
Overall Width (Y)	16.91	0.020	0.015	0.507	0.508	1314756	2	1.02
PP Grating structure 3 (4 μm)								
Pixel Width (X)	0.30	0.001	0.006	0.009	0.011	364	2	0.02
Pixel Width (Y)	0.31	0.001	0.007	0.009	0.011	230	2	0.02
Overall Width (X)	5.70	0.014	0.012	0.171	0.172	72577	2	0.34
Overall Width (Y)	5.73	0.009	0.010	0.172	0.172	339402	2	0.34

Table C.11 Uncertainty analysis and calculation for AFM based gratings depth values at μIM stage of the process chain

Measurand	Mean Value (nm)	u(cal) (nm)	u(art) (nm)	u(noise) (nm)	u(rep) (nm)	u(res) (nm)	u(proc) (nm)	u(temp) (nm)	u_c (nm)	v_{eff}	k	U (nm)
PP Grating structure 1 (20 μm)												
Pixel height	369.02	1.163	1.501	0.008	2.393	0.058	0.096	0.365	3.078	5	2.65	8.16
PP Grating structure 2 (12 μm)												
Pixel height	306.23	1.163	1.501	0.008	1.985	0.058	0.105	0.303	2.767	7	2.43	6.72
PP Grating structure 3 (4 μm)												
Pixel height	74.72	1.163	1.501	0.008	0.484	0.058	0.049	0.074	1.962	30	2.09	4.10
PC Grating structure 1 (20 μm)												
Pixel height	360.50	1.163	1.501	0.008	2.974	0.058	0.047	0.125	3.531	3	3.31	11.69
PC Grating structure 2 (12 μm)												
Pixel height	316.78	1.163	1.501	0.008	2.613	0.058	0.116	0.110	3.235	4	2.87	9.28
PP Grating structure 3 (4 μm)												
Pixel height	78.67	1.163	1.501	0.008	0.649	0.058	0.093	0.027	2.010	29	2.094	4.21

Table C.12 Uncertainty analysis and calculation for BMG insert micro-hardness values after processing steps

Measurand	Mean Value (Hv)	u(art) (Hv)	u(cal) (Hv)	u(res) (Hv)	u(hardness) (Hv)	u_c (Hv)	v_{eff}	k	U (Hv)
As Received Vit 1 B plate.	534.36	7.75	8.17	0.03	6.25	12.88	18	2.15	27.69
RTN 5 BMG insert after TPF	596.70	7.75	8.17	0.03	4.77	12.23	17	2.16	26.42
RTN 5 BMG insert after 1000 μIM cycles	597.26	7.75	8.17	0.03	5.52	12.54	18	2.15	26.97

Table C.13 Uncertainty analysis and calculation for BMG insert nano-hardness values after processing steps

Measurand	Mean Value (GPa)	u(art) (GPa)	u(cal) (GPa)	u(res) (GPa)	u(hardness) (GPa)	u_c (GPa)	v_{eff}	k	U (GPa)
As Received Vit 1 B plate.	6.05	0.116	0.007	0.003	0.015	0.117	57474	2	0.23
RTN 5 BMG insert after TPF	6.89	0.116	0.007	0.003	0.017	0.118	39341	2	0.24
RTN 5 BMG insert after 1000 µIM cycles	7.03	0.116	0.007	0.003	0.014	0.117	72202	2	0.23

The equations used to calculate the combined standard uncertainty (u_c), the effective degrees of freedom (v_{eff}) and the expanded uncertainty (U) are listed below:

$$u_c = \sqrt{\sum_{i=1}^{N} u_i^2} \qquad (1)$$

$$v_{eff} = \frac{u_c^4}{\sum_{i=1}^{N} \frac{u_i^4}{v_i}} \qquad (2)$$

$$U = k.u_c \qquad (3)$$

where,

u_i = individual standard uncertainty due to measurement variation contributor i

$N = N^{th}$ measurement variation contributor.

v_i = degrees of freedom of standard uncertainty u_i

k = coverage factor determined at a level of confidence (i.e. 95 %) for a given number of degrees of freedom (i.e. v_{eff})

APPENDIX D

DETAILS OF THE TECHNOLOGY EXPERTS WHO PROVIDED THE DATA FOR THE MATURITY ASSESSMENT OF THE INDIVIDUAL PROCESSES AND PROCESS PAIRS REPORTED IN CHAPTER 3

Table D.1 Technology Experts Details

Technology Expert Name	Domain of Expertise	Institution
Jurgen Mohr	Electroforming & E-beam Lithography & Deep Reactive Ion Etching	Karlsruhe Institute of Technology, Germany
Matthias Worgull	Hot embossing (HE) & Electroforming	Karlsruhe Institute of Technology, Germany
Wilhelm Pfleging	UV Laser & PS Laser ablation	Karlsruhe Institute of Technology, Germany
Pascal Meyer	X-ray lithography & Electroforming	Karlsruhe Institute of Technology, Germany
Stefan Dimov	Projection Mask-Less Ion Beam Patterning (PMLIBP) & Focused Ion Beam (FIB) & PS Laser ablation	Cardiff University, UK
Roussi Minev	Focused Ion Beam	Cardiff University, UK
E. Brousseau	PS Laser ablation & HE	Cardiff University, UK
Steffen Scholz	Micro-injection Moulding (μIM) & Electroforming	Cardiff University, UK
Pascal Fugier	Electroforming	CEA-Liten, France
Luca Belforte	Focused Ion Beam	Fiat SCPA (CRF), Italy
Lars Mattsson	E-beam Lithography & PS Laser ablation	KTH, Royal Institute of Technology, Sweden
Estefanía Abad	Deep Reactive Ion Etching & Electroforming	TEKNIKER, Spain
Sabino Azcarate	μMilling & μIM & PS Laser ablation	TEKNIKER, Spain
Hans Loeschner	Projection Mask-Less Ion Beam Patterning (PMLIBP) & Focused Ion Beam (FIB) & E-beam Lithography	IMS Nanofabrication AG, Austria
Richard Leach	X-ray lithography & FIB	NPL, UK
Falco van Delft	E-beam Lithography & Deep Reactive Ion Etching & FIB	MiPlaza Philips Research Europe, The Netherlands

APPENDIX E

TECHNICAL DATA FOR VIT 1b ALLOY

Table E.1 Vit 1b Properties

Supplier	Liquidmetal Technologies, Inc.	
Sample Details	Form	Square Plate
	Dimensions (mm)	30 x 30 x 2.5
	Weight (g)	~20
	Property	**Nominal Value**
Composition	Zr (wt%)	67.02%
	Ti (wt%)	8.80%
	Cu (wt%)	10.61%
	Ni (wt%)	9.80%
	Be (wt%)	3.76%
Mechanical Properties	Tensile Yield Strength (GPa)	1.9
	Elastic Strain Limit (%)	2
	Density (g/cc)	6.04
	Coefficient of Linear Thermal Expansion ($10^{-6}/\,^{o}$C)	9
	Young's Modulus (GPa)	95
	Hardness (Hv)	540
Thermal Properties	Glass Transition Temperature (^{o}C)	350
	Crystallisation Onset Temperature (^{o}C)	483
	Melting Onset Temperature (^{o}C)	659

APPENDIX F

TECHNICAL DATA FOR GRIVORY GV-2 FWA BLACK 9225

Table F.1 Grivory GV-2 FWA BLACK 9225 Properties

	Property	Nominal Value
Supplier	EMS - GRIVORY	
Material Description	Grivory GV-2 FWA black 9225 is a 20% glassfibre reinforced engineering thermoplastic material based on a combination of semicrystalline polyamide with partially aromatic copolyamide.	
	Property	Nominal Value
Mechanical Properties	Tensile E-Modulus (MPa)	8200
	Tensile strength at break (MPa)	145
	Elongation at break (%)	3
	Impact strength --- Charpy, 23 ^{o}C (kJ/m^2)	50
	Ball indentation hardness (MPa)	225
	Density (g/cm^3)	1.28
Thermal Properties	Melting point (^{o}C)	260
	Heat deflection temperature HDT/A (^{o}C)	230
	Thermal expansion coefficient long. (10^{-4}/K)	0.1
	Thermal expansion coefficient trans. (10^{-4}/K)	1.0
General Properties	Moisture absorption -- 23 ^{o}C/ 50% r.h.	1.5
	Linear mould shrinkage – Long. (%)	0.15
	Linear mould shrinkage – trans. (%)	0.75

Table F.2 Processing Data for Grivory GV-2 FWA BLACK 9225

	Parameter	Recommended Value
Drying		
Desiccant Dryer	Max. Temperature (^{o}C)	80
	Time (hours)	4 - 12
	Dew point of dryer (^{o}C)	-25
Vacuum Oven	Max. Temperature (^{o}C)	100
	Time (hours)	4 - 12
Injection Moulding Machine Settings		
Temperatures	Flange (^{o}C)	80
	Zone 1 (^{o}C)	260
	Zone 2 (^{o}C)	270
	Zone 3 (^{o}C)	275
	Nozzle (^{o}C)	270
	Tool (^{o}C)	80 - 120
	Melt (^{o}C)	270-300
Pressures / Speeds	Injection speed	Medium - high
	Hold-on pressure (bar)	300 - 800
	Dynamic pressure (bar)	50 - 100
	Screw speed (m/s)	0.1 – 0.3

REFERENCES

(HLG), H.L.E.G. (2011) **Key Enabling Technologies -- Final report**. June 2011. [online]. European Commission. Available from: http://ec.europa.eu/enterprise/sectors/ict/files/kets/hlg_report_final_en.pdf [Accessed 7 April 2015]

Abgrall, P. and Gue, A.-M. (2007) Lab-on-chip technologies: making a microfluidic network and coupling it into a complete microsystem—a review. **Journal of Micromechanics and Microengineering**, 17 (5): R15–R49.

Ali, M.Y., Hung, W. and Yongqi, F. (2010) A Review of Focused Ion Beam Sputtering. **International Journal of Precision Engineering and Manufacturing**, 11 (1): 157–170

Allen, D.M., Shore, P., Evans, R.W., et al. (2009) Ion beam , focused ion beam , and plasma discharge machining. **CIRP Annals - Manufacturing Technology**, 58 (2): 647–662

Alting, L., Kimura, F., Hansen, H.N., et al. (2003) Micro Engineering. **Annals of the CIRP**, 52 (2): 635–658

Altunok, T. and Cakmak, T. (2010) A technology readiness levels (TRLs) calculator software for systems engineering and technology management tool. **Advances in Engineering Software** , 41 (5): 769–778.

Anis, M., Rainforth, W.M. and H.A. Davies (1994) Wear behaviour of rapidly solidified Fe68 Cr18 M02 B12 alloys. **Wear**, 172 (2): 135 – 145

Aramcharoen, A. and Mativenga, P.T. (2009) Size effect and tool geometry in micromilling of tool steel. **Precision Engineering** , 33 (4): 402–407.

Arman, H., Hodgson, A. and Gindy, N. (2006) "Threat and Opportunity Analysis in Technological Development." In **2006 Technology Management for the Global Future - PICMET 2006 Conference**. **Istanbul**. **July 2006** . IEEE. pp. 9–17.

Attia, U.M., Marson, S. and Alcock, J.R. (2009) Micro-injection moulding of polymer microfluidic devices. **Microfluidics and Nanofluidics** , 7 (1): 1–28.

Ay, F., Worhoff, K., de Riddler, R.M., et al. (2012) Focused-ion-beam nanostructuring of Al 2 O 3 dielectric layers for photonic applications. **Journal of Micromechanics and Microengineering**, 22 (10): 105008 (5pp)

Azcarate, S., Uriarte, L., Schoth, A., et al. (2006) "Hybrid Tooling: A Review of Process Chains for Tooling Microfabrication Within 4M." In Dimov, S.S. and Menz, W. (eds.). **4M 2006 - Second International Conference on Multi-Material Micro Manufacture**. **Karlsruhe Germany**. **2006**. Elsevier. pp. 305–308

Bakkal, M. and Nakşiler, V. (2009) Cutting Mechanics of Bulk Metallic Glass Materials on Meso-End Milling. **Materials and Manufacturing Processes**, 24 (12): 1249–1255

Bakkal, M., Shih, A.J., McSpadden, S.B., et al. (2005) Thrust force, torque, and tool wear in drilling the bulk metallic glass. **International Journal of Machine Tools and Manufacture** , 45 (7-8): 863–872.

Bakkal, M., Shih, A.J. and Scattergood, R.O. (2004) Chip formation, cutting forces, and tool wear in turning of Zr-based bulk metallic glass. **International Journal of Machine Tools and Manufacture** , 44 (9): 915–925.

Barbero, D.R., Saifullah, M.S.M., Hoffmann, P., et al. (2007) High-Resolution Nanoimprinting with a Robust and Reusable Polymer Mold. **Advanced Functional Materials** , 17 (14): 2419–2425.

Bardt, J.A. and Sawyer, W.G. (2007) Micromolding three-dimensional amorphous metal structures. **Journal of Materials Research**, 22 (2): 339–343

Basu, J., Nagendra, N., Li, Y., et al. (2003) Microstructure and mechanical properties of a partially crystallized La-based bulk metallic glass. **Philosophical Magazine** , 83 (15): 1747–1760.

Beaumont, J.P., Nagel, R. and Sherman, R. (2002) **Sucessful Injection Moulding -- Process, Design, and simulation**. 1st edn. Hanser

Becker, H. and Gärtner, C. (2008) Polymer microfabrication technologies for microfluidic systems. **Analytical and Bioanalytical Chemistry** , 390 (1): 89–111.

Bergstrom, J., Thuvander, F., Devos, P., et al. (2001) Wear of die materials in full scale plastic injection moulding of glass fibre reinforced polycarbonate. **Wear** , 251 (1-12): 1511–1521.

Berztiss, A.T. (2002) "Management Capability maturity." <u>In</u> **Proceedings of the 13th International Workshop on Database and Expert Systems Applications (DEXA'02)**. **2002**. pp. 162–167

Bigot, S., Minev, R., Dimov, S., et al. (2011) Function and length scale integration in innovative products – technical solutions and new organisational models. **International Journal of Manufacturing Technology and Management**, 23 (3/4): 157–178

Bissacco, G., Hansen, H.N. and De Chiffre, L. (2005) Micromilling of hardened tool steel for mould making applications. **Journal of Materials Processing Technology** , 167 (2-3): 201–207.

Bolt, P.J., Azcarate, S., Malek, C.K., et al. (2008) **New manufacturing routes for micro polymer manufacturing for the next decades – Process chains to strengthen EC economic power**

Bonse, J., Kruger, J., Hohm, S., et al. (2012) Femtosecond laser-induced periodic surface structures. **Journal of Laser Applications**, 24 (4): 4207–42006

Brinksmeier, E., Riemer, O. and Stern, R. (2001) "Machining of precision parts and microstructures." In **Proceedings of the 10th International Conference on Precision Engineering, ICPE**. **Yokohama, Japan**. **2001**. pp. 3–11

Brousseau, E.B., Barton, R., Dimov, S.S., et al. (2009) "Technology Maturity Assessment of Micro and Nano Manufacturing Processes." In Saile, V., Ehmann, K.F. and Dimov, S.S. (eds.). **4M/ICOMM 2009 - The Global Conference on Micro Manufacture - Incorportating the 5th International Conference on Multi-Material Micro Manufacture (4M) and the 4th International Conference on Micro Manufacturing (ICOMM)**. **Karlsruhe, Germany**. **2009**. Charlesworth Group. pp. 23–25

Brousseau, E.B., Dimov, S.S. and Pham, D.T. (2010) Some Recent Advances in Multi-Material Micro- and Nano-manufacturing. **International Journal of Advanced Manufacturing Technology**, 47 (1-4): 161–180

Brown, M.S. and Arnold, C.B. (2010) "Fundamentals of Laser-Material Interaction and Application to Multiscale Surface Modification." In Sugioka, K., Meunier, M. and Pique, A. (eds.) **Laser Precision Microfabrication**. 1st edn. Springer-Verlag. pp. 91–120

Browne, D.J., Stratton, D., Gilchrist, M.D., et al. (2012) Bulk Metallic Glass Multiscale Tooling for Molding of Polymers with Micro to Nano Features : A Review. **Metallurgical and Materials Transactions A** , 44 (5): 2021–2030.

BS EN ISO 14577 (2002) **Metallic materials — Instrumented indentation test for hardness and materials parameters — Part 1: Test method**., p. 27

Calaon, M., Hansen, H.N., Tosello, G., et al. (2013) "A capability study of micro moulding for nano fluidic system manufacture." In **Proceedings of the 13th euspen International Conference**. **2013**. pp. 105–108

Calaon, M., Islam, A., Hansen, H.N., et al. (2011) Experimental investigation of new manufacturing process chains to create micro-metal structures on polymer substrates for lab-on-chip sensors. **The International Journal of Advanced Manufacturing Technology** , 59 (1-4): 101–109.

Câmara, M.A., Rubio, J.C.C., Abrão, A.M., et al. (2012) State of the Art on Micromilling of Materials, a Review. **Journal of Materials Science & Technology** , 28 (8): 673–685.

Cardoso, P. and Davim, J.P. (2012) A brief review on micromachining of materials. **Reviews on Advanced Materials Science**, 30: 98–102

Cardoso, P. and Davim, P. (2011) Some aspects on micromilling and machine tools. **Annals of Faculty of Engineering Hunedoara**, X (1): 209–211

Chang, C.Y., Yang, S.Y. and Sheh, J.L. (2006) A roller embossing process for rapid fabrication of microlens arrays on glass substrates. **Microsystem Technologies**, 12 (8): 754–759

Chen, C., Chen, S., Liao, W., et al. (2010) Micro injection molding of a micro- fluidic platform. **International Communications in Heat and Mass Transfer** , 37 (9): 1290–1294.

Chen, C.-Y., Chung, C.-J., Wu, B.-H., et al. (2012) Microstructure and lubricating property of ultra-fast laser pulse textured silicon carbide seals. **Applied Physics A** , 107 (2): 345–350.

Chen, M. (2011) A brief overview of bulk metallic glasses. **NPG Asia Materials**, 3 (9): 82–90

Chen, T.-C. and Darling, R.B. (2008) Laser micromachining of the materials using in microfluidics by high precision pulsed near and mid-ultraviolet Nd:YAG lasers. **Journal of Materials Processing Technology** , 198 (1-3): 248–253.

Chen, X.H., Zhang, X.C., Zhang, Y., et al. (2008) Fabrication and characterization of metallic glasses with a specific microstructure for micro-electro-mechanical system applications. **Journal of Non-Crystalline Solids**, 354 (28): 3308–3316

Chen, Y.C., Chu, J.P., Jang, J.S.C., et al. (2013) Replication of nano / micro-scale features using bulk metallic glass mold prepared by femtosecond laser and imprint. **Journal of Micromechanics and Microengineering**, 23 (3): 035030 (8pp)

Cheng, J., Liu, C., Shang, S., et al. (2013) A review of ultrafast laser materials micromachining. **Optics & Laser Technology** , 46: 88–102.

Chiu, C.-C. and Lee, Y.-C. (2011) Fabricating of aspheric micro-lens array by excimer laser micromachining. **Optics and Lasers in Engineering** , 49 (9-10): 1232–1237.

Chiu, C.-C. and Lee, Y.-C. (2013) Fabrication of hexagonally arrayed micro-structures with axially symmetrical surface profile by tri-axial excimer laser scanning. **International Journal of Machine Tools and Manufacture** , 70: 15–21.

Choi, K.H., Meijer, J., Masuzawa, T., et al. (2004) Excimer laser micromachining for 3D microstructure. **Journal of Materials Processing Technology** , 149 (1-3): 561–566.

Choi, S.H., Ryu, S.H., Choi, D.K., et al. (2007) Fabrication of WC micro-shaft by using electrochemical etching. **International Journal of Advanced Manufacturing Technology**, 31 (7-8): 682–687

Chrissis, M.B., Konrad, M. and Shrum, S. (2007) **CMMI Guidelines for Process Integration and Product Development**. 2nd edn.

Chu, J.P., Wijaya, H., Wu, C.W., et al. (2007) Nanoimprint of gratings on a bulk metallic glass. **Applied Physics Letters**, 90 (3): 034101

Chung, D.K., Shin, H.S., Park, M.S., et al. (2011) Recent researches in micro electrical machining. **International Journal of Precision Engineering and Manufacturing**, 12 (2): 371–380

Clark, W., Horrell, K., Rogelstad, T., et al. (1995) **SEMATECH Qualification Plan Guidelines for Engineering**. p. 94

Concustell, A., Alcalá, G., Mato, S., et al. (2005) Effect of relaxation and primary nanocrystallization on the mechanical properties of Cu60Zr22Ti18 bulk metallic glass. **Intermetallics** , 13 (11): 1214–1219.

Craighead, H. (2006) Future lab-on-a-chip technologies for interrogating individual molecules. **Nature** , 442 (7101): 387–93.

Crosby, P. (1979) **Quality is Free**. New York: McGraw Hill

Cui, Z. (2005) **Micro-Nanofabrication: Technologies and Applications**. 1st edn. Springer-Verlag

Dao, M., Lu, L., Asaro, R., et al. (2007) Toward a quantitative understanding of mechanical behavior of nanocrystalline metals. **Acta Materialia** , 55 (12): 4041–4065.

Denkena, B., Henjes, J. and Henning, H. (2011) Simulation-based dimensioning of manufacturing process chains. **CIRP Journal of Manufacturing Science and Technology** , 4 (1): 9–14.

Denkena, B., Rudzio, H. and Brandes, A. (2006) Methodology for Dimensioning Technological Interfaces of Manufacturing Process Chains. **Annals of the CIRP**, 55 (1): 497–500

DeVor, R.E. and Ehmann, K.F. (2005) "Introduction (Chapter 1)." In Ehmann, K.F., Bourell, D., Culpepper, M.L., et al. (eds.) **International Assessment of Research and Development in Micromanufacturing: Final Report**. WTEC Inc. pp. 1–8

Dhanorker, A. and Ozel, T. (2008) Meso/micro scale milling for micro-manufacturing. **International Journal of Mechatronics and Manufacturing Systems**, 1 (1): 23

Dickerhof, M. and Parusel, A. (2008) "Bridging the gap – from a process related documentation to an integrated process and application knowledge management in Micro Systems Technology." In Ratchev, S. and Koelemeije, S. (eds.) **Micro-Assembly Technologies and Applications -- IFIP TC5 WG5.5 Fourth International Precision Assembly Seminar (IPAS'2008) Chamonix, France February 10–13, 2008**. pp. 109–119

Dimov, S., Pham, D.T., Ivanov, A., et al. (2004) Micromilling strategies : optimization issues. **Proc Instn Mech Engrs Part B: J Engineering Manufacture**, 218 (7): 731–736

Dimov, S.S., Brousseau, E.B., Minev, R., et al. (2012) Micro- and nano-manufacturing: Challenges and opportunities. **Proc. Inst. Mechanical Engineers Part C: Journal of Mechanical Engineering Science**, 226 (3): 3–15

Dimov, S.S., Matthews, C.W., Glanfield, A., et al. (2006) "Roadmapping Study in Multi-Material Micro Manufacture." In **Second International Conference on Multi-Material Micro Manufacture, 4M2006. Grenoble, France, 20-22 September**. 2006. pp. xi–xxv

Dirckx, M., Taylor, H.K., Mazzeo, A.D., et al. (2006) "Tooling for Micro- and Nano-Imprinting and its Consequences for Manufacturing." In **Proceedings of the 4th International Symposium on Nanomanufacturing (ISNM)**. 2006. pp. 1 – 7

Dobrev, T. (2006) **Investigation of laser milling process characteristics for micro tooling applications**. Cardiff University

Dobrev, T., Dimov, S.S. and Thomas, A.J. (2006) Laser milling: Modelling crater and surface formation. **Proceedings of the Institution of Mechanical Engineers, Part C: Journal of Mechanical Engineering Science** , 220 (11): 1685–1696.

Dornfeld, D., Min, S. and Takeuchi, Y. (2006) Recent Advances in Mechanical Micromachining. **Annals of the CIRP**, 55 (2): 745–768

Dubey, A.K. and Yadava, V. (2008) Laser beam machining --- A review. **International Journal of Machine Tools & Manufacture**, 48 (6): 609–628

Eckert, J. and Das, J. (2007) Mechanical properties of bulk metallic glasses and composites. **Journal of Materials Research**, 22 (2): 285–301

Etsion, I. (2005) State of the Art in Laser Surface Texturing. **Journal of Tribology**, 127 (1): 248

Fadeeva, E., Truong, V.K., Stiesch, M., et al. (2011) Bacterial Retention on Superhydrophobic Titanium Surfaces Fabricated by Femtosecond Laser Ablation. **Langmuir** , 27 (6): 3012–3019.

Ferrara, V. La, Aneesh, P.M., Veneri, P.D., et al. (2014) Focused ion beam strategy for nanostructure milling in doped silicon oxide layer for light trapping applications. **Vacuum**, 99: 135–142

Filiz, S., Conley, C.M., Wasserman, M.B., et al. (2007) An experimental investigation of micro-machinability of copper 101 using tungsten carbide micro-endmills. **International Journal of Machine Tools and Manufacture**, 47 (7): 1088–1100

Filiz, S., Xie, L., Weiss, L.E., et al. (2008) Micromilling of microbarbs for medical implants. **International Journal of Machine Tools and Manufacture**, 48 (3): 459–472

Fleischer, J. and Kotschenreuther, J. (2007) The manufacturing of micro molds by conventional and energy-assisted processes. **The International Journal of Advanced Manufacturing Technology** , 33 (1-2): 75–85.

Flores, K.M. and Dauskardt, R.H. (2004) Fracture and deformation of bulk metallic glasses and their composites. **Intermetallics** , 12 (7-9): 1025–1029.

Ford, D. and Ryan, C. (1981) Taking technology to market. **Harvard Buisness Review**, 59 (2): 117–126

Fornell, J., González, S., Rossinyol, E., et al. (2010) Enhanced mechanical properties due to structural changes induced by devitrification in Fe–Co–B–Si–Nb bulk metallic glass. **Acta Materialia** , 58 (19): 6256–6266.

Fox-Rabinovich, G.S., Beake, B.D., Endrino, J.L., et al. (2006) Effect of mechanical properties measured at room and elevated temperatures on the wear resistance of cutting tools with TiAlN and AlCrN coatings. **Surface and Coatings Technology** , 200 (20-21): 5738–5742.

Franssila, S. (2004) **Introduction to Microfabrication**. 1st edn. John Wiley & Sons Inc.

Fraser, P., Farrukh, C. and Gregory, M. (2003) Managing product development collaborations ---- a process maturity approach. **Proc Instn Mech Engrs Part B: J Engineering Manufacture**, 217 (11): 1499–1519

Fraser, P., Moultrie, J. and Gregory, M. (2002) "The use of maturity models/ grids as a tool in assessing product development capability." In **IEEE Engineering Management Conference, 2002. IEMC'02. 2002**. pp. 244–249

Fujita, K., Hashimoto, T., Zhang, W., et al. (2008) Ultrahigh fatigue strength in Ti-based bulk metallic glass. **Reviews on Advanced Material Science**, 18: 137 – 139

Fujita, K., Morishita, Y., Nishiyama, N., et al. (2005) Cutting Characteristics of Bulk Metallic Glass. **Materials Transactions**, 46 (12): 2856–2863

Gad-el-Hak (2006) "Introduction." <u>In</u> Gad-el-Hak, M. (ed.) **The MEMS handbook**. 2nd Editio. CRC Press. pp. 1–1 – 1–5

Giboz, J., Copponnex, T. and Mele, P. (2007) Microinjection Moulding of Thermoplastic Polymers - A review. **Journal of Micromechanics and Microengineering**, 17 (6): R96 – R109

Gierak, J. (2009) Focused ion beam technology and ultimate applications. **Semiconductor Science and Technology**, 24 (4): 043001 (23pp)

Gloriant, T. (2003) Microhardness and abrasive wear resistance of metallic glasses and nanostructured composite materials. **Journal of Non-Crystalline Solids** , 316 (1): 96–103.

Gong, L., Wang, Y.., Wang, L.M., et al. (2002) Wear behavior of Bulk Zr41 Ti14 Cu12,5 Ni10 Be22.5 metallic Glasses. **Journal of Materials Research** , 17 (8): 1877 – 1880.

González, S., Pellicer, E., Suriñach, S., et al. (2012) Mechanical and corrosion behaviour of as-cast and annealed Zr60Cu20Al10Fe5Ti5 bulk metallic glass. **Intermetallics** , 28: 149–155.

Gower, M. and Rizvi, N. (2000) "Applications of laser ablation to microengineering." <u>In</u> **Proceedings of SPIE, High-Power Laser Ablation III**. **2000** . International Society for Optics and Photonics. pp. 452–460.

Grant, K.P. and Pennypacker, J.S. (2006) Project management maturity: an assessment of project management capabilities among and between selected industries. **IEEE Transactions on Engineering Management** , 53 (1): 59–68.

Greer, A.L., Rutherford, K.L. and Hutchings, I.M. (2002) Wear resistance of amorphous alloys and related materials. **International Materials Reviews** , 47 (2): 87–112.

Griffiths, C.A., Dimov, S.S., Brousseau, E.B., et al. (2007) The effects of tool surface quality in micro-injection moulding. **Journal of Materials Processing Technology**, 189 (1-3): 418–427

Griffiths, C.A., Dimov, S.S. and Brousseau, E.B. (2008a) Microinjection moulding: the influence of runner systems on flow behaviour and melt fill of multiple microcavities. **Proceedings of the Institution of Mechanical Engineers, Part B: Journal of Engineering Manufacture** , 222 (9): 1119–1130.

Griffiths, C.A., Dimov, S.S., Brousseau, E.B., et al. (2008b) The finite element analysis of melt flow behaviour in micro-injection moulding. **Proceedings of the Institution of Mechanical Engineers, Part B: Journal of Engineering Manufacture** , 222 (9): 1107–1118.

Griffiths, C.A., Dimov, S.S., Brousseau, E.B., et al. (2009) Investigation of surface treatment effects in micro-injection-moulding. **The International Journal of Advanced Manufacturing Technology** , 47 (1-4): 99–110.

Griffiths, C.A., Dimov, S.S., Scholz, S., et al. (2011) Cavity Air Flow Behavior During Filling in Microinjection Molding. **Journal of Manufacturing Science and Engineering** , 133 (1): 011006.

Grigorescu, A.E. and Hagen, C.W. (2009) Resists for sub-20-nm electron beam lithography with a focus on HSQ: state of the art. **Nanotechnology** , 20 (29): 292001.

Groover, M.P. (2007) **Fundamentals of Modern Manufacturing**. 3rd Edn.

Gu, X.J., Poon, S.J., Shiflet, G.J., et al. (2009) Ductile-to-brittle transition in a Ti-based bulk metallic glass. **Scripta Materialia** , 60 (11): 1027–1030.

Guo, L.J. (2007) Nanoimprint Lithography: Methods and Material Requirements. **Advanced Materials** , 19 (4): 495–513.

Hainberger, R., Bruck, R., Kataeva, N., et al. (2010) Nanopatterned polymethylpentene substrates fabricated by injection molding for biophotonic applications. **Microelectronic Engineering** , 87 (5-8): 821–823.

Hansen, H.N., Hocken, R.J. and Tosello, G. (2011) Replication of micro and nano surface geometries. **CIRP Annals - Manufacturing Technology** , 60 (2): 695–714.

Hansen, H.N., Prichystal, J.P., Møller, P., et al. (2007) Complex process chains for manufacturing of invisible displays integrated in bulk metal panels. **CIRP Annals - Manufacturing Technology**, 56 (1): 237–240

He, J.J., Li, N., Tang, N., et al. (2012) The precision replication of a microchannel mould by hot-embossing a Zr-based bulk metallic glass. **Intermetallics** , 21 (1): 50–55.

Heckele, M. and Schomburg, W.K. (2004) Review on micro molding of thermoplastic polymers. **Journal of Micromechanics and Microengineering** , 14 (3): R1–R14.

Henann, D.L., Srivastava, V., Taylor, H.K., et al. (2009) Metallic glasses: viable tool materials for the production of surface microstructures in amorphous polymers by micro-hot-embossing. **Journal of Micromechanics and Microengineering** , 19 (11): 115030.

Hess, P.A. and Dauskardt, R.H. (2004) Mechanisms of elevated temperature fatigue crack growth in Zr–Ti–Cu–Ni–Be bulk metallic glass. **Acta Materialia** , 52 (12): 3525–3533.

Ho, H., Saeedi, E., Kim, S.S., et al. (2008) "Contact lens with integrated inorganic semiconductor devices." In **Proceedings of the IEEE 21st International Conference on Micro electro mechanical systems (MEMS 2008)**. **Tuscon, Arizona**. **2008**. pp. 403–406

Hopman, W.C.L., Ay, F., Hu, W., et al. (2007) Focused ion beam scan routine , dwell time and dose optimizations for submicrometre period planar photonic crystal components and stamps in silicon. **Nanotechnology**, 18 (19): 195305 (11pp)

Hsieh, P.J., Lin, B. and Lin, C. (2009) The construction and application of knowledge navigator model (KNM^{TM}): An evaluation of knowledge management maturity. **Expert Systems with Applications** , 36 (2): 4087–4100.

Huang, C.K. (2007) Polymeric nanofeatures of 100 nm using injection moulding for replication. **Journal of Micromechanics and Microengineering**, 17 (8): 1518–1526

Huang, Y., Chiu, Y.L., Shen, J., et al. (2010) Mechanical performance of metallic glasses during nanoscratch tests. **Intermetallics** , 18 (5): 1056–1061.

Ihlemann, J. (2010) "Micromachining and Patterning." In Sugioka, K., Meunier, M. and Pique, A. (eds.) **Laser Precision Microfabrication**. 1st edn. Springer-Verlag. pp. 239–258

Inoue, A. (2000) Stabilization of Metallic Supercooled Liquid and Bulk Amorphous Alloys. **Acta Materialia**, 48 (1): 278–306

Ishida, M., Takeda, H., Watanabe, D., et al. (2004) Fillability and Imprintability of High-strength Ni-based Bulk Metallic Glass Prepared by the Precision Die-casting Technique. **Materials Transactions**, 45 (4): 1239–1244

ISO 4288 (1997) **Geometrical Product Specifications (GPS) -- Surface texture: Profile method -- Rules and procedures for the assessment of surface texture**

Ito, H., Suzuki, H., Kazama, K., et al. (2009) Polymer structure and properties in micro- and nanomolding process. **Current Applied Physics** , 9 (2): e19–e24.

Jahan, M.P., Bakar, A., Asad, A., et al. (2011) "Micro-Electro Discharge Machining." In Koc, M. and Ozel, T. (eds.) **Micro-Manufacturing -- Design and Manufacturing of Micro-Products**. 1st edn. John Wiley & Sons Inc. pp. 301–346

Jia, G. and Madou, M.J. (2006a) "Liga and Micromolding." In Gad-el-Hak, M. (ed.) **The MEMS handbook**. Second Edi. CRC Press. pp. 4–1 – 4–79

Jia, G. and Madou, M.J. (2006b) "MEMS Fabrication." In Gad-el-Hak, M. (ed.) **The MEMS handbook**. Second Edi. CRC Press. pp. 3–1 – 3–214

Jo, C.H., Kim, B.H. and Chu, C.N. (2009) Micro electrochemical machining for complex internal micro features. **CIRP Annals - Manufacturing Technology**, 58 (1): 181–184

Joint Committee for Guides in Metrology (JCGM) (2008) **Evaluation of measurement data — Guide to the expression of uncertainty in measurement (GUM)**

Joshi, S.S. and Marla, D. (2014) "Electrochemical Micromachining." In Rahman, M. (ed.) **Comprehensive Materials Processing**. 1st edn. Elsevier. pp. 373–403.

Judy, J.W. (2001) Microelectromechanical systems (MEMS): fabrication , design and applications. **Smart Materials and Structures**, 10 (6): 1115–1134

Kalima, V., Pietarinen, J., Siitonen, S., et al. (2007) Transparent thermoplastics: Replication of diffractive optical elements using micro-injection molding. **Optical Materials** , 30 (2): 285–291.

Kapsa, J., Robach, Y., Hollinger, G., et al. (2004) STM and FIB nano-structuration of surfaces to localise InAs / InP (0 0 1) quantum dots. **Applied Surface Science**, 226 (1): 31–35

Kautt, M., Anson, S.M., Saile, V., et al. (2009) "Facilitating Open Innovation in Micro and Nano Technology by Providing Open Access to a Pan-European Toolbox called EUMINAfab." In Saile, V., Ehmann, K.F. and Dimov, S.S. (eds.). **4M/ICOMM 2009 - The Global Conference on Micro Manufacture - Incorportating the 5th International Conference on Multi-Material Micro Manufacture (4M) and the 4th International Conference on Micro Manufacturing (ICOMM). Forschungszentrum Karlsruhe, Karlsruhe, Germany**. **2009**. pp. 11–24

Kawasegi, N., Morita, N., Yamada, S., et al. (2006) Rapid Nanopatterning of a Zr-based Metallic Glass Surface Utilizing Focused Ion Beam Induced Selective Etching. **Applied Physics Letters**, 89 (14): 143115–1431153

Kettle, J., Hoyle, R.T., Dimov, S., et al. (2008) Fabrication of complex 3D structures using Step and Flash Imprint Lithography (S-FIL). **Microelectronic Engineering** , 85 (5-6): 853–855.

Kirkup, L. and Frenkel, B. (2006) **An Introduction to Uncertainty in Measurement**. 1st edn. Cambridge University Press

Knowles, M., Kearsley, A. and Karnakis, D. (2007a) **INDUSTRIAL LASERS: Laser micromachining expands as technology develops** [online]. Available from: http://www.laserfocusworld.com/articles/print/volume-43/issue-6/features/industrial-lasers-laser-micromachining-expands-as-technology-develops.html [Accessed 7 April 2015]

Knowles, M.R.H., Rutterford, G., Karnakis, D., et al. (2007b) Micro-machining of metals, ceramics and polymers using nanosecond lasers. **The International Journal of Advanced Manufacturing Technology** , 33 (1-2): 95–102.

Koc, M. and Ozel, T. (2011) "Fundamentals of Micromanufacturing." <u>In</u> Koc, M. and Ozel, T. (eds.) **Micro-Manufacturing -- Design and Manufacturing of Micro-Products**. 1st edn. John Wiley & Sons Inc. pp. 1–23

Kolew, A., Münch, D., Sikora, K., et al. (2010) Hot embossing of micro and sub-micro structured inserts for polymer replication. **Microsystem Technologies** , 17 (4): 609–618.

Koza, J.A., Sueptitz, R., Uhlemann, M., et al. (2011) Electrochemical micromachining of a Zr-based bulk metallic glass using a micro-tool electrode technique. **Intermetallics** , 19 (4): 437–444.

Kumar, G., Desai, A. and Schroers, J. (2011) Bulk metallic glass: The smaller the better. **Advanced Materials**, 23 (4): 461–476

Kumar, G. and Schroers, J. (2008) Write and erase mechanisms for bulk metallic glass. **Applied Physics Letters**, 92 (3): 31901–31903

Kumar, G., Staffier, P.A., Blawzdziewicz, J., et al. (2010) Atomically smooth surfaces through thermoplastic forming of metallic glass. **Applied Physics Letters** , 97 (10): 101907.

Kumar, G., Tang, H.X. and Schroers, J. (2009a) Nanomoulding with amorphous metals. **Nature** , 457 (7231): 868–872.

Kumar, S., Kruth, J.P., Van Humbeeck, J., et al. (2009b) A study of degradation of laser-sintered moulds using wear tests. **Rapid Prototyping Journal** , 15 (2): 104–110.

Kundig, A.A., Cucinelli, M., Uggowitzer, P., et al. (2003) Preparation of high aspect ratio surface microstructures out of a Zr-based bulk metallic glass. **Microelectronic Engineering**, 67-68: 405–409

Kunieda, M., Lauwers, B., Rajurkar, K.P., et al. (2005) Advancing EDM through Fundamental Insight into the Process. **CIRP Annals - Manufacturing Technology**, 54 (2): 64–87

Lalev, G., Dimov, S.S., Kettle, J., et al. (2008) Data Preparation for FIB machining of complex 3D Structures. **Proc Instn Mech Engrs Part B: J Engineering Manufacture**, 222 (1): 67–76

Lalev, G., Petkov, P., Sykes, N., et al. (2009) Fabrication and validation of fused silica NIL templates incorporating different length scale features. **Microelectronic Engineering** , 86 (4-6): 705–708.

Leach, R.K. (2001) **Measurement Good Practice Guide No. 37 -- The Measurement of Surface Texture using Stylus Instruments** Laboratory, N.P. (ed.). pp. 84

Lee, B.-K., Kim, D.S. and Kwon, T.H. (2004) Replication of microlens arrays by injection molding. **Microsystem Technologies** , 10 (6-7): 531–535.

Lee, Y.-C., Chen, C.-M. and Wu, C.-Y. (2005) A new excimer laser micromachining method for axially symmetric 3D microstructures with continuous surface profiles. **Sensors and Actuators A: Physical** , 117 (2): 349–355.

Lewis, L.J. and Perez, D. (2010) "Theory and Simulation of Laser Ablation --- from Basic Mechanisms to Applications." <u>In</u> Sugioka, K., Meunier, M. and Pique, A. (eds.) **Laser Precision Microfabrication**. 1st edn. Springer-Verlag. pp. 35–61

Leyland, A. and Matthews, A. (2000) On the significance of the H/E ratio in wear control: a nanocomposite coating approach to optimised tribological behaviour. **Wear** , 246 (1-2): 1–11.

Li, W., Dimov, S. and Lalev, G. (2007a) Focused-ion-beam direct structuring of fused silica for fabrication of nano-imprinting templates. **Microelectronic Engineering** , 84 (5-8): 829–832.

Li, W., Minev, R., Dimov, S., et al. (2007b) Patterning of Amorphous and Polycrystalline Ni78B14Si8 with a Focused Ion Beam. **Applied Surface Science**, 253 (12): 5404–5410

Li, Y.J., Xie, H.M., Guo, B.Q., et al. (2010) Fabrication of high-frequency moire gratings for microscopic deformation measurement using focused ion beam milling. **Journal of Micromechanics and Microengineering**, 20 (5): 055037 (9pp)

Liang, S., He, J.Y., Chu, W.Y., et al. (2004) Nanowear of a Zr-based Bulk Metallic Glass/ Nanocrystalline Alloy. **Transactions of Materials and Heat Treatment**, 25 (5): 1195 – 1199

Lin, H.-K., Lee, C.-J., Hu, T.-T., et al. (2012) Pulsed laser micromachining of Mg-Cu-Gd bulk metallic glass. **Optics and Lasers in Engineering** , 50 (6): 883–886.

Liu, K., NiCkolov, Z., Oh, J., et al. (2012) KrF excimer laser micromachining of MEMS materials: characterization and applications. **Journal of Micromechanics and Microengineering** , 22 (1): 015012.

Löffler, J.F. (2003) Bulk metallic glasses. **Intermetallics** , 11 (6): 529–540.

Loffler, J.F., Kundig, A.A. and Dalla Torre, F.H. (2007) "Rapid Solidification and Bulk Metallic Glasses --- Processing and Properties." In Groza, J.R., Shackelford, J.F., Lavernia, E.J., et al. (eds.) **Materials Processing Handbook**. 1st edn. CRC Press. pp. 17–1 – 17–44

Madou, M.J. (2002) **Fundamentals of Microfabrication: The Science of Miniaturization**. 2nd Edn. New York: CRC Press

Mäkelä, T. and Haatainen, T. (2012) Roll-to-roll pilot nanoimprinting process for backlight devices. **Microelectronic Engineering**, 97: 89–91

Malek, C.K. and Saile, V. (2004) Applications of LIGA technology to precision manufacturing of high-aspect-ratio micro-components and -systems: a review. **Microelectronics Journal** , 35 (2): 131–143.

Mani, M.R., Surace, R., Ferreira, P., et al. (2013) Process Parameter Effects on Dimensional Accuracy of Micro-Injection Moulded Part. **Journal of Micro and Nano-Manufacturing and Nano-Manufacturing**, 1 (3): 031003

Mankins, J.C. (1995) **Technology Readiness Levels** [online]. Available from: http://www.hq.nasa.gov/office/codeq/trl/trl.pdf [Accessed 7 April 2015]

Mankins, J.C. (2002) Approaches to Strategic Research and Technology Analysis and Road Mapping. **Acta Astronautica**, 51 (1-9): 3–21

Mankins, J.C. (2009) Technology readiness assessments : A retrospective. **Acta Astronautica** , 65 (9-10): 1216–1223.

Marinello, F., Bariani, P., Carmignato, S., et al. (2009) Geometrical modelling of scanning probe microscopes and characterization of errors. **Measurement Science and Technology** , 20 (8): 084013.

Masuzawa, T. (2000) State of the Art of Micromachining. **CIRP Annals - Manufacturing Technology**, 49 (2): 473–488

Meijer, J., Du, K., Gillner, A., et al. (2002) Laser Machining by short and ultrashort pulses, state of the art and new opportunities in the age of the photons. **CIRP Annals - Manufacturing Technology**, 51 (2): 531–550

Minev, R., Ilieva, M., Kettle, J., et al. (2010) Deposition and FIB Milling of Anticorrosive CrC Coatings on Tool Steel Substrates. **International Journal of Advanced Manufacturing Technology** , 47 (1-4): 29–35.

Mondal, K., Ohkubo, T., Toyama, T., et al. (2008) The effect of nanocrystallization and free volume on the room temperature plasticity of Zr-based bulk metallic glasses. **Acta Materialia** , 56 (18): 5329–5339.

Monkkonen, K., Hietala, J., Paakkonen, P., et al. (2002) Replication of Sub-Micron Features Using Amorphous Thermoplastics. **Polymer Engineering and Science**, 42 (7): 1600–1608

Montgomery, D.C. (2009) **Design and Analysis of Experiments**. 7th edn. John Wiley & Sons Inc.

Murali, P. and Ramamurty, U. (2005) Embrittlement of a bulk metallic glass due to sub-Tg annealing. **Acta Materialia** , 53 (5): 1467–1478.

Musil, J., Kunc, F., Zeman, H., et al. (2002) Relationships between hardness , Young ' s modulus and elastic recovery in hard nanocomposite coatings. **Surface and Coatings Technology**, 154 (2): 304–313

Mutapcic, E., Iovenitti, P. and Hayes, J.P. (2005) A prototyping and microfabrication CAD/CAM tool for the excimer laser micromachining process. **The International Journal of Advanced Manufacturing Technology** , 30 (11-12): 1076–1083.

Nagahama, D., Ohkubo, T., Mukai, T., et al. (2005) Characterization of Nanocrystal Dispersed Cu 60 Zr 30 Ti 10 Metallic Glass. **Materials Transactions**, 46 (6): 1264–1270

Nayak, B.K. and Gupta, M.C. (2010) Self-organized micro/nano structures in metal surfaces by ultrafast laser irradiation. **Optics and Lasers in Engineering** , 48 (10): 940–949.

Nestler, J., Morschhauser, A., Hiller, K., et al. (2010) Polymer lab-on-chip systems with integrated electrochemical pumps suitable for large-scale fabrication. **International Journal of Advanced Manufacturing Technology**, 47 (1-4): 137–145

Nguyen, N.-T. and Wu, Z. (2005) Micromixers—a review. **Journal of Micromechanics and Microengineering** , 15 (2): R1–R16.

Nishiyama, N., Amiya, K. and Inoue, A. (2004) Bulk Metallic Glasses for Industrial Products. **Materials Transactions**, 45 (4): 1245–1250

Ohkubo, T., Nagahama, D., Mukai, T., et al. (2007) Stress − strain behaviors of Ti-based bulk metallic glass and their nanostructures. **Journal of Materials Research**, 22 (5): 1406–1413

Osswald, T.A., Turng, L.S. and Gramann, P. (2008) **Injection Molding Handbook**. 2nd edn. Hanser

Ozel, T. and Thepsonthi, T. (2011) "Mechanical Micro-machining." In Koc, M. and Ozel, T. (eds.) **Micro-Manufacturing -- Design and Manufacturing of Micro-Products**. 1st edn. John Wiley & Sons Inc. pp. 235–274

Packard, C.E., Schroers, J. and Schuh, C.A. (2009) In situ measurements of surface tension-driven shape recovery in a metallic glass. **Scripta Materialia** , 60 (12): 1145–1148.

Pan, C.T., Wu, T.T., Chen, M.F., et al. (2008) Hot embossing of micro-lens array on bulk metallic glass. **Sensors and Actuators** , 141 (2): 422–431.

Pan, C.T., Wu, T.T., Liu, C.F., et al. (2010) Study of scratching Mg-based BMG using nanoindenter with Berkovich probe. **Materials Science and Engineering: A** , 527 (9): 2342–2349.

Paulk, M.C., Weber, C. V, Curtis, B., et al. (eds.) (1995) **The Capability Maturity Model: Guidelines for Improving the Software Process**. Addison-Wesley

Pavey, J. (2013) **Study of Conventional Annealing and Laser Annealing of Vitreloy 1b Zr-based BMG**. University of Birmingham

Peng, L., Deng, Y., Yi, P., et al. (2014) Micro hot embossing of thermoplastic polymers : a review. **Journal of Micromechanics and Microengineering**, 24 (1): 013001 (23pp)

Petkov, P. (2011) **Laser Milling: Surface Integrity, Removal Strategies and Process Accuracy**. Cardiff University

Petkov, P. V, Dimov, S.S., Minev, R.M., et al. (2008a) Laser milling: Pulse duration effects on surface integrity. **Proceedings of the Institution of Mechanical Engineers, Part B: Journal of Engineering Manufacture** , 222 (1): 35–45.

Petkov, P. V, Scholz, S. and Dimov, S.S. (2008b) "Strategies for material removal in laser milling." In Dimov, S.S. and Menz, W. (eds.). **4M 2008 - Fourth International Conference on Multi-Material Micro Manufacture Proceedings** . **Cardiff, Wales, UK**. **2008**. Whittles Publishing. pp. 249–252

Pham, D.T., Dimov, S.S., Bigot, S., et al. (2004a) Micro-EDM -recent developments and research issues. **Journal of Materials Processing Technology**, 149 (1-3): 50–57

Pham, D.T., Dimov, S.S., Ji, C., et al. (2004b) Laser milling as a "rapid" micromanufacturing process. **Proc. Instn Mech. Engrs Part B: J. Engineering Manufacture**, 218 (1): 1–7

Pham, D.T., Dimov, S.S., Petkov, P. V, et al. (2002) Laser Milling. **Proc Instn Mech Engrs Part B: J Engineering Manufacture**, 216 (5): 657–667

Pham, D.T., Dimov, S.S. and Petkov, P. V (2007) Laser milling of ceramic Components. **International Journal of Machine Tools and Manufacture**, 47 (3): 618–626

Pham, D.T., Elkaseer, A.M., Popov, K.P., et al. (2009) "Micromiling of coarse-grained and ultrafine-grained Cu99.9E: Effects of material microstructure on machining conditions and surface quality." In **Proceedings of 4M/ICOMM Conference**. **2009** . pp. 241–244.

Platzgummer, E., Loeschner, H. and Gross, G. (2008) "Projection Maskless Patterning for Nanotechnology Applications." In **52nd International Conference on Electron, Ion and Photon Beam Technology and Nanofabrication**. **AVS**. **2008**. pp. 2059–2063

Popov, K.B., Dimov, S.S., Pham, D.T., et al. (2006) Micromilling: Material Microstructure Effects. **Proceedings of the Institution of Mechanical Engineers, Part B, J. of Engineering Manufacture (IMechE)**, 220 (11): 1807–1813

Prenitzer, B.I., Giannuzzi, L.A., Brown, S.R., et al. (2003) The Correlation between Ion Beam / Material Interactions and Practical FIB Specimen Preparation. **Microscopy and Microanalysis**, 9 (03): 216–236

Qian, L., Li, M., Zhou, Z., et al. (2005) Comparison of nano-indentation hardness to microhardness. **Surface and Coatings Technology** , 195 (2-3): 264–271.

Qin, Y. (2010) "Overview of micro-manufacturing." In Qin, Y. (ed.) **Micro-Manufacturing Engineering and Technology**. 1st edn. . Elsevier Ltd. p. 1-23.

Quintana, I., Dobrev, T., Aranzabe, A., et al. (2009) Investigation of Amorphous and Crystalline Ni Alloys Response to Machining with Micro-second and Pico-second Lasers. **Applied Surface Science**, 255 (13-14): 6641–6646

Rajurkar, K.P., Levy, G., Malshe, A., et al. (2006) Micro and Nano Machining by Electro-Physical and Chemical Processes . **Annals of the CIRP**, 55 (2): 643–666

Reinhart, G. and Schindler, S. (2010) "A Strategic Evaluation Approach for Defining the Maturity of Manufacturing Technologies." In **Proceedings of the International Conference on Engineering and Technology Management (ICETM 2010)**. **Venice, Italy**. **2010**. pp. 920–925

Ren, Y.T. and Yeo, K.T. (2004) "Risk management capability maturity model for complex product systems (CoPS) projects." In **Engineering Management Conference, 2004. Proceedings. 2004 IEEE International**. **2004** . IEEE. p. Vol 2. 807–811.

Saarikoski, I., Suvanto, M. and Pakkanen, T.A. (2009) Modification of polycarbonate surface properties by nano-, micro-, and hierarchical micro–nanostructuring. **Applied Surface Science** , 255 (22): 9000–9005.

Salant, P. and Dillman, D.A. (1994) **How to Conduct Your Own Survey**. Wiley

Saotome, Y., Fukuda, Y., Yamaguchi, I., et al. (2007) Superplastic nanoforming of optical components of Pt-based metallic glass. **Journal of Alloys and Compounds** , 434-435: 97–101.

Saotome, Y., Miwa, S., Zhang, T., et al. (2001) The micro-formability of Zr-based amorphous alloys in the supercooled liquid state and their application to micro-dies. **Journal of Materials Processing Technology** , 113 (1-3): 64–69.

Schaller, T., Heckele, M., Ruprecht, R., et al. (1999) "Microfabrication of a mold insert made of hardened steel and first molding results." In **Proceedings of the 14th Annual Meeting - American Society for Precision Engineering**. **1999**. pp. 225 – 228

Schmidt, J., Knoll, M. and Masuzawa, T. (2005) "Micro-EDM for Mold Inserts." In Baltes, H., Brand, O., Fedder, G.K., et al. (eds.) **Microengineering of Metals and Ceramics -- Part I: Design, Tooling, and Injection Moulding**. Wiley-VCH. pp. 161–185

Schmidt, J. and Tritschler, H. (2004) Micro cutting of steel. **Microsystem Technologies** , 10 (3): 167–174.

Scholz, S., Griffiths, C.A., Dimov, S.S., et al. (2009) "New Process Chains for Replicating Micro and Nano Structured Surfaces with Bio-mimetic Applications." In **ANTEC 2009 - Proceedings of the 67th Annual Technical Conference & Exhibition**. **Chicago**. **2009**. pp. 3021–3027

Scholz, S.G., Griffiths, C.A., Dimov, S.S., et al. (2011) Manufacturing routes for replicating micro and nano surface structures with bio-mimetic applications. **CIRP Journal of Manufacturing Science and Technology** , 4 (4): 347–356.

Schroers, B.J. (2010) Processing of Bulk Metallic Glass. **Advanced Materials**, 22 (14): 1566–1597

Schroers, J. (2005) The Superplastic Forming of Bulk Metallic Glasses. **The Journal of The Minerals, Metals & Materials Society (TMS)**, 57 (5): 35–39

Schroers, J. (2008) On the formability of bulk metallic glass in its supercooled liquid state. **Acta Materialia**, 56 (3): 471–478

Schroers, J., Nguyen, T., O'Keeffe, S., et al. (2007a) Thermoplastic forming of bulk metallic glass—Applications for MEMS and microstructure fabrication. **Materials Science and Engineering: A** , 449-451: 898–902.

Schroers, J. and Paton, N. (2006) Amorphous Metal Alloys Form Like Plastics. **Advanced Materials and Processes**, pp. 61–63

Schroers, J., Pham, Q. and Desai, A. (2007b) Thermoplastic Forming of Bulk Metallic Glass — A Technology for MEMS and Microstructure Fabrication. **Journal of Microelectromechanical Systems**, 16 (2): 240–247

Schuh, C., Hufnagel, T. and Ramamurty, U. (2007) Mechanical behavior of amorphous alloys. **Acta Materialia** , 55 (12): 4067–4109.

Sha, B., Dimov, S., Griffiths, C., et al. (2006) Micro-injection moulding: Factors affecting the achievable aspect ratios. **The International Journal of Advanced Manufacturing Technology** , 33 (1-2): 147–156.

Shah, L., Siadat, A. and Vernadat, F. (2009) "Maturity assessment in risk management in manufacturing engineering." In **3rd Annual IEEE International Systems Conference**. **Vancouver, Canada**. **March 2009** . IEEE. pp. 296–301.

Sharma, P., Kaushik, N., Kimura, H., et al. (2007) Nano-fabrication with metallic glass --- an exotic material for nano-electromechanical systems. **Nanotechnology** , 18 (3): 035302 (6pp).

Smith, J.D. (2005) "An Alternative to Technology Readiness Levels for Non-Developmental Item (NDI) Software." In **Proceedings of the 38th Hawaii International Conference on System Sciences**. **2005**. pp. 1–8

Stephen, A. and Vollertsen, F. (2005) "3D Microstructuring of Mold Inserts by Laser-based Removal." In Baltes, H., Brand, O., Fedder, G.K., et al. (eds.) **Microengineering of Metals and Ceramics -- Part I: Design, Tooling, and Injection Moulding**. Wiley-VCH. pp. 131–160

Sueptitz, R., Tschulik, K., Becker, C., et al. (2012) Micropatterning of Fe-based bulk metallic glass surfaces by pulsed electrochemical micromachining. **Journal of Materials Research**, 27 (23): 3033–3040

Suryanarayana, C. and Inoue, A. (2011) **Bulk Metallic Glasses**. 1st Edn. CRC Press Taylor & Francis Group

Svintsov, A., Zaitsev, S., Lalev, G., et al. (2009) FIB sputtering optimization using Ion Reverse Software. **Microelectronic Engineering** , 86 (4-6): 544–547.

Tam, R.C.Y. and Shek, C.H. (2004) Abrasion resistance of Cu based bulk metallic glasses. **Journal of Non-Crystalline Solids** , 347 (1-3): 268–272.

Tanaka, H. and Wood, R.J. (2010) Fabrication of corrugated artificial insect wings using laser micromachined molds. **Journal of Micromechanics and Microengineering**, 20 (7): 075008 (8pp)

Tang, P.T. (2008) "Utilising Electrochemical Deposition for Micro Manufacturing." In **Proceedings of the 4th International Conference on Multi-Material Micro Manufacture**. **Cardiff, Wales, UK**. **2008**. pp. 9–11

Tang, P.T., Fugl, J., Uriarte, L., et al. (2006) "Indirect tooling based on micromilling , electroforming and selective etching." In **4M 2006 - Second International Conference on Multi-Material Micro Manufacture**. **2006**. pp. 183 − 186

Telford, J.K. (2007) A Brief Introduction to Design of Experiments. **John Hopkins APL Technical Digest**, 27 (3): 224–232

Tiku, S., Azarian, M. and Pecht, M. (2007) Using a reliability capability maturity model to benchmark electronics companies. **International Journal of Quality & Reliability Management** , 24 (5): 547–563.

Ting, C., Chang, F., Chen, C., et al. (2008) Fabrication of an antireflective polymer optical film with subwavelength structures using a roll-to-roll micro-replication process. **Journal of Micromechanics and Microengineering**, 18 (7): 075001 (9pp)

Tosello, G. (2008) **Precision Moulding of Polymer Micro Components - Optimistation, Simulation , Tooling, Quality Control and Multi-material Application**. DTU

Tosello, G., Bissacco, G., Tang, P.T., et al. (2008) High Aspect Ratio Micro Tool Manufacturing for Polymer Replication using μEDM of Silicon, Selective Etching and Electroforming. **Micosyetem Technologies**, 14 (9-11): 1757–1764

Tosello, G. and Chiffre, L. De (2004) **Standard Traceability and Measurement Uncertainty**

Tosello, G., Fillon, B., Azcarate, S., et al. (2007) "Application of different process chains for polymer microfluidics fabrication including hybrid tooling technologies , standardization and replication : a benchmark investigation within 4M Polymer Division." In **4M 2007 Third International Conference on Multi-Material Manufacture Proceedings**. **2007**. pp. 3–6

Tosello, G., Gava, A., Hansen, H.N., et al. (2009a) Characterization and analysis of weld lines on micro-injection moulded parts using atomic force microscopy (AFM). **Wear** , 266 (5-6): 534–538.

Tosello, G., Gava, A., Hansen, H.N., et al. (2010a) Study of process parameters effect on the filling phase of micro-injection moulding using weld lines as flow markers. **International Journal of Advanced Manufacturing Technology**, 47 (1-4): 81–97

Tosello, G., Hansen, H.N. and Gasparin, S. (2009b) Applications of dimensional micro metrology to the product and process quality control in manufacturing of precision polymer micro components. **CIRP Annals - Manufacturing Technology** , 58 (1): 467–472.

Tosello, G., Hansen, H.N., Marinello, F., et al. (2010b) Replication and dimensional quality control of industrial nanoscale surfaces using calibrated AFM measurements and SEM image processing. **CIRP Annals - Manufacturing Technology** , 59 (1): 563–568.

Tosello, G., Marinello, F. and Hansen, H.N. (2012) Characterisation and analysis of microchannels and submicrometre surface roughness of injection moulded microfluidic systems using optical metrology. **Plastics, Rubber and Composites** , 41 (1): 29–39.

Trexler, M.M. and Thadhani, N.N. (2010) Mechanical properties of bulk metallic glasses. **Progress in Materials Science** , 55 (8): 759–839.

Tseng, A.A. (2004) Recent developments in micromilling using focused ion beam technology. **Journal of Micromechanics and Microengineering** , 14 (4): R15–R34.

Tseng, A.A. (2005) Recent Developments in Nanofabrication Using Focused Ion Beams. **Small**, 1 (10): 924–939

United Kingdom Accreditation Service (UKAS) (2007) **The Expression of Uncertainty and Confidence in Measurement**

Urbanek, M., Uhlir, V., Babor, P., et al. (2010) Focused ion beam fabrication of spintronic nanostructures : an optimization of the milling process. **Nanotechnology**, 21 (14): 145304 (7pp)

Uriarte, L., Herrero, A., Ivanov, A., et al. (2006) Comparison between microfabrication technologies for metal tooling. **Proceedings of the Institution of Mechanical Engineers, Part C: Journal of Mechanical Engineering Science** , 220 (11): 1665–1676.

Vaidyanathan, R., Dao, M., Ravichandran, G., et al. (2001) Study of mechanical deformation in bulk metallic glass through instrumented indentation. **Acta Materialia** , 49 (18): 3781–3789.

Van Steenberge, N., Concustell, A., Sort, J., et al. (2008) Microstructural inhomogeneities introduced in a Zr-based bulk metallic glass upon low-temperature annealing. **Materials Science and Engineering: A** , 491 (1-2): 124–130.

Vázquez, E., Rodríguez, C.A., Elías-Zúñiga, A., et al. (2010) An experimental analysis of process parameters to manufacture metallic micro-channels by micro-milling. **The International Journal of Advanced Manufacturing Technology** , 51 (9-12): 945–955.

Vazquez, R.M., Osellame, R., Nolli, D., et al. (2009) Integration of femtosecond laser written optical waveguides in a lab-on-chip. **Lab on a chip**, 9 (1): 91–96

Vehse, M., Lobler, M., Schmitz, K.P., et al. (2012) Laser induced surface structure on stainless steel influences cell viability. **Biomed Tech**, 57 (Suppl. 1): 419–421

Velkova, V. (2011) **Focused Ion Beam Technology: Implementation in Manufacturing Platforms and Process Optimisation**. Cardiff University

Velkova, V., Lalev, G., Hirshy, H., et al. (2010) Design and validation of a novel master-making process chain for organic and large area electronics on flexible substrates. **Microelectronic Engineering** , 87 (11): 2139–2145.

Velkova, V., Lalev, G., Hirshy, H., et al. (2011) Process chain for serial manufacture of 3D micro- and nano-scale structures. **CIRP Journal of Manufacturing Science and Technology** , 4 (4): 340–346.

Velten, T., Bauerfeld, F., Schuck, H., et al. (2011) Roll-to-roll hot embossing of microstructures. **Microsystem Technologies**, 17 (4): 619–627

Velten, T., Schuck, H., Haberer, W., et al. (2010) Investigations on reel-to-reel hot embossing. **International Journal of Advanced Manufacturing Technology**, 47 (1-4): 73–80

Vick, D., Sauer, V., Fraser, A.E., et al. (2010) Bulk focused ion beam fabrication with three-dimensional shape control of nanoelectromechanical systems. **Journal of Micromechanics and Microengineering**, 20 (10): 105005 (9pp)

Wang, G., Liaw, P.K., Yokoyama, Y., et al. (2008a) Investigations of the Factors that Affected Fatigue Behavior of Zr-Based Bulk-Metallic Glasses. **Advanced Engineering Materials** , 10 (11): 1030–1033.

Wang, G.Y. and Liaw, P.K. (2007) Effects of partial crystallization on compression and fatigue behavior of Zr-based bulk metallic glasses. **Journal of Materials Research**, 22 (2): 493–500

Wang, G.Y. and Liaw, P.K. (2010) "Fatigue and Fracture Behavior." <u>In</u> Miller, M. and Liaw, P. (eds.) **Bulk Metallic Glasses**. 1st edn. Springer. pp. 169–203

Wang, G.Y., Liaw, P.K., Yokoyama, Y., et al. (2008b) Fatigue behavior of Zr-based bulk-metallic glasses. **Materials Science and Engineering: A** , 494 (1-2): 314–323.

Wang, G.Y., Liaw, P.K., Yokoyama, Y., et al. (2011) Size effects on the fatigue behavior of bulk metallic glasses. **Journal of Applied Physics** , 110 (11): 113507.

Wang, J.G., Choi, B.W. and Nieh, T.G. (2000) Nano-scratch Behavior of a Zr-10Al-5Ti-17.9Cu-14.6Ni amorphous alloy. **Journal of Materials Research**, 15 (4): 913–922

Wang, Q., Luo, Q. and Gu, C.Z. (2007a) Nickel silicide nanowires formed in pre-patterned SiO 2 trenches and their electrical transport properties. **Nanotechnology**, 18 (19): 195304 (5pp)

Wang, X., Lu, P., Dai, N., et al. (2007b) Noncrystalline Micromachining of Amorphous Alloys Using Femtosecond Laser Pulses. **Materials Letters**, 61 (21): 4290–4293

Waniuk, T., Schroers, J. and Johnson, W.L. (2003) Timescales of crystallization and viscous flow of the bulk glass-forming Zr-Ti-Ni-Cu-Be alloys. **Physical Review B** , 67 (18): 184203–184209.

Washio, K. (2010) "Laser Devices and Optical Systems for Laser Precision Microfabrication." In Sugioka, K., Meunier, M. and Pique, A. (eds.) **Laser Precision Microfabrication**. 1st edn. Springer Verlag. pp. 63–89

Watts, H.S. (1989) **Managing the Software Process**. Addison-Wesley Professional

Whitesides, G.M. (2006) The origins and the future of microfluidics. **Nature** , 442 (7101): 368 –373.

Worgull, M. (2009) **Hot Embossing: Theory and Technology of Microreplication**. 1st edn. William Andrew

Wu, B. and Ozel, T. (2011) "Micro-Laser Processing." In Koc, M. and Ozel, T. (eds.) **Micro-Manufacturing -- Design and Manufacturing of Micro-Products**. 1st edn. John Wiley & Sons Inc. pp. 159–198

Wu, P.H., Cheng, C.W., Chang, C.P., et al. (2011) Fabrication of large-area hydrophobic surfaces with femtosecond-laser-structured molds. **Journal of Micromechanics and Microengineering**, 21 (11): 115032

Xu, J., Ramamurty, U. and Ma, E. (2010) The Fracture Toughness of Bulk Metallic Glasses. **The Journal of The Minerals, Metals & Materials Society (TMS)**, 64 (4): 10–18

Yao, D. (2011) "Polymer Micro-Molding/Forming Processes." In Koc, M. and Ozel, T. (eds.) **Micro-Manufacturing -- Design and Manufacturing of Micro-Products**. 1st edn. John Wiley & Sons Inc. pp. 197–234

Yeo, L.P., Ng, S.H., Wang, Z.F., et al. (2010) Investigation of hot roller embossing for microfluidic devices. **Journal of Micromechanics and Microengineering**, 20 (1): 015017 (10pp)

Yeo, S.H., Tan, P.C., Aligiri, E., et al. (2009) Processing of Zirconium-Based Bulk Metallic Glass (BMG) Using Micro Electrical Discharge Machining (Micro-EDM). **Materials and Manufacturing Processes**, 24 (12): 1242–1248

Yokoyama, Y., Liaw, P.K., Nishijima, M., et al. (2006) Fatigue-Strength Enhancement of Cast Zr50Cu40Al10 Glassy Alloys. **Materials Transactions** , 47 (5): 1286–1293.

Yong, L., Di, Z., Yongbin, Z., et al. (2010) Experimental investigation on complex structures machining by electrochemical micromachining technology. **Chinese Journal of Aeronautics** , 23 (5): 578–584.

Yoo, Y.E., Kim, T.H., Choi, D.S., et al. (2009) Injection molding of a nanostructured plate and measurement of its surface properties. **Current Applied Physics** , 9 (2): e12–e18.

Youn, S.-W., Okuyama, C., Takahashi, M., et al. (2008) A study on fabrication of silicon mold for polymer hot-embossing using focused ion beam milling. **Journal of Materials Processing Technology** , 201 (1-3): 548–553.

Youn, S.W., Takahashi, M., Goto, H., et al. (2006) Microstructuring of glassy carbon mold for glass embossing -- Comparison of focused ion beam, nano/femtosecond-pulsed laser and mechanical machining. **Microelectronic Engineering** , 83 (11- 12): 2482–2492.

Youn, S.W., Takahashi, M., Goto, H., et al. (2007) Fabrication of micro-mold for glass embossing using focused ion beam, femto-second laser, eximer laser and dicing techniques. **Journal of Materials Processing Technology** , 187-188: 326–330.

Zhang, G., Liu, Y. and Zhang, B. (2006) Effect of Annealing Close to Tg on Notch Fracture Toughness of Pd-based Thin-film Metallic Glass for MEMS Applications. **Scripta Materialia**, 54 (5): 897–901

Zhang, N., Byrne, C.J., Browne, D.J., et al. (2012a) Towards nano-injection molding. **Materials Today** , 15 (5): 216–221.

Zhang, N., Chu, J.S., Byrne, C.J., et al. (2012b) Replication of micro/nano-scale features by micro injection molding with a bulk metallic glass mold insert. **Journal of Micromechanics and Microengineering**, 22 (6): 065019 (13pp)

Zhang, X., Ma, J., Fang, G., et al. (2014) Polymer micro molding with bulk metallic glass mold. **Microsystem TechnologiesMicrosystem Technologies** , pp. 1–5.

Zheng, H.Y., Liu, H., Wan, S., et al. (2005) Ultrashort pulse laser micromachined microchannels and their application in an optical switch. **The International Journal of Advanced Manufacturing Technology** , 27 (9-10): 925–929.

Zhu, Z., Yi, C., Shi, T., et al. (2014) Fabricating Zr-Based Bulk Metallic Glass Microcomponent by Suction Casting Using Silicon Micromold. **Advances in Mechanical Engineering**, 2014: 1–8

Zhu, Z.W., Zheng, S.J., Zhang, H.F., et al. (2008) Plasticity of bulk metallic glasses improved by controlling the solidification condition. **Journal of Materials Research**, 23 (4): 941–948

Ziaie, B., Baldi, A., Lei, M., et al. (2004) Hard and soft micromachining for BioMEMS: review of techniques and examples of applications in microfluidics and drug delivery. **Advanced Drug Delivery Reviews** , 56 (2): 145–172.

Zorzi, J.E. and Perottoni, C.A. (2013) Estimating Young's modulus and Poisson's ratio by instrumented indentation test. **Materials Science and Engineering: A** , 574: 25–30.

LIST OF PUBLICATIONS

Vella, P.C., Brousseau, E.B., Minev, R., et al. (2010) "A Methodology for Technology Maturity Assessment of Micro and Nano Manufacturing Processes and Process Chains." In Pfefferkorn, F.E. (ed.). **The 5th International Conference on MicroManufacturing (ICOMM/4M 2010)**. **Madison, Wisconsin, USA**. **2010**. pp. 327–334

Vella, P.C., Dimov, S.S., Brousseau, E.B., et al. (2011) "Length Scale Integration: Implementation of a New Process Chain for Producing Replication Masters with Micro and Nano Scale Features." In Kuck, H., Reinecke, H. and Dimov, S.S. (eds.). **8th International Conference on Multi-Material Micro Manufacture**. **Stuttgart, Germany**. **2011**. Research Publishing. pp. 343–347

Vella, P.C., Dimov, S.S., Kolew, A., et al. (2012) "Bulk Metallic Glass Based Tool-making Process Chain for Micro- and Nano-Replication." In Noll, H., Adamovic, N. and Dimov, S.S. (eds.). **9th International Conference on Multi-Material Micro Manufacture**. **Vienna, Austria**. **2012**. Research Publishing. pp. 309–314

Vella, P.C., Dimov, S.S., Whiteside, B.R., et al. (2013) "Validation of a New Process Chain for Producing Bulk Metallic Glass Replication Masters with Micro and Nano-scale Features." In Azcarate, S. and Dimov, S.S. (eds.). **10th International Conference on Multi-Material Micro Manufacture**. **San Sebastian, Spain**. **2013**. Research Publishing. pp. 103–108

Vella, P.C., Dimov, S.S., Brousseau, E.B., et al. (2014) A New Process Chain for Producing Bulk Metallic Glass Replication Masters with Micro- and Nano-scale Features. **International Journal of Advanced Manufacturing Technology**, 76 (1-4): 523–543

Vella, P., Dimov, S.S. and Kolew, A. (2014) Process Chain for Serial Manufacture of Polymer Components with Micro- and Nano-scale Features: Optimisation Issues. **Proceedings of the Institution of Mechanical Engineers, Part B: Journal of Engineering Manufacture.** (Submitted for Review)

Vella, P., Dimov, S.S., Minev, R., et al. (2015) Technology Maturity Assessment of Micro and Nano Manufacturing Processes and Process Chains. **Proceedings of the Institution of Mechanical Engineers, Part B: Journal of Engineering Manufacture.** (Submitted for Review)

Vella, P.C., Dimov, S.S. and Kolew, A. (2015) A Novel Master Making Process Chain for Producing Bulk Metallic Glass Injection Moulding Inserts with Different Length Scale Features. (Manuscript in Preparation)